Timescales of Oceanic Lithosphere Hydration: Constraints from Rodingites, Apennines, Italy

A thesis prepared by Charlotte Lorthioir

Master of Science – Geology

Department of Earth and Environmental Sciences

Boston College

Morrissey College of Arts and Sciences

Graduate School

April 2023

Timescales of Oceanic Lithosphere Hydration: Constraints from Rodingites, Apennines, Italy

By Charlotte Lorthioir

Advisor: Ethan Baxter

Abstract:

Serpentinites assume a critical role in geochemical and geophysical cycles, from recycling fluid into the sub-arc mantle to facilitating exhumation within subduction zones. Rodingite dikes can be used as a lens to investigate the hydration of the oceanic lithosphere as their development is synchronous with serpentinization, and while serpentinites lack sufficient mineral phases for geochronology, rodingite dikes are rich in andradite and grossular garnet which are potentially amenable for geochronology. This research seeks to constrain the timescales and duration of hydration of the oceanic lithosphere within the Alpine Tethys ocean basin, and associated serpentinization, by examining Apennines rodingites from the Internal Ligurides (Italy). These rodingites experienced seafloor hydrothermal alteration and were obducted onto the continental margin during Alpine orogenesis. As a result, they are ideal for studying seafloor metasomatism as they were not affected by prograde subduction zone metamorphism and dehydration. Sr isotopic and trace element profiles were constructed across two rodingite-serpentinite transects, revealing a complex, multi-stage hydration history consisting of 1) Widespread serpentinization, 2) Gabbroic intrusions, 3) Rodingitization, and 4) Localized, late-stage advective fluid flow. Serpentinizing fluids locally display strong continental crustal isotopic signatures, while rodingitization fluids are characterized by seawater-like values. U-Pb geochronology on rodingite garnets produced an age of 96.1 ± 8.9 Ma, which could represent either the main rodingitization phase or the late-stage advective alteration.

Table of Contents

List of Tables

List of Figures

Acknowledgements:

This endeavor would not have been possible without my advisor and chair of my committee, Ethan Baxter, and his invaluable insight and feedback. Thank you so much for your support and encouragement as well as your genuine enthusiasm and passion for the world we live in. I am also deeply indebted to my committee members Seth Kruckenberg and Jeremy Shakun, as well as Mark Behn, who generously contributed their time and knowledge to the development of this thesis. An immense thank you to Steph Walker and Paul Starr, whose mentorship and expertise were foundational to this research and who were always available to answer my questions. Steph, your insights and contributions were invaluable and I truly could not have done this without you. You also have my deep thanks for keeping the lab stocked during a pandemic, an incredibly impressive feat. Thank you to all the members of the Isotope Geochemistry cohort for their assistance and moral support in and out of the lab, I am so grateful to have worked with every one of you.

Kat O'Blenes thank you so much for your assistance in navigating the challenges of graduate school. You were always willing to lend an ear and your support was truly indispensable throughout this process. Sky Goliber, I have leaned on you so much during the last few years— when I try to thank you there is truly too much to list, but know I would not have been able to accomplish this without you. Jose Cuevas your ability to troubleshoot is unparalleled and I cannot tell you how much I value both your insight and comradery. I would also like to acknowledge the entire graduate student body of the Earth and Environmental Sciences Department for their encouragement and friendship. I am very proud to have been a part of the EESC community and I am truly grateful for the time spent learning, teaching, and collaborating with you all.

Preface:

This research investigates the timescales and rates of hydration of oceanic lithosphere by examining isotopic profiles throughout rodingite dikes and across rodingite-serpentinite contacts. I am investigating a suite of rodingite dikes from Apennines ophiolites that were exhumed prior to slab subduction. The Apennines ophiolites, exposed in northern Italy, represent unsubducted oceanic lithosphere from the Liguro-Piemont domain and are mainly composed of serpentinized peridotite. Samples collected are therefore reflective of seafloor environment conditions of the Tethys ocean and are ideal for studying fluid uptake by oceanic lithosphere as they have not been introduced to a subduction zone setting. Objectives include determining the age and timescale of fluid infiltration that formed rodingite dikes and associated serpentinites as well as assessing fluid source and history.

The objectives for this study will be addressed through Sr isotope collection, ICPMS trace element data, U/Pb geochronology, and SEM and petrologic characterization. Two rodingite-serpentinite samples from the northern Apennines were analyzed over the course of this study. One was collected by myself in the Fall of 2021 while the other was previously collected in 2019. Field work was completed with assistance from collaborators Marco Scambelluri and Donato Belmonte from the University of Genoa. Samples were processed and analyzed for Sr isotope compositions and concentrations via TIMS at the Boston College Center for Isotope Geochemistry with assistance and training from Paul Starr and Steph Walker. Whole rock samples were analyzed for trace element compositions with an LA-ICPMS at the Center for Elemental Mass Spectrometry at the University of South Carolina with assistance from Besim Dragovic. To address the absolute timing of rodingite formation, we performed garnet U/Pb geochronology utilizing MC-LA-ICPMS courtesy of Horst Marschall and Leo Millonig at the University of Frankfurt. Thin sections were analyzed at Boston College with the assistance of Paul Starr and Seth Kruckenberg using a SEM. The results of this study will consist of a paper published in Chemical Geology, presented in chapter one of this thesis.

CHAPTER 1

1. Introduction

Hydration of oceanic lithosphere through serpentinization involves a critical transfer of water from the hydrosphere to the lithosphere as seawater interacts with oceanic lithosphere. At 10 wt% H_2O, serpentinites are a major reservoir of rock-bound water that contribute to the global geo-cycling of water (Ulmer and Trommsdorff, 1995; Scambelluri et al., 1995). Water and fluid mobile elements are then transported to subduction zones along the conveyer belt created by seafloor spreading (Guillot & Hattori, 2013; Deschamps et al., 2011). Within subduction zones serpentinites are critically influential to a wide array of processes, including earthquake genesis (Kerrick and Connolly, 2001; Hacker et al., 2003; Husen et al., 2003), arc magmatism (e.g. Schmidt and Poli, 1998; Tatsumi and Kogiso, 2003), exhumation (Hermann et al., 2000), and the global cycling of volatiles (e.g. Scambelluri et al., 1997; Rüpke et al., 2004), including mantle refertilization (Alt et al., 2012).

Serpentinites develop from the hydrothermal alteration of mantle peridotite associated with the infiltration of seawater into oceanic lithosphere. The mechanism of seawater-rock interaction varies considerably between fast and slow-spreading ridges, but large volumes of water are universally circulated through oceanic lithosphere, both on and off the mid-ocean ridge (MOR) axis. Fluid movement at slow-spreading centers is dominated by infiltration along tectonic fractures, where serpentinization is assisted by the exposure of mantle peridotite through crustal thinning (Seyfried et al., 2007). These circulating fluids are responsible for the alteration of rock through large mass transfers of elements, mainly the removal of Ca and Al and enrichment of Fe and Mg, where the degree of serpentinization is reliant on the availability of H_2O and its ability to penetrate the bedrock (Evans et al., 2013; Seyfried et al., 2007). Mineralogically, serpentinite

development is marked by the alteration of Mg-rich olivine and pyroxene to sheet silicate, serpentine minerals. A generalized serpentinization reaction is described as:

MgFe Olivine + H_2O → Serpentine + Magnetite + Brucite + H_2 (1)

However, petrographic and chemical analyses indicate that serpentinization is a multistage process marked by an initial stage of low fluid flux that produces Fe-serpentine and Fe-brucite, followed by magnetite formation (Bach et al., 2006; Seyfried et al., 2007). The increase in fluid flux responsible for reaction progress enhances Mg-Fe and Mg-Ca exchange, causing Fe-bearing phases to be replaced with Mg-dominated serpentine, brucite, and magnetite (Seyfried et al., 2007).

Rodingitization involves the infiltration of fluids, altered from serpentinization reactions, that facilitate a diffusional mass transfer between peridotite and gabbro, driven by a chemical potential difference present across the mafic-ultramafic contact. These rodingitizing pore fluids were altered from serpentinization and are characterized by high Ca, low Mg, high pH, high fH_2, and low $aSiO_2$ and produce Ca-rich, SiO_2-poor rodingites (Evans et al., 2013). Rodingitization produces a Ca enrichment and SiO_2 depletion within the gabbro, where the enrichment in Ca is a consequence of both the breakdown of Na-Ca plagioclase within the gabbro alongside the removal of Na from the system, as well as the addition of Ca sourced from the breakdown of pyroxene in the adjacent serpentinite. The Ca-rich phases present in rodingites are stable in low silica environments and are primarily diopside, grossular, and andradite, which are observed along with chlorite, prehnite, epidote, zeolite, and vesuvianite. Rodingitization proceeds at

temperatures between 200-300˚ C at a pressure of 50 MPa and does not proceed above 400˚ C (Bach & Klein, 2009).

This study seeks to investigate how rodingitization can elucidate the processes and timescale of hydration of the oceanic lithosphere. Seafloor rodingites, chemically and mineralogically distinct from surrounding serpentinites, inform on sources, chemistry, and duration of infiltrating fluids associated with serpentinization.

2. Geologic Background

Ophiolites provide accessibility to the study of oceanic lithosphere, especially lower crust and upper mantle environments. This study examines unmetamorphosed, seafloor rodingites exposed in ophiolites of the Internal Ligurides within the Apennines orogenic belt (Fig. 1). Examined rodingites originated from the sea floor of the Liguro-Piemont domain within the Alpine-Tethys ocean basin that formed in the Jurassic from the separation of Eurasia from the Adriatic promontory of the African plate. The Liguro-Piemont domain was a narrow, embryonic ocean basin with a broad ocean-continent transition that opened ~170 Ma and was active for 50 Ma (Agard, 2021). Spreading within the Liguro-Piemont domain is comparable to modern slow and ultra-slow spreading ridges; extension was mainly accommodated by faulting rather than extensive magmatism with spreading rates of <2 cm/yr (Agard & Handy, 2021). Ultra-slow extension was accompanied by the exhumation of considerable mantle peridotite via detachment faults.

Mantle peridotite underlying the Alpine Tethys, exposed to seawater during spreading, was heterogeneous; Alpine-Apennine ophiolites originate from either subcontinental lithosphere or an intra-oceanic domain. Within the Internal Ligurides, mantle peridotite was likely from a

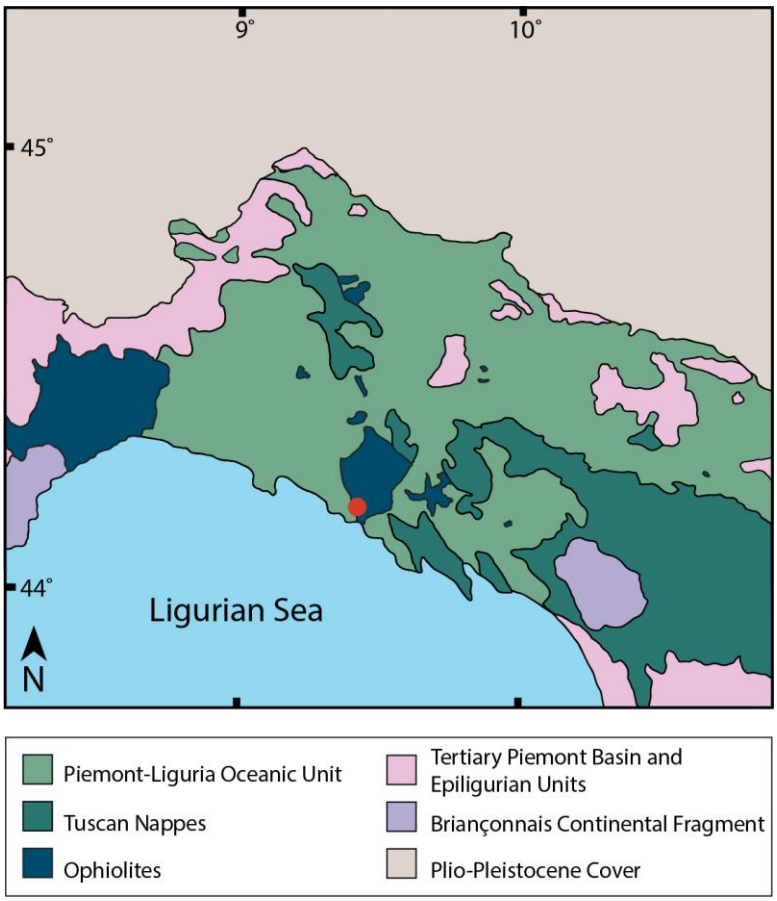

Figure 1. Simplified geological map of the Apennines and Western Alps, depicting the locations of ophiolites of the Internal Ligurides (after Schmid et al., 2004). Bargone and Pavareto outcrops are within the area marked by the red dot.

depleted, oceanic source that was modified by several melt-migration events, culminating in peridotite with variable trace element and isotopic signatures (Rampone & Sanfilippo, 2021). Exposure of this peridotite to seawater resulted in widespread serpentinization characterized by multiple stages of fluid-rock interaction (Schwarzenbach et al., 2021). Basement of the Liguro-Piemont domain consisted of discrete gabbroic bodies intruded into serpentinites as oceanic core complexes (OCCs) and dikes near the MOR axis. The age of gabbro intrusions in the Internal Ligurides was dated with zircon U-Pb geochronology as 163.0 ± 0.5 to 161.2 ± 0.9 Ma (Tribuzio et al., 2016).

The northern Apennines represents a unique junction of Alpine and Apennine orogens marked by a polyphase deformation history. The Apennines is a NW/SE oriented fold and thrust belt related to the westward collision of the Adriatic and European plates. The convergence of

the Adriatic and European plates created a complex collisional environment, characterized by a diachronous subduction zone that evolved from eastward Alpine subduction to westward Apennine subduction during the Late Eocene-Oligocene (Marroni et al., 2010; Molli & Malavieille, 2011). The Ligurides are a series of Jurassic mafic and ultramafic units and their overlying sedimentary cover that represent the top of the Apennines nappe stack (Marroni & Pandolfi, 1996). Ophiolites of both the Internal and External Ligurides represent oceanic lithosphere of the Liguro-Piemont oceanic domain accreted onto the continental margin. However, the Internal Ligurides represent a continuous ophiolite sequence, whereas the External Ligurides are regarded as isolated blocks within a sedimentary melange.

3. Field and Petrographic Observations

3.1 Field Description

Rodingites were obtained from ophiolite units within the Internal Ligurides. Samples were collected from riverbeds near the town of Pavareto (PAV-2D) located at 44.27496˚, 9.58931˚ by Paul Starr and Ethan Baxter, and from road cuts near the town of Bargone (21LAP-2C, 21LAP-2D, 21LAP-2E, 21LAP-2F, and 21LAP-2H) located at 44.29742˚, 9.47711˚ by Charlotte Lorthioir and Marco Scambelluri. Rodingites are present as dikes and boudins and were easily distinguished in the field by their chalky white color (Fig. 2a,b). Some size variation was observed across field sites, where rodingite thickness was observed between 80 and 10 cm. Chlorite rims were occasionally observed at the contact between serpentinite and the rodingite dike, most notably at Bargone where a 2.5 cm chlorite margin was observed at the lower contact (LC). Texture varies by outcrop, between massive and moderately foliated. Bargone rodingite displays alternating bands of white hydro-garnet and pale green chlorite intermixed with slightly

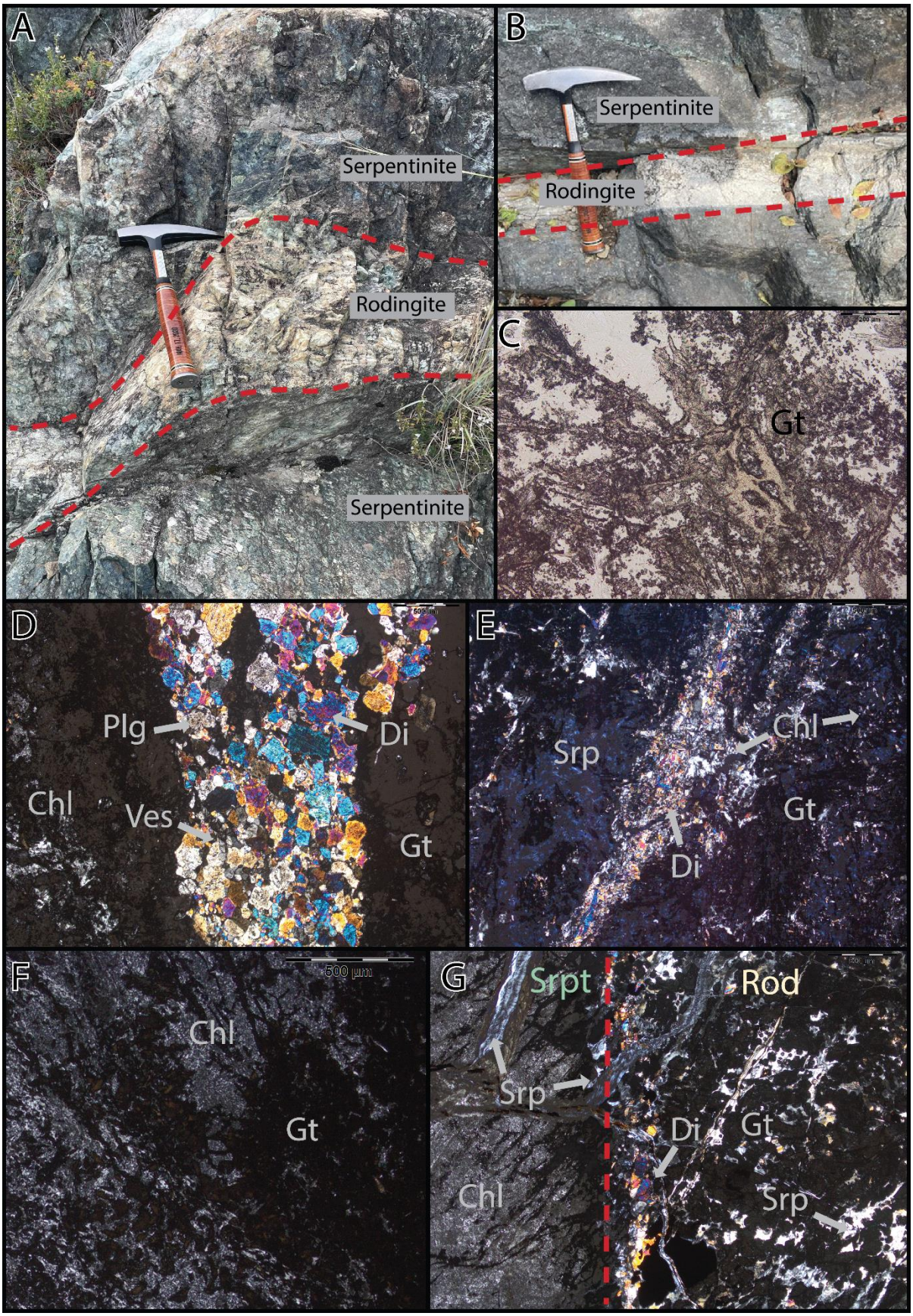
A
Serpentinite
Rodingite
Serpentinite
B
Serpentinite
Rodingite
C
Gt
D
Plg
Di
Chl
Ves
Gt
E
Chl
Srp
Gt
Di
F
500 µm
Chl
Gt
G
Srpt
Rod
Srp
Di
Gt
Chl
Srp

Figure 2. Field and microscope images of Apennines rodingites. A) Field photo of rodingite dikes within serpentinite at the Bargone outcrop where 21LAP-2C, D, E, F, and H were collected. B) Field photo of rodingite dike within serpentinite at Pavareto where PAV-2D was collected. C) Thin section photo of Pavareto garnets in plane-polarized light in thin section PAV-2D.2. D) Thin section photo of Bargone rodingite showing a vein of diopside + plagioclase + vesuvianite within a garnet and chlorite matrix in thin section 21LAP-2C-2. E) Thin section photo of a diopside + chlorite vein hosted within a garnet + serpentine + chlorite matrix in this section PAV-2D.2. F) Thin section photo of Bargone bulk rodingite matrix, mainly composed of chlorite and garnet in this section 21LAP-2C-1. G) 21LAP-2Dc thin section photo of the upper contact of the Bargone transect, with the lithologic boundary marked in red. The serpentinite (srpt) displays a serpentine and chlorite mineralogy. At the contact, the rodingite (rod) displays a garnet + diopside + serpentine mineralogy, where the majority of diopside has precipitated at the contact. Veins of serpentine are observed cross-cutting the contact, dissipating into the rodingite.

darker, gray bands of hydrothermal diopside parallel to contacts. Adjacent serpentinite is dark green to black and displays tectonic cleavage. Samples from the Pavareto outcrop do not exhibit foliation. Unaltered gabbro units within the Internal Ligurides display coarse-grained, pegmatitic textures, where the main mineral phases are pyroxene and plagioclase with minor olivine.

3.2 Mineral and Petrographic Description

Mineral identifications of Bargone samples are based on petrographic analyses, while mineral identifications of Pavareto samples are based on both petrographic and SEM analyses. Rodingite samples from Pavareto and Bargone are predominantly characterized by a hydro-garnet, diopside, and chlorite mineralogy and display similar textural characteristics. Garnets are fine-grained and chalky in hand sample, brown to black in thin section, and when present as distinct crystals display some birefringence, confirming their high water contents. Diopside is present as either hydrothermal precipitations or pseudomorphs of igneous pyroxene. Hydrothermally precipitated diopside is anhedral, fine-grained, and rarely displays distinct cleavage. Psuedomorphed pyroxenes are coarse-grained and display well-defined cleavage often accompanied by fine-grained precipitations of garnet. These large phenocrysts often show alteration to chlorite as well as evidence of deformation, including kink bands and orthogonal fractures. Chlorite and serpentine are present as fibrous matrix intergrowths, although serpentine

is also commonly seen within veins intruding into the rodingite from adjacent serpentinite. Fine-grained magnetite is present and commonly observed alongside serpentine.

3.2.1 Bargone Outcrop

Bargone rodingites are composed of garnet + diopside + chlorite + vesuvianite + plagioclase + serpentine + magnetite, where garnet and chlorite make up the bulk of the matrix (Fig. 2f) and diopside is present as both igneous pseudomorphs and hydrothermal precipitations. Garnets are predominantly a clear brown, but do display some of the murky coloring that was abundant at the Pavareto outcrop. Bargone garnets are also present as distinct phenocrysts and account for a larger modal portion of the groundmass than at Pavareto. Chlorite is less abundant by modal proportion than in Pavareto, but is still present in both fine-grained matrix growth and within contact-parallel veins. Serpentine is observed in the rodingite only near the upper contact (UC) (Fig. 2g). Contact-parallel veins of diopside + plagioclase + vesuvianite are thicker, yet less interconnected than Pavareto veins and are often centered around hydrothermally psuedomorphed igneous grains (Fig. 2d). Similar to Pavareto, these veins become more well-established away from rodingite boundaries and contact-perpendicular serpentine veins are present at the UC (Fig. 2g). Serpentinite above the UC displays massive fine-grained texture of serpentine and pseudomorphed chlorite (Fig. 2g). Beneath the LC, pyroxene grains are present as pseudo morphs of the primary mantle mineralogy, whereas olivine and plagioclase were completely replaced.

3.2.2 Pavareto Outcrop

Pavareto rodingite consists of garnet + diopside + chlorite + titanite + serpentine + magnetite, where garnet, chlorite, and serpentine are present as fine-grained matrix intergrowths. Garnet is dark brown and displays disseminated, patchy growth (Fig. 2c). Pale brown diopside is present as igneous pseudomorphs with well-defined cleavage or as secondary metasomatic products. Both psuedomorphed and hydrothermally precipitated diopside are commonly observed with chlorite overgrowths. Diopside is also present alongside chlorite in large-scale, contact-parallel vein networks that appear to crosscut garnet and serpentine matrix growth (Fig. 2e). These diopside + chlorite veins become more established deeper into the rodingite and are not present near the contact. Instead, the Pavareto rodingite-serpentinite contact is dominated by contact-perpendicular veins of serpentine that originate from the serpentinite and ultimately merge with the rodingite matrix. Magnetite is observed in association with serpentine veins and with fibrous serpentine growth within the rodingite. Hydrothermal titanite is also observed, likely the product of the highly alkaline rodingitization fluids that are capable of mobilizing Ti^{4+} (Barriga & Fyfe, 1983). Within serpentinite, olivine is completely replaced with ribbon-textured serpentine and magnetite.

4. Methods

4.1 Sr Isotopic Analysis

Five samples from Bargone comprising a complete rodingite dike and adjacent serpentinite, as well as one sample from Pavareto of a serpentinite-rodingite contact, were processed into wafers using a micro-saw. The location of each wafer was carefully documented, taking into account the kerf of the saw. Wafers were on average cut 1 mm thick, except in the

interior of the Bargone rodingite where wafers were cut 5 mm thick. Forty-one wafers from Bargone were analyzed for $^{87}Sr/^{86}Sr$ and Sr concentrations and 26 wafers from Pavareto were analyzed for $^{87}Sr/^{86}Sr$ ratios to create a representative isotopic profile along the serpentinite-rodingite-serpentinite transect and serpentinite-rodingite contact respectively. Isotopic profiles were then compared to major Sr reservoirs to assess fluid history. A gabbro sample (Apen-1) and an alternate serpentinite sample (Apen-2) from the Internal Ligurides were analyzed as well for comparison. Whole rock samples were crushed using a tungsten carbide hammer and agate mortar and pestle into powders that were dissolved over three stages of HF, HNO_3, and Aqua Regia. Depending on available concentration data, between 50-100 mg of dissolved sample was then aliquoted and spiked with a well-calibrated ^{84}Sr tracer. Sr was then isolated using a Sr-Spec resin in column chemistry and brought up in 2N HNO_3 in preparation for TIMS analysis using methods established by the Center for Isotope Geochemistry staff. Samples were loaded onto Re-outgassed filaments with TaF and analyzed on an IsotopX Phoenix TIMS at the Boston College Center for Isotope Geochemistry. SRM 987 standards were analyzed at the beginning and end of each session, yielding an average $^{87}Sr/^{86}Sr$ value of 0.710246 ± 0.000017 (2SD) during the duration of analysis for this study.

4.2 Whole Rock Trace Element Compositions

Trace element concentrations were analyzed in 38 Bargone whole rock samples and 20 Pavareto whole rock samples at the Center for Elemental Mass Spectrometry at the School of Earth, Ocean and Environment, University of South Carolina. About 10 mg of sample was aliquoted and dissolved in 2% HNO_3 for analysis on a Thermo-Fisher Scientific Element 2, HR-ICP-MS, where a combination of low-, medium-, and high-resolution modes were used to

resolve $ArOH^+$ on $^{57}Fe^+$ isobaric interferences. USGS reference material BHVO-2 (Jochum et al., 2016) was used as an external standard for this analysis. Dating processing was performed in-house at the University of South Carolina, where drift was corrected via a linear fit established from analyzing standards every 10 bulk rock analyses. The precision of all ICP-MS trace element analyses was calculated to be less than 5%.

4.3 Garnet Geochronology

In situ U-Pb geochronology was conducted on two polished thin sections of rodingite samples from the Pavareto outcrop, where multiple laser analyses were taken across a series of rodingite garnets, assumed to all be the same age. Rodingite thin sections were analyzed at the Frankfurt Isotope and Element Research Center at the Goethe University Frankfurt with a Thermo-Finnegan Element 2 ICP-MS combined with a Resonetics RESOLution-LR 193 nm ArF Excimer laser using the methods described in Millonig et al. (2020).

4.4 Petrographic Analyses

Petrographic analysis of all thin sections was conducted to mineralogically characterize rodingites and to provide insight into the extent of hydrothermal alteration. Additionally, rodingite thin sections PAV-2D.1 and PAV-2D.2 from the Pavareto outcrop were analyzed with Tescan Mira 3 Schottky Field Emission SEM at the Department of Earth and Environmental Sciences at Boston College following the methods of Kruckenberg et al. (2019). Backscattered electron maps and mineral chemical characterizations were acquired for two rodingite samples and were significant for identifying garnet grains for in situ U-Pb geochronology.

5. Data

5.1 Whole Rock Chemistry

Whole rock isotopic and trace element analyses are reported in Table 1. Both Pavareto and Bargone rodingite samples are Si-poor and Ca-rich. Both rodingites display high CaO and Al_2O_3 contents, along with lower MgO, Ni, and Cr concentrations, compared to their adjacent serpentinite, where the greatest discrepancies are observed within the interior of the Bargone rodingite dike (Figs. 4 b,d & 5 b,d). This is in agreement with a gabbro protolith and rodingite mineralogy. Variations in isotopic and trace element data are observed within the rodingite analyses, both throughout the interior and at the contacts. Within rodingites, $^{87}Sr/^{86}Sr$ values range between 0.704227–0.707444 at Bargone (Fig. 4a) and 0.705021–0.707771 at Pavareto (Fig. 5a). Bargone serpentinite $^{87}Sr/^{86}Sr$ values are more radiogenic, with a range of 0.706599–0.709036, while at Pavareto, Sr ratios of 0.706861–0.707588 are clustered near seawater values. Within the rodingite dikes, localized zones of similar chemistry, illustrated with pink bands in Figures 4 and 5, are characterized by peaks in $^{87}Sr/^{86}Sr$ that approach seawater values and depletions in LILEs, REEs, Ni, Cr, Sc, and Zr. The primary gabbro, assumed to be representative of the rodingite protolith, gives an $^{87}Sr/^{86}Sr$ value of 0.703397. The alternate serpentinite sample, collected in the vicinity of the Pavareto outcrop, but beyond the range of the rodingite dikes, has an $^{87}Sr/^{86}Sr$ value of 0.705158. Bulk rock REE patterns of both rodingites and serpentinites are characterized by low LREE concentrations and greater HREE enrichments with positive Eu anomalies (Fig. 3). Serpentinite REE concentrations tend to be lower than rodingites and display nearly flat trends. Sr, Cs, Ni, Sc, and Cr were normalized to Th and Zr (Figs. 4 & 5) to assess enrichment and depletion trends. Th was employed over other immobile elements, such as Zr or

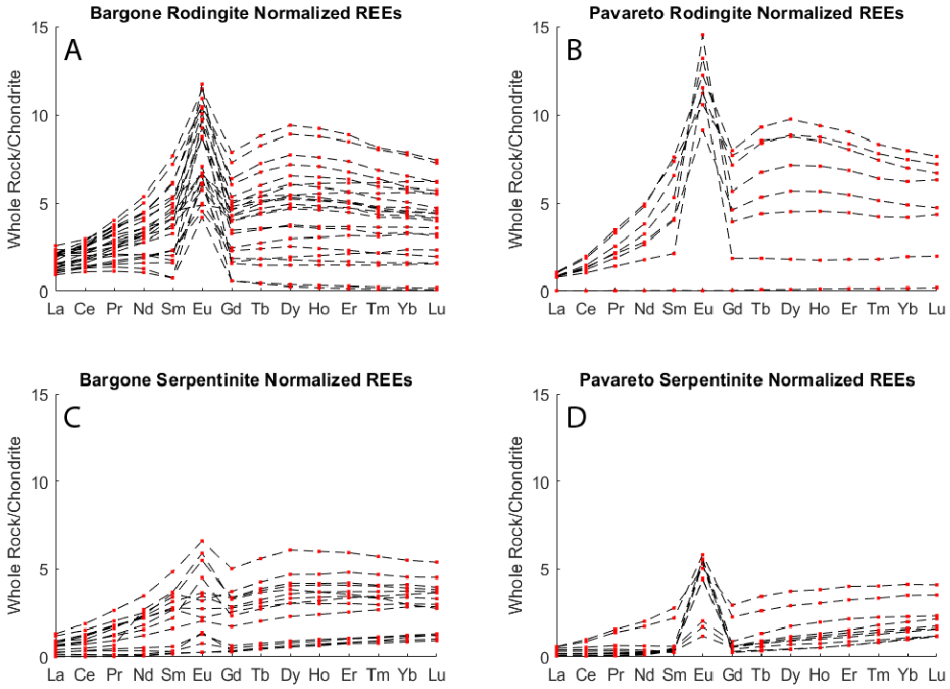

Figure 3. Chondrite-normalized REE diagrams of rodingites and serpentinites from both the Bargone and Pavareto outcrops (normalizing values after McDonough & Sun, 1995). A) Bargone rodingites show weak LREE enrichments compared to MREEs and HREEs, with strong Eu anomalies. B) Pavareto rodingites show weak LREE enrichments and stronger enrichments in MREEs and HREEs, similar to Bargone, but with a larger Eu anomaly. C) Bargone serpentinites display near-flat REE trends with slight HREE enrichment and mild positive Eu anomalies, although anomalies in some samples are negative or absent. D) Pavareto serpentinites display the lowest REE values, with particularly low LREE concentrations and only slightly higher HREE concentrations. Positive Eu anomalies are present, but slight.

TiO_2, as it displayed the least variability within the transects, especially within the serpentinite sections. Zr and TiO_2 do not display typical immobile behavior.

5.1.1 Bargone Isotopic and Trace Element Analyses

Relevant whole rock analyses of the investigated rodingite-serpentinite transect are illustrated in Figure 4. Ca concentrations peak in the interior of the rodingite, a trend potentially related to calcic garnet growth (Fig. 4b). REE and HFSE (Zr, Hf, Nb, Ta, Ti) concentrations are higher than surrounding serpentinites and are not homogenized. LILE concentrations are consistent across the rodingite dike and the lower serpentinite section, but rise considerably in

Bargone

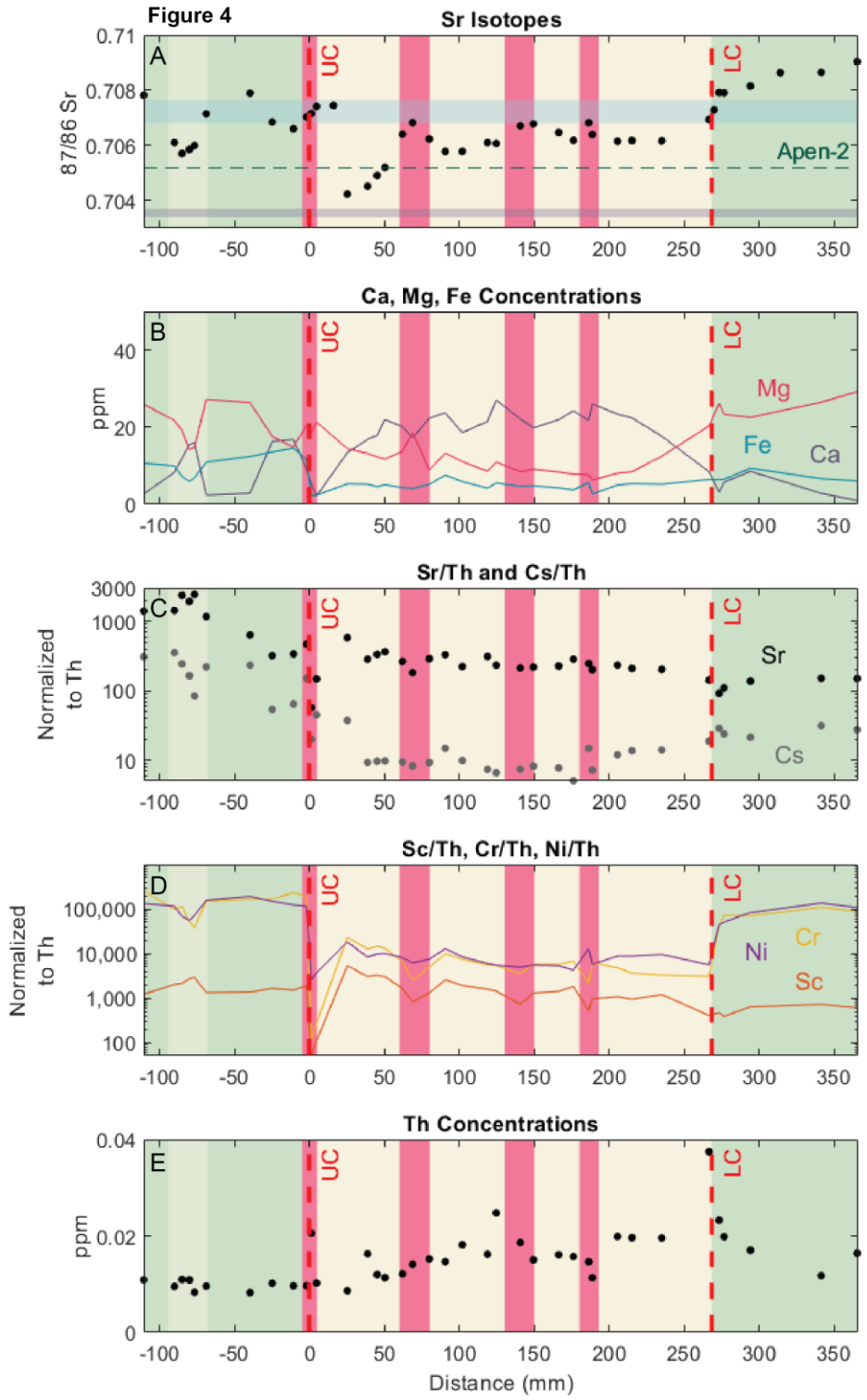
Figure 4
Sr Isotopes
A
UC
LC
87/86 Sr
0.71
0.708
0.706
0.704
Apen-2
Ca, Mg, Fe Concentrations
B
ppm
40
20
0
Mg
Fe
Ca
Sr/Th and Cs/Th
C
Normalized to Th
3000
1000
100
10
Sr
Cs
Sc/Th, Cr/Th, Ni/Th
D
100,000
10,000
1,000
100
Ni
Cr
Sc
Th Concentrations
E
0.04
0.02
0
-100
-50
0
50
100
150
200
250
300
350
Distance (mm)

Bargone

Figure 4 cont.

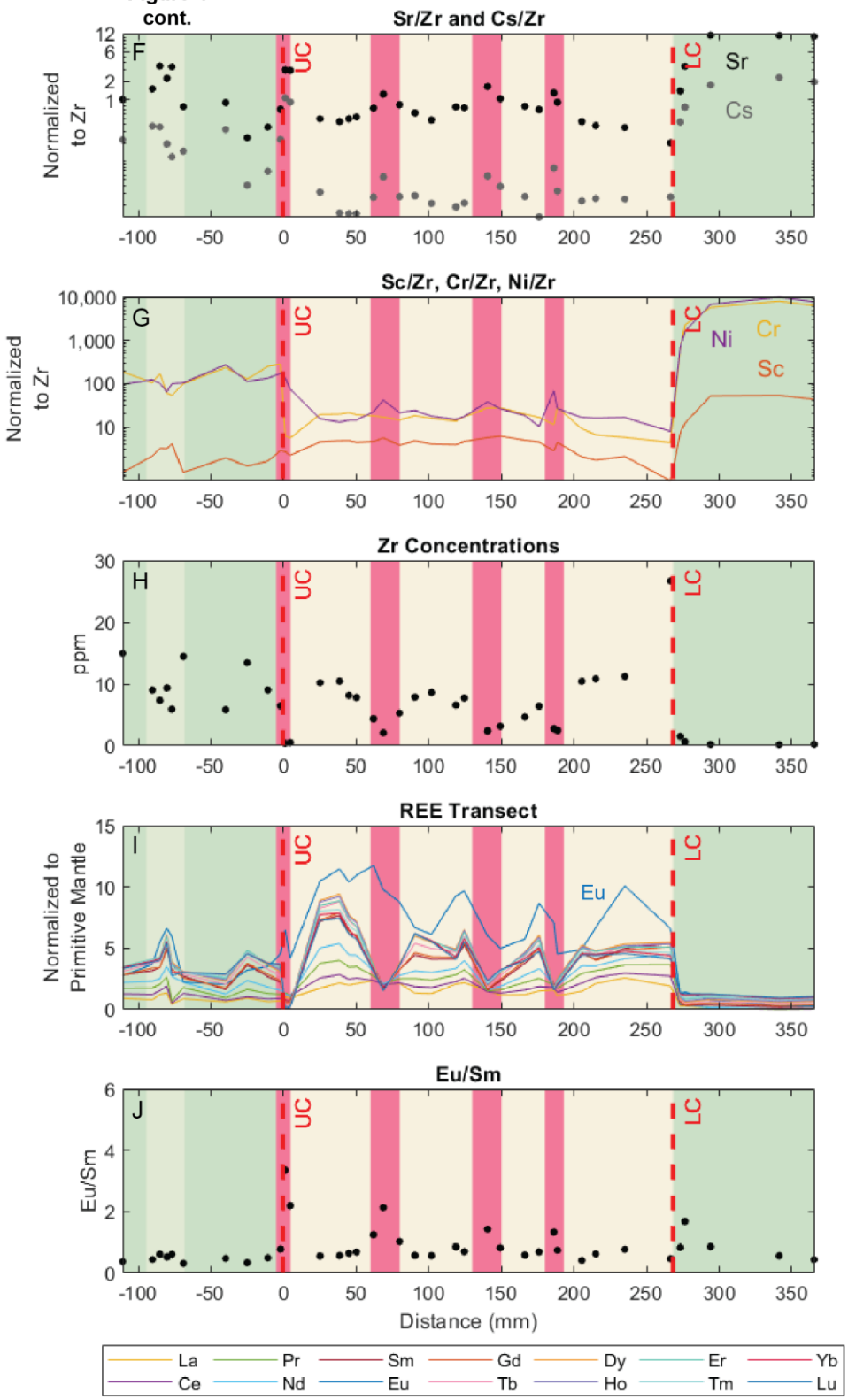

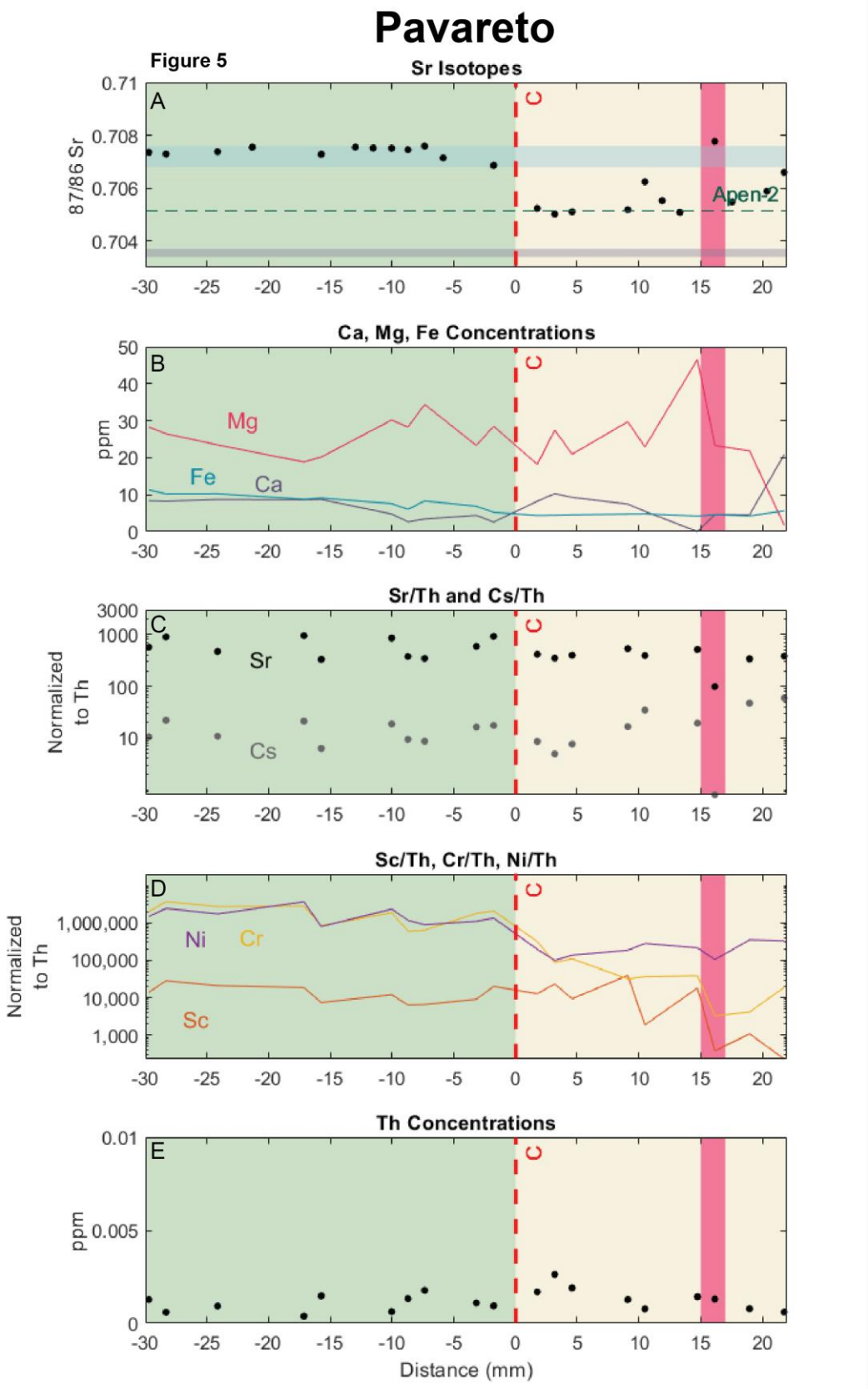
Pavareto
Figure 5
Sr Isotopes
A
87/86 Sr
0.71
0.708
0.706
0.704
C
Apen-2
Ca, Mg, Fe Concentrations
B
ppm
50
40
30
20
10
0
Mg
Fe
Ca
Sr/Th and Cs/Th
C
Normalized to Th
3000
1000
100
10
Sr
Cs
Sc/Th, Cr/Th, Ni/Th
D
Normalized to Th
1,000,000
100,000
10,000
1,000
Ni
Cr
Sc
Th Concentrations
E
ppm
0.01
0.005
0
-30 -25 -20 -15 -10 -5 0 5 10 15 20
Distance (mm)

Pavareto

Figure 5 cont.

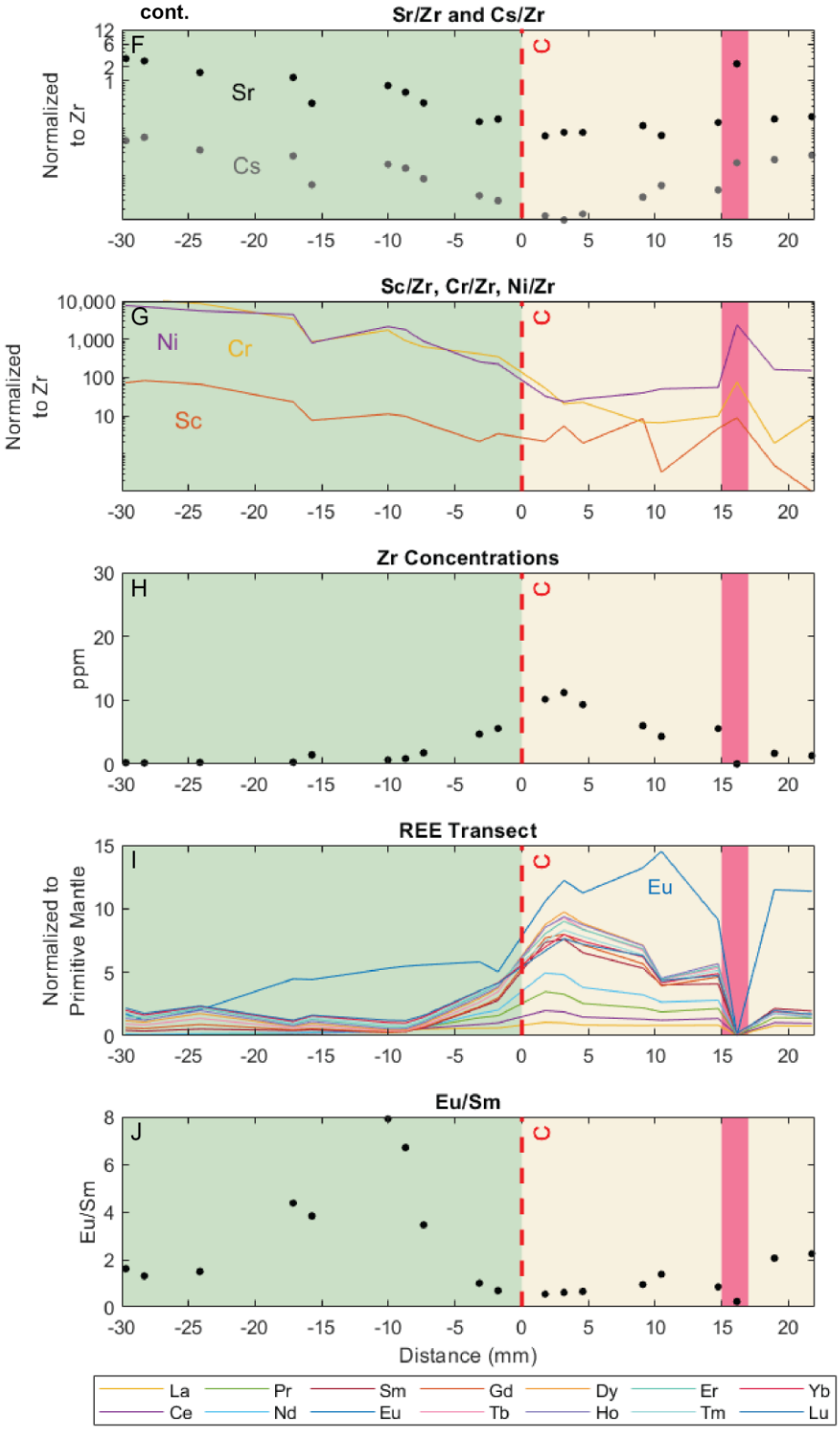

Figure 4. Isotopic and trace elements plotted against the location of samples within the Bargone rodingite transect, where UC denotes the upper contact at 0.0 mm and LC denotes the lower contact at 268.2 mm. A) $^{87}Sr/^{86}Sr$ ratios of rodingite and adjacent serpentinites. Rodingites (beige) display values between their gabbro protoliths (gray) and Jurassic-Cretaceous seawater (blue), with peaks present in advective zones (pink). Serpentinites (green) display radiogenic Sr ratios greater than that of seawater, while serpentinites above the UC display some variability. The Apen-2 serpentinite sample (green dashed line) displays a value of 0.705158. Error bars are smaller than plotted markers. B) Concentrations of Ca, Mg, and Fe. Ca concentrations are the greatest within the center of the rodingite, while Mg concentrations are the greatest within the serpentinites. Fe concentrations are relatively flat across the transect. C) Transect of Sr and Cs normalized to Th. Both Sr and Cs are relatively flat throughout the rodingite and below the LC, while dipping within most advective zones. However, both trend up towards the UC and into the upper serpentinites. Within the rodingite veinlet (pale beige) Sr enrichment peaks, while Cs dips. D) Sc, Cr, and Ni normalized to Th. Sc, Cr, and Ni display flat trends throughout the rodingite and serpentinite sections, but dip within advective zones, suggesting mobility. E) Th concentrations, where Th displays relatively flat behavior. F) Transect of Sr and Cs normalized to Zr, showing significant peaks within pink advective zones. G) Sc, Cr, and Ni normalized to Zr, where values peak slightly within pink advective zones. H) Zr concentrations, where values dip significantly within advective zones. I) REE transect shows enrichment within rodingites and the upper serpentinites, while lower serpentinites are fairly depleted. Advective zones display significant REE depletions, except for Eu. Values normalized after McDonough and Sun (1995). J) Eu/Sm transect; values peak within the advective zones implying the presence of plagioclase and reducing fluids.

Figure 5. Isotopic and trace elements plotted against the location of samples within the Pavareto rodingite transect, where C denotes the contact at 0.0 mm. A) $^{87}Sr/^{86}Sr$ ratios of rodingite vary between primary gabbro and seawater values, except within the pink advective zone where it peaks at 0.707771, suggesting crustal input of fluids. $^{87}Sr/^{86}Sr$ ratios of serpentinites are observed within or slightly above seawater values. A smaller peak is observed at 10.5 mm. The Apen-2 serpentinite sample (green dashed line) displays a value of 0.705158, lower than that of transect serpentinites. Error bars are smaller than plotted markers. B) Concentrations of Ca, Mg, and Fe. Ca and Fe are fairly flat throughout the transect, while Mg displays the most variability. C) Sr and Cs normalized to Th, where Sr/Th and Cs/Th values are relatively consistent across the lithologic contact but dip within the pink advective zone. D) Sc, Cr, and Ni normalized to Th, where serpentinite values surpass rodingites' and dips are observed within the advective zone. E) Th concentrations, which present a flat trend across the transect. F) Sr and Cs normalized to Zr. Values slightly decrease in the serpentinite towards the contact and are consistent within the rodingite, but peak in the advective zone. G) Sc, Cr, and Ni normalized to Zr, where values steadily decrease from the serpentinite into the rodingite, but peak in the advective zone. H) Zr concentrations, which peak within the rodingite just beyond the contact and dip within the advective zone. I) REE transect that shows rodingites are enriched in REEs compared to serpentinites, except within the advective zone which displays significant depletion. A smaller dip is observed at 10.5 mm. Values normalized after McDonough and Sun (1995). J) Eu/Sm transect that displays a peak within the serpentinite section, while values dip within the advective zone.

the upper serpentinite section. Within the rodingite dike, there are localized zones of similar chemistry illustrated with pink bands in Figure 4, marked by $^{87}Sr/^{86}Sr$ values that approach Jurassic-Cretaceous seawater, depletions of LILEs, REES excluding Eu, Ni, Cr, Sc, and Zr, as well as high values of Eu/Sm. Within the Bargone transect there is also a distinction between the upper and lower serpentinite sections, where upper serpentinites chemically more resemble

rodingite. Upper serpentinites are considerably more enriched in HFSE, LILE, REEs, and Zr compared to the fairly depleted serpentinites below the LC. Lower serpentinites also display values of $^{87}Sr/^{86}Sr$ that exceed the range of Jurassic-Cretaceous seawater, while upper serpentinites display variation between 0.706599-0.707892 (Fig. 4a). A small rodingite veinlet is present within the upper serpentinite section and displays trace element and isotopic values similar to that of the majority of the rodingite transect.

5.1.2 Pavareto Isotopic and Trace Element Analyses

Analyses of the Pavareto rodingite-serpentinite transect encompass a narrower range focused on the contact, as shown in Figure 5. At this scale, there are only slight deviations in CaO, Al_2O_3, and MgO concentrations between the serpentinite and rodingite sections (Fig. 5b). Similar to Bargone, REE and Zr concentrations are higher within the rodingite, while rodingites also display lower Ni, Cr, Sc, and Fe_2O_3 concentrations. LILE concentrations display flat trends within the serpentinite and rodingite. One zone of alternate chemistry comparable to those at Bargone, designated in pink, is observed within the rodingite. This zone is characterized by $^{87}Sr/^{86}Sr$ values more radiogenic than Jurassic-Cretaceous seawater, depletions in LILEs, REEs including Eu, Cr, Ni, and Sc, low Eu/Sm values, and a slight dip in Zr concentrations (Fig. 5). An additional mild peak in $^{87}Sr/^{86}Sr$ and slight dip in REEs is observed at 10.5 mm, but chemical deviations are not significant enough to classify this as a zone of alternate chemistry analogous to those previously identified. Serpentinites show $^{87}Sr/^{86}Sr$ values within and slightly above the range of seawater, high concentrations of Cr, Ni, and Sc, and low REE concentrations.

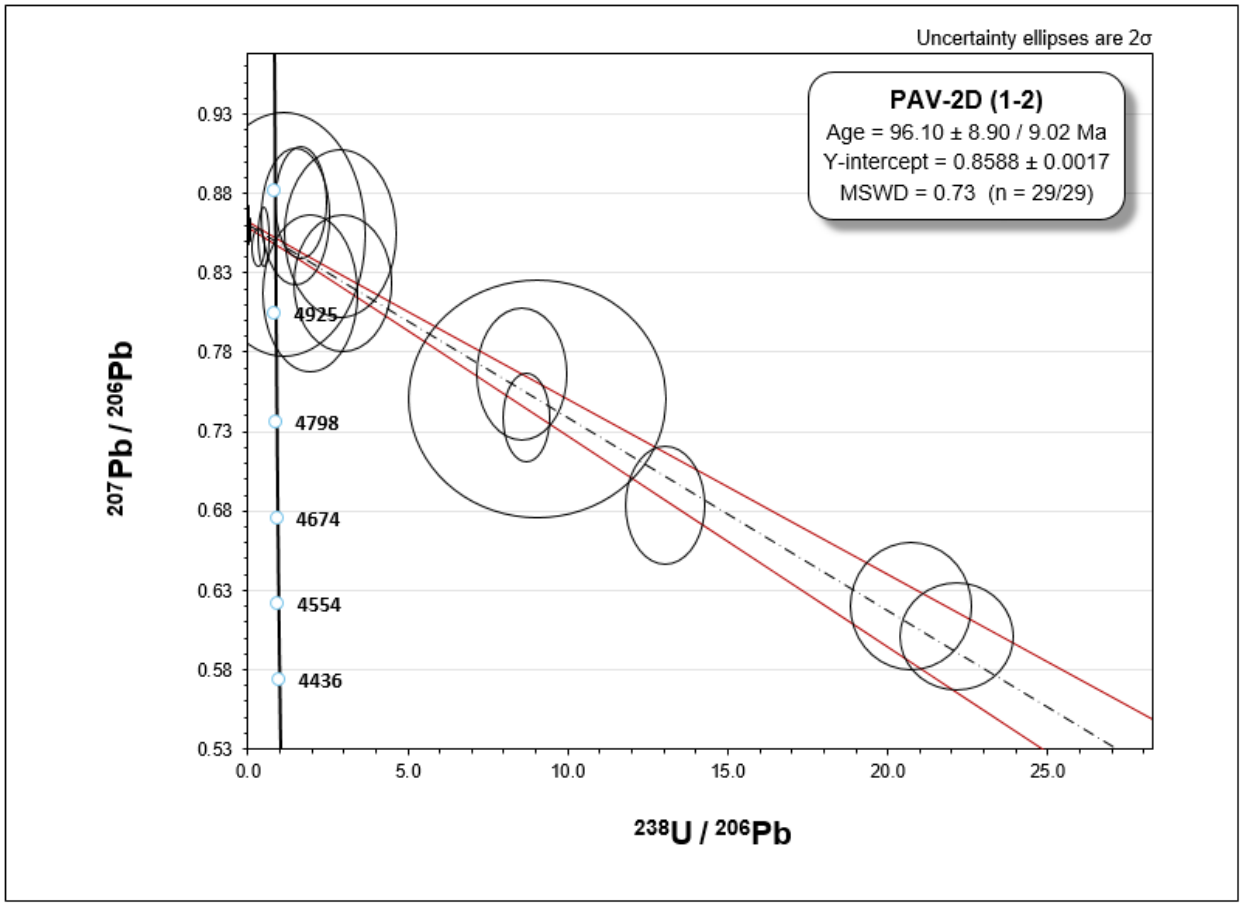

Figure 6. Isochron of U-Pb data from Apennines rodingite garnets plotted on a Terra-Wasserburg diagram, showing an age of 96.10 ± 8.90 Ma with an MSWD of 0.73. Garnets sampled from PAV-2D.1.

5.2 Garnet Geochronology

U-Pb data from Pavareto rodingite garnets plotted on a Tera-Wasserburg diagram presents an age of 96.10 ± 8.90 Ma with an MSWD of 0.73 (Fig. 6). U-Pb geochronology was utilized as preliminary attempts to date Apennines rodingites with Sm-Nd failed due to low $^{147}Sm/^{144}Nd$ ratios (Haws et al., 2021). Additional attempts to date Bargone rodingite garnets were unsuccessful due to low U concentrations for samples 21LAP-2C-2, 21LAP-2C-3, 21LAP-2Dc, and PAV-2D.2 (Table 2).

6. Discussion

Sr isotope signatures and trace element data of serpentinite-rodingite transects suggest oceanic lithosphere of the Liguro-Piemont domain experienced a multi-stage hydrothermal alteration history. The chemical signatures of serpentinite-rodingite transects can be ascribed to at least four stages, illustrated in Figure 7: (1) Widespread serpentinization of peridotite, (2) Intrusion of gabbro dikes along zones of weakness, (3) Rodingitization of gabbro from post-serpentinization fluids, (4) Localized, late-stage alteration of rodingites by seawater-like fluids. The garnet U-Pb age of 96.10 ± 8.90 either represents the age of initial rodingitization or late-stage advective alteration. Below I discuss each of these stages in greater detail.

6.1 Widespread serpentinization

Serpentinization was initiated early on in the development of the Alpine Tethys when mantle peridotite was exhumed along detachment faults at the ridge axis (Fig. 7a). Field relationships indicate that mantle peridotite had been serpentinized before gabbros intruded, (Desmurs et al., 2001; Schaltegger et al., 2002), confirming serpentinization occurred at the MOR. Variable $^{87}Sr/^{86}Sr$ ratios are documented within serpentinites emplaced in Alpine and Apennine ophiolites, ranging between peridotite protolith and continental crustal values (Cannaò et al., 2016; Schwarzenbach et al., 2021). Transect serpentinites are characterized by $^{87}Sr/^{86}Sr$ ratios within and greater than the established range of 0.7068–0.7076 for Cretaceous-Jurassic seawater (McArthur et al., 2020), and approach values of 0.709 in Bargone (Fig. 4a). Conversely, the Apen-2 serpentinite provides an $^{87}Sr/^{86}Sr$ value of 0.705158, considerably lower than that of rodingite-adjacent serpentinites and close to the range of 0.7053–0.7069 published by Cannaò et al. (2016). The higher-than-seawater-$^{87}Sr/^{86}Sr$ values observed in rodingite-

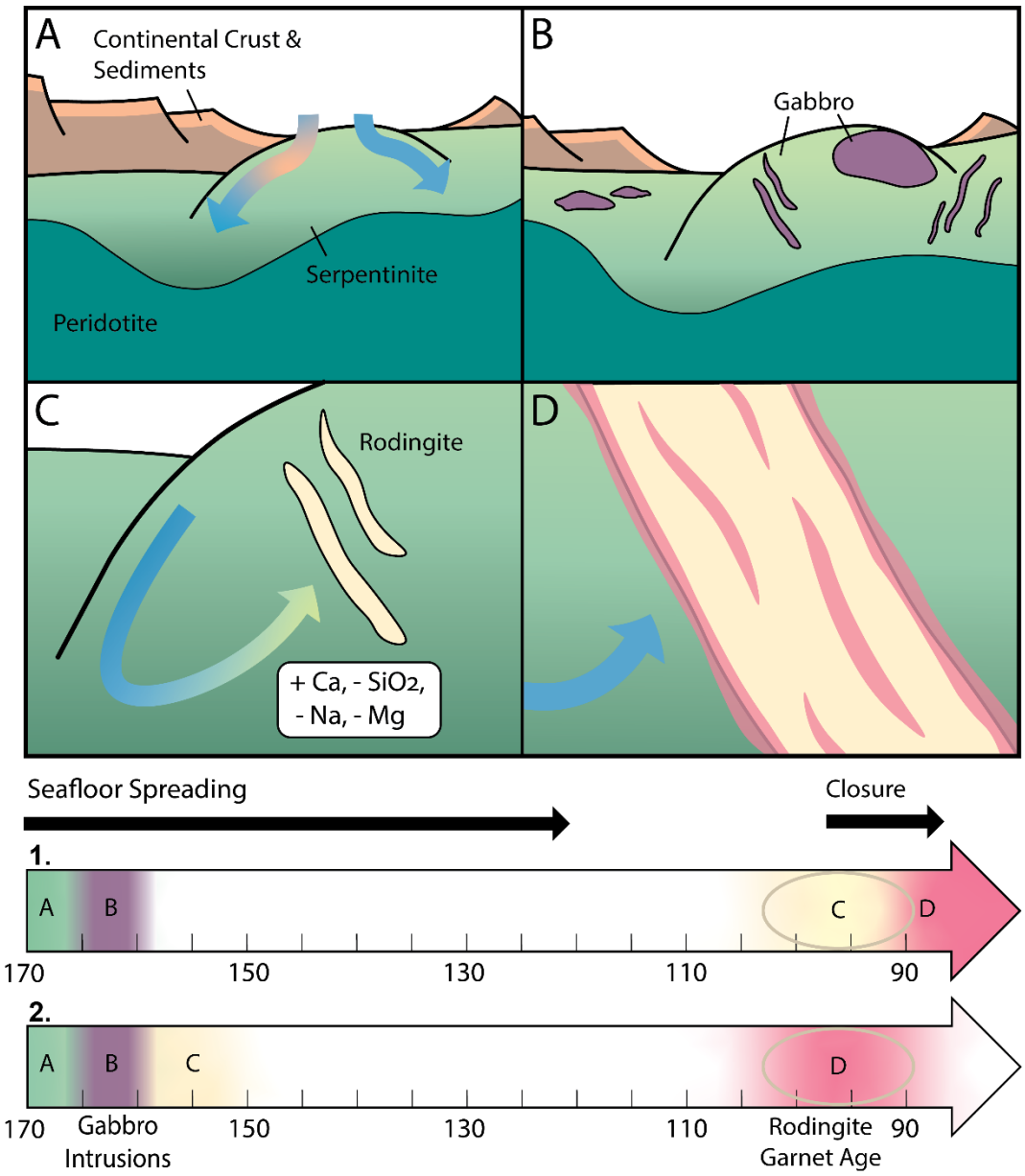

Figure 7. Two potential timelines of events in the Liguro-Piedmont domain within the Alpine Tethys starting 170 Ma with the onset of seafloor spreading through 90 Ma where Alpine subduction had already initiated ocean basin closure. A) Serpentinization: detachment faults allowed for the exhumation of mantle peridotite and the infiltration of seawater, leading to widespread serpentinization. Interaction between seawater and an unspecified continental source locally produced serpentinites with highly radiogenic Sr isotope signatures. B) Gabbro Intrusions: short-lived magmatism at the slow-spreading center produced MORB-like gabbro bodies in the form of plutons and dike systems, all dated to a relatively short period of 166-158 Ma (Tribuzio et al., 2016). C) Rodingitization: as serpentinization continued, infiltrating seawater was modified by serpentinization reactions, creating Ca-rich, SiO_2-depleted fluids that altered gabbros to produce rodingite dikes. D) Late-Stage Advective Alteration: The continued presence of fluids with seawater signatures contributed to further alteration within rodingite dikes. In Timeline 1, serpentinization and gabbro intrusions occur shortly after the onset of seafloor spreading. The garnet age of 96.10 ± 8.90 Ma represents the main rodingitization event depicted in panel C with late-stage advective alteration occurring shortly after. In Timeline 2, bulk rodingitization immediately followed gabbro emplacement and the garnet age instead represents the late-stage advective alteration shown in panel D.

adjacent serpentinites suggest they formed from serpentinizing fluids that were modified by interaction with either continental detrital sediments produced during rifting and ocean basin development or continental basement still present in an embryonic ocean basin marked by a well-documented ocean-continent transition (Fig. 7a) (Marroni et al., 2010). Serpentinites not associated with rodingites do not display crustal signatures and were likely produced from fluids dominated by seawater chemistry. The disparity in Sr isotopic signatures observed within Apennines serpentinites indicates that serpentinization was varied and involved compositionally distinct fluids. A potential mechanism for the introduction of crustally-sourced, radiogenic fluids in the areas surrounding rodingites may be physical zones of weakness related to gabbro emplacement that were later exploited by late-stage fluid infiltration.

6.2 Gabbroic Intrusions

The Apennines display a range of gabbroic intrusions hosted within serpentinized peridotite, from OCCs to smaller-scale dike systems (Fig. 7b). Intrusive magmatism within Alpine-Apennines ophiolites occurred between 166–158 Ma at the MOR axis and produced gabbroic bodies similar in structure and composition to those generated at modern-day ultra-slow spreading ridges from N-MORB magmas (Tribuzio et al., 2016). Gabbro bodies appear to have intruded into already serpentinized mantle peridotite (Desmurs et al., 2001; Schaltegger et al., 2002). The Sr isotopic analysis and literature values of primary gabbros in the Apennines show an expectedly low $^{87}Sr/^{86}Sr$ range of 0.703397–0.7037 (Codillo et al., 2022). This creates a representative baseline for rodingites whose values of $^{87}Sr/^{86}Sr$ were then inflated during alteration by hydrothermal fluids, over at least two stages, illustrated in Figure 8.

6.3 Rodingitization

Petrographic and chemical analyses of rodingites suggest the Pavareto and Bargone transects share analogous gabbro protoliths based on their mineralogy, but experienced slightly different metasomatic histories. For both rodingite transects, Ca was sourced from the breakdown of pyroxene and plagioclase, leading to the development of hydrogarnet and chlorite in the first phase of rodingitization (Frost & Beard, 2007):

$$5\ Di + 4\ An + 8\ H_2O \rightarrow 3\ Grs + Chl + 6\ SiO_{2\ (aq)} \quad (2)$$

$$Grs + 2\ H_2O \rightarrow Hgr + x\ SiO_{2\ (aq)} \quad (3)$$

The formation of hydrogrossular is consistent with the enrichment in Ca and desilication of the gabbro protolith that occurs alongside serpentinization. This reaction is also evidenced by the presence of chlorite and garnet intergrowths within the matrix of the rodingite in PAV-2D and 21LAP-2C thin sections. Garnet formation is followed by diopside development according to the reaction of Li et al. (2008):

$$Grs + Chl + H_2O \pm C_m \rightarrow Di + SiO_{2(aq)} \quad (4)$$

Where C_m represents mobile components such as Ca, Na, and Si. These psuedomorphed pyroxene grains are characterized by well-defined cleavage lined with garnet growth, suggesting synchronous development. Andradite garnet and chlorite were likely produced from the following reaction (Li et al., 2008):

$$Grs + Di + H_2O \pm C_m \rightarrow Adr + Chl \quad (5)$$

Vesuvianite is not observed in the Pavareto transect and is only present in Bargone within the contact-parallel veins alongside diopside + plagioclase in thin sections 21LAP-2C-1 and 21LAP-2C-2. Vesuvianite likely formed from the reactions (Li et al., 2008):

$$Grs + Chl + H_2O \rightarrow Ves \pm C_m \quad (6)$$

$$Chl + H_2O \rightarrow Ves + Di \pm C_m \quad (7)$$

The vesuvianite development in the Bargone transect suggests that rodingitization was more advanced than at Pavareto. The restriction of vesuvianite formation to contact-parallel veins suggests that this final rodingitization stage was locally contained within advective fluid zones. Unexplained is the presence of fine-grained plagioclase within contact-parallel veins in thin sections 21LAP-2C-1, 21LAP-2C-2, 21LAP-2C-3, and 21LAP-2C-4, typically not found in silica-undersaturated rodingites. Vesuvianite and plagioclase were identified on the basis of petrographic analysis alone and need to be confirmed with probe analysis. Garnets are one of the first mineral phases to form during rodingitization, therefore the age of 96.10 ± 8.90 Ma produced from garnet U-Pb geochronology may represent the initial bulk stage of rodingite formation. However, two generations of complexly zoned garnets were identified at the Bargone outcrop, but were not successfully dated (Haws et al., 2021), which may potentially alter this timeline.

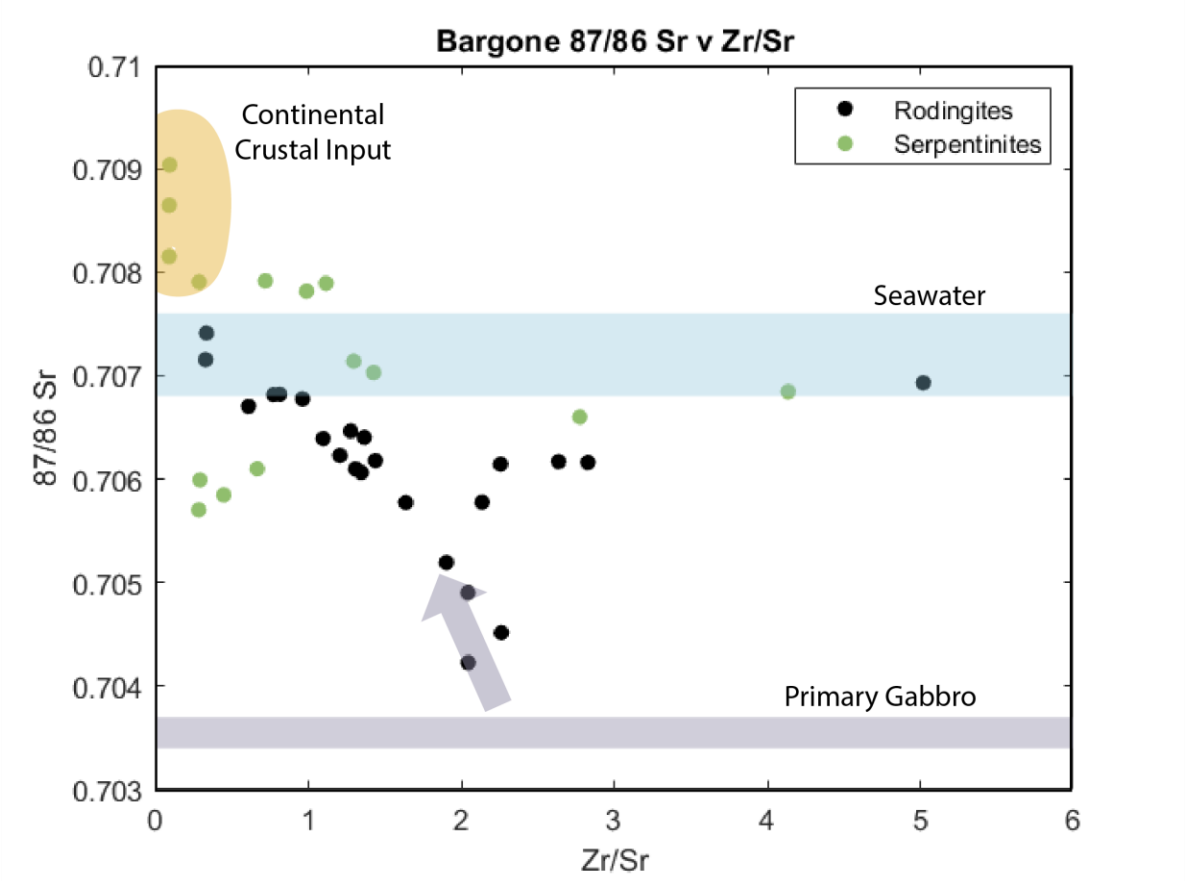

Figure 8. Plot of $^{87}Sr/^{86}Sr$ versus Zr/Sr ratios of Bargone serpentinites and rodingites. The range of $^{87}Sr/^{86}Sr$ values of the primary gabbro protoliths (gray) is 0.703397– 0.7037 (Codillo et al., 2022). Between 170-100 Ma, seawater $^{87}Sr/^{86}Sr$ values ranged from 0.7068–0.7074, shown as the blue bar (McArthur et al., 2020). Serpentinites show the most radiogenic Sr values and the lowest Zr/Sr values, suggesting serpentinizing fluids were affected by continental crustal and/or sedimentary sources (yellow). Both rodingites and serpentinites appear to have interacted with fluid with seawater isotopic ratios and high Zr/Sr ratios.

The metasomatic fluids responsible for rodingitization at Bargone and Pavareto were likely seawater that had been altered by its interaction with peridotite during serpentinization (Fig. 7c), allowing for the development of Ca-Al and Ca-Mg silicates and raising Sr isotope signatures from gabbro protolith values. LILEs are generally consistent across both rodingite transects, however, at Bargone LILEs become enriched towards the UC with the greatest enrichments observed in the upper serpentinite section (Fig. 4b). The Bargone upper serpentinite section also displays considerable enrichments in REEs compared to the lower serpentinite section and Pavareto serpentinites (Fig. 4d). Enrichment of REEs within both rodingite transects

and the Bargone upper serpentinites suggest that high REE values are related to mobilization during rodingitization and are not entirely a signature of the primary gabbro. REE mobilization implies that fluid/rock ratios were greater than 100 and that the composition of the fluid overrode that of the protolith (Tsikouras et al., 2009). The enrichment trends present at Bargone suggest that the seawater-derived fluids responsible for rodingitization were potentially present as a large-scale fluid flow regime, where fluid movement was facilitated along an artery of mechanical weakness greater than the scale of the transect.

6.4 Late-Stage, Localized Advective Fluid Alteration

Zones of advective fluid flow are seemingly manifested as contact-parallel veins at both Bargone and Pavareto. Advective zones at both localities represent continued metasomatism related to further interaction with seawater-like fluids compared to the rest of the rodingite dike (Fig. 7d). At Pavareto, advective-phase alteration is marked by diopside formation at the expense of garnet, whereas contact-parallel veins at Bargone present a more advanced phase of diopside and vesuvianite development as well as a more mature structure (Fig. 2c,d). Advective fluids within the Bargone transect appear to have progressed rodingitization beyond what is observed at Pavareto. However, the plagioclase development in the Bargone contact-parallel veins diverges from a typical rodingitization sequence, but is in line with the high Eu anomalies (Figs. 3 & 4e).

The chemistry of the advective fluid that produced late-stage alteration is distinct from the fluids that produced the bulk of rodingitization. Advective zones in Pavareto and Bargone display high $^{87}Sr/^{86}Sr$ ratios, low Sr/Th and Cs/Th ratios, low REE concentrations, and low Zr concentrations. The late-stage fluids that potentially produced these contact-parallel veins are chemically more similar to seawater than the post-serpentinization fluids that prompted bulk

rodingitization. Pavareto and Bargone differ in that advective zones at Bargone show depletions in all REEs except for Eu and contain peak values of Eu/Sm. The Pavareto advective zone is depleted in all REEs and displays the lowest values of Eu/Sm, although this can be explained by the lack of plagioclase within contact-parallel veins. Eu anomalies indicate that Eu was present in its divalent state, suggesting reducing conditions were present during late-stage alteration (Tsikouras et al., 2009). Additionally, depletions of Zr, a typically immobile element, within advective zones suggest mobilization occurred— behavior that is possible within alkaline fluid systems with available F^- and OH^- ligands (Tsikouras et al., 2009). Ni, Cr, and Sc appear to behave as mobile elements within advective zones and were likely mobilized as $Ni(OH)_2$, $Cr(OH)_3$, and $Sc(OH)_3$ complexes. The formation of these hydroxides suggests relatively high CO_2/H_2O ratios of the advective fluids, and high fluid CO_2 levels may have contributed to the REE mobilization that caused advective zone depletions (Rogkala et al., 2022).

6.5 Timing of Infiltrating Fluids

While widespread serpentinization and gabbro intrusions into oceanic lithosphere of the Alpine Tethys certainly occurred near the MOR axis, the timing and location of rodingitization and late-stage, localized advective alteration is up for debate. There are two potential interpretations of the 96.10 ± 8.90 Ma age produced from garnet geochronology; both indicate that some form of metasomatism occurred shortly before subduction. In the first interpretation (Timeline 1 in Figure 7) the garnet age represents the main rodingitization phase, where the bulk of the metasomatic alteration of gabbro to rodingite occurred (Fig. 7c). The gap between gabbro intrusions at 166–158 Ma and the main rodingitization phase would therefore suggest that serpentinization not only occurred at the MOR, but was reignited again at the outer rise some 20

Ma after seafloor spreading concluded within the Liguro-Piemont domain (Agard & Handy, 2021). Metasomatism would have likely been induced by water percolating through flexure cracks that developed from bending-related faulting as the oceanic slab underwent subduction (Ranero et al., 2003). In this scenario, the post-rodingitization, local fluid alteration seen in the chemical data likely occurred shortly thereafter. The second interpretation (Timeline 2 in Figure 7) relates that the 96 Ma age represents only the late-stage, localized fluid alteration (Fig. 7d). Here, the bulk of rodingitization could have occurred near the MOR axis, shortly after the emplacement of gabbros. Then 60 Ma later, shortly before the slab is subducted, seawater-like fluids infiltrating through flexure cracks resulted in localized partial alteration that reset garnet ages. In both hypotheses, fluid reintroduction occurred around 96 Ma through the development of flexure cracks.

7. Conclusion

The two investigated rodingite transects share similar protoliths, but slightly different metasomatic histories based on chemical, textural, and mineralogic criteria. At both localities, rodingitization was initiated by the development of garnet from the Ca-Fe and Ca-Mg exchange related to the breakdown of pyroxene and plagioclase by post-serpentinization fluids. The metasomatic mineral assemblages at both localities are similar; as metasomatism progressed, hydrogrossular formed, diopside crystallized with the breakdown of garnet, which was subsequently followed by the development of chlorite and andradite. Late-stage alteration was constrained within advective fluid zones and likely manifested as contact-parallel veins of diopside + chlorite at Pavareto and diopside + vesuvianite + plagioclase at Bargone. The presence of vesuvianite indicates rodingitization progressed slightly more at Bargone than

Pavareto either due to longer or more intense fluid interactions. Eu enrichments and Zr depletions suggest that late-stage rodingitization within advective zones occurred under reducing and alkaline conditions. Metasomatism within the Bargone transect appears to be influenced by high levels of fluid movement at an outcrop scale, potentially facilitated by preexisting mechanical weakness. More extensive fluid interaction is observed in Bargone upper serpentinites compared to lower serpentinites, evidenced by the chloritization within the Bargone upper serpentinite section, along with the high REE and LILE concentrations. Serpentinite samples adjacent to rodingite transects present values of $^{87}Sr/^{86}Sr$ more radiogenic than Jurassic-Cretaceous seawater, while other Apennines serpentinites display values intermediate between peridotite protoliths and seawater. High $^{87}Sr/^{86}Sr$ values within rodingite-adjacent serpentinites may be related to the presence of crustally-sourced, radiogenic fluids that infiltrated the mechanically weak zones that allowed for gabbro intrusions and further faulting related to plate-bending. Garnet U-Pb ages from Pavareto either represent the initial phase of rodingitization, which proposes a near 60 Ma gap between the intrusion of the gabbro protolith and the main rodingitization event, or the localized late-stage advective alteration. Flexure cracks created from the bending of the brittle lithosphere during subduction present a potential mechanism for the fluid infiltration responsible for this age and would have developed shortly after the onset of subduction, estimated to be ~100-95 Ma (Agard, 2021).

Overall, hydrothermal alteration of oceanic lithosphere of the Liguro-Piemont domain experienced a complex, multi-stage history characterized by: 1) Widespread, variable serpentinization, 2) Discontinuous magmatism that produced gabbro intrusions from 166-158 Ma, 3) Rodingitization of gabbro dikes, and 4) Late-stage alteration constrained within advective fluid zones.

References:

Agard, P. (2021). Subduction of oceanic lithosphere in the Alps: Selective and archetypal from (slow-spreading) oceans. Earth-Science Reviews, 214, 103517. https://doi.org/10.1016/j.earscirev.2021.103517

Agard, P., & Handy, M. R. (2021). Ocean Subduction Dynamics in the Alps. Elements, 17(1), 9–16. https://doi.org/10.2138/gselements.17.1.9

Alt, J. C., Garrido, C. J., Shanks, W. C., Turchyn, A., Padrón-Navarta, J. A., López Sánchez-Vizcaíno, V., Gómez Pugnaire, M. T., & Marchesi, C. (2012). Recycling of water, carbon, and sulfur during subduction of serpentinites: A stable isotope study of Cerro del Almirez, Spain. Earth and Planetary Science Letters, 327–328, 50–60. https://doi.org/10.1016/j.epsl.2012.01.029

Bach, W., & Klein, F. (2009). The petrology of seafloor rodingites: Insights from geochemical reaction path modeling. Lithos, 112(1), 103–117. https://doi.org/10.1016/j.lithos.2008.10.022

Bach, W., Paulick, H., Garrido, C. J., Ildefonse, B., Meurer, W. P., & Humphris, S. E. (2006). Unraveling the sequence of serpentinization reactions: Petrography, mineral chemistry, and petrophysics of serpentinites from MAR 15°N (ODP Leg 209, Site 1274). Geophysical Research Letters, 33(13). https://doi.org/10.1029/2006GL025681

Barriga, F., & Fyfe, W. S. (1983). Development of rodingite in basaltic rocks in serpentinites, East Liguria, Italy. Contributions to Mineralogy and Petrology, 84(2), 146–151. https://doi.org/10.1007/BF00371281

Cannaò, E., Scambelluri, M., Agostini, S., Tonarini, S., & Godard, M. (2016). Linking serpentinite geochemistry with tectonic evolution at the subduction plate-interface: The Voltri Massif case study (Ligurian Western Alps, Italy). Geochimica et Cosmochimica Acta, 190, 115–133. https://doi.org/10.1016/j.gca.2016.06.034

Codillo, E. A., Klein, F., Dragovic, B., Marschall, H. R., Baxter, E., Scambelluri, M., & Schwarzenbach, E. (2022). Fluid-Mediated Mass Transfer Between Mafic and Ultramafic Rocks in Subduction Zones. Geochemistry, Geophysics, Geosystems, 23(8), e2021GC010206. https://doi.org/10.1029/2021GC010206

Deschamps, F., Guillot, S., Godard, M., Andreani, M., & Hattori, K. (2011). Serpentinites act as sponges for fluid-mobile elements in abyssal and subduction zone environments. Terra Nova, 23(3), 171–178. https://doi.org/10.1111/j.1365-3121.2011.00995.x

Desmurs, L., Manatschal, G., & Bernoulli, D. (2001). The Steinmann Trinity revisited: Mantle exhumation and magmatism along an ocean-continent transition: The Platta nappe, Eastern Switzerland. Geological Society, London, Special Publications, 187, 235–266. https://doi.org/10.1144/GSL.SP.2001.187.01.12

Evans, B. W., Hattori, K., & Baronnet, A. (2013). Serpentinite: What, Why, Where? Elements, 9(2), 99–106. https://doi.org/10.2113/gselements.9.2.99

Frost, B. R., & Beard, J. S. (2007). On Silica Activity and Serpentinization. Journal of Petrology, 48(7), 1351–1368. https://doi.org/10.1093/petrology/egm021

Guillot, S., & Hattori, K. (2013). Serpentinites: Essential Roles in Geodynamics, Arc Volcanism, Sustainable Development, and the Origin of Life. Elements, 9(2), 95–98. https://doi.org/10.2113/gselements.9.2.95

Hacker, B. R., Abers, G. A., & Peacock, S. M. (2003). Subduction factory 1. Theoretical mineralogy, densities, seismic wave speeds, and H2O contents. Journal of Geophysical Research: Solid Earth, 108(B1). https://doi.org/10.1029/2001JB001127

Haws, A. A., Starr, P. G., Dragovic, B., Scambelluri, M., Belmonte, D., Caddick, M. J., Broadwell, K. S., Ague, J. J., & Baxter, E. F. (2021). Meta-rodingite dikes as recorders of subduction zone metamorphism and serpentinite dehydration: Voltri Ophiolite, Italy. Chemical Geology, 565, 120077. https://doi.org/10.1016/j.chemgeo.2021.120077

Hermann, J., Müntener, O., & Scambelluri, M. (2000). The importance of serpentinite mylonites for subduction and exhumation of oceanic crust. Tectonophysics, 327, 225–238. https://doi.org/10.1016/S0040-1951(00)00171-2

Husen, S., Quintero, R., Kissling, E., & Hacker, B. (2003). Subduction-zone structure and magmatic processes beneath Costa Rica constrained by local earthquake tomography and petrological modelling. https://doi.org/10.1046/J.1365-246X.2003.01984.X

Jochum, K., Weis, U., Schwager, B., Stoll, B., Wilson, S., Haug, G., Andreae, M., & Enzweiler, J. (2015). Reference Values Following ISO Guidelines for Frequently Requested Rock Reference Materials. Geostandards and Geoanalytical Research, 40, n/a-n/a. https://doi.org/10.1111/j.1751-908X.2015.00392.x

Kerrick, D. M., & Connolly, J. A. D. (2001). Metamorphic devolatilization of subducted oceanic metabasalts: Implications for seismicity, arc magmatism and volatile recycling. Earth and Planetary Science Letters, 189(1), 19–29. https://doi.org/10.1016/S0012-821X(01)00347-8

Kruckenberg, S. C., Michels, Z. D., & Parsons, M. M. (2019). From intracrystalline distortion to plate motion: Unifying structural, kinematic, and textural analysis in heterogeneous shear zones through crystallographic orientation-dispersion methods. Geosphere, 15(2), 357–381. https://doi.org/10.1130/GES01585.1

Li, X.-P., Zhang, L. F., & Wang, Z. L. (2008). Geochemistry of rodingite derived from eclogite in western Tianshan, China. Acta Petrologica Sinica, 24, 711–717.

Marroni, M., Meneghini, F., & Pandolfi, L. (2010). Anatomy of the Ligure-Piemontese subduction system: Evidence from Late Cretaceous–middle Eocene convergent margin deposits in the Northern Apennines, Italy. International Geology Review, 52(10–12), 1160–1192. https://doi.org/10.1080/00206810903545493

Marroni, M., & Pandolfi, L. (1996). The deformation history of an accreted ophiolite sequence: The Internal Liguride units (Northern apennines, Italy). Geodinamica Acta, 9(1), 13–29. https://doi.org/10.1080/09853111.1996.11417260

McArthur, J. M., Howarth, R. J., Shields, G. A., & Zhou, Y. (2020). Chapter 7—Strontium Isotope Stratigraphy. In F. M. Gradstein, J. G. Ogg, M. D. Schmitz, & G. M. Ogg (Eds.), Geologic Time Scale 2020 (pp. 211–238). Elsevier. https://doi.org/10.1016/B978-0-12-824360-2.00007-3

McDonough, W. F., & Sun, S. -s. (1995). The composition of the Earth. Chemical Geology, 120(3), 223–253. https://doi.org/10.1016/0009-2541(94)00140-4

Millonig, L., Gerdes, A., Avigad, D., Dietsch, C., & Albert, R. (2020). Exploring laser ablation U–Pb dating of regional metamorphic garnet – The Straits Schist, Connecticut, USA. Earth and Planetary Sciences Letters, 552. https://doi.org/10.1016/j.epsl.2020.116589

Molli, G., & Malavieille, J. (2011). Orogenic processes and the Corsica/Apennines geodynamic evolution: Insights from Taiwan. International Journal of Earth Sciences, 100(5), 1207–1224. https://doi.org/10.1007/s00531-010-0598-y

Rampone, E., & Sanfilippo, A. (2021). The Heterogeneous Tethyan Oceanic Lithosphere of the Alpine Ophiolites. Elements, 17(1), 23–28. https://doi.org/10.2138/gselements.17.1.23

Ranero, C., Morgan, J., Mcintosh, K., & Reichert, C. (2003). Bending-related faulting and mantle serpentinization at the Middle America trench. Nature, 425, 367–373. https://doi.org/10.1038/nature01961

Rogkala, A., Petrounias, P., Koutsovitis, P., Giannakopoulou, P., Pomonis, P., Lampropoulou, P., & Hatzipanagiotou, K. (2022). Rodingites from the Veria-Naousa ophiolite (Greece): Mineralogical evolution, metasomatism and petrogenetic processes. Geochemistry, 125860. https://doi.org/10.1016/j.chemer.2021.125860

Rüpke, L. H., Morgan, J. P., Hort, M., & Connolly, J. A. D. (2004). Serpentine and the subduction zone water cycle. Earth and Planetary Science Letters, 223(1), 17–34. https://doi.org/10.1016/j.epsl.2004.04.018

Scambelluri, M., Müntener, O., Hermann, J., Piccardo, G. B., & Trommsdorff, V. (1995). Subduction of water into the mantle: History of an Alpine peridotite. Geology, 23(5), 459–462. https://doi.org/10.1130/0091-7613(1995)023<0459:SOWITM>2.3.CO;2

Scambelluri, M., Piccardo, G. B., Philippot, P., Robbiano, A., & Negretti, L. (1997). High salinity fluid inclusions formed from recycled seawater in deeply subducted alpine serpentinite. Earth and Planetary Science Letters, 148(3), 485–499. https://doi.org/10.1016/S0012-821X(97)00043-5

Schaltegger, U., Desmurs, L., Manatschal, G., Müntener, O., Meier, M., Frank, M., & Bernoulli, D. (2002). The transition from rifting to sea-floor spreading within a magma-poor rifted margin: Field and isotopic constraints. Terra Nova, 14, 156–162. https://doi.org/10.1046/j.1365-3121.2002.00406.x

Schmid, S. M., Fügenschuh, B., Kissling, E., & Schuster, R. (2004). Tectonic map and overall architecture of the Alpine orogen. Eclogae Geologicae Helvetiae, 97(1), 93–117. https://doi.org/10.1007/s00015-004-1113-x

Schmidt, M. W., & Poli, S. (1998). Experimentally based water budgets for dehydrating slabs and consequences for arc magma generation. Earth and Planetary Science Letters, 163(1), 361–379. https://doi.org/10.1016/S0012-821X(98)00142-3

Schwarzenbach, E. M., Vogel, M., Früh-Green, G. L., & Boschi, C. (2021). Serpentinization, Carbonation, and Metasomatism of Ultramafic Sequences in the Northern Apennine Ophiolite (NW Italy). Journal of Geophysical Research: Solid Earth, 126(5), e2020JB020619. https://doi.org/10.1029/2020JB020619

Seyfried, W. E., Foustoukos, D. I., & Fu, Q. (2007). Redox evolution and mass transfer during serpentinization: An experimental and theoretical study at 200°C, 500bar with implications for ultramafic-hosted hydrothermal systems at Mid-Ocean Ridges. Geochimica et Cosmochimica Acta, 71(15), 3872–3886. https://doi.org/10.1016/j.gca.2007.05.015

Tatsumi, Y., & Kogiso, T. (2003). The subduction factory: Its role in the evolution of the Earth's crust and mantle. Geological Society, London, Special Publications, 219, 55–80. https://doi.org/10.1144/GSL.SP.2003.219.01.03

Tribuzio, R., Garzetti, F., Corfu, F., Tiepolo, M., & Renna, M. R. (2016). U–Pb zircon geochronology of the Ligurian ophiolites (Northern Apennine, Italy): Implications for continental breakup to slow seafloor spreading. Tectonophysics, 666, 220–243. https://doi.org/10.1016/j.tecto.2015.10.024

Tsikouras, B., Karipi, S., Rigopoulos, I., Perraki, M., Pomonis, P., & Hatzipanagiotou, K. (2009). Geochemical processes and petrogenetic evolution of rodingite dykes in the ophiolite complex of Othrys (Central Greece). Lithos, 113(3), 540–554. https://doi.org/10.1016/j.lithos.2009.06.013

Ulmer, P., & Trommsdorff, V. (1995). Serpentine Stability to Mantle Depths and Subduction-Related Magmatism. Science, 268(5212), 858–861. https://doi.org/10.1126/science.268.5212.858

Table 1

Bargone

	Rodingite				
Sample	**21LAP-UCR-1.15-2F**	**21LAP-UCR-4.62-2F**	**21LAP-UCR-15.92-2F**	**21LAP-UCR-25.17-2C**	**21LAP-UCR-38.66-2C**
Location	1.2	4.6	15.9	25.2	38.7
$^{87}Sr/^{86}Sr$	0.7071529	0.707410	0.7074441	0.7042272	0.7045154
2 Std Error	0.0000054	0.000010	0.0000051	0.0000034	0.0000064
MgO	18.6	21.3		14.4	13.2
Al_2O_3	11.5	10.4		8.49	9.61
CaO	5.24	2.17		13.4	16.8
TiO_2	0.082	0.083		0.420	0.415
MnO	0.131	0.152		0.148	0.153
Fe_2O_3	2.33	2.38		5.34	5.24
Y	0.273	0.437		12.7	13.2
Zr	0.384	0.502		10.2	10.5
W	0.101	0.036		0.074	0.043
Rb	0.056	0.066		0.069	0.065
Sr	1.17	1.51		5.00	4.63
Nb	0.013	0.008		0.033	0.035
Mo	-	-		0.006	-
Cd	-	0.003		0.064	0.064
Sn	0.063	0.126		0.238	0.209
Sb	0.046	0.000		0.000	0.000
Te	1.10	1.41		2.71	2.22
Cs	0.411	0.459		0.323	0.152
Ba	-	-		-	-
Hf	0.054	0.035		0.410	0.444
Ta	0.073	0.070		0.004	0.028
Tl	-	-		0.003	-
Pb	-	-		0.003	-
Bi	0.001	-		0.003	0.002
Th	0.021	0.010		0.009	0.016
U	0.007	-		0.002	0.001
Sc	1.03	1.11		46.0	49.7
V	15.9	9.33		178	179
Cr	2.38	2.79		199	207
Co	11.9	5.59		28.1	25.6
Ni	52.2	37.6		157	135
Cu	0.291	4.30		95.1	74.6
Zn	49.3	77.5		36.3	30.0
La	0.238	0.216		0.410	0.510
Ce	0.795	0.663		1.57	1.73
Pr	0.126	0.103		0.347	0.370
Nd	0.577	0.474		2.29	2.45
Sm	0.109	0.107		1.06	1.13
Eu	0.365	0.235		0.589	0.644
Gd	0.110	0.111		1.45	1.57
Tb	0.014	0.016		0.298	0.317
Dy	0.061	0.086		2.19	2.31
Ho	0.011	0.017		0.478	0.503
Er	0.023	0.042		1.36	1.42
Tm	0.003	0.005		0.198	0.201
Yb	0.016	0.032		1.24	1.26
Lu	0.002	0.004		0.178	0.182

Table 1

Bargone

	Rodingite				
Sample	**21LAP-UCR-45.04-2C**	**21LAP-UCR-50.29-2C**	**21LAP-UCR-61.95-2C**	**21LAP-UCR-68.72-2C**	**21LAP-UCR-79.91-2C**
Location	45.0	50.3	62.0	68.7	79.9
$^{87}Sr/^{86}Sr$	0.7049024	0.705194	0.7064034	0.7068201	0.7062277
2 Std Error	0.0000072	0.000017	0.0000061	0.0000028	0.0000062
MgO	12.3	11.8	13.7	18.7	8.97
Al_2O_3	9.88	12.2	15.4	20.7	13.0
CaO	17.9	22.0	20.1	17.3	22.3
TiO_2	0.354	0.357	0.258	0.203	0.253
MnO	0.150	0.154	0.151	0.147	0.115
Fe_2O_3	4.59	5.08	4.35	4.11	5.21
Y	10.8	9.98	5.20	2.18	5.42
Zr	8.16	7.82	4.37	2.09	5.30
W	0.043	15.5	15.9	5.54	14.2
Rb	0.036	0.036	0.039	0.031	0.032
Sr	3.99	4.11	3.20	2.57	4.39
Nb	0.025	0.033	0.030	0.026	0.040
Mo	-	0.123	0.245	0.034	0.042
Cd	0.048	0.044	0.023	0.014	0.028
Sn	0.256	0.167	0.200	0.151	0.163
Sb	0.001	-	-	0.001	-
Te	1.05	2.20	3.06	2.44	2.75
Cs	0.115	0.110	0.114	0.116	0.141
Ba	-	-	-	-	-
Hf	0.342	0.333	0.195	0.100	0.197
Ta	0.004	0.006	0.005	0.003	0.015
Tl	0.013	0.029	0.035	0.029	0.037
Pb	-	-	-	-	-
Bi	0.005	0.025	-	0.012	-
Th	0.012	0.011	0.012	0.014	0.015
U	-	-	-	-	-
Sc	39.1	34.2	20.0	11.6	20.1
V	164	184	130	99.7	106
Cr	176	150	78.8	35.0	75.9
Co	22.7	26.8	25.4	20.9	24.8
Ni	117	113	98.3	87.1	113
Cu	45.1	43.1	35.2	48.2	16.1
Zn	28.4	28.4	35.9	63.7	26.7
La	0.467	0.497	0.557	0.481	0.501
Ce	1.51	1.57	1.44	1.24	1.32
Pr	0.319	0.323	0.252	0.195	0.233
Nd	2.03	2.01	1.44	0.943	1.26
Sm	0.909	0.896	0.529	0.257	0.480
Eu	0.584	0.616	0.660	0.549	0.493
Gd	1.27	1.20	0.684	0.310	0.644
Tb	0.261	0.243	0.128	0.053	0.126
Dy	1.90	1.76	0.899	0.360	0.920
Ho	0.414	0.385	0.193	0.080	0.199
Er	1.18	1.08	0.562	0.235	0.583
Tm	0.169	0.157	0.080	0.036	0.089
Yb	1.05	0.944	0.531	0.242	0.582
Lu	0.151	0.141	0.076	0.038	0.088

Table 1

Bargone

	Rodingite				
Sample	**21LAP-UCR-90.51-2C**	**21LAP-UCR-101.88-2C**	**21LAP-UCR-118.67-2C**	**21LAP-UCR-124.52-2C**	**21LAP-UCR-140.55-2C**
Location	90.5	101.9	118.7	124.5	140.6
$^{87}Sr/^{86}Sr$	0.705775	0.705778	0.7060975	0.7060638	0.7067043
2 Std Error	0.000049	0.000040	0.0000053	0.0000048	0.0000044
MgO	13.3	11.1	8.58	11.0	8.46
Al_2O_3	12.5	9.87	10.8	13.6	12.5
CaO	23.7	18.6	21.5	27.1	22.1
TiO_2	0.400	0.281	0.258	0.345	0.203
MnO	0.152	0.126	0.117	0.144	0.101
Fe_2O_3	7.59	5.91	4.20	5.56	4.68
Y	8.86	7.66	6.77	8.87	2.86
Zr	7.89	8.63	6.58	7.74	2.40
W	7.69	21.3	23.1	36.3	12.8
Rb	0.069	0.051	0.044	0.061	0.045
Sr	4.82	4.04	5.03	5.74	3.95
Nb	0.046	0.075	0.045	0.047	0.020
Mo	-	0.737	0.107	0.136	0.054
Cd	0.056	0.034	0.027	0.034	0.019
Sn	0.179	0.097	0.095	0.163	0.089
Sb	-	-	0.002	-	0.002
Te	7.13	1.23	2.54	2.04	3.63
Cs	0.218	0.179	0.120	0.163	0.138
Ba	-	-	-	-	-
Hf	0.290	0.310	0.253	0.329	0.112
Ta	0.006	0.016	0.006	0.007	0.003
Tl	0.042	-	0.025	0.032	0.027
Pb	-	-	-	-	-
Bi	-	-	0.002	-	0.003
Th	0.015	0.018	0.016	0.025	0.019
U	-	-	0.0004	0.008	-
Sc	37.5	34.8	25.7	35.4	13.6
V	141	112	121	155	68.2
Cr	143	135	90.0	133	65.9
Co	44.1	38.8	24.8	33.8	26.3
Ni	189	153	96.9	135	91.7
Cu	139	81.4	13.6	27.2	7.44
Zn	37.9	32.5	26.8	32.5	29.2
La	0.314	0.303	0.488	0.514	0.360
Ce	1.14	1.09	1.39	1.56	0.879
Pr	0.234	0.221	0.261	0.300	0.140
Nd	1.43	1.37	1.52	1.82	0.728
Sm	0.656	0.608	0.610	0.777	0.236
Eu	0.375	0.344	0.521	0.544	0.338
Gd	0.919	0.852	0.844	1.07	0.326
Tb	0.194	0.180	0.169	0.216	0.065
Dy	1.47	1.34	1.22	1.61	0.475
Ho	0.333	0.302	0.264	0.352	0.110
Er	0.979	0.897	0.758	1.01	0.341
Tm	0.151	0.137	0.107	0.146	0.054
Yb	0.997	0.903	0.687	0.929	0.379
Lu	0.152	0.136	0.100	0.136	0.057

Table 1

Bargone

	Rodingite				
Sample	**21LAP-UCR-149.29-2C**	**21LAP-UCR-166.20-2C**	**21LAP-UCR-175.99-2C**	**21LAP-UCR-186.19-2C**	**21LAP-UCR-188.62-2C**
Location	149.3	166.2	176.0	186.2	188.6
$^{87}Sr/^{86}Sr$	0.7067745	0.7064641	0.7061800	0.706817	0.7063913
2 Std Error	0.0000051	0.0000030	0.0000079	0.000013	0.0000042
MgO	9.12	8.37	7.87	7.70	6.31
Al_2O_3	11.8	11.1	11.1	12.3	11.0
CaO	19.8	22.0	24.3	21.8	26.0
TiO_2	0.247	0.257	0.266	0.150	0.101
MnO	0.108	0.122	0.134	0.085	0.131
Fe_2O_3	4.81	4.26	3.74	5.67	2.65
Y	4.30	6.20	7.98	2.43	3.30
Zr	3.16	4.66	6.41	2.78	2.49
W	0.084	14.2	0.132	0.070	65.6
Rb	0.045	0.052	0.040	0.043	0.041
Sr	3.29	3.65	4.46	3.59	2.27
Nb	0.024	0.032	0.022	0.046	0.091
Mo	-	0.057	-	-	2.76
Cd	0.015	0.014	0.022	0.019	0.023
Sn	0.270	0.154	0.151	0.195	0.117
Sb	0.000	0.002	-	-	0.003
Te	3.83	2.20	2.19	2.80	1.17
Cs	0.123	0.124	0.079	0.217	0.082
Ba	-	-	-	-	-
Hf	0.140	0.228	0.299	0.114	0.109
Ta	0.014	0.005	0.004	0.133	0.020
Tl	-	0.024	-	-	-
Pb	-	-	-	-	-
Bi	0.001	-	-	-	-
Th	0.015	0.016	0.016	0.015	0.011
U	-	-	-	-	0.001
Sc	19.5	22.8	28.6	7.71	10.9
V	82.8	81.1	90.2	58.9	64.0
Cr	87.0	92.3	106	31.7	70.7
Co	24.6	21.4	17.0	30.1	23.5
Ni	82.6	85.5	66.3	189	65.9
Cu	12.5	9.08	6.53	33.8	2.92
Zn	30.7	27.3	27.3	29.4	19.0
La	0.271	0.280	0.355	0.376	0.259
Ce	0.811	0.972	1.14	1.09	0.849
Pr	0.148	0.203	0.235	0.185	0.159
Nd	0.854	1.27	1.52	0.950	0.895
Sm	0.341	0.554	0.706	0.297	0.344
Eu	0.280	0.322	0.487	0.397	0.254
Gd	0.489	0.786	0.989	0.368	0.456
Tb	0.099	0.157	0.203	0.066	0.087
Dy	0.733	1.15	1.49	0.435	0.624
Ho	0.166	0.251	0.321	0.093	0.132
Er	0.502	0.714	0.906	0.267	0.371
Tm	0.077	0.103	0.129	0.040	0.053
Yb	0.519	0.666	0.814	0.257	0.333
Lu	0.079	0.097	0.116	0.039	0.048

Table 1

Bargone

	Rodingite				
Sample	**21LAP-UCR-205.40-2C**	**21LAP-UCR-215.02-2C**	**21LAP-UCR-234.94-2C**	**21LAP-LCR-1.98-2E**	**21LAP-LCC-0.86-2E**
Location	205.4	215.0	234.9	266.5	269.8
$^{87}Sr/^{86}Sr$	0.7061456	0.7061698	0.7061616	0.7069310	0.7072816
2 Std Error	0.0000052	0.0000039	0.0000032	0.0000042	0.0000036
MgO	8.09	8.45	12.5	20.3	
Al_2O_3	10.8	11.1	11.1	9.58	
CaO	23.4	22.4	17.7	8.47	
TiO_2	0.252	0.379	0.310	0.920	
MnO	0.109	0.108	0.125	0.229	
Fe_2O_3	5.02	5.39	5.24	6.45	
Y	7.11	6.33	7.24	7.50	
Zr	10.5	10.8	11.2	26.7	
W	0.429	0.150	0.190	0.020	
Rb	0.076	0.058	0.082	0.110	
Sr	4.63	4.11	3.97	5.32	
Nb	0.121	0.194	0.147	1.00	
Mo	-	-	-	-	
Cd	0.033	0.035	0.036	0.029	
Sn	0.198	0.295	0.472	0.246	
Sb	0.000	-	-	0.001	
Te	2.63	1.42	1.86	1.68	
Cs	0.237	0.270	0.274	0.702	
Ba	0.208	-	-	1.48	
Hf	0.354	0.369	0.423	0.785	
Ta	0.065	0.186	0.084	0.070	
Tl	-	-	-	-	
Pb	-	-	-	-	
Bi	-	0.004	-	-	
Th	0.020	0.020	0.020	0.037	
U	0.002	0.003	0.012	0.005	
Sc	21.3	18.5	23.4	15.2	
V	62.0	73.4	81.8	106	
Cr	94.5	71.6	64.3	116	
Co	33.2	34.8	34.0	22.1	
Ni	173	172	185	210	
Cu	19.0	38.2	20.8	26.9	
Zn	23.0	27.3	32.5	33.7	
La	0.349	0.497	0.611	0.449	
Ce	1.31	1.60	1.81	1.67	
Pr	0.271	0.292	0.336	0.337	
Nd	1.62	1.62	1.90	2.04	
Sm	0.672	0.603	0.736	0.792	
Eu	0.276	0.376	0.568	0.371	
Gd	0.919	0.797	0.957	1.02	
Tb	0.182	0.160	0.185	0.195	
Dy	1.29	1.17	1.31	1.34	
Ho	0.280	0.258	0.282	0.290	
Er	0.798	0.754	0.816	0.812	
Tm	0.117	0.111	0.118	0.115	
Yb	0.730	0.723	0.763	0.704	
Lu	0.109	0.108	0.112	0.102	

Table 1

Bargone

	Serpentinite				
Sample	**21LAP-UCS-110.68-2H**	**21LAP-UCS-90.19-2H**	**21LAP-UCS-85.11-2H**	**21LAP-UCS-80.23-2H**	**21LAP-UCS-76.82-2H**
Location	-110.7	-90.2	-85.1	-80.2	-76.8
$^{87}Sr/^{86}Sr$	0.7078154	0.7060988	0.7057023	0.7058462	0.7059913
2 Std Error	0.0000040	0.0000088	0.0000041	0.0000046	0.0000042
MgO	25.9	21.8	19.1	14.2	14.8
Al_2O_3	3.07	4.42	9.62	8.58	8.70
CaO	2.69	8.29	11.9	15.5	16.0
TiO_2	0.211	0.212	0.267	0.290	0.253
MnO	0.169	0.150	0.190	0.193	0.207
Fe_2O_3	10.7	9.96	7.20	5.99	6.88
Y	4.88	5.83	5.99	8.56	5.61
Zr	15.0	9.01	7.35	9.35	5.92
W	0.499	0.028	2.25	0.035	0.019
Rb	0.637	0.513	0.421	0.210	0.0
Sr	15.1	13.5	25.9	20.9	20.2
Nb	0.063	0.030	0.048	0.034	0.020
Mo	-	-	1.58	-	-
Cd	0.027	0.041	0.052	0.065	0.039
Sn	1.137	0.167	0.132	0.247	0.124
Sb	-	-	0.000004	-	-
Te	6.45	6.37	4.02	3.76	0.161
Cs	3.34	3.36	2.66	1.78	0.697
Ba	-	-	-	-	-
Hf	0.508	0.349	0.305	0.362	0.155
Ta	0.009	0.005	0.075	0.067	0.042
Tl	0.034	0.038	0.009	0.005	-
Pb	0.073	0.037	0.011	0.013	-
Bi	0.002	0.004	0.003	0.006	-
Th	0.011	0.010	0.011	0.011	0.008
U	0.0002	-	-	0.001	-
Sc	13.2	19.2	23.4	29.3	24.3
V	82.3	84.1	107	133	109
Cr	2803	938	1251	569	313
Co	92.6	86.8	56.1	43.5	48.0
Ni	1443	1106	744	605	591
Cu	61.9	158	221	268	218
Zn	80.7	51.9	55.8	44.5	43.8
La	0.217	0.188	0.287	0.316	0.100
Ce	0.770	0.737	0.944	1.16	0.311
Pr	0.161	0.162	0.189	0.246	0.062
Nd	1.01	1.05	1.15	1.59	1.24
Sm	0.414	0.467	0.506	0.716	0.548
Eu	0.154	0.207	0.310	0.373	0.333
Gd	0.554	0.671	0.675	1.000	0.655
Tb	0.111	0.137	0.141	0.202	0.133
Dy	0.823	1.00	1.04	1.50	0.948
Ho	0.186	0.225	0.230	0.329	0.202
Er	0.555	0.657	0.679	0.952	0.574
Tm	0.083	0.100	0.101	0.141	0.084
Yb	0.548	0.636	0.667	0.887	0.482
Lu	0.082	0.095	0.098	0.133	0.068

Table 1

Bargone

	Serpentinite				
Sample	**21LAP-UCS-68.94-2H**	**21LAP-UCS-39.72-2H**	**21LAP-UCS-24.93-2F**	**21LAP-UCS-10.76-2F**	**21LAP-UCS-2.04-2F**
Location	-68.9	-39.7	-24.9	-10.8	-2.0
$^{87}Sr/^{86}Sr$	0.7071382	0.7078921	0.7068454	0.7065992	0.7070286
2 Std Error	0.0000060	0.0000066	0.0000061	0.0000059	0.0000043
MgO	27.2	26.4	17.6	14.8	20.5
Al_2O_3	2.23	2.72	2.48	3.60	6.58
CaO	2.41	2.89	16.3	16.8	9.18
TiO_2	0.168	0.177	0.261	0.245	0.251
MnO	0.150	0.138	0.098	0.097	0.119
Fe_2O_3	11.0	12.4	13.6	14.6	11.6
Y	4.36	3.43	6.71	5.35	4.54
Zr	14.5	5.83	13.5	9.03	6.47
W	4.97	0.021	0.073	0.052	0.046
Rb	0.332	0.185	0.082	0.079	0.179
Sr	11.2	5.23	3.25	3.25	4.53
Nb	0.055	0.023	0.030	0.023	0.023
Mo	0.523	-	-	-	-
Cd	0.027	0.018	0.041	0.033	0.036
Sn	0.131	0.091	0.710	0.390	0.144
Sb	-	-	-	-	-
Te	3.55	8.29	4.04	5.81	5.42
Cs	2.12	1.91	0.549	0.621	1.46
Ba	-	-	-	-	-
Hf	0.470	0.255	0.658	0.450	0.326
Ta	0.012	0.008	0.082	0.004	0.234
Tl	0.021	0.017	0.004	0.038	0.003
Pb	0.014	0.107	0.242	0.863	0.770
Bi	-	0.063	0.001	-	0.008
Th	0.010	0.008	0.010	0.010	0.010
U	0.001	0.001	-	-	0.006
Sc	12.8	11.3	16.8	14.6	18.4
V	62.4	51.8	76.6	80.0	84.6
Cr	1438	1369	1700	2256	1823
Co	98.5	111	103	95.4	113
Ni	1511	1586	1510	1195	1115
Cu	36.0	53.5	30.2	32.0	67.2
Zn	68.9	68.8	48.9	76.3	98.4
La	0.207	0.145	0.220	0.148	0.164
Ce	0.793	0.457	0.621	0.528	0.552
Pr	0.166	0.087	0.152	0.119	0.114
Nd	1.01	0.565	1.08	0.828	0.715
Sm	0.401	0.241	0.536	0.396	0.327
Eu	0.126	0.115	0.180	0.196	0.254
Gd	0.510	0.345	0.744	0.570	0.465
Tb	0.104	0.074	0.155	0.118	0.098
Dy	0.753	0.567	1.15	0.888	0.756
Ho	0.166	0.132	0.256	0.203	0.175
Er	0.488	0.407	0.770	0.598	0.542
Tm	0.074	0.066	0.116	0.092	0.086
Yb	0.488	0.459	0.731	0.607	0.575
Lu	0.074	0.071	0.111	0.092	0.090

Table 1

Bargone

	Serpentinite				
Sample	**21LAP-LCS-3.76-2E**	**21LAP-LCS-6.55-2E**	**21LAP-LCS-25.85-2E**	**21LAP-LCS-49.91-2E**	**21LAP-LCS-76.81-2E**
Location	272.0	274.8	294.0	314.0	341.3
$^{87}Sr/^{86}Sr$	0.7079137	0.707904	0.7081513	0.7086356	0.7086460
2 Std Error	0.0000057	0.000033	0.0000048	0.0000060	0.0000044
MgO	26.2	23.3	22.6		26.5
Al_2O_3	4.68	2.76	2.15		1.89
CaO	3.14	5.74	8.58		2.86
TiO_2	0.054	0.044	0.044		0.034
MnO	0.101	0.097	0.085		0.091
Fe_2O_3	6.41	6.50	9.34		6.68
Y	1.38	0.952	1.35		0.894
Zr	1.53	0.624	0.209		0.160
W	0.019	0.028	0.037		0.155
Rb	0.100	0.086	0.077		0.069
Sr	2.13	2.18	2.34		1.78
Nb	0.008	0.005	0.004		0.002
Mo	-	-	-		-
Cd	0.008	0.015	0.017		0.012
Sn	0.057	0.044	0.097		0.088
Sb	0.003	0.003	-		0.002
Te	0.884	2.34	3.97		2.61
Cs	0.668	0.472	0.364		0.369
Ba	-	-	-		-
Hf	0.075	0.031	0.027		0.022
Ta	0.058	0.051	0.005		0.056
Tl	-	-	-		0.010
Pb	-	-	-		-
Bi	-	-	0.000		-
Th	0.023	0.020	0.017		0.012
U	0.076	0.037	0.050		0.004
Sc	10.9	7.68	10.8		8.55
V	37.4	36.3	50.6		39.7
Cr	960	1426	1200		1283
Co	93.5	93.2	90.3		82.0
Ni	1027	1008	1413		1595
Cu	14.5	18.7	19.3		19.1
Zn	40.4	44.2	38.3		39.3
La	0.059	0.066	0.036		0.003
Ce	0.226	0.215	0.085		0.007
Pr	0.044	0.033	0.012		0.002
Nd	0.243	0.162	0.068		0.026
Sm	0.089	0.047	0.051		0.028
Eu	0.074	0.079	0.044		0.015
Gd	0.129	0.072	0.101		0.058
Tb	0.028	0.016	0.024		0.016
Dy	0.225	0.141	0.201		0.143
Ho	0.055	0.037	0.050		0.036
Er	0.172	0.134	0.167		0.124
Tm	0.029	0.023	0.027		0.020
Yb	0.201	0.182	0.195		0.140
Lu	0.033	0.031	0.031		0.023

Table 1

	Bargone	**Pavareto**					
	Serpentinite	Rodingite					
Sample	**21LAP-LCS-100.85-2E**	**PAV-2D-R-24**	**PAV-2D-R-25.1**	**PAV-2D-R-25.2**	**PAV-2D-R-27**	**PAV-2D-R-28**	**PAV-2D-R-29**
Location	365.3	1.8	3.2	4.6	9.1	10.5	11.9
$^{87}Sr/^{86}Sr$	0.7090363	0.705234	0.705021	0.705103	0.705181	0.706238	0.705524
2 Std Error	0.0000052	0.000027	0.000042	0.000011	0.000007	0.000021	0.000017
MgO	29.2	18.2	27.5	20.9	29.7	22.9	21.7
Al_2O_3	1.04	5.49	15.8	6.87	16.2	6.40	6.48
CaO	1.01	8.22	10.3	9.27	7.45	5.48	7.87
TiO_2	0.042	0.343	0.420	0.379	0.297	0.188	0.302
MnO	0.083	0.140	0.148	0.157	0.139	0.126	0.164
Fe_2O_3	6.08	4.38	4.46	4.56	4.77	4.81	4.08
Y	1.00	10.9	11.9	10.6	8.66	5.54	7.98
Zr	0.230	10.1	11.2	9.32	6.01	4.33	31.9
W	0.019	0.113	0.130	16.3	0.128	32.0	23.9
Rb	0.125	0.002	-	-	-	-	171
Sr	2.45	0.702	0.919	0.758	0.683	0.305	369
Nb	0.009	0.019	0.026	0.048	0.016	0.060	1.33
Mo	-	0.065	0.056	1.33	0.023	2.81	55.0
Cd	0.013	0.012	0.064	0.015	0.006	0.012	16.1
Sn	0.099	0.504	0.635	0.614	0.735	0.699	648
Sb	0.003	-	0.006	-	-	0.011	52.3
Te	2.14	3.05	2.79	3.55	1.73	0.889	5080
Cs	0.448	0.014	0.013	0.015	0.021	0.027	7.20
Ba	0.063	0.109	0.085	0.066	0.125	0.089	159.8
Hf	0.023	0.512	0.538	0.476	0.294	0.192	2.25
Ta	0.009	0.008	0.008	0.013	0.064	0.012	0.464
Tl	0.010	0.003	0.003	0.002	0.002	0.004	2.12
Pb	0.609	0.026	0.030	0.043	0.114	0.027	42.5
Bi	0.003	0.019	0.012	0.004	0.001	0.038	2.10
Th	0.016	0.002	0.003	0.002	0.001	0.001	0.171
U	0.034	0.001	0.001	0.001	0.001	0.001	0.182
Sc	9.89	21.5	61.0	17.7	50.2	1.45	10.1
V	39.9	163	175	148	125	98.9	211
Cr	1449	534	229	208	40.4	28.1	230
Co	87.4	20.9	17.7	21.8	16.1	17.0	16.8
Ni	1777	332	260	260	236	218	169
Cu	16.0	0.654	0.705	0.901	1.13	1.43	1863
Zn	37.9	69.4	332	95.0	50.4	37.7	8006
La	0.012	0.249	0.237	0.199	0.189	0.193	2.21
Ce	0.030	1.21	1.15	0.895	0.792	0.740	3.27
Pr	0.005	0.321	0.304	0.236	0.202	0.174	0.522
Nd	0.040	2.26	2.20	1.73	1.47	1.21	2.90
Sm	0.034	1.09	1.13	0.967	0.787	0.593	0.857
Eu	0.015	0.596	0.689	0.633	0.744	0.817	1.77
Gd	0.071	1.53	1.59	1.42	1.13	0.781	25.5
Tb	0.019	0.308	0.336	0.303	0.243	0.158	0.140
Dy	0.161	2.15	2.40	2.18	1.75	1.11	1.49
Ho	0.041	0.465	0.512	0.476	0.387	0.247	0.225
Er	0.134	1.28	1.44	1.34	1.09	0.710	0.061
Tm	0.022	0.183	0.206	0.193	0.157	0.104	0.088
Yb	0.156	1.12	1.28	1.20	0.998	0.672	1.68
Lu	0.026	0.164	0.188	0.177	0.155	0.107	0.577

Table 1

Pavareto

	Rodingite							Serpentinite
Sample	**PAV-2D-R-30**	**PAV-2D-R-31**	**PAV-2D-R-32**	**PAV-2D-R-33**	**PAV-2D-R-34**	**PAV-2D-R-35**	**PAV-2D-R-36.1**	**PAV-2D-S-18.1**
Location	13.3	14.7	16.1	17.6	19.0	20.4	21.8	-29.7
$^{87}Sr/^{86}Sr$	0.705085	0.70637	0.707771	0.705478	0.70550	0.70588	0.706599	0.707352
2 Std Error	0.000071	0.00074	0.000016	0.000018	0.00055	0.00010	0.000028	0.000018
MgO		46.6	23.3		21.8		1.75	28.3
Al_2O_3		4.70	5.24		5.68		4.23	5.17
CaO		0.03	4.63		4.57		20.8	8.35
TiO_2		0.005	0.145		0.145		0.285	0.049
MnO		0.081	0.135		0.125		-	0.111
Fe_2O_3		4.22	4.58		4.26		5.62	11.3
Y		6.64	0.163		2.51		2.21	1.89
Zr		5.57	0.056		1.71		1.33	0.246
W		0.092	0.279		0.051		13.3	48.4
Rb		-	-		-		-	0.003
Sr		0.736	0.128		0.267		0.233	0.725
Nb		0.017	0.002		0.010		0.032	0.059
Mo		0.060	0.134		0.039		1.47	2.11
Cd		0.008	-		-		0.005	0.013
Sn		0.434	-		0.448		0.572	0.713
Sb		0.005	-		-		-	-
Te		3.32	0.460		0.738		1.58	3.88
Cs		0.028	0.001		0.037		0.036	0.013
Ba		0.112	0.052		0.091		0.051	0.213
Hf		0.287	0.003		0.063		0.043	0.037
Ta		0.005	0.000		0.002		0.019	0.014
Tl		0.013	0.003		0.004		0.003	0.004
Pb		0.029	0.009		0.006		0.008	0.050
Bi		0.012	0.001		0.002		0.005	0.004
Th		0.001	0.001		0.001		0.001	0.001
U		0.001	0.008		0.000		0.000	0.001
Sc		25.9	0.491		0.847		0.138	17.7
V		112	12.0		82.1		71.2	70.9
Cr		54.8	4.24		3.25		11.4	2542
Co		19.2	26.5		13.9		13.6	108
Ni		307	135		274		201	1874
Cu		0.531	0.371		0.533		0.897	13.4
Zn		58.4	9.89		48.8		52.7	37.6
La		0.194	0.007		0.183		0.180	0.021
Ce		0.823	0.015		0.626		0.593	0.043
Pr		0.197	0.003		0.131		0.128	0.008
Nd		1.27	0.015		0.812		0.804	0.064
Sm		0.604	0.008		0.315		0.286	0.060
Eu		0.514	0.002		0.648		0.641	0.097
Gd		0.917	0.009		0.368		0.339	0.123
Tb		0.193	0.003		0.067		0.056	0.033
Dy		1.40	0.024		0.444		0.375	0.290
Ho		0.309	0.007		0.095		0.079	0.073
Er		0.875	0.023		0.287		0.235	0.246
Tm		0.127	0.004		0.044		0.037	0.045
Yb		0.787	0.026		0.314		0.272	0.320
Lu		0.116	0.005		0.049		0.041	0.053

Table 1

Pavareto

	Serpentinite								
Sample	**PAV-2D-S-17**	**PAV-2D-S-14**	**PAV-2D-S-12**	**PAV-2D-S-9**	**PAV-2D-S-6**	**PAV-2D-S-5**	**PAV-2D-S-8**	**PAV-2D-S-4**	**PAV-2D-S-3**
Location	-28.3	-24.1	-21.3	-17.1	-13.0	-11.5	-15.7	-10.0	-8.7
$^{87}Sr/^{86}Sr$	0.707290	0.707379	0.707548	-	0.707550	0.707516	0.707283	0.707508	0.707454
2 Std Error	0.000014	0.000012	0.000037	-	0.000011	0.000052	0.000076	0.000016	0.000049
MgO	26.5	23.5		18.8			20.2	30.2	28.3
Al_2O_3	4.60	3.05		2.26			1.77	2.98	2.76
CaO	8.22	8.69		8.62			8.72	4.77	2.65
TiO_2	0.031	0.032		0.036			0.025	0.049	0.045
MnO	0.095	0.091		0.076			0.075	0.093	0.094
Fe_2O_3	10.2	10.3		8.76			9.09	7.58	6.01
Y	1.60	2.46		1.10			1.53	0.781	0.815
Zr	0.204	0.292		0.310			1.454	0.680	0.873
W	0.033	0.049		0.085			0.107	54.5	0.106
Rb	0.001	-		0.003			0.006	0.007	0.005
Sr	0.537	0.438		0.364			0.489	0.540	0.500
Nb	0.008	0.012		0.006			0.006	0.063	0.006
Mo	0.035	0.041		0.067			0.057	2.32	0.079
Cd	0.008	0.012		0.003			0.004	0.010	0.006
Sn	0.199	0.343		0.776			0.844	0.924	0.942
Sb	-	0.001		0.003			0.010	0.004	0.010
Te	2.67	4.15		3.52			2.12	3.32	3.09
Cs	0.013	0.010		0.008			0.009	0.012	0.013
Ba	0.122	0.128		0.143			0.631	0.201	0.211
Hf	0.029	0.037		0.017			0.053	0.021	0.026
Ta	0.002	0.001		0.002			0.001	0.013	0.001
Tl	0.004	0.005		0.006			0.005	0.010	0.003
Pb	0.033	0.041		0.052			0.063	0.153	0.222
Bi	0.001	0.034		0.002			0.001	0.002	0.003
Th	0.001	0.001		0.000			0.001	0.001	0.001
U	0.000	0.000		0.000			0.001	0.000	0.000
Sc	16.9	19.5		7.08			11.0	7.54	8.46
V	55.0	58.7		44.4			44.4	39.1	35.0
Cr	2200	2538		1063			1245	1172	796
Co	77.8	90.3		80.6			71.2	105	102
Ni	1447	1612		1394			1176	1463	1548
Cu	13.3	20.2		11.8			9.74	10.5	10.7
Zn	32.8	39.8		19.1			21.6	29.3	31.7
La	0.013	0.019		0.039			0.048	0.080	0.096
Ce	0.030	0.047		0.097			0.124	0.204	0.257
Pr	0.006	0.009		0.017			0.022	0.033	0.042
Nd	0.051	0.078		0.097			0.120	0.140	0.180
Sm	0.052	0.077		0.058			0.065	0.038	0.046
Eu	0.067	0.115		0.251			0.248	0.298	0.308
Gd	0.111	0.177		0.090			0.111	0.052	0.064
Tb	0.031	0.049		0.021			0.028	0.013	0.014
Dy	0.262	0.429		0.177			0.236	0.107	0.114
Ho	0.067	0.108		0.043			0.061	0.029	0.029
Er	0.224	0.347		0.142			0.203	0.109	0.108
Tm	0.038	0.056		0.024			0.035	0.021	0.020
Yb	0.262	0.370		0.178			0.251	0.167	0.161
Lu	0.043	0.058		0.030			0.040	0.030	0.029

Table 1

	Pavareto				Apennines	
	Serpentinite				Gabbro	Serpentinite
Sample	**PAV-2D-S-2B**	**PAV-2D-S-1**	**PAV-2D-S-19**	**PAV-2D-S-20**	**Apen-1**	**Apen-2**
Location	-7.4	-5.9	-3.2	-1.8		
$^{87}Sr/^{86}Sr$	0.707588	0.707143	-	0.706861	0.7033971	0.705158
2 Std Error	0.000038	0.000017	-	0.000094	0.0000044	0.000027
MgO	34.4		23.3	28.5		
Al_2O_3	3.02		4.60	9.71		
CaO	3.41		4.41	2.59		
TiO_2	0.057		0.122	0.159		
MnO	0.119		0.101	0.101		
Fe_2O_3	8.30		6.88	5.23		
Y	1.51		4.19	5.19		
Zr	1.78		4.71	5.59		
W	0.107		0.244	0.148		
Rb	0.019		0.011	0.010		
Sr	0.612		0.647	0.872		
Nb	0.009		0.012	0.011		
Mo	0.156		0.053	0.040		
Cd	0.006		0.007	0.007		
Sn	0.949		0.680	0.307		
Sb	-		0.009	0.010		
Te	2.03		5.07	8.19		
Cs	0.015		0.018	0.017		
Ba	0.229		0.144	0.101		
Hf	0.045		0.153	0.207		
Ta	0.002		0.003	0.003		
Tl	0.003		0.006	0.004		
Pb	0.321		1.264	0.802		
Bi	0.001		0.034	0.013		
Th	0.002		0.001	0.001		
U	0.001		0.000	0.001		
Sc	11.6		9.95	18.9		
V	44.5		70.1	71.3		
Cr	1125		1958	1965		
Co	100		82.9	81.4		
Ni	1578		1206	1262		
Cu	15.0		10.1	3.81		
Zn	30.2		25.8	31.6		
La	0.120		0.138	0.141		
Ce	0.346		0.546	0.614		
Pr	0.061		0.131	0.146		
Nd	0.293		0.795	0.921		
Sm	0.091		0.326	0.412		
Eu	0.314		0.328	0.284		
Gd	0.134		0.453	0.587		
Tb	0.028		0.095	0.125		
Dy	0.226		0.719	0.924		
Ho	0.056		0.168	0.210		
Er	0.183		0.522	0.646		
Tm	0.032		0.083	0.100		
Yb	0.234		0.566	0.669		
Lu	0.039		0.087	0.102		

Table 2

Analysis	Name / Sample	^{207}Pb[a] (cps)	U[b] (µg/g)	Pb[b] (µg/g)	Th[b] / U	^{238}U[c] / ^{206}Pb	±2s (%)	^{207}Pb[c] / ^{206}Pb	±2s (%)	rho[d]
486_U	**21LAP-2C-2**	73232	0.018	0.26	0.47	0.1032	21	0.6929	4.0	0.00
487_U		*2278*	*bdl*	*bdl*	*na*	*na*	*481*	*0.7035*	*12*	*0.00*
488_U		7464	0.0030	0.041	0.38	0.1120	69	0.7927	4.2	0.00
489_U		2937	0.00082	0.013	na	0.09284	157	0.6593	7.9	0.00
490_U		1825	0.0013	0.0044	0.56	0.4162	77	0.5783	12	0.00
491_U		2220	0.00018	0.0019	5.37	0.1295	416	0.5130	11	0.00
492_U		3034	0.00057	0.011	0.87	0.08095	253	0.7259	11	0.00
481_U	**21LAP-2C-3**	21865	0.0013	0.069	2.65	0.03764	167	1.261	4.2	0.00
482_U		*2143*	*0.00055*	*bdl*	*0.74*	*na*	*2511*	*0.7274*	*12*	*0.00*
483_U		3587	0.00001	0.00016	na	0.08120	9387	0.8049	7.0	0.00
484_U		*3219*	*0.00016*	*bdl*	*0.82*	*na*	*579*	*0.7379*	*7.9*	*0.00*
485_U		339745	0.0084	0.73	2.83	0.02124	25	1.111	3.2	0.00
476_U	**21LAP-2Dc**	16959	0.00036	0.048	1.94	0.01181	359	0.8462	2.8	0.00
477_U		175283	0.013	0.61	1.58	0.03851	35	1.144	3.3	0.00
478_U		9735	0.00021	0.013	3.77	0.02501	441	0.8323	3.7	0.00
479_U		14462	0.00049	0.025	0.72	0.03176	226	0.9021	3.9	0.00
480_U		8085	0.00057	0.0092	1.93	0.09905	152	0.8397	5.3	0.00
376_U	**PAV-2D (2-2)**	2614	0.0049	0.0012	0.48	6.720	38	0.8419	5.8	0.00
377_U		1144	0.0044	0.0011	0.51	5.983	13	0.7637	5.6	0.00
378_U		10313	0.0027	0.0100	0.64	0.4356	22	0.8458	2.0	0.00
379_U		18226	0.0045	0.016	0.67	0.4411	16	0.8484	1.5	0.00
380_U		3840	0.0016	0.0044	0.18	0.5795	119	0.8361	4.4	0.00
381_U	*Pb saturated*	*23896*	*0.0011*	*0.026*	*0.97*	*0.06655*	*45*	*0.8154*	*1.5*	*0.00*
382_U	*Pb saturated*	*27392*	*0.0014*	*0.021*	*0.77*	*0.1058*	*29*	*0.8120*	*1.3*	*0.00*
383_U		406076	0.015	0.30	1.68	0.07938	17	0.8364	1.0	0.00
384_U		324585	0.014	0.24	1.71	0.09052	17	0.8237	1.2	0.00
385_U		288412	0.012	0.27	1.44	0.06888	14	0.8190	1.3	0.00
386_U		179646	0.0076	0.14	1.03	0.08990	21	0.8373	1.3	0.00
327_U	**PAV-2D (1-2)**	3875	0.001	0.0030	1.67	0.4966	32	0.8510	2.2	0.00
328_U		1448	0.007	0.0012	1.50	8.699	8.4	0.7371	3.7	0.00
329_U		405	0.004	0.00043	0.70	13.03	9.5	0.6819	5.5	0.00
330_U		405	0.007	0.00042	0.34	22.16	8.0	0.5990	5.6	0.00
331_U		278	0.005	0.00032	0.12	20.71	9.2	0.6183	6.5	0.00
332_U		428	0.002	0.00040	0.44	8.558	16	0.7650	5.4	0.00
333_U		504749	0.013	0.69	1.50	0.03080	22	0.8551	0.78	0.00
334_U		535806	0.005	0.56	1.31	0.01409	31	0.8598	0.77	0.00
335_U		276373	0.007	0.45	1.11	0.02541	29	0.8588	0.80	0.00
336_U		328997	0.002	0.41	1.08	0.007706	30	0.8607	0.78	0.00
337_U		664709	0.016	0.57	1.36	0.04425	15	0.8530	0.81	0.00
338_U		406032	0.004	0.46	1.11	0.01416	30	0.8584	0.79	0.00
339_U		204341	0.008	0.17	1.11	0.08082	12	0.8556	0.83	0.00
340_U		150800	0.006	0.028	1.29	0.3376	57	0.8443	1.3	0.00
341_U		924676	0.005	4.0	1.18	0.001935	65	0.8593	0.77	0.00
342_U		438423	0.012	0.67	1.28	0.02991	25	0.8575	0.79	0.00
343_U		685402	0.007	0.77	1.20	0.01551	35	0.8600	0.77	0.00
344_U		861324	0.001	2.6	0.93	0.000688	196	0.8598	0.77	0.00
345_U		98166	0.004	0.22	0.85	0.02755	54	0.8635	0.88	0.00
346_U		289732	0.010	0.48	1.28	0.03329	24	0.8568	0.81	0.00
347_U		587406	0.004	0.83	0.88	0.008521	34	0.8608	0.76	0.00

Analysis	Name / Sample	^{207}Pb[a] (cps)	U[b] (µg/g)	Pb[b] (µg/g)	Th/U[b]	$^{238}U/^{206}Pb$[c]	±2s (%)	$^{207}Pb/^{206}Pb$[c]	±2s (%)	rho[d]
348_U	**PAV-2D (1-2)**	686484	0.002	0.53	0.66	0.006423	38	0.8617	0.77	0.00
349_U		276	0.000	0.00052	0.48	1.124	226	0.8528	9.0	0.00
350_U		164	0.001	0.00011	0.096	9.051	44	0.7491	10.0	0.00
359_U		426	0.001	0.00031	0.060	2.876	61	0.8530	6.1	0.00
360_U		552	0.001	0.00037	0.14	2.957	52	0.8218	5.2	0.00
361_U		1079	0.001	0.00063	0.84	1.651	49	0.8724	4.0	0.00
362_U		519	0.001	0.00068	0.086	1.484	73	0.8641	5.0	0.00
363_U		397	0.000	0.00035	0.20	1.939	76	0.8153	6.0	0.00

a Within run background-corrected mean 207Pb signal in cps (counts per second).

b U and Pb concentrations and Th/U ratio were calculated relative to the primary reference material.

c Corrected for background, within-run Pb/U fractionation (in case of 206Pb/238U) and subsequently normalised to the primary reference material (ID-TIMS value/measured value).

d Rho is the 206Pb/238U - 207Pb/206Pb uncertainty correlation coefficient.

Accuracy and reproducibilty was checked by repeated analyses of secondary reference materials; data given as mean with 2 standard deviation uncertainties.

bdl = below detection limit; na = not available (e.g., for Th/U, if Th or U are bdl)

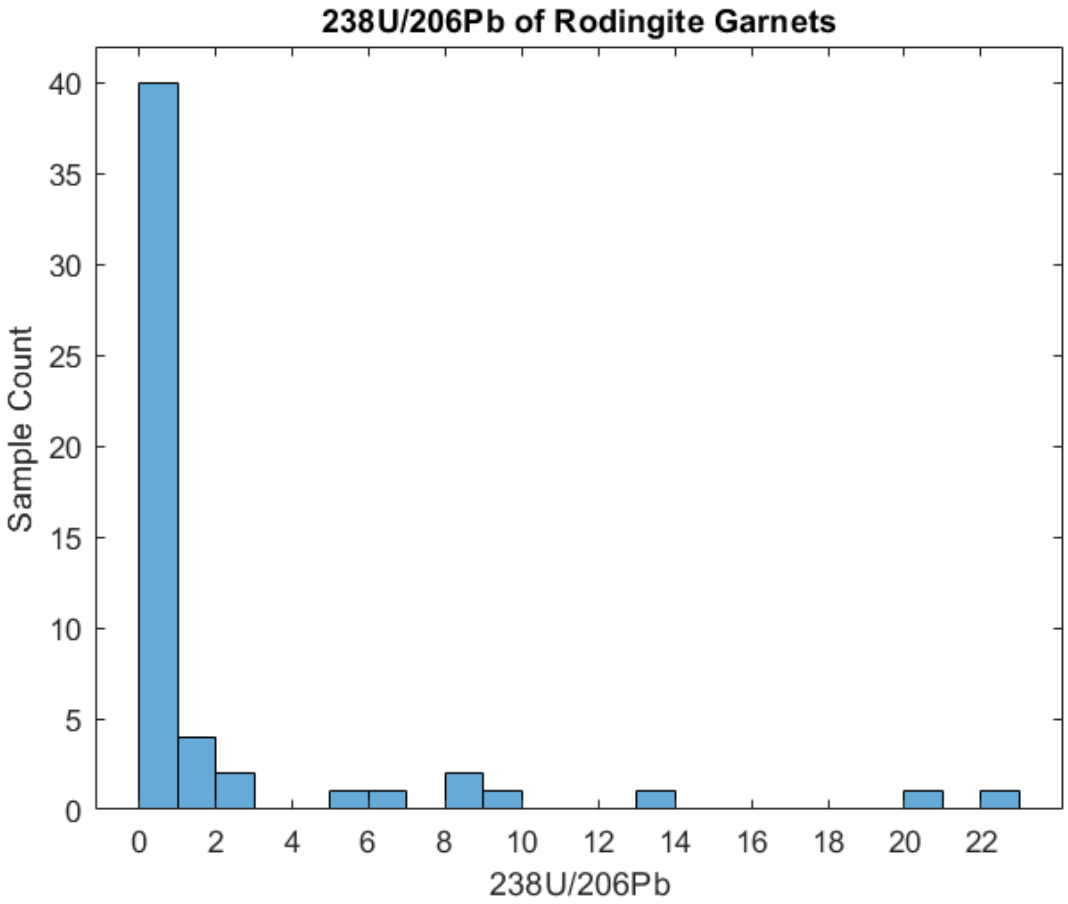

Figure S1. Histogram of $^{238}U/^{206}Pb$ ratios of garnets from Apennines rodingites listed in Table 2. The majority of samples have ratios of <1, and only one sample (PAV-2D.1) had high enough ratios to generate an isochron.

Table 3

Hand Sample	Formation	Outcrop	Coordinates	Lithology	Notes
21LAP-1A	Internal Ligurides	Libiola	44°18'11.1"N 9°26'57.5"E	Rodingite	Contact at bottom of dike
21LAP-1B	Internal Ligurides	Libiola	44°18'11.1"N 9°26'57.5"E	Serpentinite	Serpentinite adjacent to 21LAP-1B
21LAP-1C	Internal Ligurides	Libiola	44°18'11.1"N 9°26'57.5"E	Rodingite-Serpentinite	Contact at top of dike
21LAP-1D	Internal Ligurides	Libiola	44°18'11.1"N 9°26'57.5"E	Rodingite-Serpentinite	Contact at top of dike
21LAP-1E	Internal Ligurides	Libiola	44°18'11.1"N 9°26'57.5"E	Rodingite	Center of rodingite
21LAP-2C	Internal Ligurides	Bargone	44°17'50.7"N 9°28'37.6"E	Rodingite	Rodingite dike
21LAP-2D	Internal Ligurides	Bargone	44°17'50.7"N 9°28'37.6"E	Rodingite-Serpentinite	Upper contact serpentinite-rodingite
21LAP-2E	Internal Ligurides	Bargone	44°17'50.7"N 9°28'37.6"E	serpentinite	Lower Contact, mostly serpentinite
21LAP-2F	Internal Ligurides	Bargone	44°17'50.7"N 9°28'37.6"E	rodingite-serpentinite	Upper contact serpentinite-rodingite
21LAP-2G	Internal Ligurides	Bargone	44°17'50.7"N 9°28'37.6"E	Serpentinite	Serpentinite beneath LC
21LAP-2H	Internal Ligurides	Bargone	44°17'50.7"N 9°28'37.6"E	Serpentinite	Serpentinite above UC
21LAP-3A	Internal Ligurides	Pipocilla	44°18'07.7"N 9°26'59.0"E	Fresh olivine gabbro	
21LAP-4A	Internal Ligurides	Pavareto	44°16'29.9"N 9°35'21.5"E	Rodingite-Serpentinite	Full rodingite dike
21LAP-4B	Internal Ligurides	Pavareto	44°16'29.9"N 9°35'21.5"E	Serpentinite	Serpentinite above upper contact
21LAP-4C	Internal Ligurides	Pavareto	44°16'29.9"N 9°35'21.5"E	Serpentinite	Serpentinite directly adjacent to contact
21LAP-4D	Internal Ligurides	Pavareto	44°16'29.9"N 9°35'21.5"E	Serpentinite	Serpentinite beneath the lower contact
21LAP-4F	Internal Ligurides	Pavareto	44°16'29.9"N 9°35'21.5"E	Serpentinite	Serpentinite above upper contact
21LAP-5A	Internal Ligurides	Bonnasola	44°10'49.6"N 9°35'03.2"E	Gabbro	Oceanic Core Complex
PAV-2D	Internal Ligurides	Pavareto	44°16'29.9"N 9°35'21.5"E	Rodingite-Serpentinite	Rodingite-serpentinite contact

Table 4

Sample Name	Hand Sample	Rod	Cut	Lithology	Increment Cut	Saw Kerf	Distance Along Transect
21LAP-UCS-90.19-2H	21LAP-2H	1	2	Serpentinite	1.6	0.6	-90.2
21LAP-UCS-88.58-2H	21LAP-2H	1	3	Serpentinite	1.6	0.6	-88.6
21LAP-UCS-86.84-2H	21LAP-2H	1	4	Serpentinite	1.6	0.6	-86.8
21LAP-UCS-85.11-2H	21LAP-2H	1	5	Serpentinite	1.6	0.6	-85.1
21LAP-UCS-83.55-2H	21LAP-2H	1	6	Serpentinite	1.6	0.6	-83.5
21LAP-UCS-81.99-2H	21LAP-2H	1	7	Serpentinite	1.6	0.6	-82.0
21LAP-UCS-80.23-2H	21LAP-2H	1	8	Serpentinite	1.6	0.6	-80.2
21LAP-UCS-78.47-2H	21LAP-2H	1	9	Serpentinite	1.6	0.6	-78.5
21LAP-UCS-76.82-2H	21LAP-2H	1	10	Serpentinite	1.6	0.6	-76.8
21LAP-UCS-75.14-2H	21LAP-2H	1	11	Serpentinite	1.6	0.6	-75.1
21LAP-UCS-73.41-2H	21LAP-2H	1	12	Serpentinite	1.6	0.6	-73.4
21LAP-UCS-71.87-2H	21LAP-2H	1	13	Serpentinite	1.6	0.6	-71.9
21LAP-UCS-70.31-2H	21LAP-2H	1	14	Serpentinite	1.6	0.6	-70.3
21LAP-UCS-68.44-2H	21LAP-2H	1	15	Serpentinite	1.6	0.6	-68.4
21LAP-UCS-66.69-2H	21LAP-2H	1	16	Serpentinite	1.6	0.6	-66.7
21LAP-UCS-65.16-2H	21LAP-2H	1	17	Serpentinite	1.6	0.6	-65.2
21LAP-UCS-62.98-2H	21LAP-2H	1	17 RR	Serpentinite	1.6	0.6	-63.0
21LAP-UCS-110.68-2H	21LAP-2H	1	18	Serpentinite	1.6	0.6	-110.7
21LAP-UCS-108.40-2H	21LAP-2H	1	19	Serpentinite	1.6	0.6	-108.4
21LAP-UCS-106.44-2H	21LAP-2H	1	20	Serpentinite	1.6	0.6	-106.4
21LAP-UCS-104.94-2H	21LAP-2H	1	21	Serpentinite	1.6	0.6	-104.9
21LAP-UCS-103.09-2H	21LAP-2H	1	22	Serpentinite	1.6	0.6	-103.1
21LAP-UCS-101.40-2H	21LAP-2H	1	23	Serpentinite	1.6	0.6	-101.4
21LAP-UCS-99.76-2H	21LAP-2H	1	24	Serpentinite	1.6	0.6	-99.8
21LAP-UCS-97.97-2H	21LAP-2H	1	25	Serpentinite	1.6	0.6	-98.0
21LAP-UCS-96.33-2H	21LAP-2H	1	26	Serpentinite	1.6	0.6	-96.3
21LAP-UCS-94.77-2H	21LAP-2H	1	27	Serpentinite	1.6	0.6	-94.8
21LAP-UCS-92.90-2H	21LAP-2H	1	28	Serpentinite	1.6	0.6	-92.9
21LAP-UCS-90.73-2H	21LAP-2H	1	28 RR	Serpentinite	1.6	0.6	-90.7
21LAP-UCS-62.41-2H	21LAP-2H	2	3	Serpentinite	5.6	0.6	-62.4
21LAP-UCS-59.38-2H	21LAP-2H	2	4	Serpentinite	1.6	0.6	-59.4
21LAP-UCS-57.72-2H	21LAP-2H	2	5	Serpentinite	1.6	0.6	-57.7
21LAP-UCS-56.11-2H	21LAP-2H	2	6	Serpentinite	1.6	0.6	-56.1
21LAP-UCS-54.63-2H	21LAP-2H	2	7	Serpentinite	1.6	0.6	-54.6
21LAP-UCS-53.05-2H	21LAP-2H	2	8	Serpentinite	1.6	0.6	-53.0
21LAP-UCS-51.26-2H	21LAP-2H	2	9	Serpentinite	1.6	0.6	-51.3
21LAP-UCS-49.57-2H	21LAP-2H	2	10	Serpentinite	1.6	0.6	-49.6
21LAP-UCS-47.97-2H	21LAP-2H	2	11	Serpentinite	1.6	0.6	-48.0
21LAP-UCS-46.30-2H	21LAP-2H	2	12	Serpentinite	1.6	0.6	-46.3
21LAP-UCS-44.63-2H	21LAP-2H	2	13	Serpentinite	1.6	0.6	-44.6
21LAP-UCS-43.03-2H	21LAP-2H	2	14	Serpentinite	1.6	0.6	-43.0
21LAP-UCS-41.40-2H	21LAP-2H	2	15	Serpentinite	1.6	0.6	-41.4
21LAP-UCS-39.72-2H	21LAP-2H	2	16	Serpentinite	1.6	0.6	-39.7
21LAP-UCS-37.66-2H	21LAP-2H	2	16 RR	Serpentinite	1.6	0.6	-37.7

Table 4

Sample Name	Hand Sample	Rod	Cut	Lithology	Increment Cut	Saw Kerf	Distance Along Transect
21LAP-UCS-76.60-2H	21LAP-2H	2	17	Serpentinite	1.6	0.6	-76.6
21LAP-UCS-68.94-2H	21LAP-2H	2	17 RR	Serpentinite	1.6	0.6	-68.9
21LAP-UCS-10.76-2F	21LAP-2F	3	2	Serpentinite	1.6	0.6	-10.8
21LAP-UCS-8.745-2F	21LAP-2F	3	3	Serpentinite	1.6	0.6	-8.7
21LAP-UCS-6.95-2F	21LAP-2F	3	4	Serpentinite	1.6	0.6	-6.9
21LAP-UCS-5.70-2F	21LAP-2F	3	5	Serpentinite	1.6	0.6	-5.7
21LAP-UCS-3.90-2F	21LAP-2F	3	6	Serpentinite	1.6	0.6	-3.9
21LAP-UCS-2.04-2F	21LAP-2F	3	7	Serpentinite	1.6	0.6	-2.0
21LAP-UCS-0.47-2F	21LAP-2F	3	8	Serpentinite	1.6	0.6	-0.5
21LAP-UCR-1.15-2F	21LAP-2F	3	9	Contact	1.6	0.6	1.2
21LAP-UCR-2.79-2F	21LAP-2F	3	10	Rodingite	1.6	0.6	2.8
21LAP-UCR-4.62-2F	21LAP-2F	3	11	Rodingite	1.6	0.6	4.6
21LAP-UCR-6.28-2F	21LAP-2F	3	12	Rodingite	1.6	0.6	6.3
21LAP-UCR-7.61-2F	21LAP-2F	3	13	Rodingite	1.6	0.6	7.6
21LAP-UCR-9.27-2F	21LAP-2F	3	14	Rodingite	1.6	0.6	9.3
21LAP-UCR-11.06-2F	21LAP-2F	3	15	Rodingite	1.6	0.6	11.1
21LAP-UCR-12.64-2F	21LAP-2F	3	16	Rodingite	1.6	0.6	12.6
21LAP-UCR-14.27-2F	21LAP-2F	3	17	Rodingite	1.6	0.6	14.3
21LAP-UCR-15.92-2F	21LAP-2F	3	18	Rodingite	1.6	0.6	15.9
21LAP-UCR-17.69-2F	21LAP-2F	3	18 RR	Rodingite	1.6	0.6	17.7
21LAP-UCS-43.30-2F	21LAP-2F	3	19	Serpentinite	1.6	0.6	-43.3
21LAP-UCS-39.15-2F	21LAP-2F	3	20	Serpentinite	1.6	0.6	-39.2
21LAP-UCS-37.23-2F	21LAP-2F	3	21	Serpentinite	1.6	0.6	-37.2
21LAP-UCS-35.31-2F	21LAP-2F	3	22	Serpentinite	1.6	0.6	-35.3
21LAP-UCS-33.68-2F	21LAP-2F	3	23	Serpentinite	1.6	0.6	-33.7
21LAP-UCS-32.00-2F	21LAP-2F	3	24	Serpentinite	1.6	0.6	-32.0
21LAP-UCS-30.31-2F	21LAP-2F	3	25	Serpentinite	1.6	0.6	-30.3
21LAP-UCS-28.53-2F	21LAP-2F	3	26	Serpentinite	1.6	0.6	-28.5
21LAP-UCS-26.61-2F	21LAP-2F	3	27	Serpentinite	1.6	0.6	-26.6
21LAP-UCS-24.93-2F	21LAP-2F	3	28	Serpentinite	1.6	0.6	-24.9
21LAP-UCS-23.44-2F	21LAP-2F	3	29	Serpentinite	1.6	0.6	-23.4
21LAP-UCS-21.48-2F	21LAP-2F	3	30	Serpentinite	1.6	0.6	-21.5
21LAP-UCS-19.47-2F	21LAP-2F	3	31	Serpentinite	1.6	0.6	-19.5
21LAP-UCS-17.83-2F	21LAP-2F	3	32	Serpentinite	1.6	0.6	-17.8
21LAP-UCS-16.42-2F	21LAP-2F	3	33	Serpentinite	1.6	0.6	-16.4
21LAP-UCS-14.99-2F	21LAP-2F	3	34	Serpentinite	1.6	0.6	-15.0
21LAP-UCS-13.25-2F	21LAP-2F	3	35	Serpentinite	1.6	0.6	-13.2
21LAP-UCS-11.99-2F	21LAP-2F	3	35 RR	Serpentinite	1.6	0.6	-12.0
21LAP-UCR-166.20-2C	21LAP-2C	4	3	Rodingite	1.6	0.6	166.2
21LAP-UCR-164.59-2C	21LAP-2C	4	4	Rodingite	1.6	0.6	164.6
21LAP-UCR-162.80-2C	21LAP-2C	4	5	Rodingite	1.6	0.6	162.8
21LAP-UCR-160.96-2C	21LAP-2C	4	6	Rodingite	1.6	0.6	161.0
21LAP-UCR-159.27-2C	21LAP-2C	4	7	Rodingite	1.6	0.6	159.3

Table 4

Sample Name	Hand Sample	Rod	Cut	Lithology	Increment Cut	Saw Kerf	Distance Along Transect
21LAP-UCR-157.64-2C	21LAP-2C	4	8	Rodingite	1.6	0.6	157.6
21LAP-UCR-155.95-2C	21LAP-2C	4	9	Rodingite	1.6	0.6	155.9
21LAP-UCR-154.29-2C	21LAP-2C	4	10	Rodingite	1.6	0.6	154.3
21LAP-UCR-152.65-2C	21LAP-2C	4	11	Rodingite	1.6	0.6	152.7
21LAP-UCR-150.94-2C	21LAP-2C	4	12	Rodingite	1.6	0.6	150.9
21LAP-UCR-149.29-2C	21LAP-2C	4	13	Rodingite	1.6	0.6	149.3
21LAP-UCR-146.00-2C	21LAP-2C	4	14	Rodingite	5	0.6	146.0
21LAP-UCR-140.55-2C	21LAP-2C	4	14 RR	Rodingite	5	0.6	140.6
21LAP-UCR-189.54-2C	21LAP-2C	4	15	Rodingite	5	0.6	189.5
21LAP-UCR-186.19-2C	21LAP-2C	4	16	Rodingite	1.6	0.6	186.2
21LAP-UCR-184.38-2C	21LAP-2C	4	17	Rodingite	1.6	0.6	184.4
21LAP-UCR-182.60-2C	21LAP-2C	4	18	Rodingite	1.6	0.6	182.6
21LAP-UCR-180.93-2C	21LAP-2C	4	19	Rodingite	1.6	0.6	180.9
21LAP-UCR-179.26-2C	21LAP-2C	4	20	Rodingite	1.6	0.6	179.3
21LAP-UCR-177.61-2C	21LAP-2C	4	21	Rodingite	1.6	0.6	177.6
21LAP-UCR-175.99-2C	21LAP-2C	4	22	Rodingite	1.6	0.6	176.0
21LAP-UCR-173.92-2C	21LAP-2C	4	23	Rodingite	1.6	0.6	173.9
21LAP-UCR-171.76-2C	21LAP-2C	4	24	Rodingite	1.6	0.6	171.8
21LAP-UCR-170.03-2C	21LAP-2C	4	25	Rodingite	1.6	0.6	170.0
21LAP-UCR-168.32-2C	21LAP-2C	4	26	Rodingite	1.8	0.6	168.3
21LAP-UCR-167.15-2C	21LAP-2C	4	26 RR	Rodingite	1.8	0.6	167.2
21LAP-UCR-135.79-2C	21LAP-2C	4	27	Rodingite	5.6	0.6	135.8
21LAP-UCR-130.21-2C	21LAP-2C	4	28	Rodingite	5.6	0.6	130.2
21LAP-UCR-124.52-2C	21LAP-2C	4	29	Rodingite	5.6	0.6	124.5
21LAP-UCR-118.67-2C	21LAP-2C	4	30	Rodingite	5.6	0.6	118.7
21LAP-UCR-112.81-2C	21LAP-2C	4	30 RR	Rodingite	5.6	0.6	112.8
21LAP-UCR-85.35-2C	21LAP-2C	4	32	Rodingite	5.6	0.6	85.4
21LAP-UCR-90.51-2C	21LAP-2C	4	33	Rodingite	5.6	0.6	90.5
21LAP-UCR-96.07-2C	21LAP-2C	4	34	Rodingite	5.6	0.6	96.1
21LAP-UCR-101.88-2C	21LAP-2C	4	35	Rodingite	5.6	0.6	101.9
21LAP-UCR-107.90-2C	21LAP-2C	4	35 RR	Rodingite	5.6	0.6	107.9
21LAP-UCR-68.72-2C	21LAP-2C	4	37	Rodingite	5.6	0.6	68.7
21LAP-UCR-74.29-2C	21LAP-2C	4	38	Rodingite	5.6	0.6	74.3
21LAP-UCR-79.91-2C	21LAP-2C	4	38 RR	Rodingite	5.6	0.6	79.9
21LAP-UCR-13.94-2C	21LAP-2C	4	41	Rodingite	1.6	0.6	13.9
21LAP-UCR-15.62-2C	21LAP-2C	4	42	Rodingite	1.6	0.6	15.6
21LAP-UCR-17.22-2C	21LAP-2C	4	43	Rodingite	1.6	0.6	17.2
21LAP-UCR-18.89-2C	21LAP-2C	4	44	Rodingite	1.6	0.6	18.9
21LAP-UCR-20.35-2C	21LAP-2C	4	45	Rodingite	1.6	0.6	20.3
21LAP-UCR-21.82-2C	21LAP-2C	4	46	Rodingite	1.6	0.6	21.8
21LAP-UCR-23.48-2C	21LAP-2C	4	47	Rodingite	1.6	0.6	23.5
21LAP-UCR-25.17-2C	21LAP-2C	4	48	Rodingite	1.6	0.6	25.2
21LAP-UCR-26.89-2C	21LAP-2C	4	49	Rodingite	1.6	0.6	26.9

Table 4

Sample Name	Hand Sample	Rod	Cut	Lithology	Increment Cut	Saw Kerf	Distance Along Transect
21LAP-UCR-28.56-2C	21LAP-2C	4	50	Rodingite	1.6	0.6	28.6
21LAP-UCR-30.23-2C	21LAP-2C	4	51	Rodingite	1.6	0.6	30.2
21LAP-UCR-31.88-2C	21LAP-2C	4	52	Rodingite	1.6	0.6	31.9
21LAP-UCR-33.56-2C	21LAP-2C	4	53	Rodingite	1.6	0.6	33.6
21LAP-UCR-35.26-2C	21LAP-2C	4	54	Rodingite	1.6	0.6	35.3
21LAP-UCR-36.79-2C	21LAP-2C	4	55	Rodingite	1.6	0.6	36.8
21LAP-UCR-38.66-2C	21LAP-2C	4	55 RR	Rodingite	1.6	0.6	38.7
21LAP-UCR-6.17-2C	21LAP-2C	4	56	Rodingite	1.6	0.6	6.2
21LAP-UCR-8.70-2C	21LAP-2C	4	57	Rodingite	1.8	0.6	8.7
21LAP-UCR-10.96-2C	21LAP-2C	4	57 RR	Rodingite	1.8	0.6	11.0
21LAP-UCR-61.95-2C	21LAP-2C	4	59	Rodingite	5.6	0.6	61.9
21LAP-UCR-56.04-2C	21LAP-2C	4	60	Rodingite	5.6	0.6	56.0
21LAP-UCR-50.29-2C	21LAP-2C	4	61	Rodingite	5.6	0.6	50.3
21LAP-UCR-46.70-2C	21LAP-2C	4	62	Rodingite	1.6	0.6	46.7
21LAP-UCR-45.04-2C	21LAP-2C	4	63	Rodingite	1.6	0.6	45.0
21LAP-UCR-43.33-2C	21LAP-2C	4	64	Rodingite	1.6	0.6	43.3
21LAP-UCR-41.65-2C	21LAP-2C	4	65	Rodingite	1.6	0.6	41.6
21LAP-UCR-39.98-2C	21LAP-2C	4	66	Rodingite	1.6	0.6	40.0
21LAP-UCR-37.32-2C	21LAP-2C	4	66 RR	Rodingite	1.6	0.6	37.3
21LAP-UCR-206.94-2C	21LAP-2C	5	3	Rodingite	1.6	0.6	206.9
21LAP-UCR-205.40-2C	21LAP-2C	5	4	Rodingite	1.6	0.6	205.4
21LAP-UCR-203.59-2C	21LAP-2C	5	5	Rodingite	1.6	0.6	203.6
21LAP-UCR-199.85-2C	21LAP-2C	5	6	Rodingite	1.6	0.6	199.9
21LAP-UCR-194.25-2C	21LAP-2C	5	7	Rodingite	1.6	0.6	194.3
21LAP-UCR-188.62-2C	21LAP-2C	5	8	Rodingite	1.6	0.6	188.6
21LAP-UCR-182.69-2C	21LAP-2C	5	8 RR	Rodingite	1.6	0.6	182.7
21LAP-UCR-234.94-2C	21LAP-2C	5	9	Rodingite	3.3	0.6	234.9
21LAP-UCR-232.14-2C	21LAP-2C	5	10	Rodingite	2	0.6	232.1
21LAP-UCR-230.25-2C	21LAP-2C	5	11	Rodingite	1.6	0.6	230.3
21LAP-UCR-228.58-2C	21LAP-2C	5	12	Rodingite	1.6	0.6	228.6
21LAP-UCR-226.85-2C	21LAP-2C	5	13	Rodingite	1.6	0.6	226.8
21LAP-UCR-225.19-2C	21LAP-2C	5	14	Rodingite	1.6	0.6	225.2
21LAP-UCR-223.49-2C	21LAP-2C	5	15	Rodingite	1.6	0.6	223.5
21LAP-UCR-221.62-2C	21LAP-2C	5	16	Rodingite	1.6	0.6	221.6
21LAP-UCR-219.74-2C	21LAP-2C	5	17	Rodingite	1.6	0.6	219.7
21LAP-UCR-217.99-2C	21LAP-2C	5	18	Rodingite	1.6	0.6	218.0
21LAP-UCR-216.53-2C	21LAP-2C	5	19	Rodingite	1.6	0.6	216.5
21LAP-UCR-215.02-2C	21LAP-2C	5	20	Rodingite	1.6	0.6	215.0
21LAP-UCR-213.38-2C	21LAP-2C	5	21	Rodingite	1.6	0.6	213.4
21LAP-UCR-211.83-2C	21LAP-2C	5	22	Rodingite	1.6	0.6	211.8
21LAP-UCR-210.09-2C	21LAP-2C	5	23	Rodingite	1.7	0.6	210.1
21LAP-UCR-207.90-2C	21LAP-2C	5	23 RR	Rodingite	1.7	0.6	207.9
21LAP-LCS-21.60-2E	21LAP-2E	6	2	Serpentinite	1.4	0.6	289.8

Table 4

Sample Name	Hand Sample	Rod	Cut	Lithology	Increment Cut	Saw Kerf	Distance Along Transect
21LAP-LCS-23.01-2E	21LAP-2E	6	3	Serpentinite	1.4	0.6	291.2
21LAP-LCS-24.39-2E	21LAP-2E	6	4	Serpentinite	1.4	0.6	292.6
21LAP-LCS-25.85-2E	21LAP-2E	6	5	Serpentinite	1.5	0.6	294.0
21LAP-LCS-27.36-2E	21LAP-2E	6	6	Serpentinite	1.5	0.6	295.6
21LAP-LCS-28.84-2E	21LAP-2E	6	7	Serpentinite	1.5	0.6	297.0
21LAP-LCS-30.39-2E	21LAP-2E	6	8	Serpentinite	1.6	0.6	298.6
21LAP-LCS-32.03-2E	21LAP-2E	6	9	Serpentinite	1.6	0.6	300.2
21LAP-LCS-33.64-2E	21LAP-2E	6	10	Serpentinite	1.6	0.6	301.8
21LAP-LCS-35.24-2E	21LAP-2E	6	11	Serpentinite	1.6	0.6	303.4
21LAP-LCS-36.82-2E	21LAP-2E	6	12	Serpentinite	1.6	0.6	305.0
21LAP-LCS-38.62-2E	21LAP-2E	6	13	Serpentinite	1.6	0.6	306.8
21LAP-LCS-40.47-2E	21LAP-2E	6	14	Serpentinite	1.6	0.6	308.7
21LAP-LCS-42.03-2E	21LAP-2E	6	15	Serpentinite	1.6	0.6	310.2
21LAP-LCS-43.59-2E	21LAP-2E	6	16	Serpentinite	1.6	0.6	311.8
21LAP-LCS-45.22-2E	21LAP-2E	6	17	Serpentinite	1.6	0.6	313.4
21LAP-LCS-46.85-2E	21LAP-2E	6	18	Serpentinite	1.6	0.6	315.0
21LAP-LCS-48.60-2E	21LAP-2E	6	18 RR	Serpentinite	1.6	0.6	316.8
21LAP-LCR-6.68-2E	21LAP-2E	6	19	Rodingite	1.4	0.4	261.5
21LAP-LCR-3.59-2E	21LAP-2E	6	20	Rodingite	1.4	0.4	264.6
21LAP-LCR-1.98-2E	21LAP-2E	6	21	Rodingite	1.4	0.4	266.2
21LAP-LCR-1.20-2E	21LAP-2E	6	22	Rodingite	1.4	0.4	267.0
21LAP-LCC-0.86-2E	21LAP-2E	6	23	Contact	1.4	0.4	269.1
21LAP-LCS-2.36-2E	21LAP-2E	6	24	Serpentinite	1.4	0.4	270.6
21LAP-LCS-3.76-2E	21LAP-2E	6	25	Serpentinite	1.4	0.4	272.0
21LAP-LCS-5.16-2E	21LAP-2E	6	26	Serpentinite	1.4	0.4	273.4
21LAP-LCS-6.55-2E	21LAP-2E	6	27	Serpentinite	1.4	0.4	274.8
21LAP-LCS-7.95-2E	21LAP-2E	6	28	Serpentinite	1.4	0.4	276.2
21LAP-LCS-9.39-2E	21LAP-2E	6	29	Serpentinite	1.4	0.4	277.6
21LAP-LCS-10.84-2E	21LAP-2E	6	30	Serpentinite	1.4	0.4	279.0
21LAP-LCS-12.30-2E	21LAP-2E	6	31	Serpentinite	1.4	0.4	280.5
21LAP-LCS-13.75-2E	21LAP-2E	6	32	Serpentinite	1.4	0.4	282.0
21LAP-LCS-15.17-2E	21LAP-2E	6	33	Serpentinite	1.4	0.4	283.4
21LAP-LCS-16.56-2E	21LAP-2E	6	34	Serpentinite	1.4	0.4	284.8
21LAP-LCS-17.96-2E	21LAP-2E	6	35	Serpentinite	1.4	0.4	286.2
21LAP-LCS-20.29-2E	21LAP-2E	6	35 RR	Serpentinite	1.4	0.4	288.5
21LAP-LCS--74.12-2E	21LAP-2E	7	3	Serpentinite	1.6	0.6	338.8
21LAP-LCS-72.61-2E	21LAP-2E	7	4	Serpentinite	1.6	0.6	337.3
21LAP-LCS-70.95-2E	21LAP-2E	7	5	Serpentinite	1.6	0.6	335.6
21LAP-LCS-69.26-2E	21LAP-2E	7	6	Serpentinite	1.6	0.6	333.9
21LAP-LCS-67.70-2E	21LAP-2E	7	7	Serpentinite	1.6	0.6	332.4
21LAP-LCS-66.03-2E	21LAP-2E	7	8	Serpentinite	1.6	0.6	330.7
21LAP-LCS-64.37-2E	21LAP-2E	7	9	Serpentinite	1.6	0.6	329.0
21LAP-LCS-62.70-2E	21LAP-2E	7	10	Serpentinite	1.6	0.6	327.4

Table 4

Sample Name	Hand Sample	Rod	Cut	Lithology	Increment Cut	Saw Kerf	Distance Along Transect
21LAP-LCS-61.06-2E	21LAP-2E	7	11	Serpentinite	1.6	0.6	325.7
21LAP-LCS-59.57-2E	21LAP-2E	7	12	Serpentinite	1.6	0.6	324.2
21LAP-LCS-58.05-2E	21LAP-2E	7	13	Serpentinite	1.6	0.6	322.7
21LAP-LCS-56.46-2E	21LAP-2E	7	14	Serpentinite	1.6	0.6	321.1
21LAP-LCS-54.82-2E	21LAP-2E	7	15	Serpentinite	1.6	0.6	319.5
21LAP-LCS-53.20-2E	21LAP-2E	7	16	Serpentinite	1.6	0.6	317.9
21LAP-LCS-51.60-2E	21LAP-2E	7	17	Serpentinite	1.6	0.6	316.3
21LAP-LCS-49.91-2E	21LAP-2E	7	18	Serpentinite	1.6	0.6	314.6
21LAP-LCS-47.40-2E	21LAP-2E	7	18 RR	Serpentinite	1.6	0.6	312.1
21LAP-LCS-107.51-2E	21LAP-2E	7	19	Serpentinite	1.6	0.6	372.0
21LAP-LCS-102.45-2E	21LAP-2E	7	20	Serpentinite	1.6	0.6	366.9
21LAP-LCS-100.85-2E	21LAP-2E	7	21	Serpentinite	1.6	0.6	365.3
21LAP-LCS-99.27-2E	21LAP-2E	7	22	Serpentinite	1.6	0.6	363.7
21LAP-LCS-97.73-2E	21LAP-2E	7	23	Serpentinite	1.6	0.6	362.2
21LAP-LCS-96.27-2E	21LAP-2E	7	24	Serpentinite	1.6	0.6	360.7
21LAP-LCS-94.77-2E	21LAP-2E	7	25	Serpentinite	1.6	0.6	359.2
21LAP-LCS-93.16-2E	21LAP-2E	7	26	Serpentinite	1.6	0.6	357.6
21LAP-LCS-91.52-2E	21LAP-2E	7	27	Serpentinite	1.6	0.6	356.0
21LAP-LCS-89.78-2E	21LAP-2E	7	28	Serpentinite	1.6	0.6	354.3
21LAP-LCS-88.08-2E	21LAP-2E	7	29	Serpentinite	1.6	0.6	352.5
21LAP-LCS-86.50-2E	21LAP-2E	7	30	Serpentinite	1.6	0.6	351.0
21LAP-LCS-85.02-2E	21LAP-2E	7	31	Serpentinite	1.6	0.6	349.5
21LAP-LCS-83.50-2E	21LAP-2E	7	32	Serpentinite	1.6	0.6	348.0
21LAP-LCS-81.95-2E	21LAP-2E	7	33	Serpentinite	1.6	0.6	346.4
21LAP-LCS-80.30-2E	21LAP-2E	7	34	Serpentinite	1.6	0.6	344.8
21LAP-LCS-78.52-2E	21LAP-2E	7	35	Serpentinite	1.6	0.6	343.0
21LAP-LCS-76.81-2E	21LAP-2E	7	36	Serpentinite	1.6	0.6	341.3
21LAP-LCS-75.18-2E	21LAP-2E	7	36 RR	Serpentinite	1.6	0.6	339.6

Table 5

Sample Name	Hand Sample	Cut	Lithology	Increment Cut	Saw Kerf	Distance Along Transect
PAV-2D-S-18.2	PAV-2D	19 RR	Serpentinite	1.4	0.36	-31.1
PAV-2D-S-18.1	PAV-2D	19	Serpentinite	1.4	0.36	-29.7
PAV-2D-S-17	PAV-2D	18	Serpentinite	1.4	0.36	-28.3
PAV-2D-S-16	PAV-2D	17	Serpentinite	1.4	0.36	-26.9
PAV-2D-S-15	PAV-2D	16	Serpentinite	1.4	0.36	-25.5
PAV-2D-S-14	PAV-2D	15	Serpentinite	1.4	0.36	-24.1
PAV-2D-S-13	PAV-2D	14	Serpentinite	1.4	0.36	-22.7
PAV-2D-S-12	PAV-2D	13	Serpentinite	1.4	0.36	-21.3
PAV-2D-S-11	PAV-2D	12	Serpentinite	1.4	0.36	-19.9
PAV-2D-S-10	PAV-2D	11	Serpentinite	1.4	0.36	-18.5
PAV-2D-S-9	PAV-2D	10	Serpentinite	1.4	0.36	-17.1
PAV-2D-S-8	PAV-2D	9	Serpentinite	1.4	0.36	-15.7
PAV-2D-S-7	PAV-2D	8	Serpentinite	1.4	0.36	-14.5
PAV-2D-S-6	PAV-2D	7	Serpentinite	1.4	0.36	-13.0
PAV-2D-S-5	PAV-2D	6	Serpentinite	1.4	0.36	-11.5
PAV-2D-S-4	PAV-2D	5	Serpentinite	1.5	0.36	-10.0
PAV-2D-S-3	PAV-2D	4	Serpentinite	1.4	0.36	-8.7
PAV-2D-S-2	PAV-2D	3	Serpentinite	1.4	0.36	-7.4
PAV-2D-S-1	PAV-2D	2	Serpentinite	1.5	0.36	-5.9
PAV-2D-S-19	PAV-2D	20	Serpentinite	1.4	0.36	-3.2
PAV-2D-S-20	PAV-2D	21	Serpentinite	1.4	0.36	-1.8
PAV-2D-S-21	PAV-2D	22	Serpentinite	1.4	0.36	-0.8
PAV-2D-S/R-22	PAV-2D	23	Contact	1.4	0.36	0.0
PAV-2D-R-23	PAV-2D	24	Rodingite	1.4	0.36	0.9
PAV-2D-R-24	PAV-2D	25	Rodingite	1.4	0.36	1.8
PAV-2D-R-25.1	PAV-2D	26	Rodingite	1.4	0.36	3.2
PAV-2D-R-25.2	PAV-2D	26 RR	Rodingite	1.4	0.36	4.6
PAV-2D-R-26	PAV-2D	27	Rodingite	1.4	0.36	7.6
PAV-2D-R-27	PAV-2D	28	Rodingite	1.4	0.36	9.1
PAV-2D-R-28	PAV-2D	29	Rodingite	1.4	0.36	10.5
PAV-2D-R-29	PAV-2D	30	Rodingite	1.4	0.36	11.9
PAV-2D-R-30	PAV-2D	31	Rodingite	1.4	0.36	13.3
PAV-2D-R-31	PAV-2D	32	Rodingite	1.4	0.36	14.7
PAV-2D-R-32	PAV-2D	33	Rodingite	1.4	0.36	16.1
PAV-2D-R-33	PAV-2D	34	Rodingite	1.4	0.36	17.6
PAV-2D-R-34	PAV-2D	35	Rodingite	1.4	0.36	19.0
PAV-2D-R-35	PAV-2D	36	Rodingite	1.4	0.36	20.4
PAV-2D-R-36.1	PAV-2D	37	Rodingite	1.4	0.36	21.8
PAV-2D-R-36.2	PAV-2D	37 RR	Rodingite	1.4	0.36	22.1

Thin Section Photo Compilations

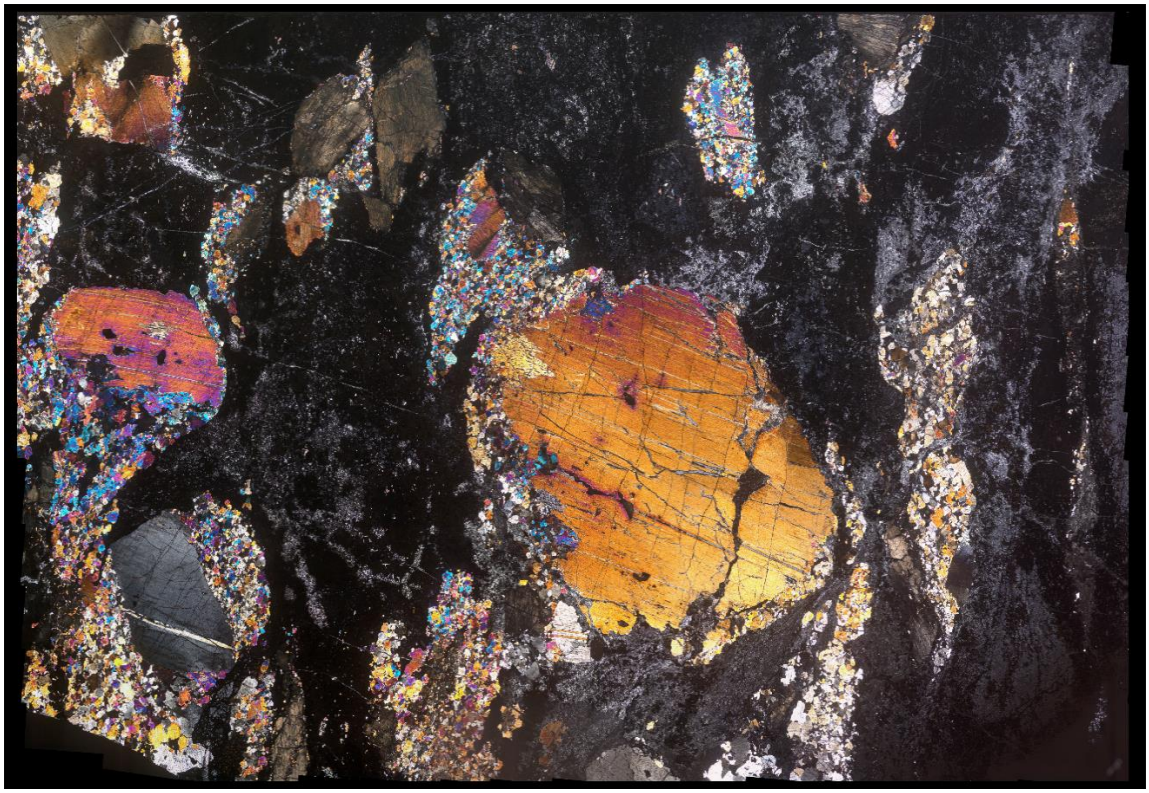

Figure S2. Thin section photo compilation of 21LAP-2C-1 in XPL, a rodingite thin section taken from the interior of the Bargone rodingite dike. Large psuedomorphed grains of diopside displaying second-order and first-order interference colors are present within a groundmass of fine-grained garnet (isotropic) and chlorite (low first-order gray) and display variable alteration. Fine-grained garnet is also present within the fractures defined by cpx cleavage planes. Discontinuous bands of diopside, plagioclase, and vesuvianite precipitations are present in the matrix and are generally parallel to the contact. They also display deformation mechanics around large pyroxene grains.

Figure S3. Thin section photo compilation of 21LAP-2C-1 in PPL. Garnet is pale to dark brown and intergrown with clear chlorite. Precipitated and psuedomorphed diopside are light brown, although more heavily altered diopside is darker in color.

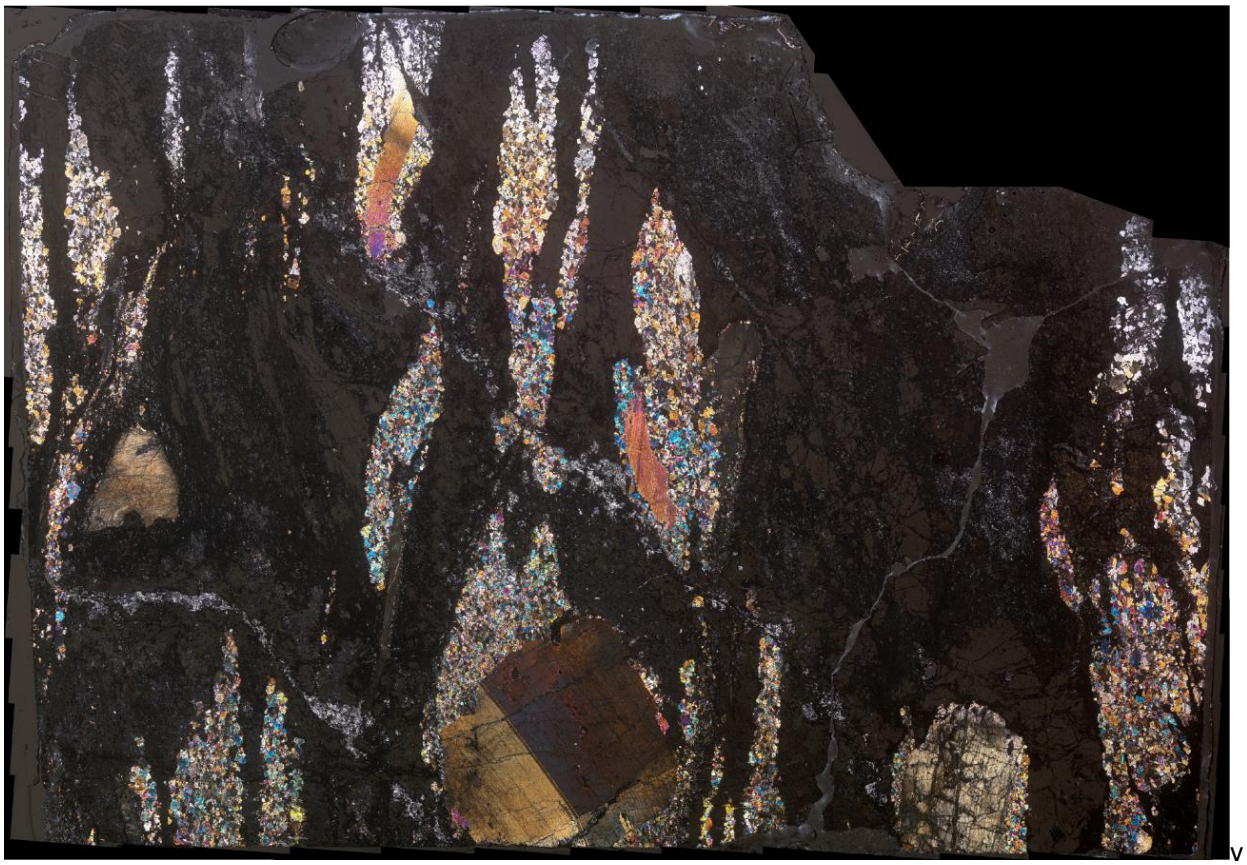

Figure S4. Thin section photo compilation of 21LAP-2C-2 in XPL, a thin section taken from the interior of the Bargone rodingite dike. Ground mass is composed predominantly of garnet (isotropic) with minor chlorite. Discontinuous bands of hydrothermal diopside, plagioclase, and vesuvianite are present and predominantly parallel to the contact. Two bands notably encase deformed and altered diopside grains. Large, psuedomorphed diopside grains display second-order and first-order interference colors. Some hydrogarnets display slight birefringence, a product of their high water contents.

Figure S5. Thin section photo compilation of 21LAP-2C-2 in PPL. Garnet grains are present with both dark-brown and pale-brown coloring, presenting the possibility of two generations of garnet. Lighter garnets are more idiomorphic and correlate to areas with mild birefringence in Figure S3. Large, psuedomorphed diopside grains are a darker brown than the diopside present in the contact-parallel bands.

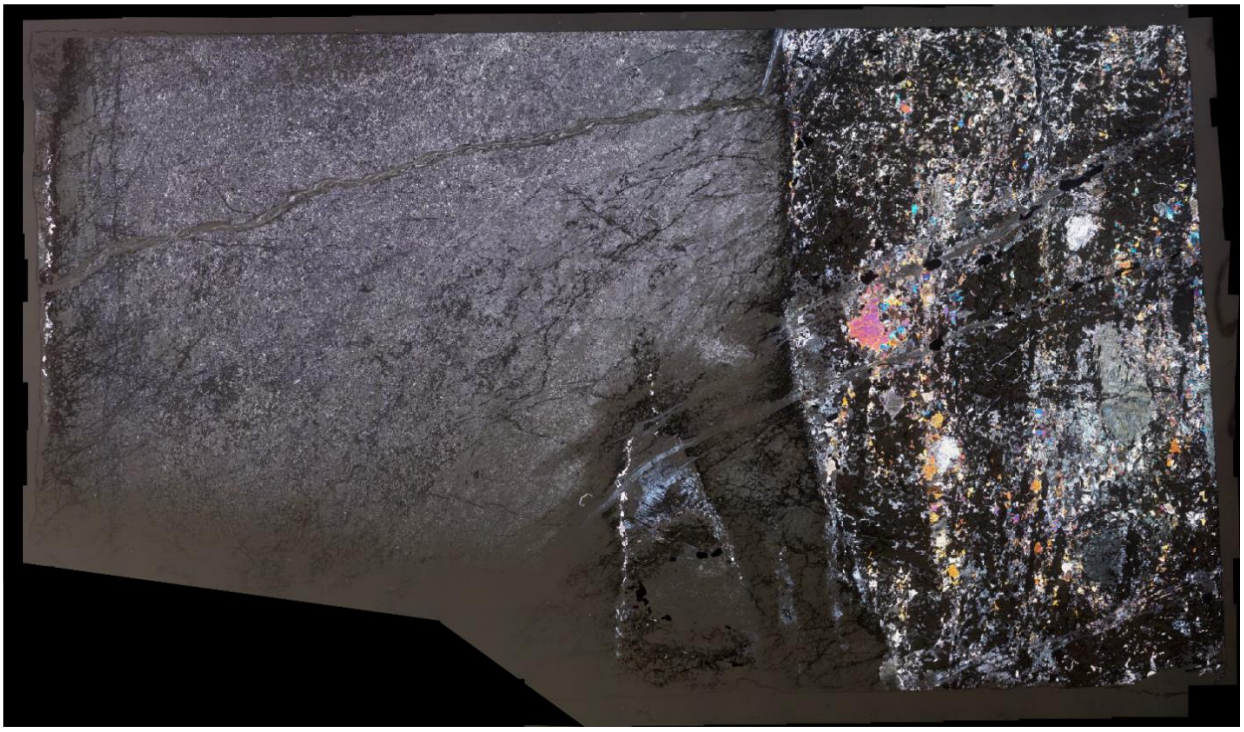

Figure S6. Thin section photo compilation of 21LAP-2Dc in XPL of the Upper Contact (UC) of the Bargone transect. The contact between serpentinite (left) and rodingite (right) is sharp, but irregular. However, some fine-grained garnet has developed along veins infiltrating the serpentinite. Serpentinite veins are also observed traversing the contact from the serpentinite into the rodingite. The serpentinite is composed largely of serpentine with additional chlorite and magnetite. Serpentinite near the contact displays ribbon textures and mild blue birefringence. Rodingite mineralogy includes garnet + chlorite + diopside + serpentine with additional magnetite. Garnets are uniquely euhedral to subhedral compared to the rest of the rodingite dike. Diopside displays second-order interference colors.

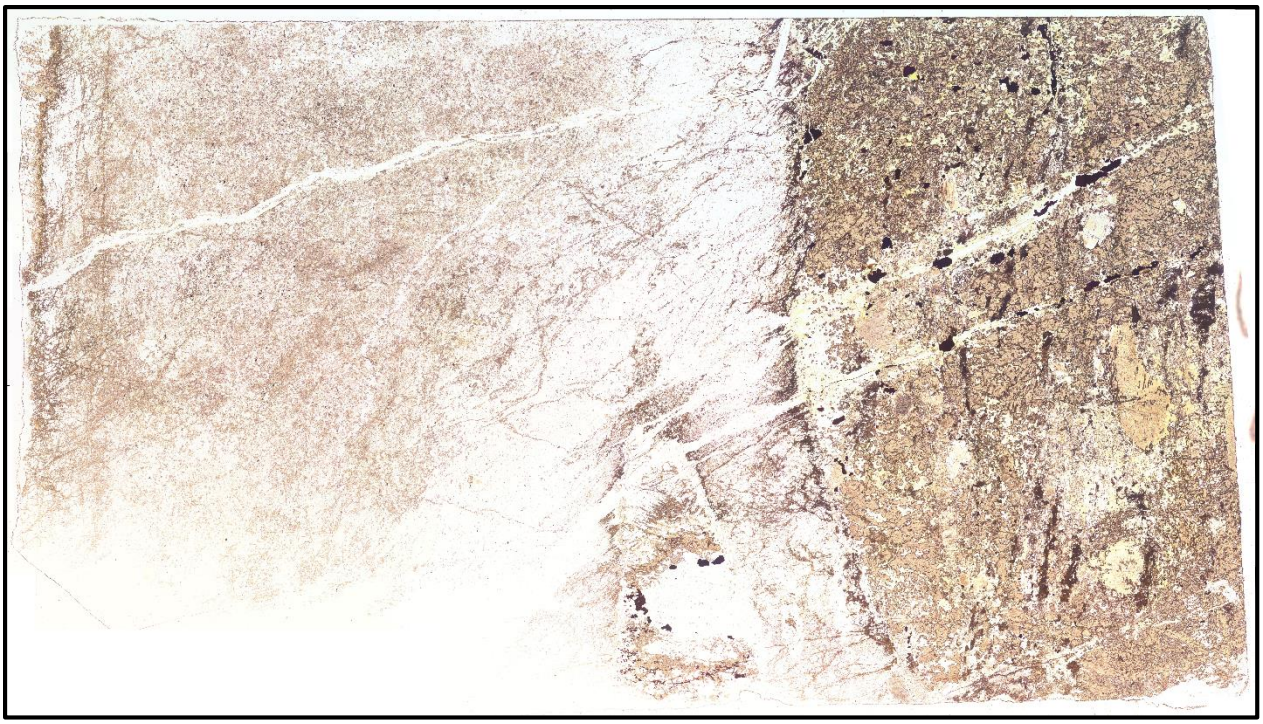

Figure S7. Thin section photo compilation of 21LAP-2Dc in PPL. Serpentine is clear to pale brown within the serpentinite and rodingite. Fine-grained chlorite is clear and pervasive within the serpentinite. Garnets are brown and do not display color variation. Diopside is present as pale brown hydrothermally precipitated grains (no psuedomorphed grains are present).

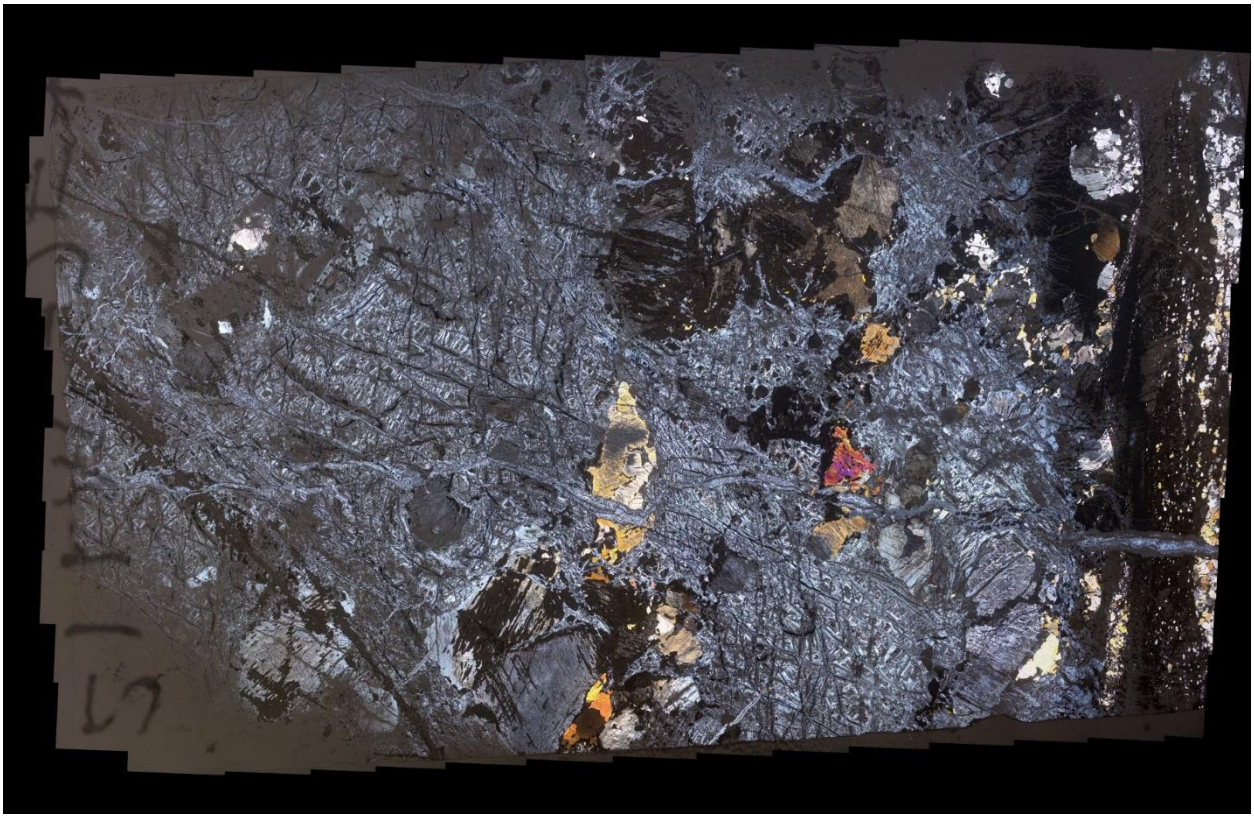

Figure S8. Thin section photo compilation of 21LAP-2Ec in XPL of the Lower Contact (LC) of the Bargone transect. The LC is more diffuse than the UC; mineralogy grades from garnet (isotropic) and diopside (first-order interference colors) to ribbon-textured serpentine. Large grains of altered diopside (first-order and second-order interference colors) with garnet overgrowths are present within the serpentinite matrix. Garnet veins are observed throughout the serpentinite matrix. Serpentine displays first-order gray and mild Berlin-blue interference colors.

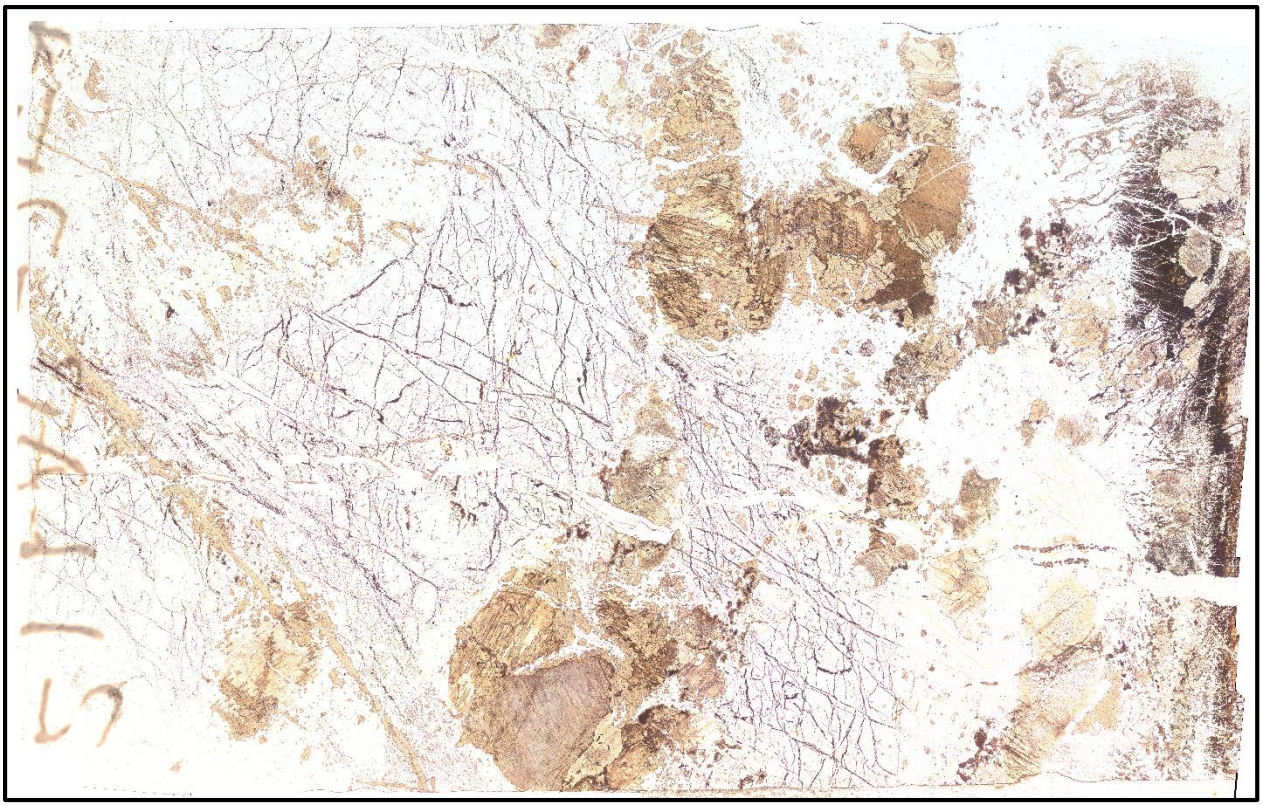

Figure S9. Thin section photo compilation 21LAP-2Ec in PPL of the Bargone LC. Colorless serpentine makes up the serpentinite matrix. Brown diopside grains with slightly paler brown garnet growths are present within the serpentinite. Garnet present near the contact is a darker brown and more fine-grained. Brown garnet growth along veins is observed throughout the interior of the serpentinite.

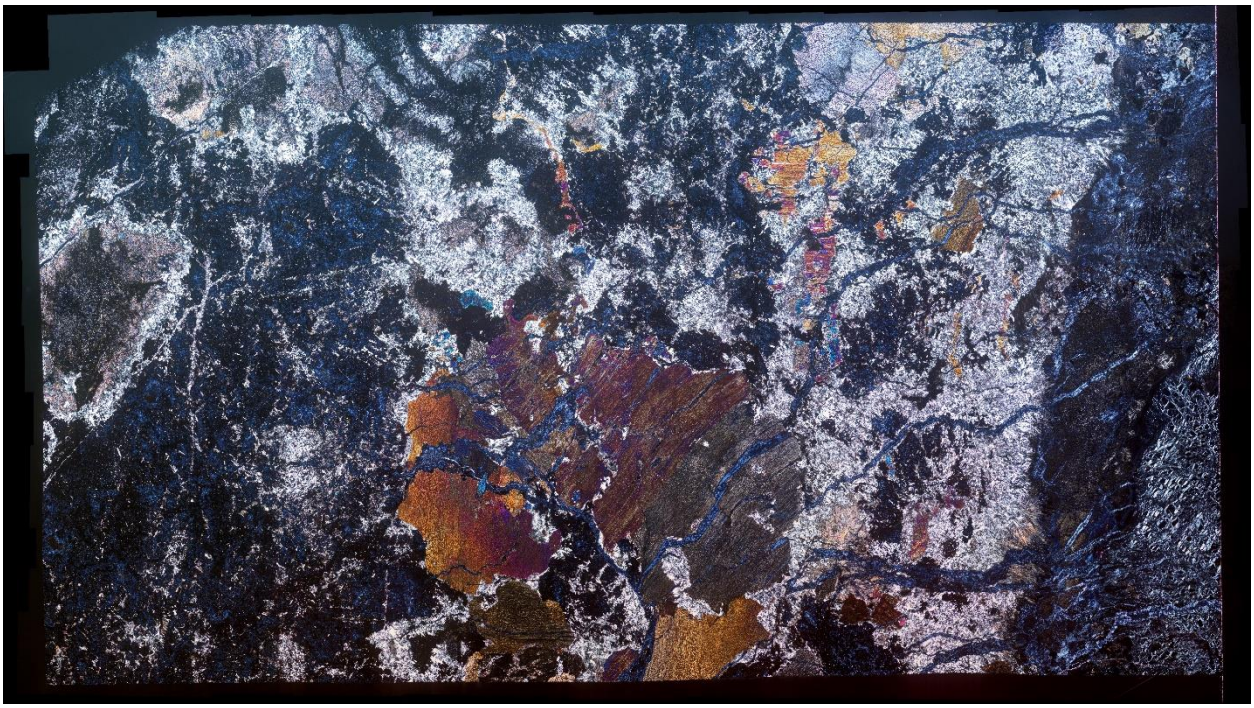

Figure S10. Thin section photo compilation of PAV-2D-1 in XPL showing the rodingite (left) – serpentinite (right) contact. Rodingite matrix is composed of garnet (isotropic), chlorite (first-order gray), and serpentinite (Berlin-blue interference colors). Diopside is present as hydrothermal precipitations or large psuedomorphed grains. Psuedomorphed grains of diopside show varying degrees of alteration, where some grains display reaction rims of chlorite alteration. Fine-grained precipitations of garnet are present within cleavage planes of diopside grains. Veins of serpentine transverse the lithologic contact and crosscut diopside grains. Serpentinite is mainly composed of ribbon-textured serpentine, with garnet growth present close to the contact.

Figure S11. Thin section photo of PAV-2D-1 in PPL. Garnets are dark-brown to black and display patchy disseminated textures. Chlorite and serpentine are both clear, although serpentine is accompanied by fine-grained magnetite. Both psuedomorphed and precipitated diopside is brown.

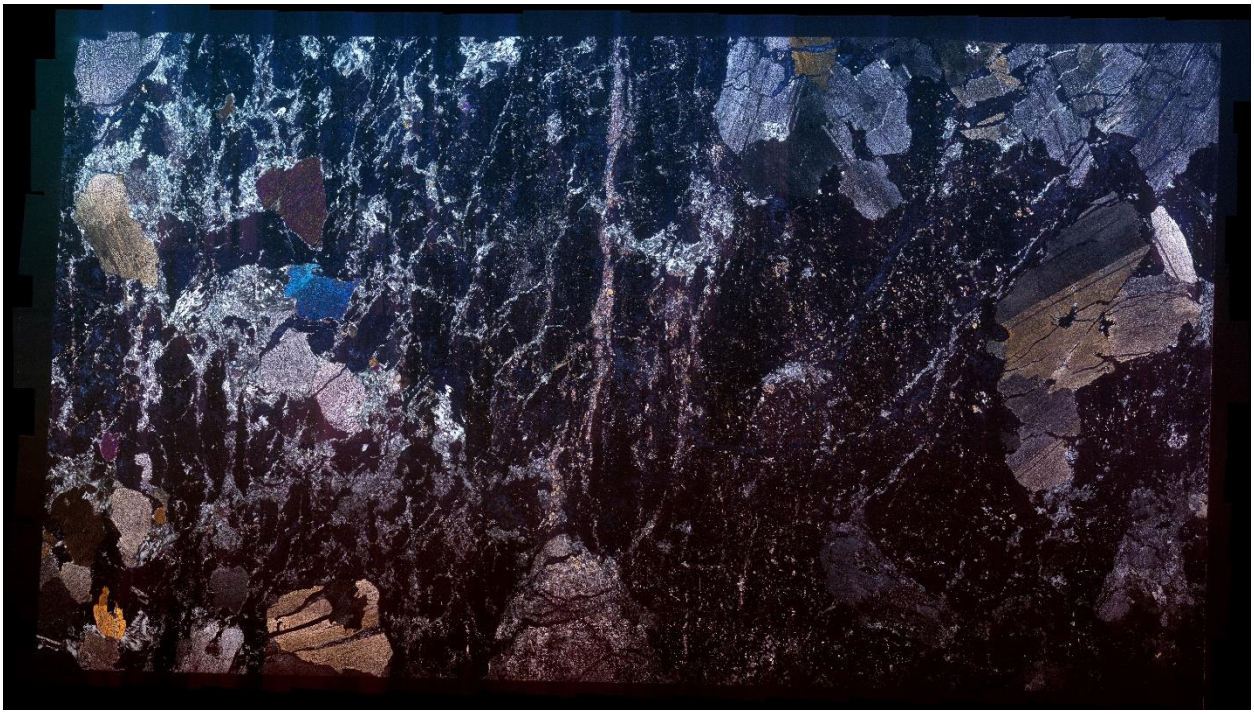

Figure S12. Thin section photo compilation of PAV-2D-2 in XPL, showing the interior of the Pavareto rodingite. The matrix is predominantly isotropic garnet with minor chlorite and serpentine. Psuedomorphed diopside displays first-order and second-order interference colors. Vein networks of diopside and chlorite have developed towards the interior of the rodingite and are overwhelmingly parallel to the contact. Minor amounts of hydrothermal titanite are present.

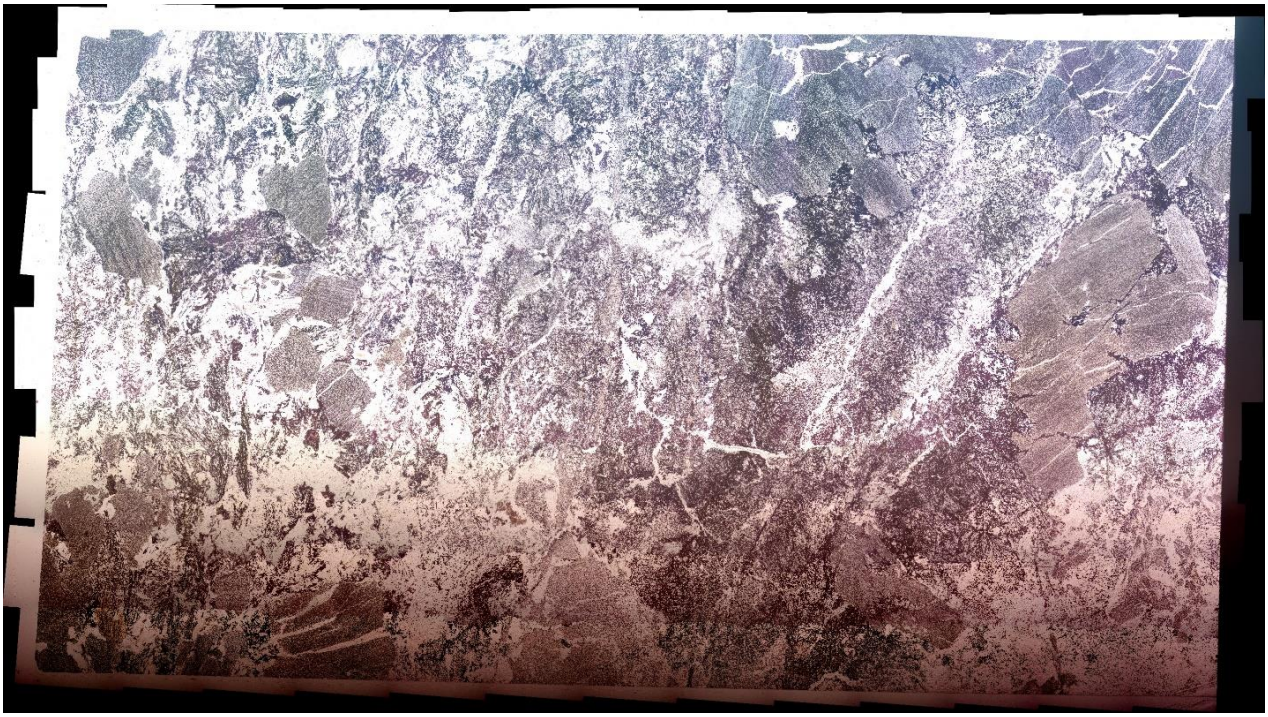

Figure S13. Thin section photo compilation of PAV-2D-2 in PPL. Garnets are brown to black and display amorphous growth. Titanite is brown in thin section and displays high relief. Stress-related fractures are observed infilled with clear chlorite and serpentine growth.

PAV-2D BSE Maps

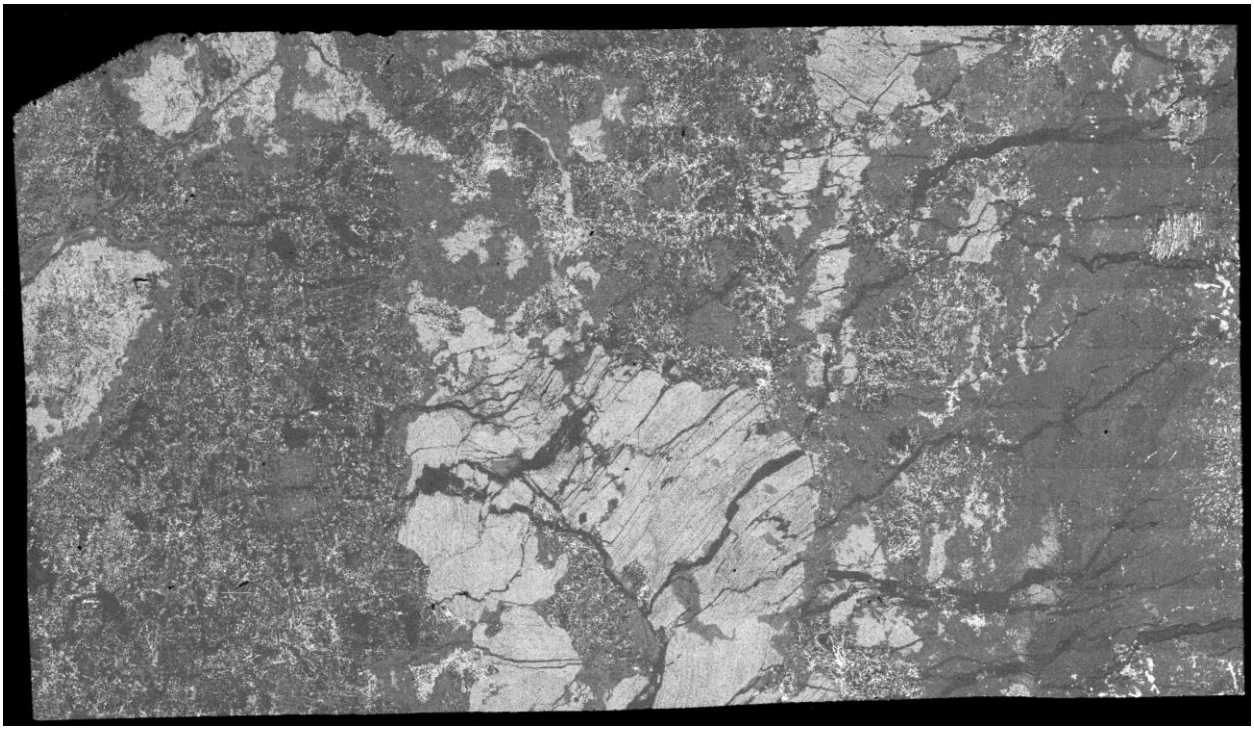

Figure S14. BSE map of PAV-2D-1. Fine-grained garnet is visibly the palest, followed by diopside. Serpentine is slightly darker than chlorite. Garnet was identified as andradite.

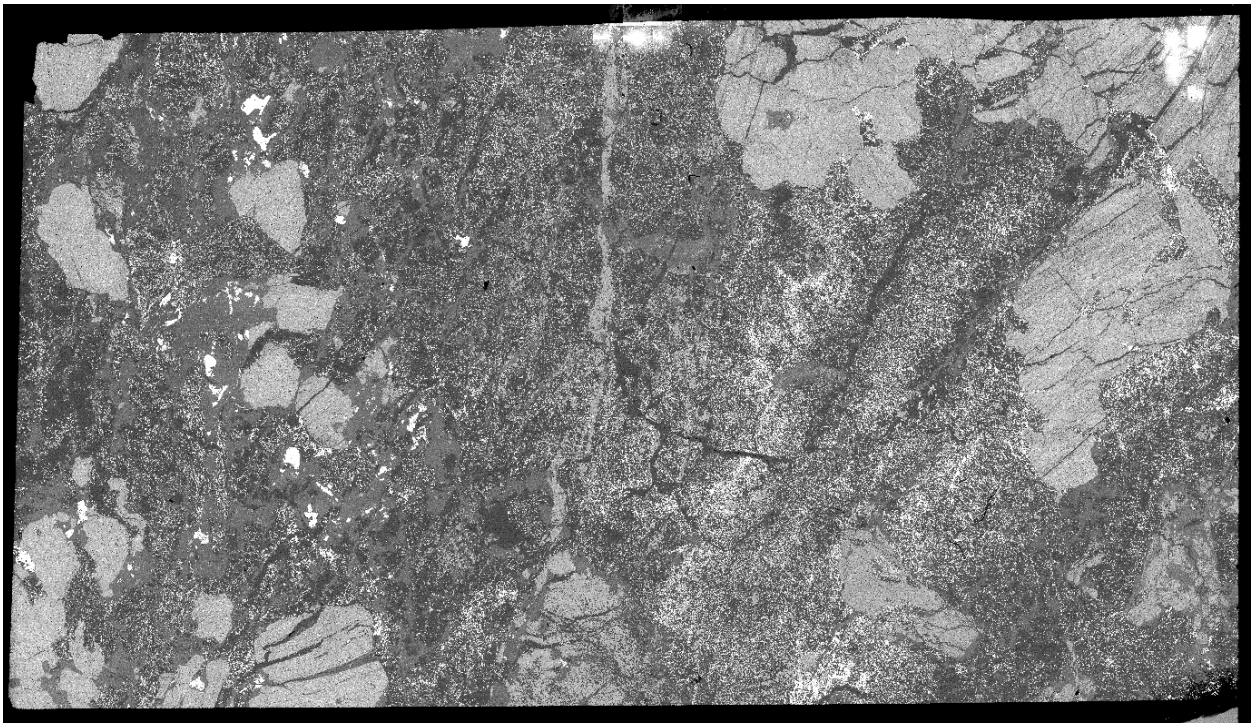

Figure S15. BSE map of PAV-2D-2. Hydrothermal titanite is the brightest mineral identified. Pale, fine-grained garnet displays extremely patchy textures, along with chlorite and serpentine. Garnet was identified as andradite.

PAV-2D BSE Reports

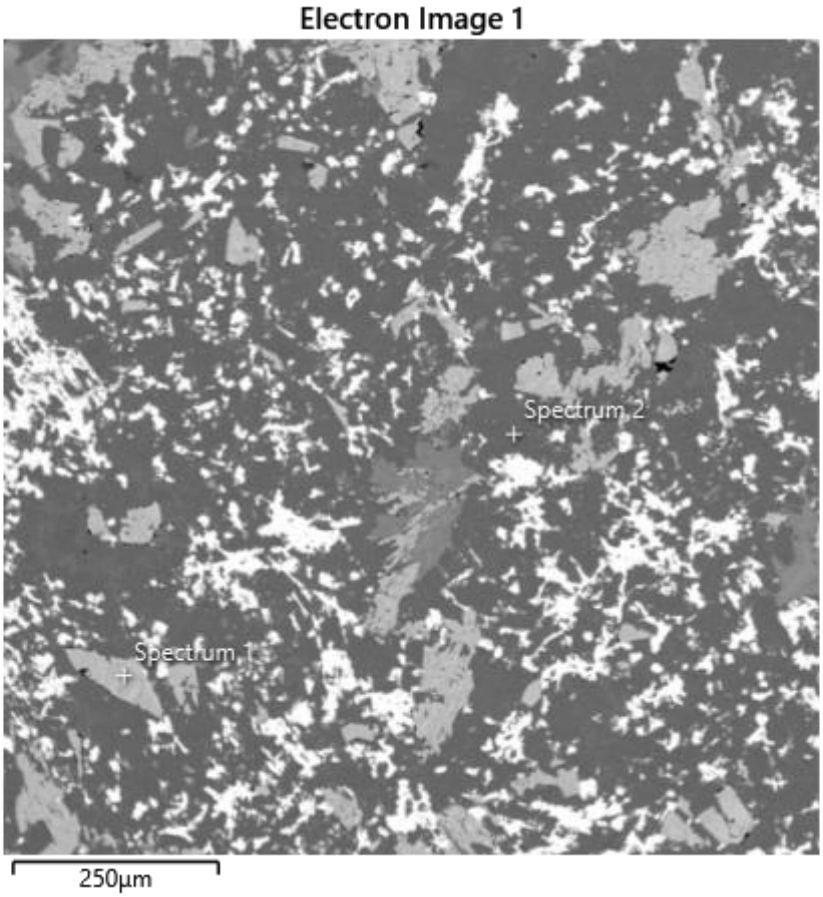

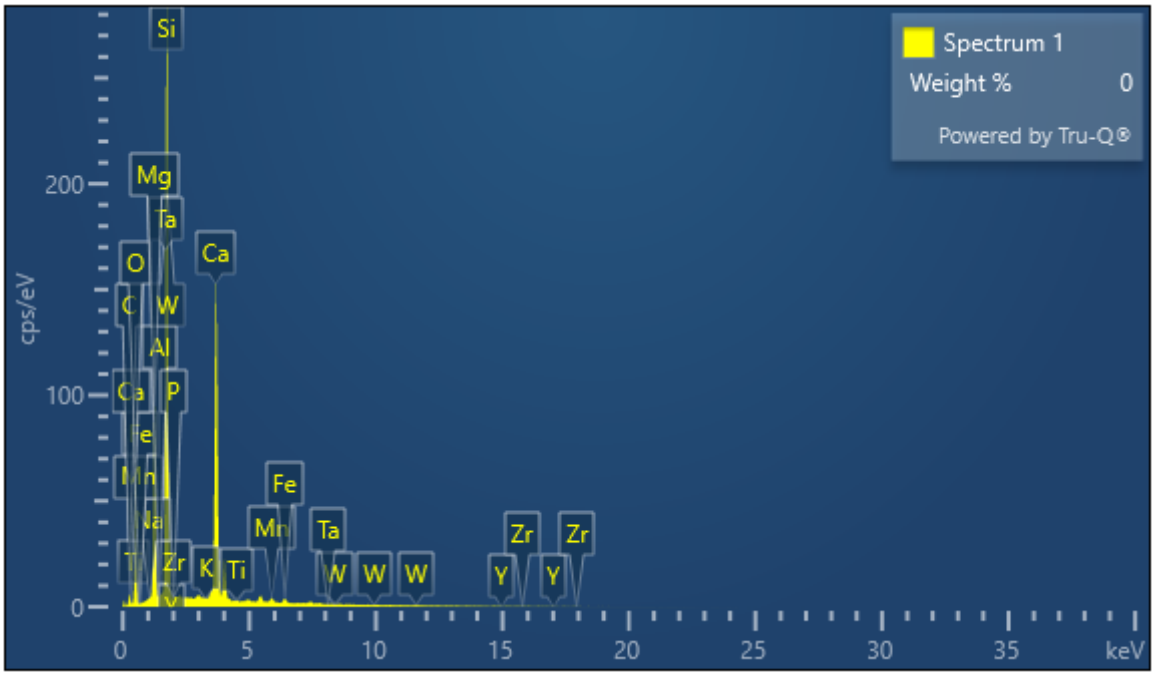

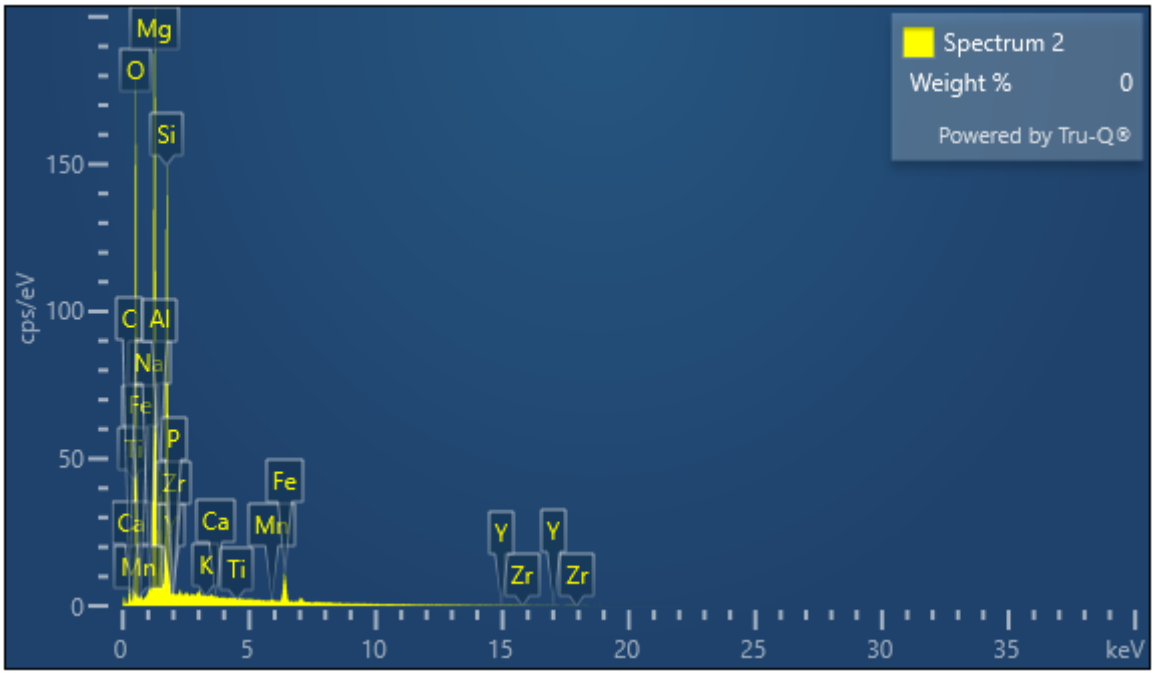
Spectrum 2
Weight % 0
Powered by Tru-Q®
cps/eV
150
100
50
0
0
5
10
15
20
25
30
35
keV
Mg
O
Si
C
Al
Na
Fe
Ti
P
Zr
Ca
Mn
Ca
K
Ti
Fe
Mn
Y
Zr
Y
Zr

Electron Image 2

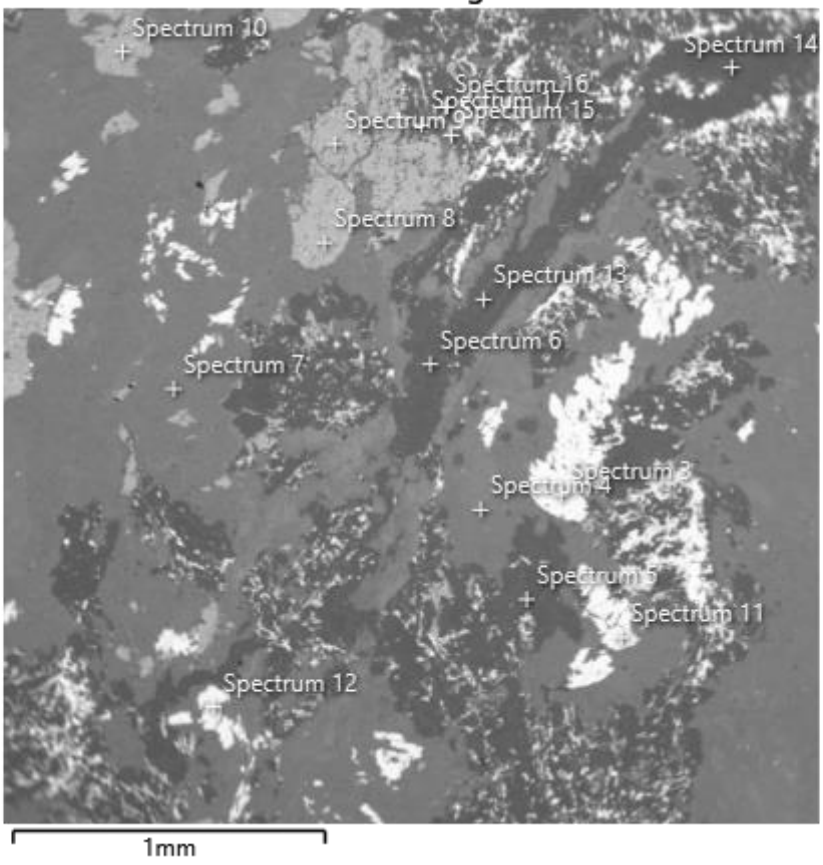

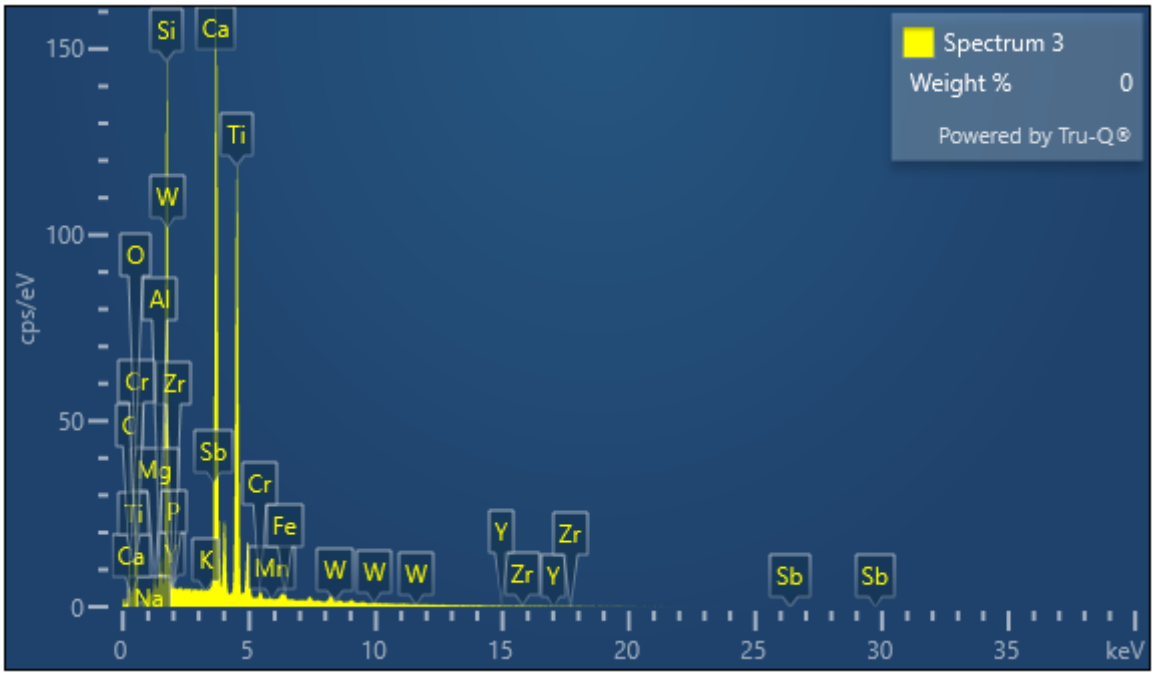

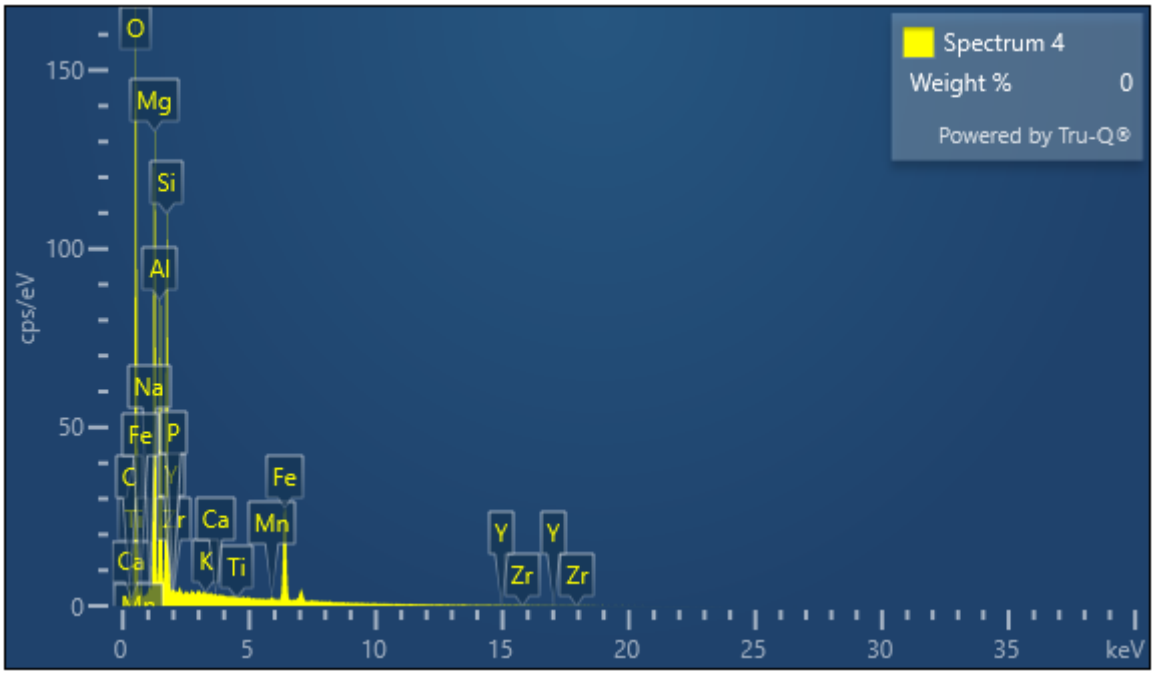
Spectrum 4
Weight % 0
Powered by Tru-Q®
cps/eV
keV
O
Mg
Si
Al
Na
Fe
P
C
Ca
K
Ti
Mn
Y
Zr

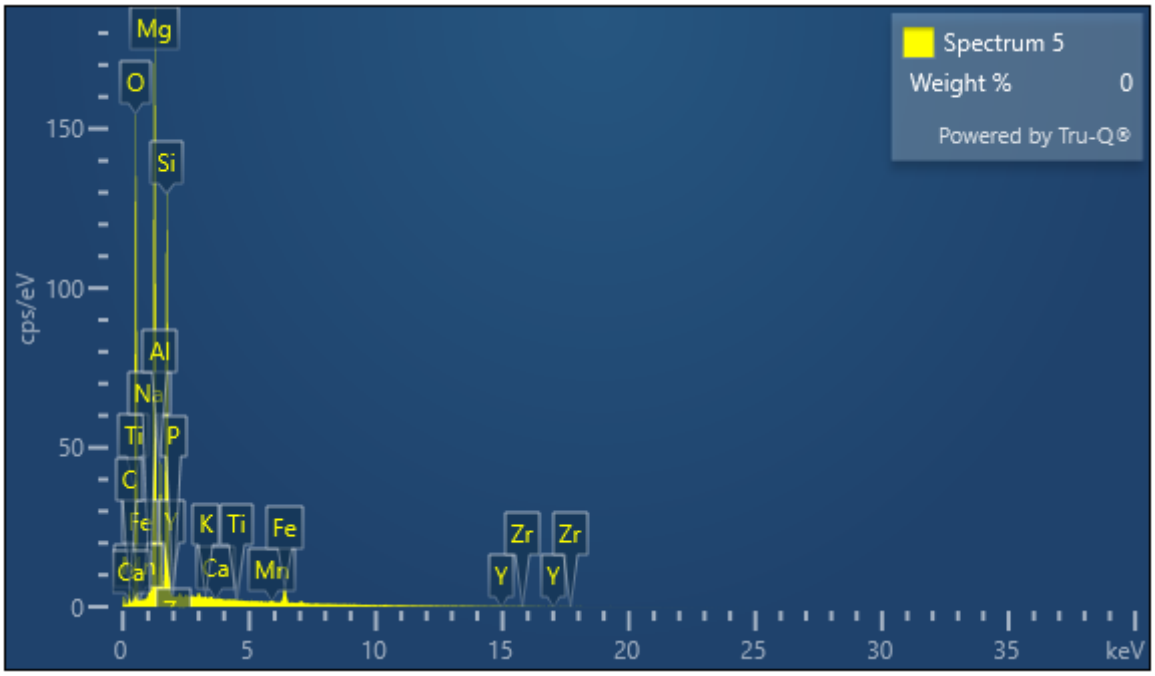
Spectrum 5
Weight % 0
Powered by Tru-Q®
cps/eV
keV
Mg
O
Si
Al
Na
Ti
P
C
K
Fe
Ca
Mn
Zr
Y

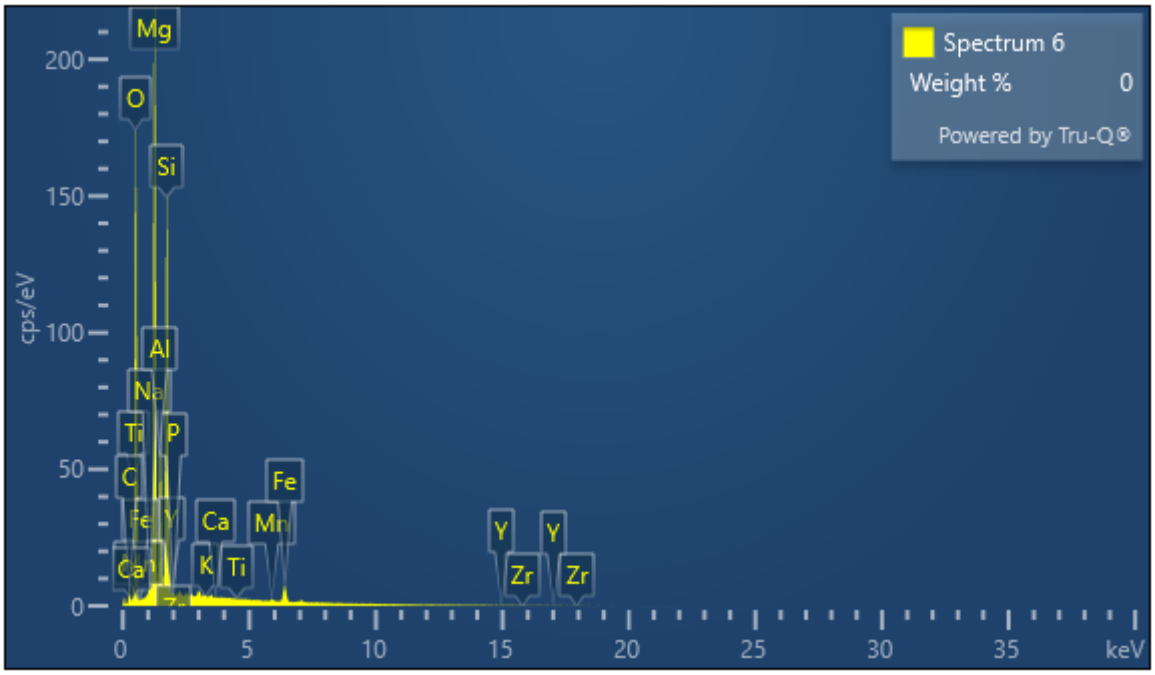
Spectrum 6
Weight % 0
Powered by Tru-Q®
cps/eV
keV
Mg
O
Si
Al
Na
Ti
P
C
Fe
Ca
Mn
K
Y
Zr

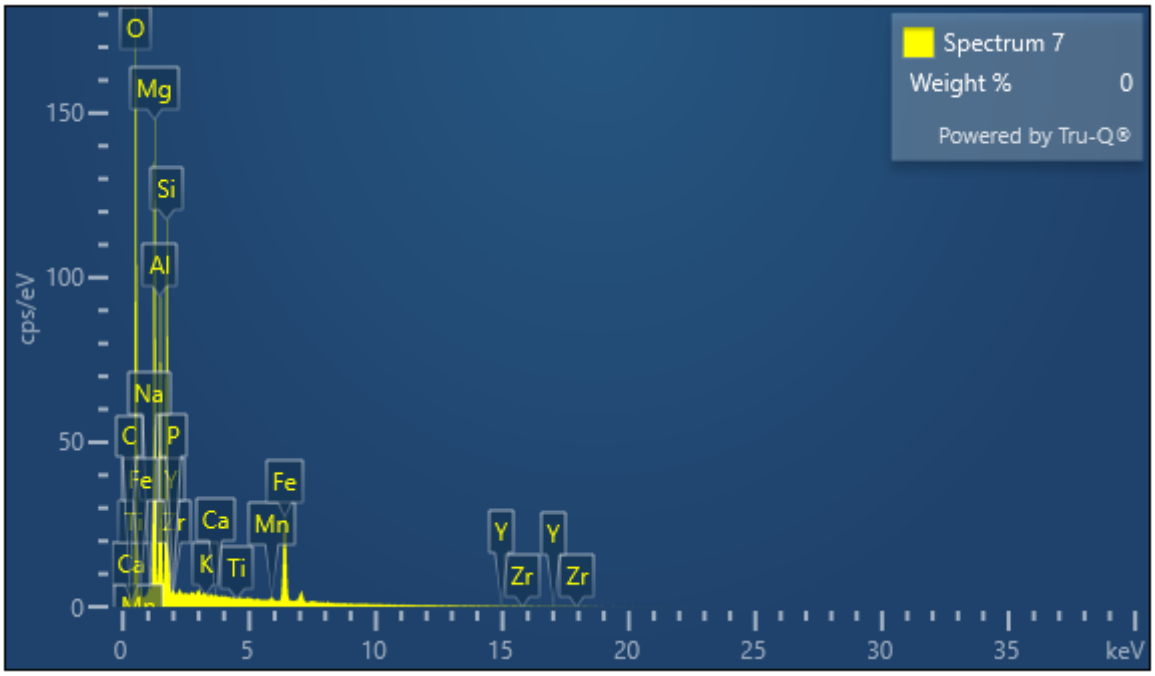
Spectrum 7
Weight % 0
Powered by Tru-Q®
cps/eV
keV
O
Mg
Si
Al
Na
C
P
Fe
Ca
K
Ti
Mn
Y
Zr

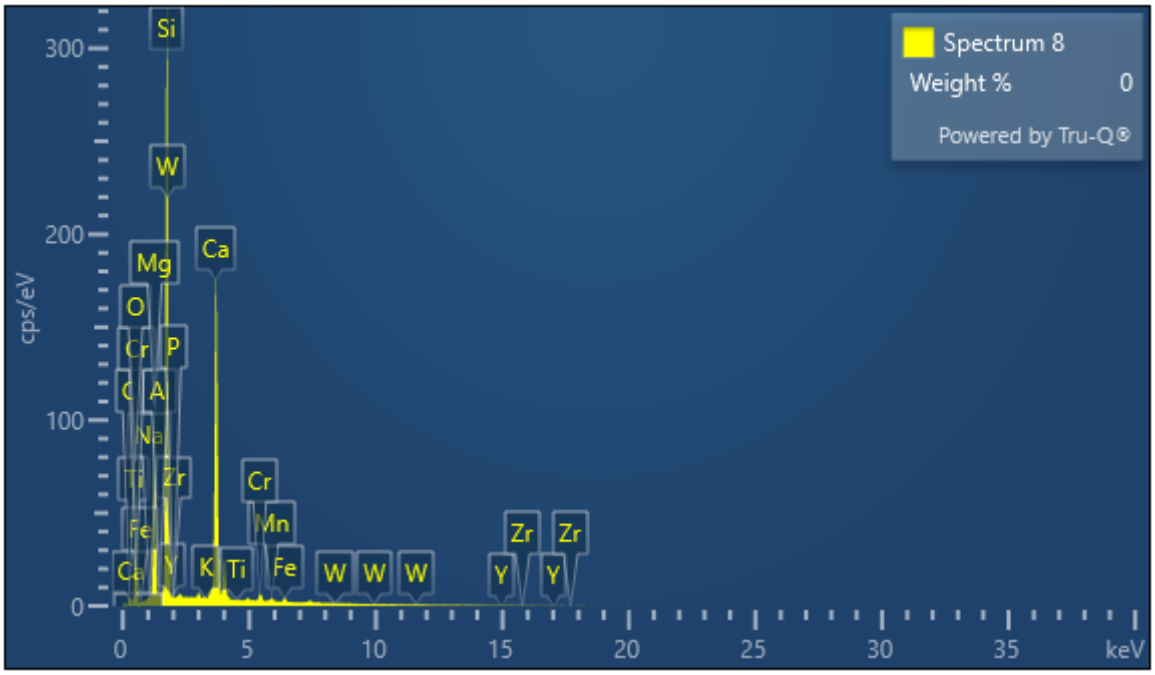
Spectrum 8
Weight % 0
Powered by Tru-Q®
cps/eV
keV
Si
W
Mg
Ca
O
Cr
P
C
Al
Na
Ti
Zr
Mn
Fe
K
Y

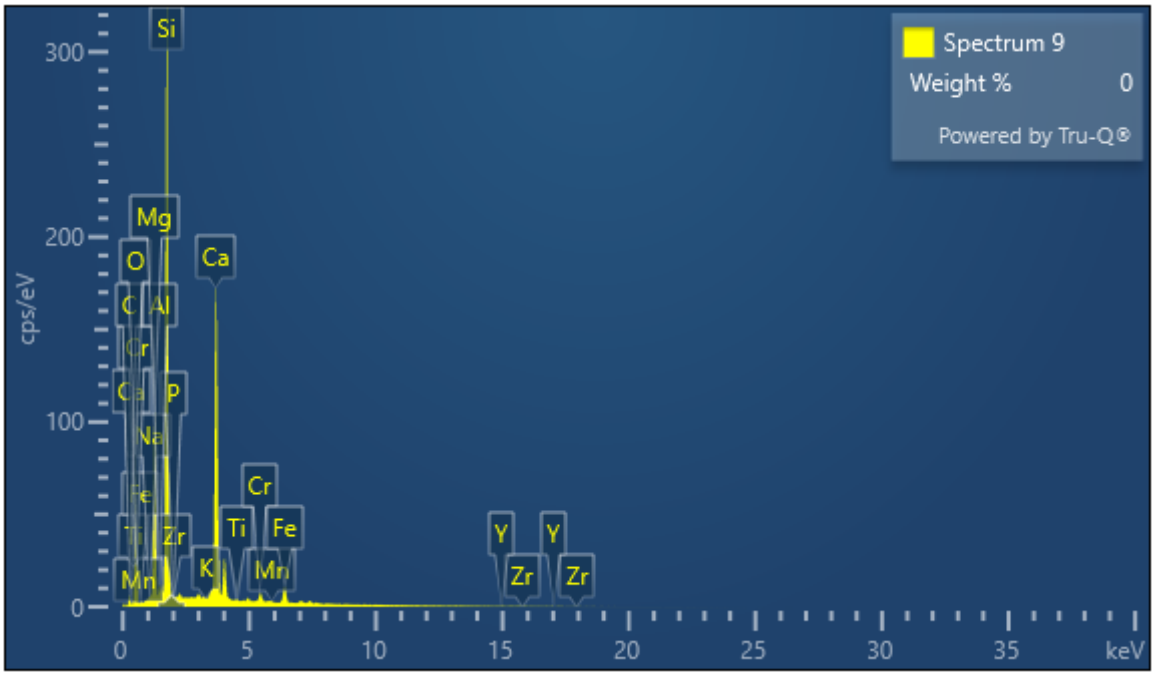
Spectrum 9
Weight % 0
Powered by Tru-Q®
cps/eV
keV
Si
Mg
Ca
O
C
Al
Cr
P
Na
Fe
Ti
Zr
Mn
K
Y

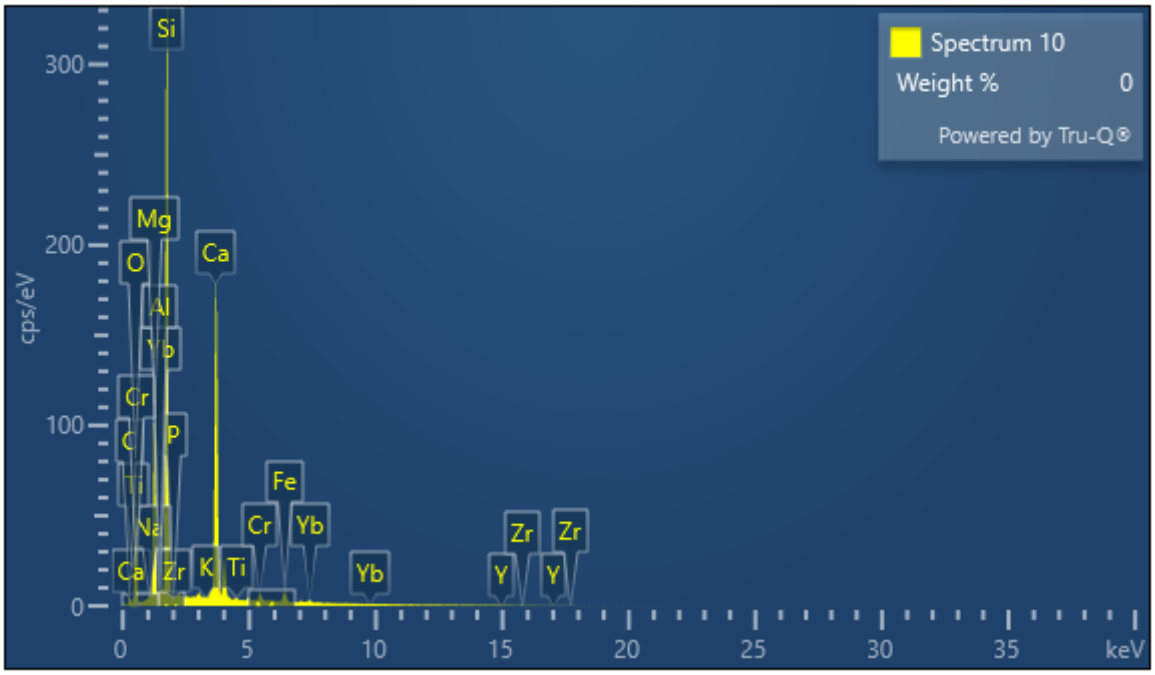
Spectrum 10
Weight % 0
Powered by Tru-Q®
cps/eV
keV
Si
Mg
O
Ca
Al
Cr
C
P
Fe
Cr
Yb
Zr
Zr
Na
Ca
Zr
K
Ti
Yb
Y
Y

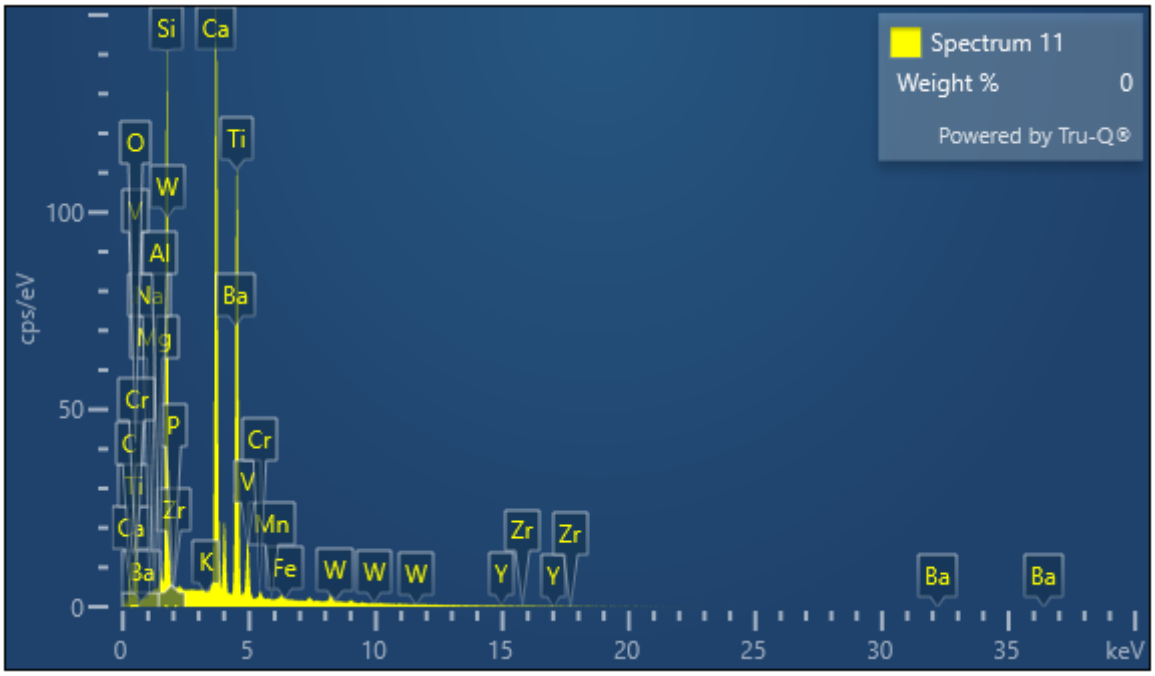
Spectrum 11
Weight % 0
Powered by Tru-Q®
cps/eV
keV
Si
Ca
O
Ti
W
Al
Ba
Cr
C
P
Cr
V
Zr
Mn
K
Fe
W
W
W
Zr
Zr
Y
Y
Ba
Ba

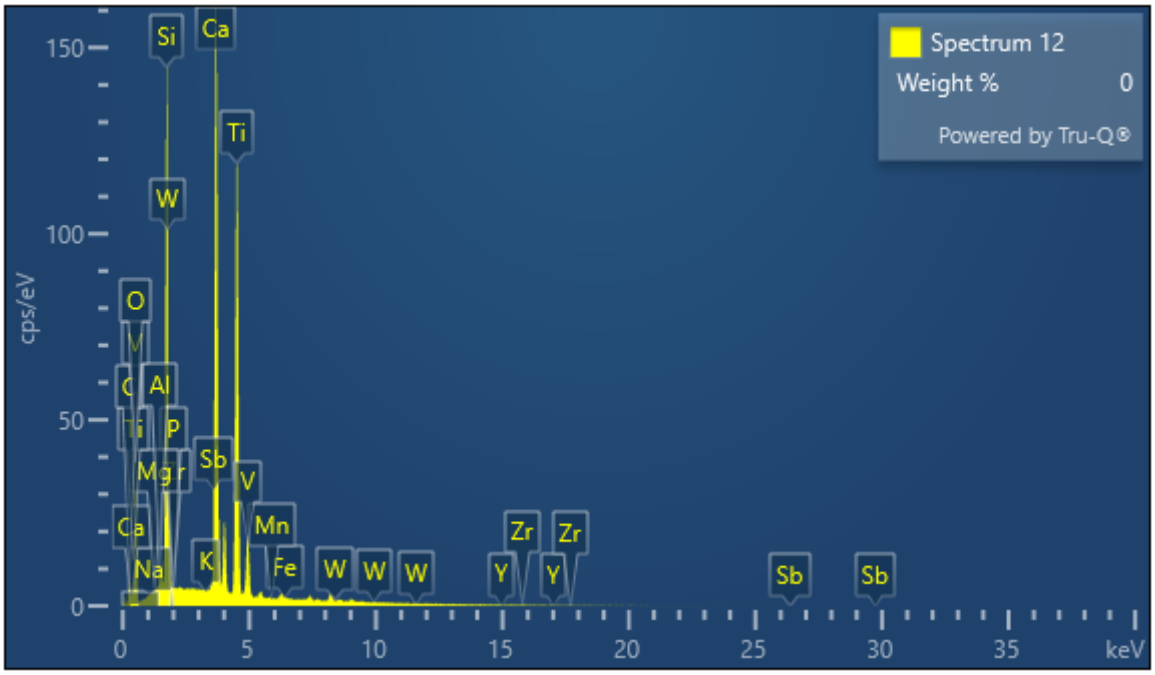
Spectrum 12
Weight % 0
Powered by Tru-Q®
cps/eV
keV
Si
Ca
Ti
W
O
Al
P
Sb
V
Mn
Fe
K
Na
Zr
Y
Sb

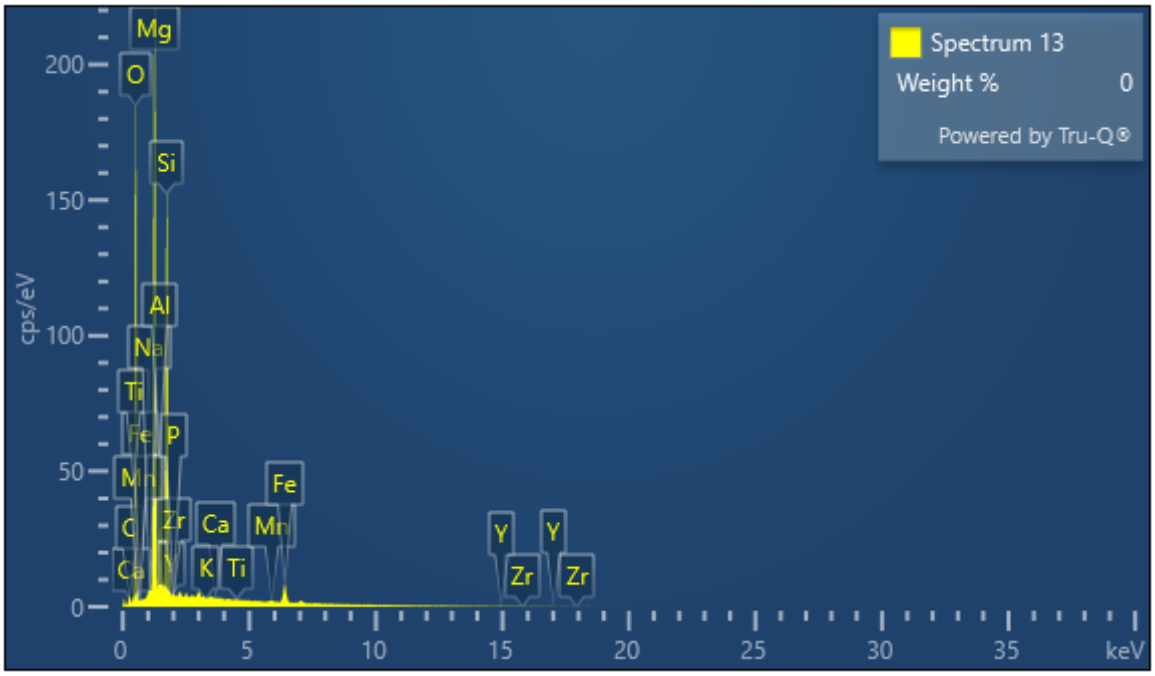
Spectrum 13
Weight % 0
Powered by Tru-Q®
cps/eV
keV
Mg
O
Si
Al
Na
Ti
Fe
P
Mn
Zr
Ca
K
Y

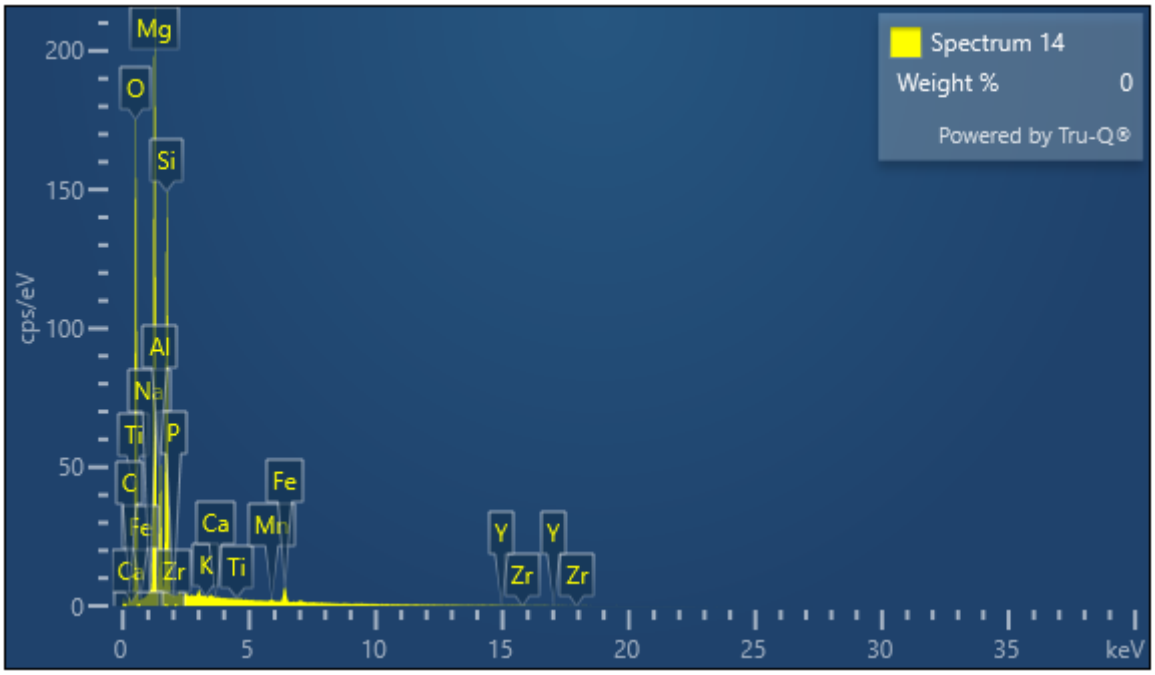
Spectrum 14
Weight % 0
Powered by Tru-Q®
cps/eV
keV
Mg
O
Si
Al
Na
Ti
P
C
Fe
Ca
Mn
K
Zr
Y

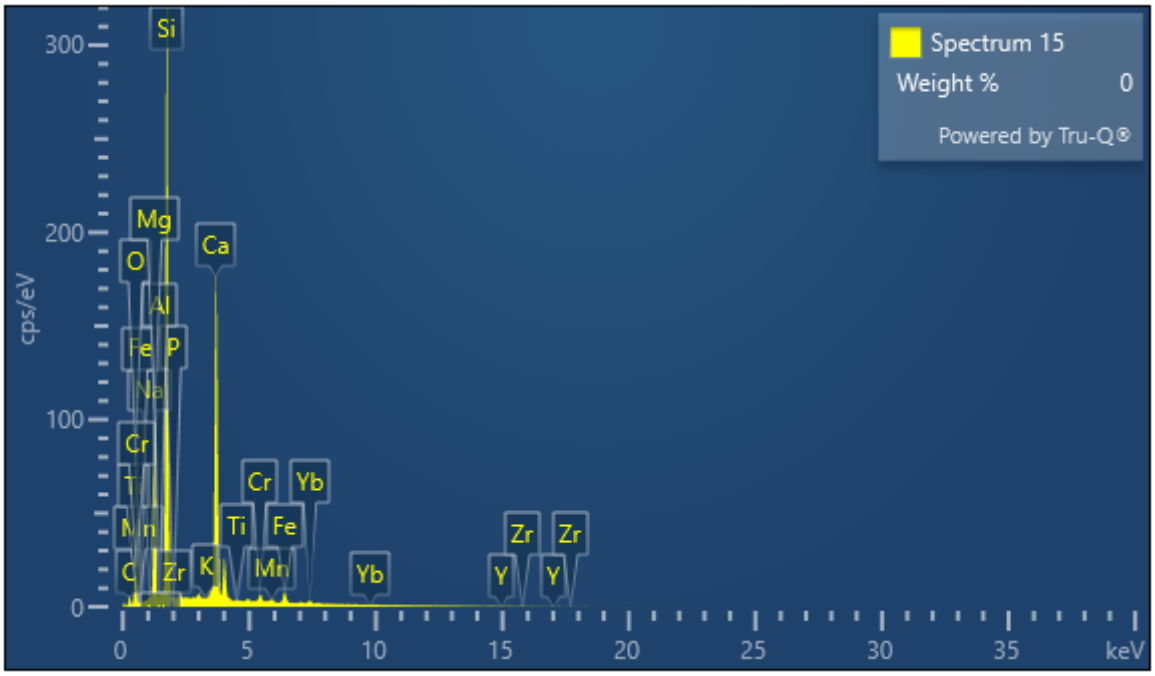
Spectrum 15
Weight % 0
Powered by Tru-Q®
cps/eV
keV
Si
Mg
Ca
O
Al
Fe
P
Na
Cr
Ti
Mn
C
Zr
K
Yb
Y

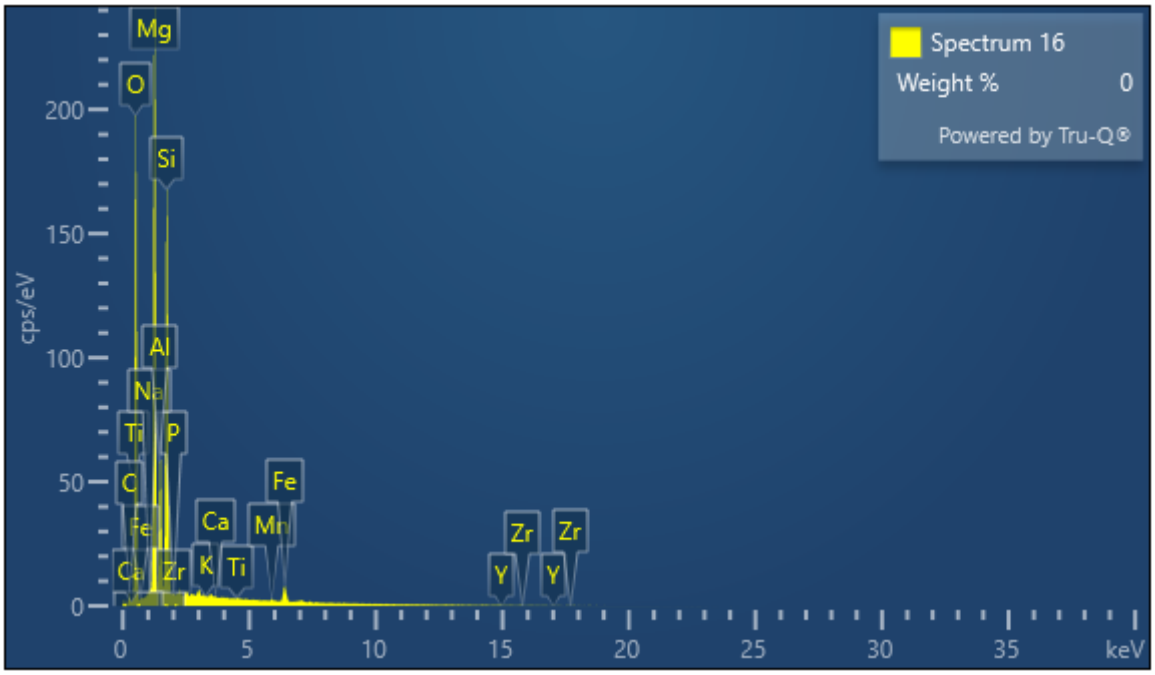
Spectrum 16
Weight % 0
Powered by Tru-Q®
cps/eV
keV
Mg
O
Si
Al
Na
Ti
P
C
Fe
Ca
Mn
Zr
K
Y

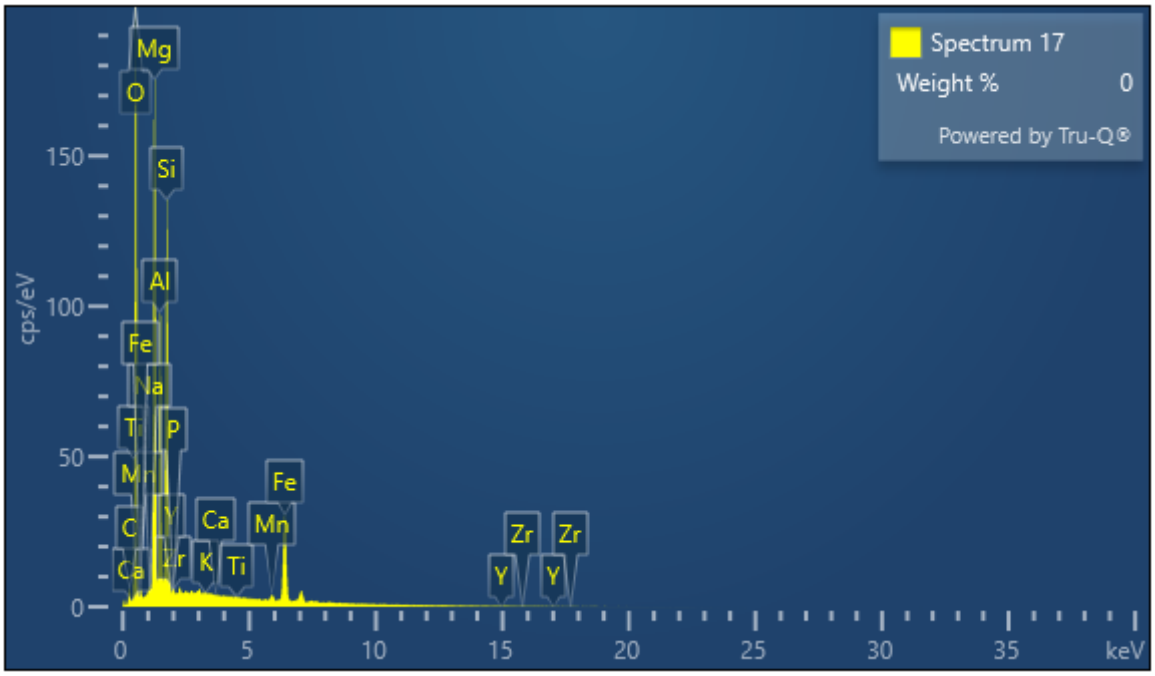
Spectrum 17
Weight % 0
Powered by Tru-Q®
cps/eV
keV
Mg
O
Si
Al
Fe
Na
Ti
P
Mn
C
Ca
Zr
K
Y

Electron Image 3

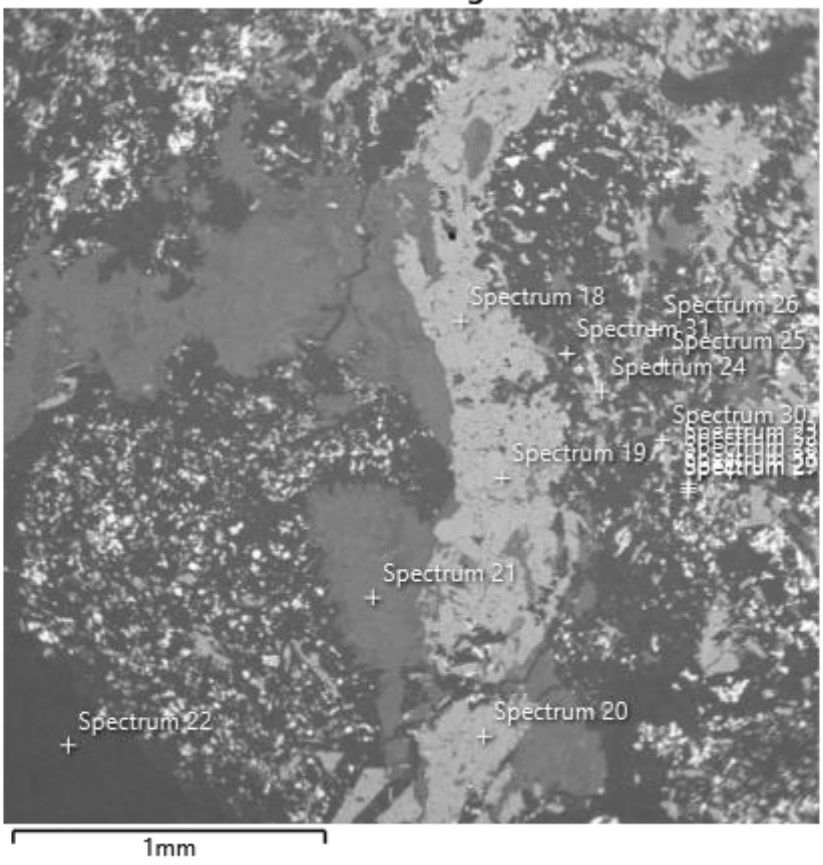

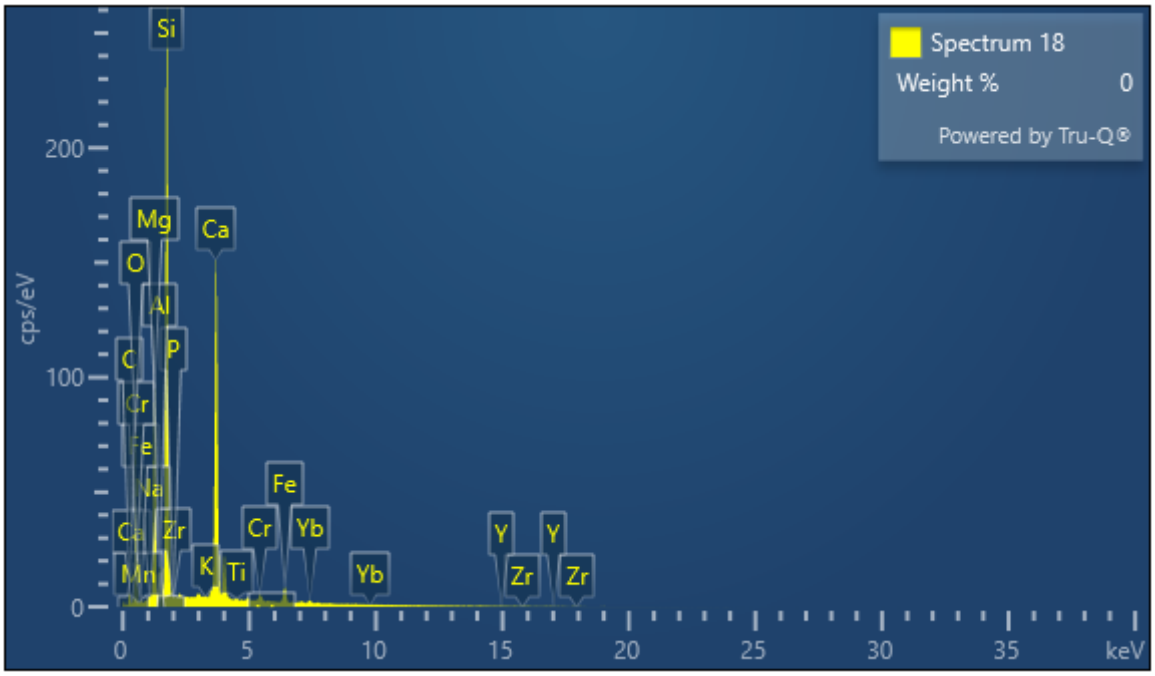

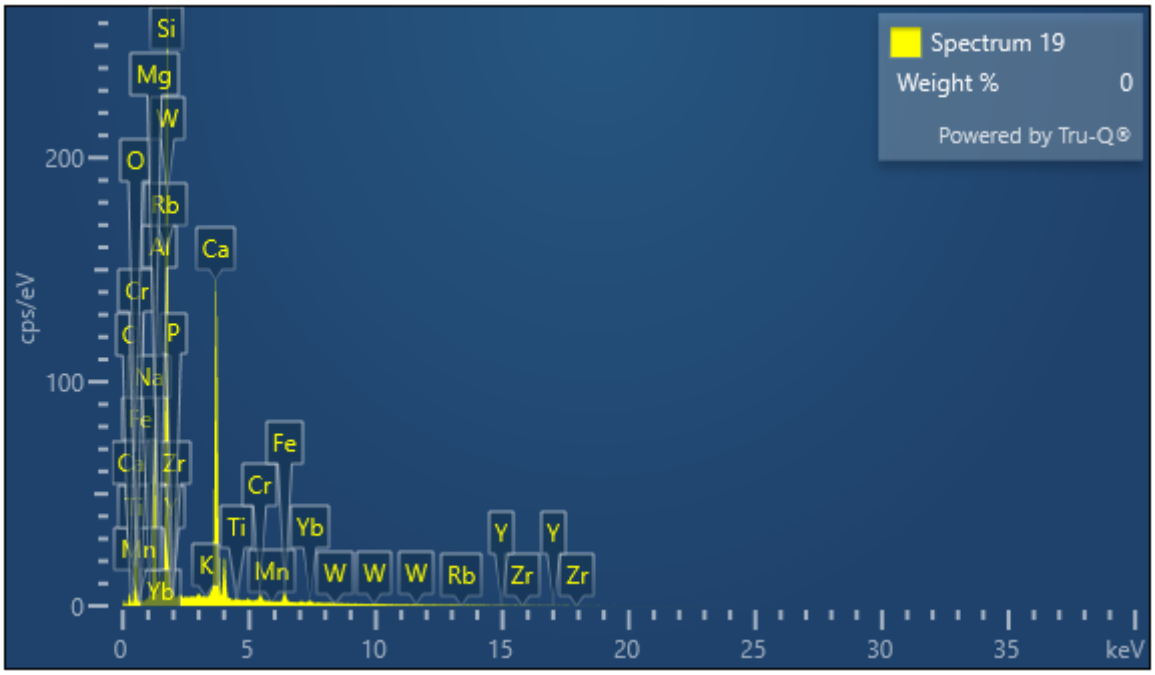
Spectrum 19
Weight % 0
Powered by Tru-Q®
cps/eV
keV
Si
Mg
W
O
Rb
Al
Ca
Cr
C
P
Na
Fe
Zr
Ti
Yb
Mn
K
Y

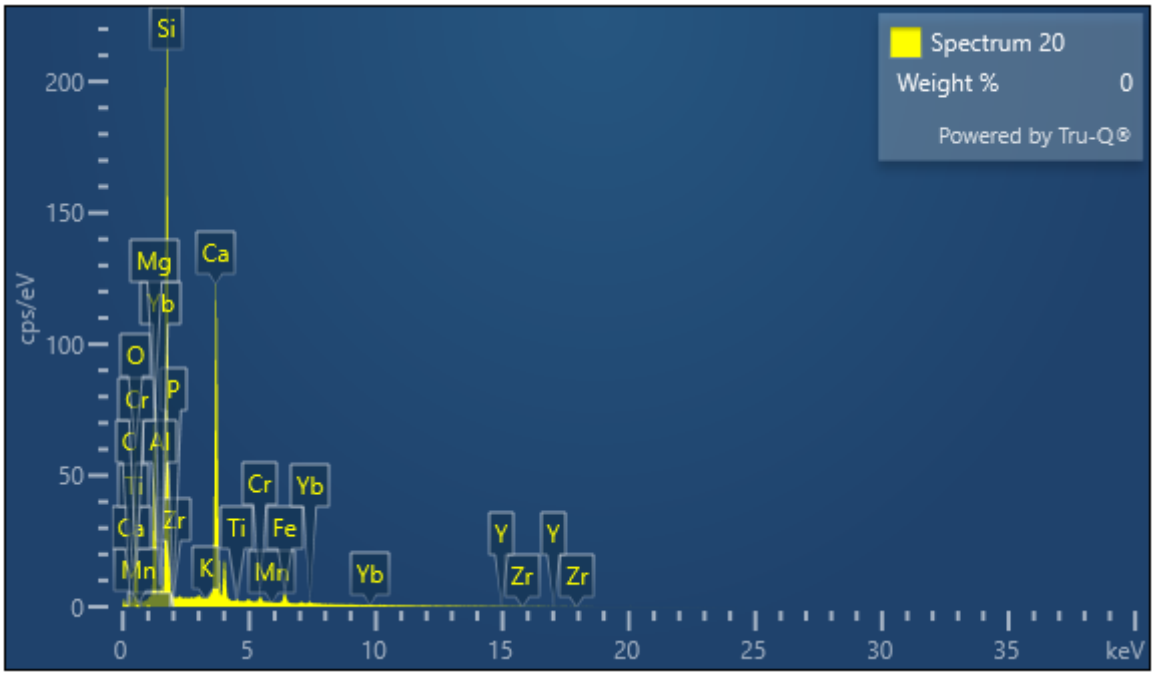
Spectrum 20
Weight % 0
Powered by Tru-Q®
cps/eV
keV
Si
Mg
Ca
Yb
O
Cr
P
C
Al
Ti
Zr
Fe
K
Mn
Y

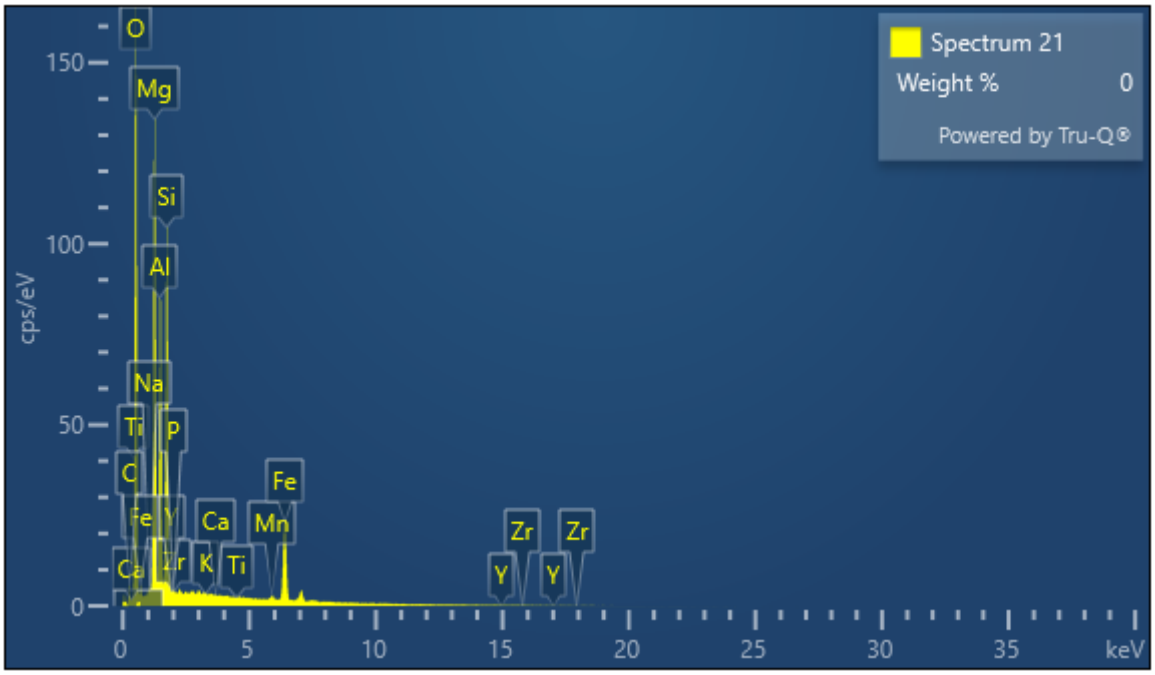
Spectrum 21
Weight % 0
Powered by Tru-Q®
cps/eV
keV
O
Mg
Si
Al
Na
Ti
P
C
Fe
Ca
Mn
Zr
K
Y

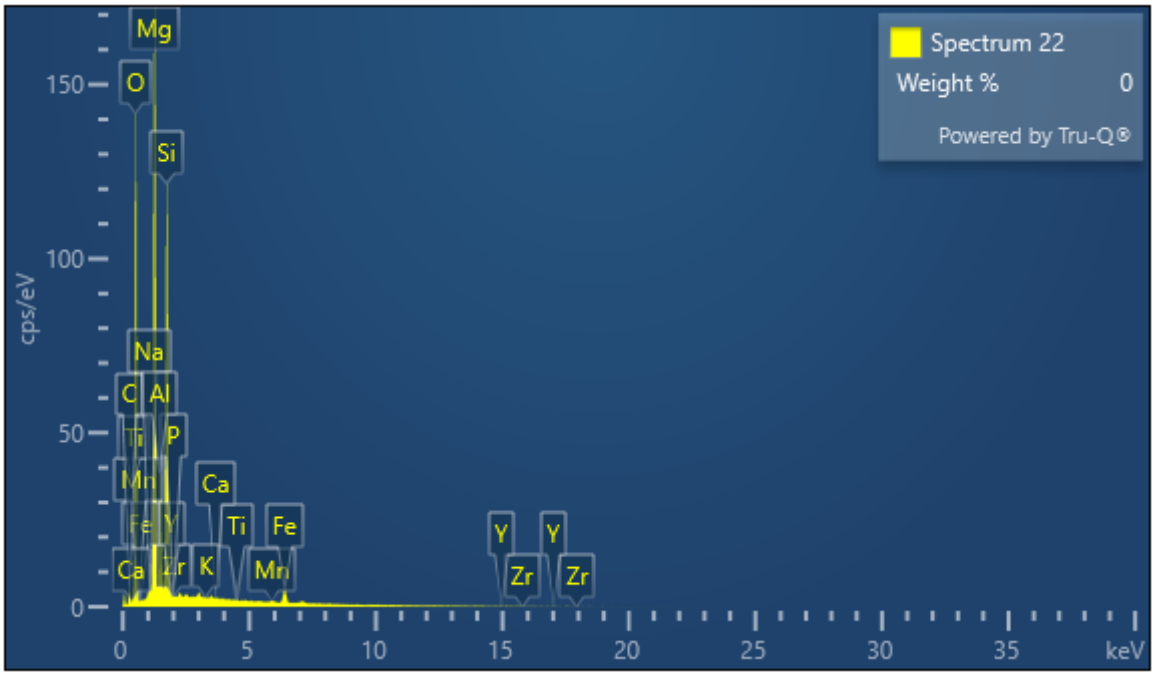
Spectrum 22
Weight % 0
Powered by Tru-Q®
cps/eV
keV
Mg
O
Si
Na
C
Al
Ti
P
Mn
Ca
Fe
Y
Zr
K

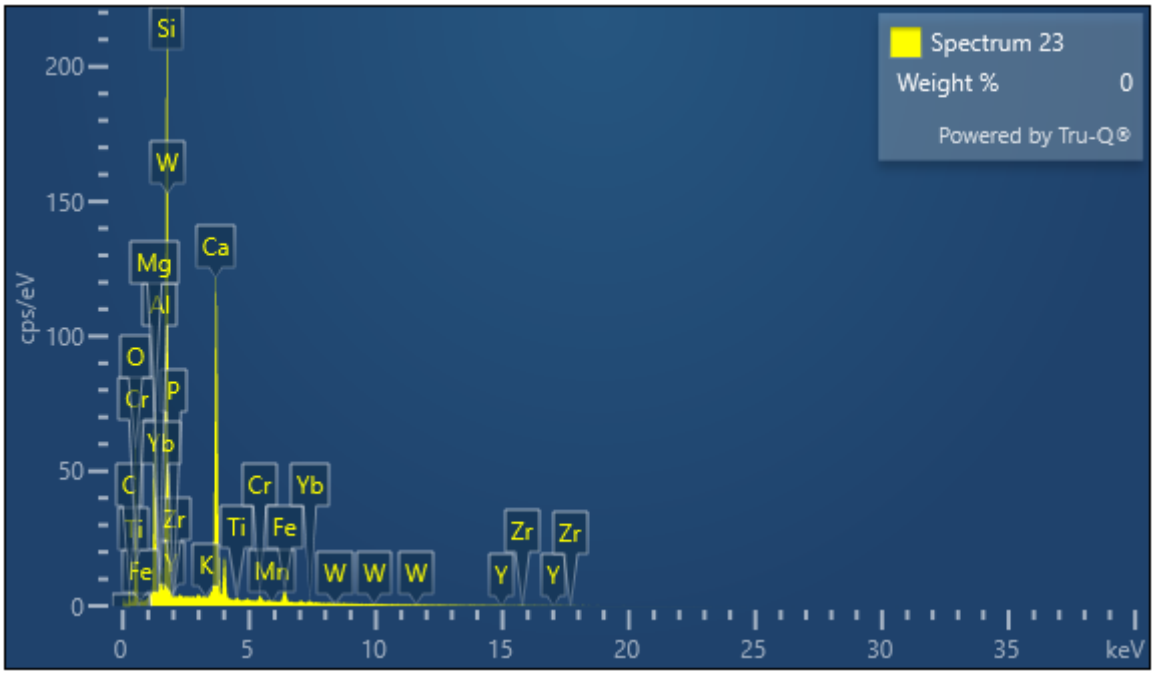
Spectrum 23
Weight % 0
Powered by Tru-Q®
cps/eV
keV
Si
W
Ca
Mg
Al
O
Cr
P
Yb
C
Ti
Zr
Fe
K
Mn
Y

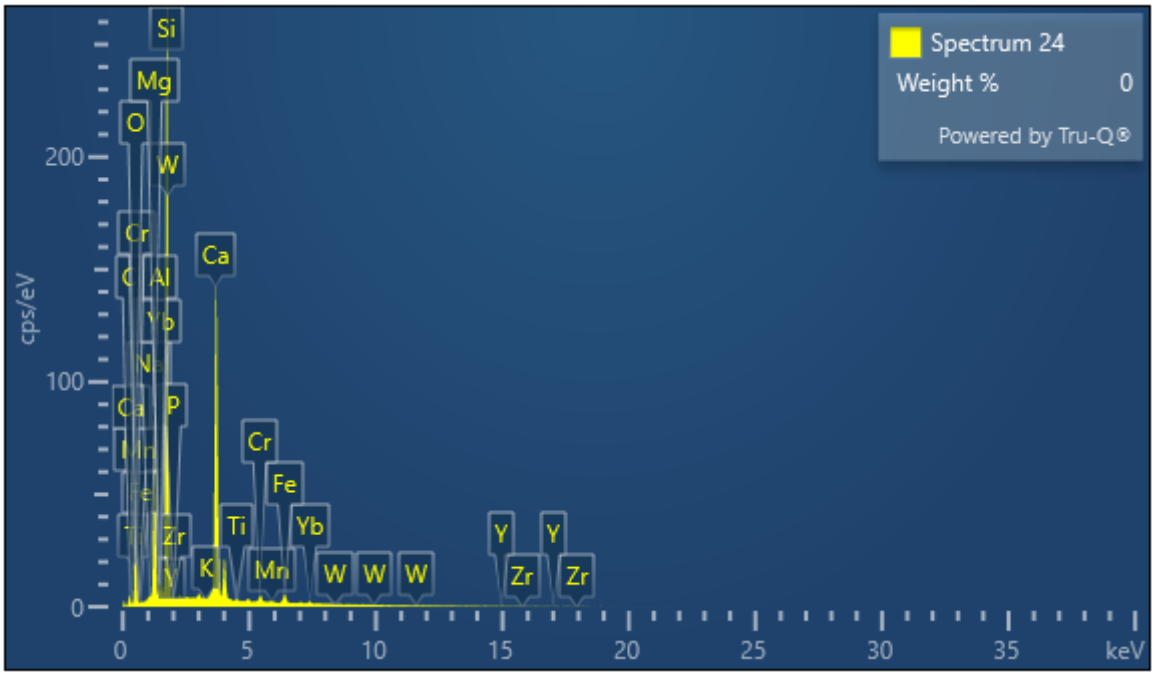
Spectrum 24
Weight % 0
Powered by Tru-Q®
cps/eV
keV
Si
Mg
O
W
Cr
Ca
Al
P
Fe
Yb
Ti
Zr
K
Mn
Y

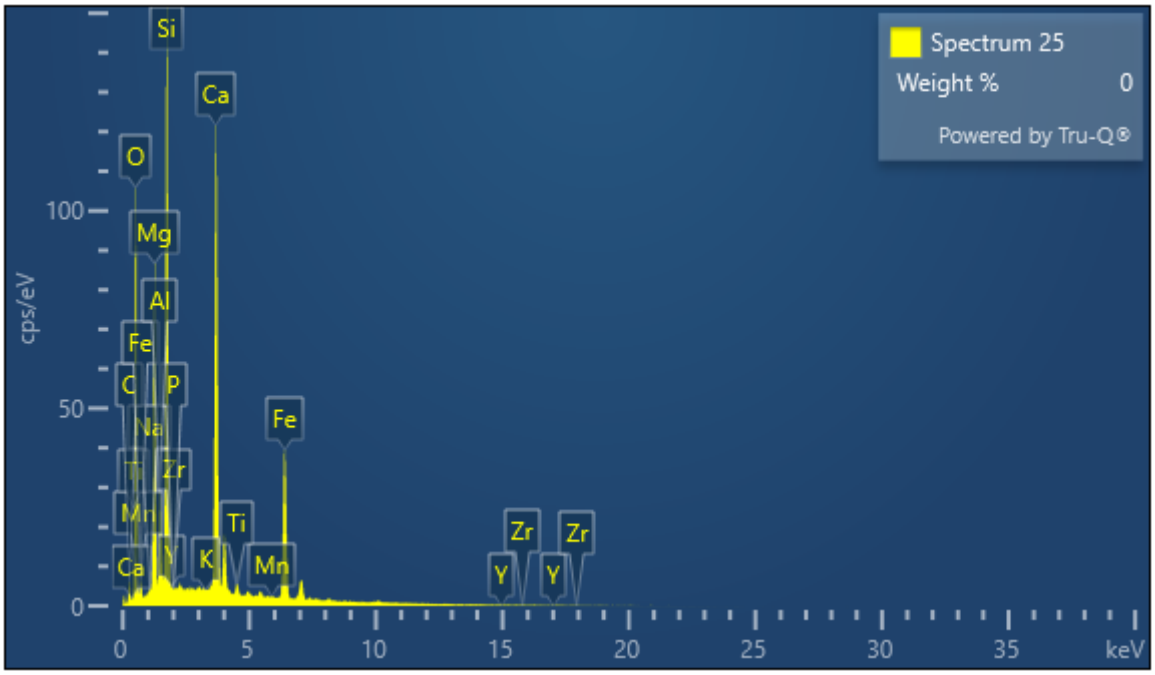
Spectrum 25
Weight % 0
Powered by Tru-Q®
cps/eV
keV
Si
Ca
O
Mg
Al
Fe
C
P
Na
Zr
Mn
Ti
K
Y

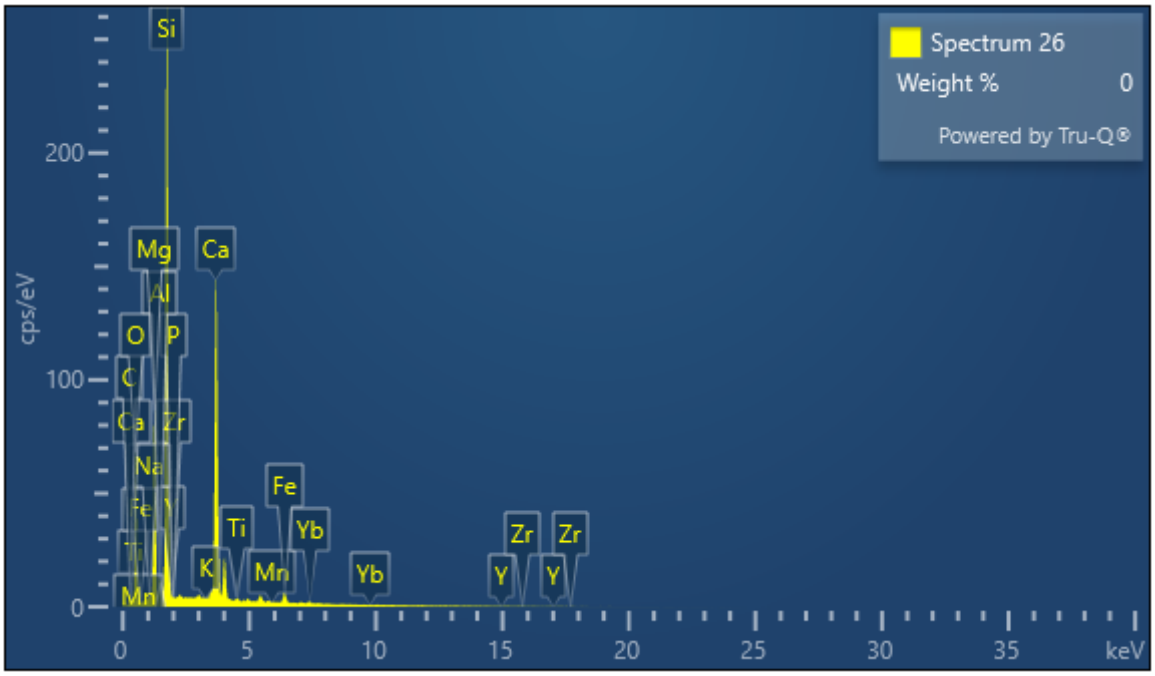
Spectrum 26
Weight % 0
Powered by Tru-Q®
cps/eV
keV
Si
Mg
Ca
Al
O
P
C
Ca
Zr
Na
Fe
Ti
Yb
K
Mn
Y

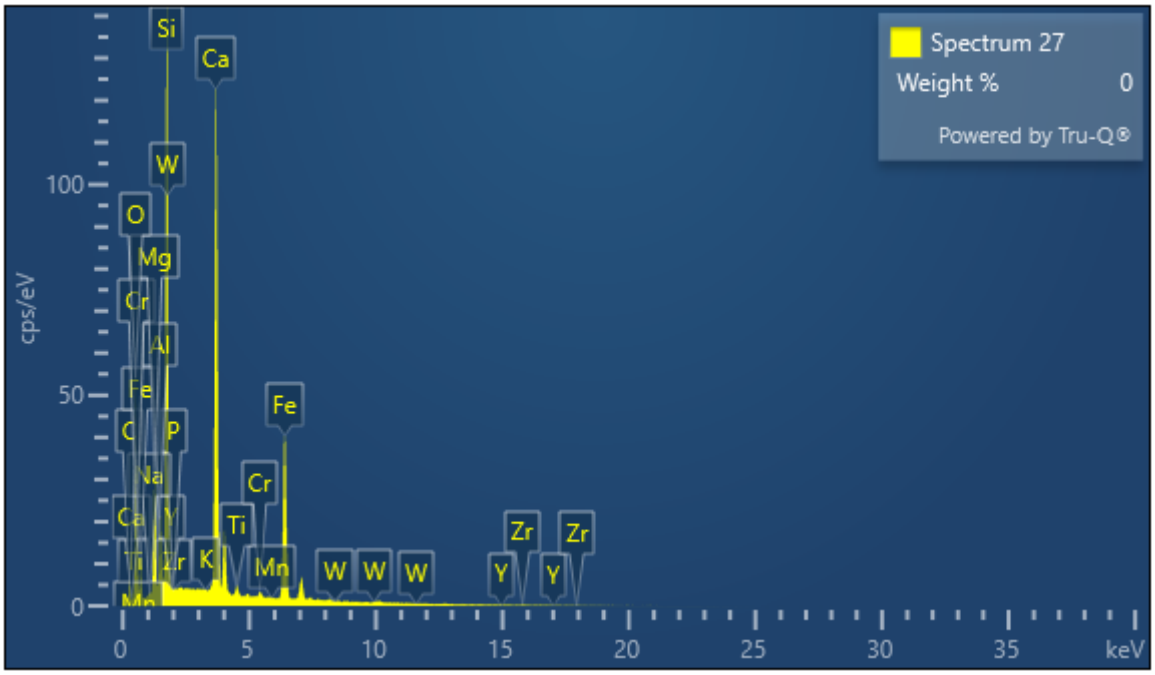
Spectrum 27
Weight % 0
Powered by Tru-Q®
cps/eV
keV
Si
Ca
W
O
Mg
Cr
Al
Fe
C
P
Na
Ca
Ti
Zr
K
Mn
Y
0
5
10
15
20
25
30
35
50
100

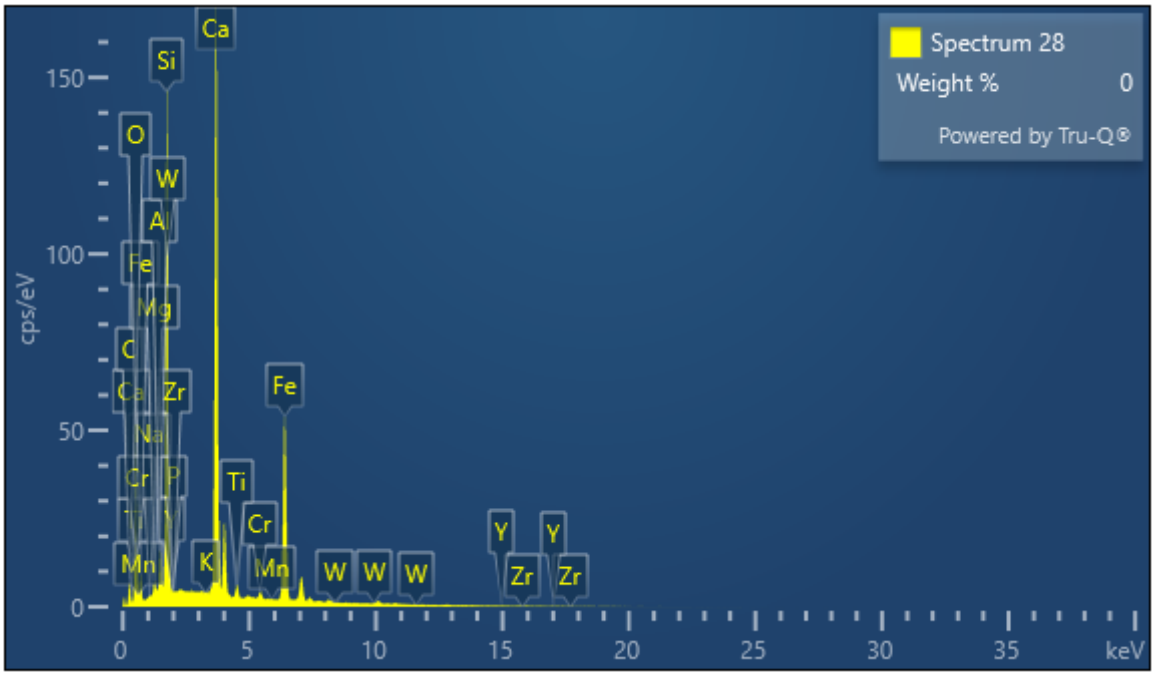
Spectrum 28
Weight % 0
Powered by Tru-Q®
cps/eV
keV
Ca
Si
O
W
Al
Fe
Mg
C
Ca
Zr
Na
Cr
P
Ti
Mn
K
Y
0
5
10
15
20
25
30
35
50
100
150

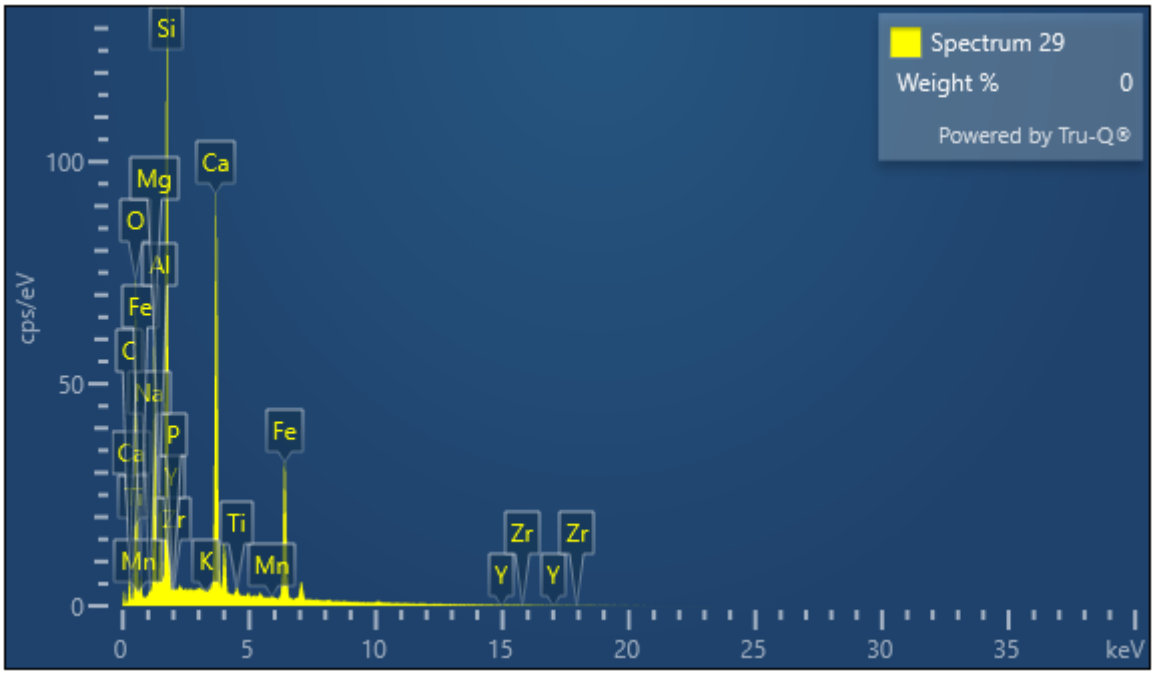
Spectrum 29
Weight % 0
Powered by Tru-Q®
cps/eV
keV
Si
Ca
Mg
O
Al
Fe
C
Na
P
Ti
Mn
K
Zr
Y

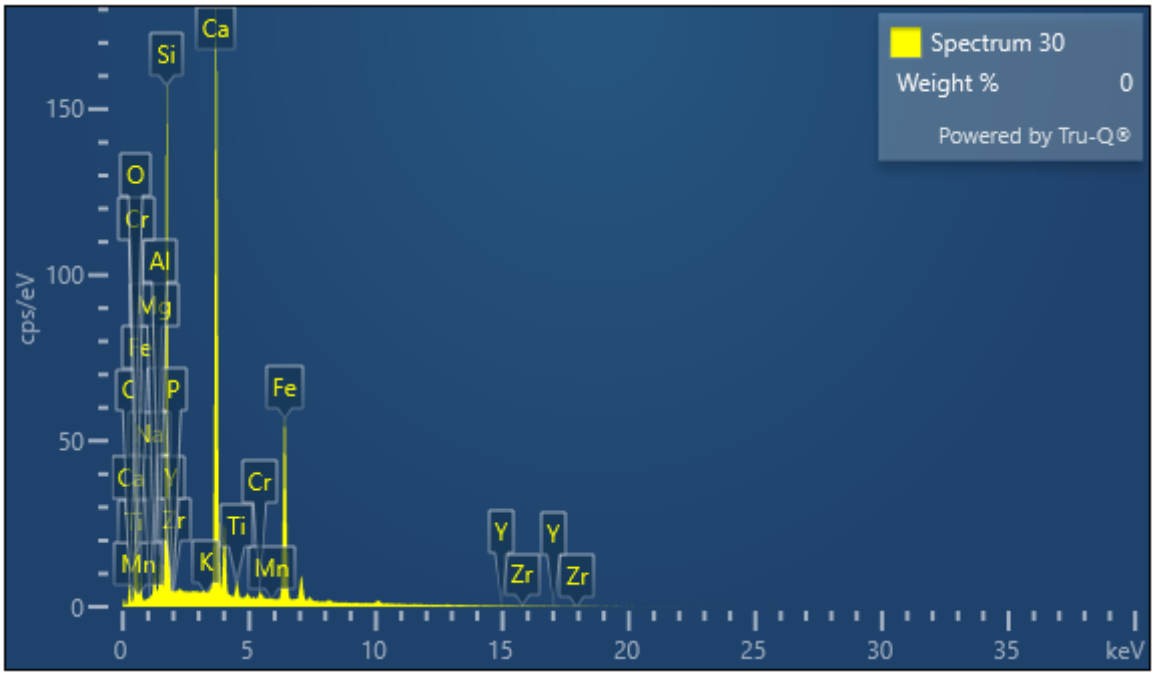
Spectrum 30
Weight % 0
Powered by Tru-Q®
cps/eV
keV
Si
Ca
O
Cr
Al
Fe
P
Ti
Mn
K
Zr
Y

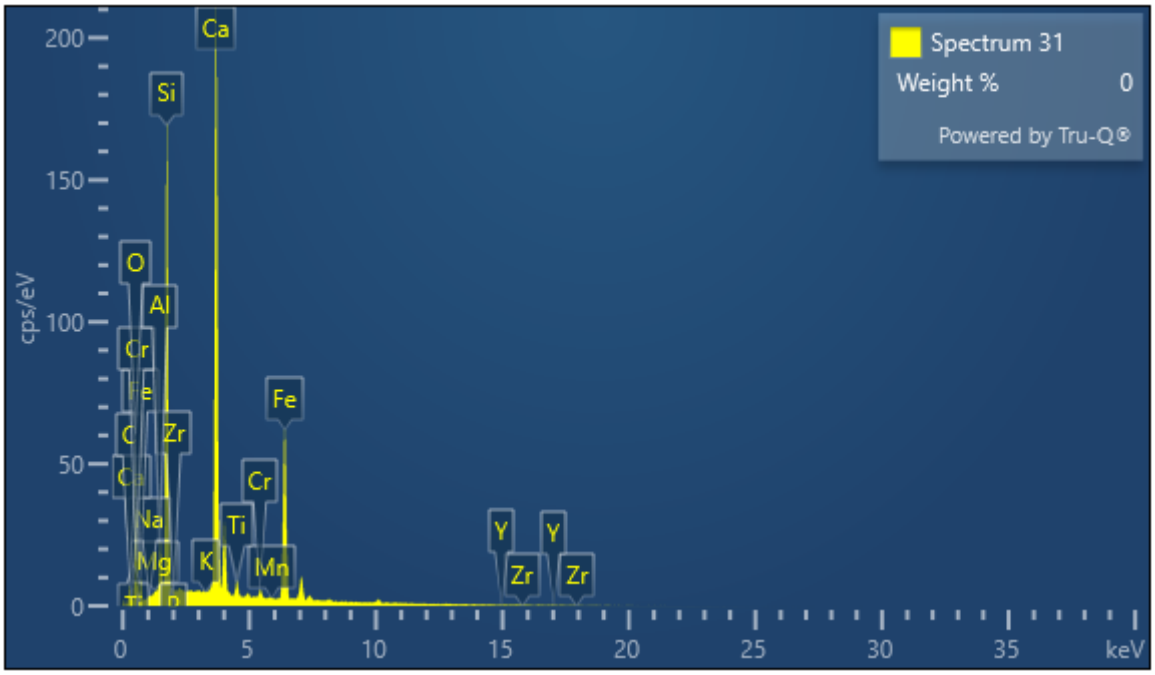
Spectrum 31
Weight % 0
Powered by Tru-Q®
cps/eV
keV
Ca
Si
O
Al
Cr
Fe
C
Zr
Na
Mg
K
Mn
Ti
Y
Zr

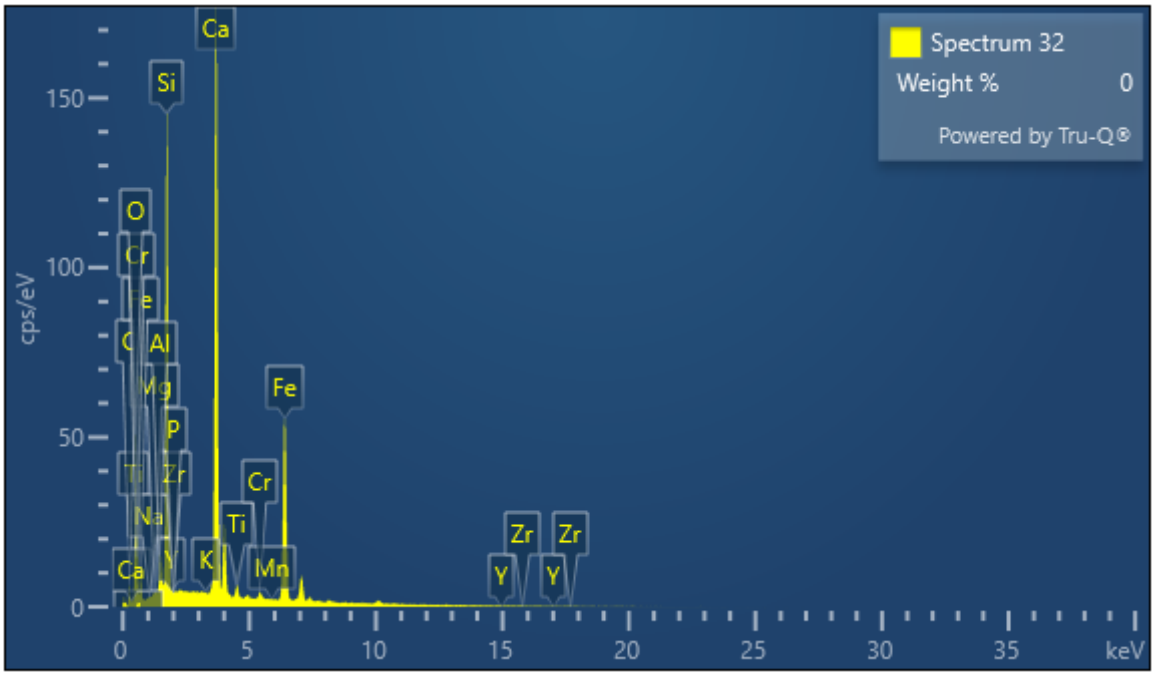
Spectrum 32
Weight % 0
Powered by Tru-Q®
cps/eV
keV
Ca
Si
O
Cr
Fe
C
Al
Mg
P
Zr
Na
Ti
K
Mn
Y
Zr

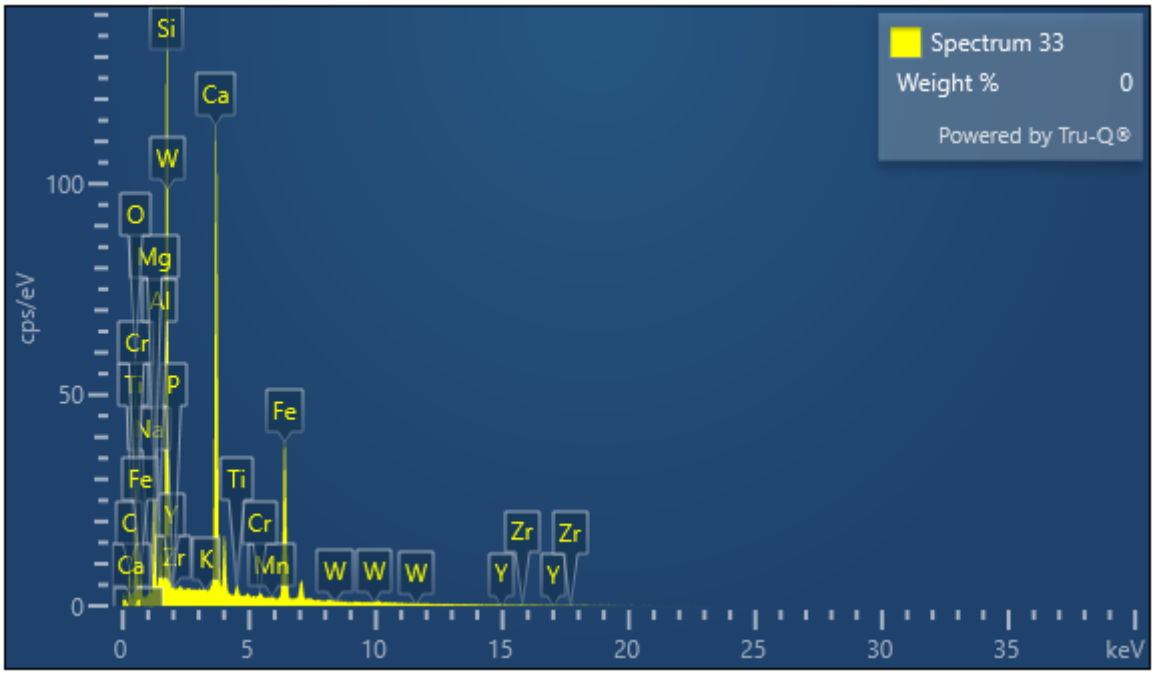
Spectrum 33
Weight % 0
Powered by Tru-Q®
cps/eV
100
50
0
0
5
10
15
20
25
30
35
keV
Si
Ca
W
O
Mg
Al
Cr
Ti
P
Na
Fe
C
Y
Zr
K
Mn
Zr
Zr
Y
Y
W
W
W

Electron Image 4

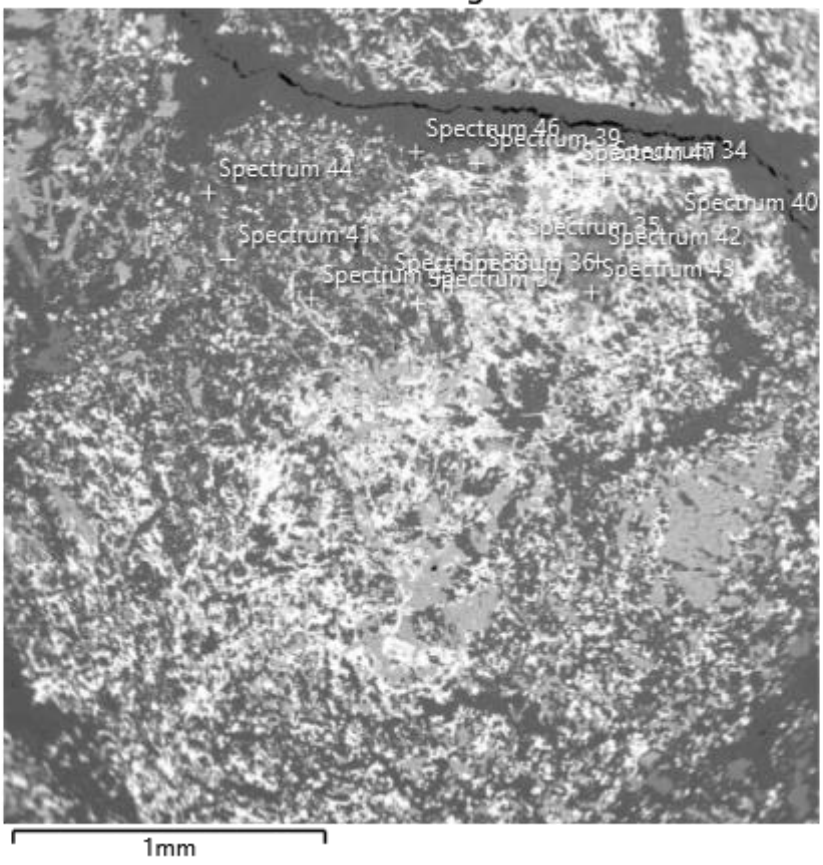

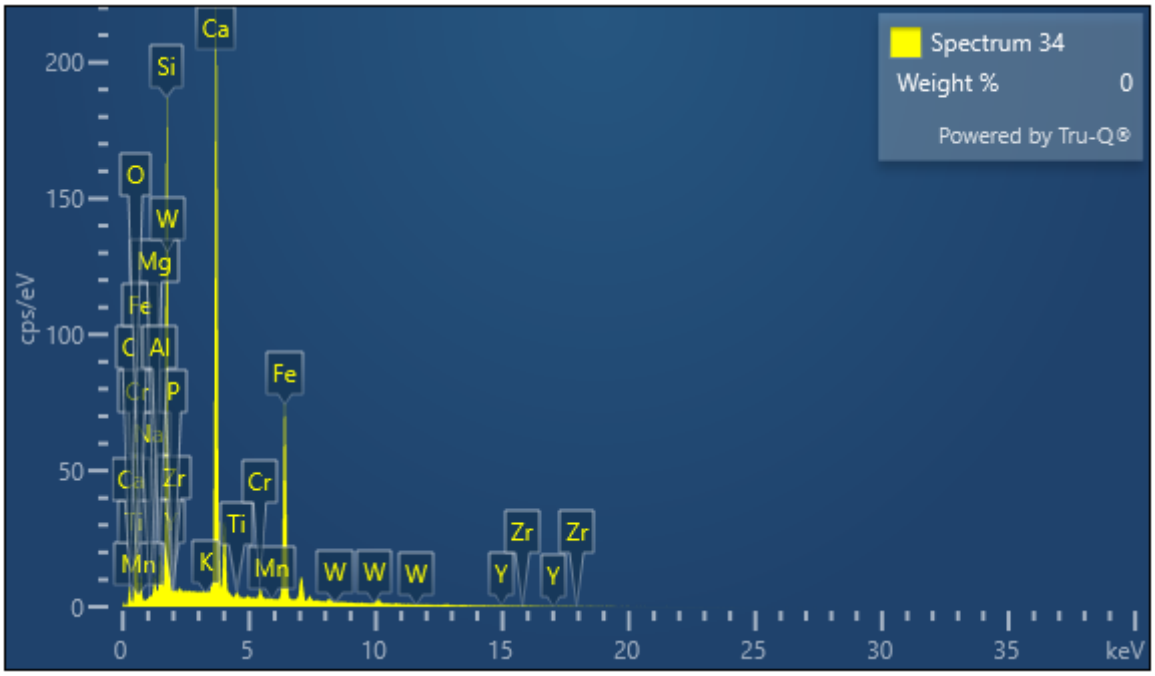

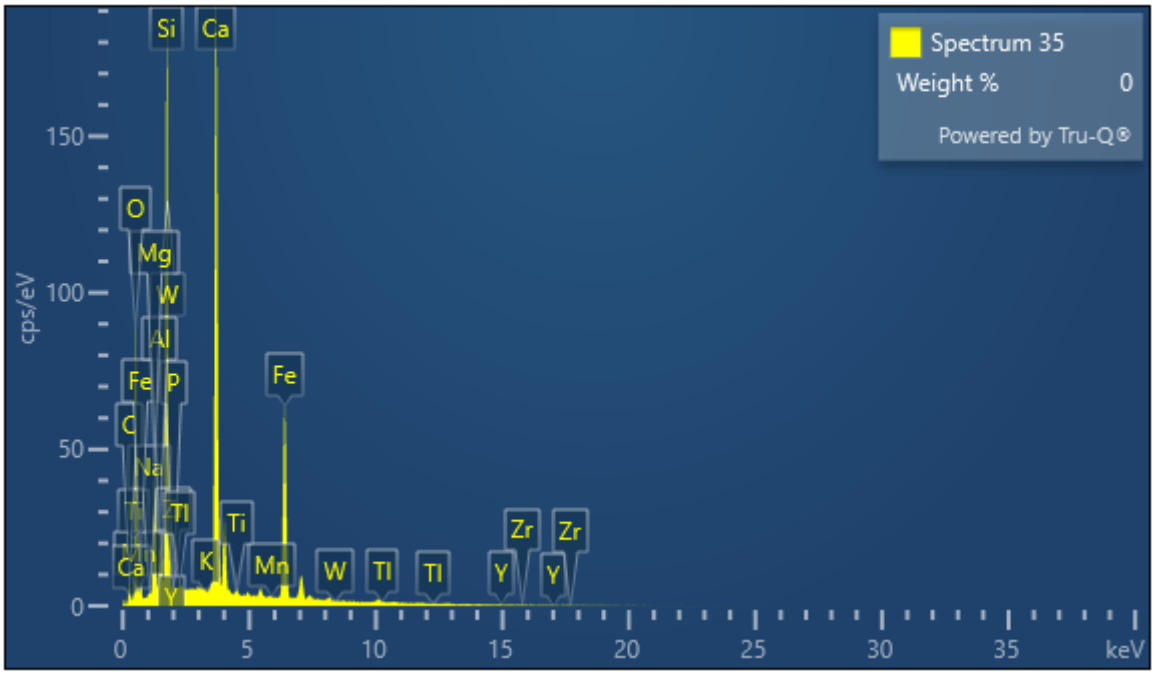
Spectrum 35
Weight % 0
Powered by Tru-Q®
cps/eV
keV
Si
Ca
O
Mg
W
Al
Fe
P
C
Na
Tl
Ti
K
Mn
Y
Zr

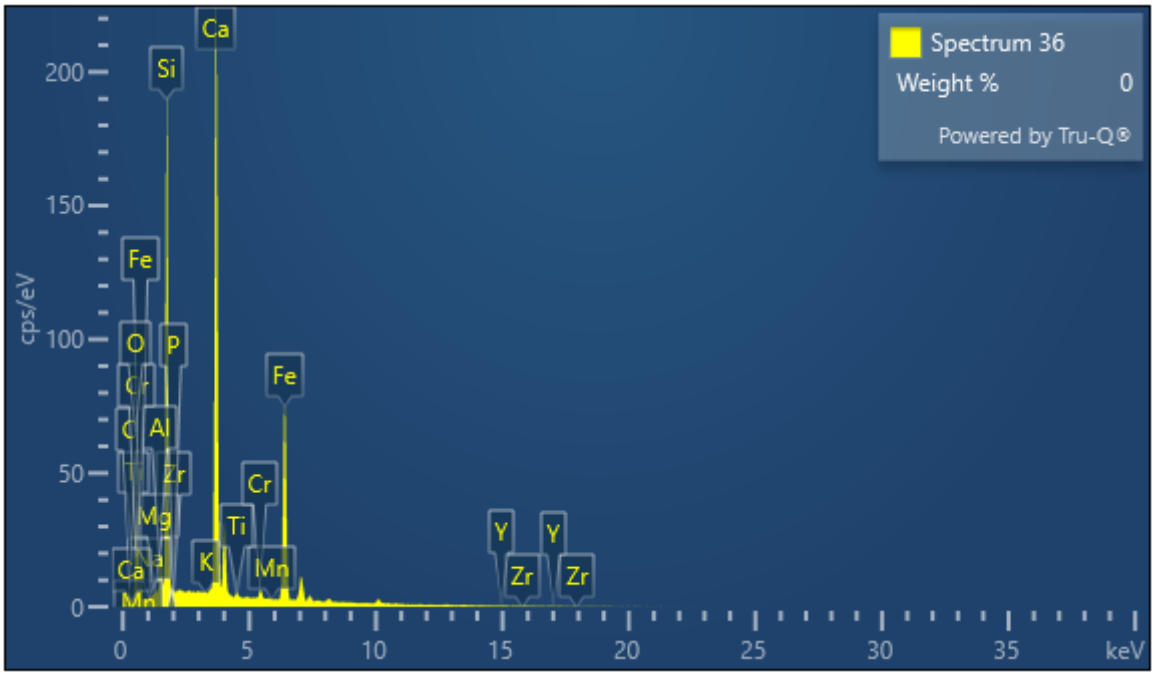
Spectrum 36
Weight % 0
Powered by Tru-Q®
cps/eV
keV
Ca
Si
Fe
O
P
Cr
C
Al
Zr
Mg
Ti
K
Mn
Y

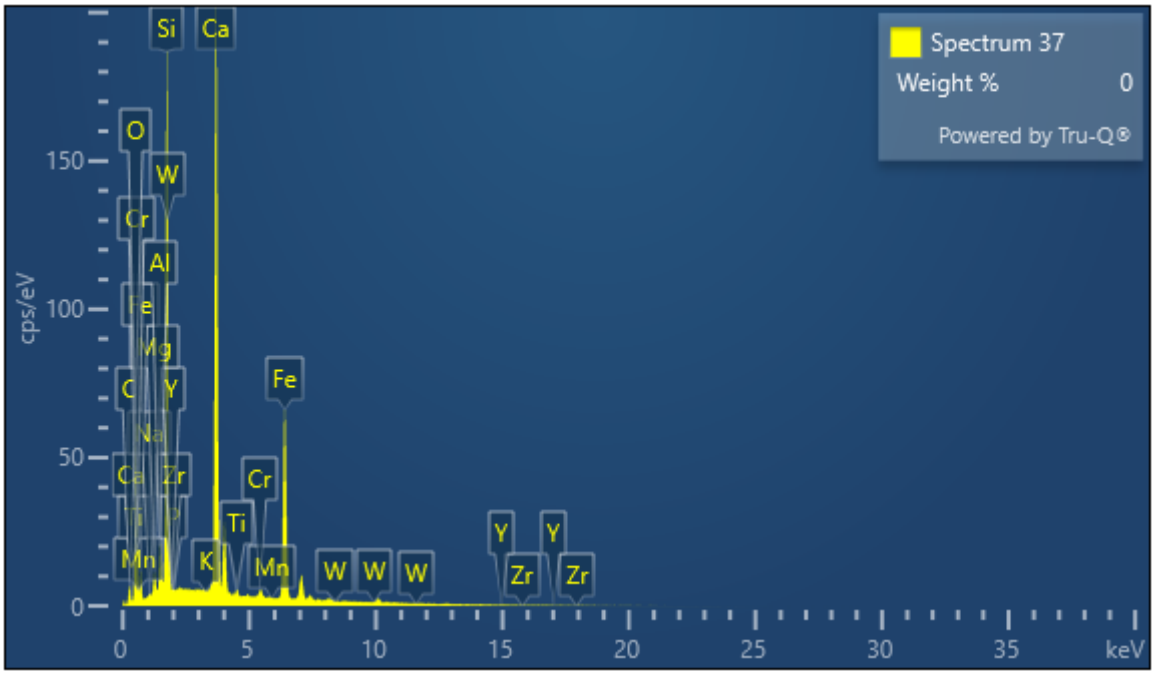
Spectrum 37
Weight % 0
Powered by Tru-Q®
cps/eV
keV
Si
Ca
O
W
Cr
Al
Mg
Fe
Y
Zr
Ti
Mn
K

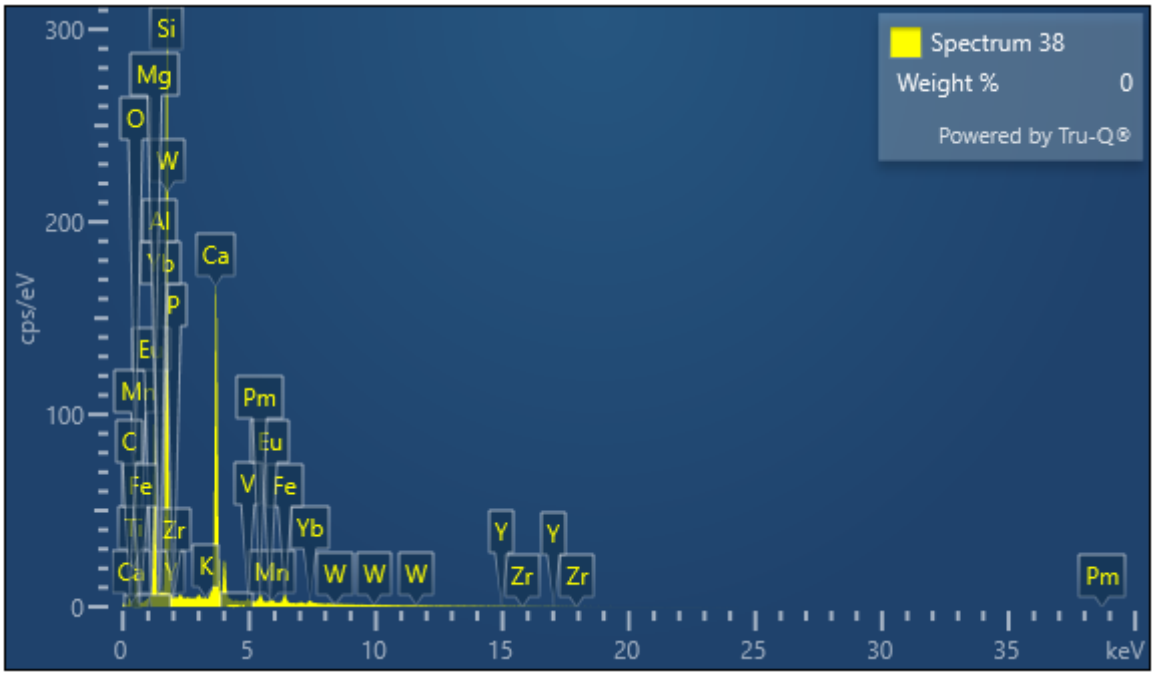
Spectrum 38
Weight % 0
Powered by Tru-Q®
cps/eV
keV
Si
Mg
O
W
Al
Ca
P
Pm
Eu
Fe
Yb
Y
Zr
Mn
K
Pm

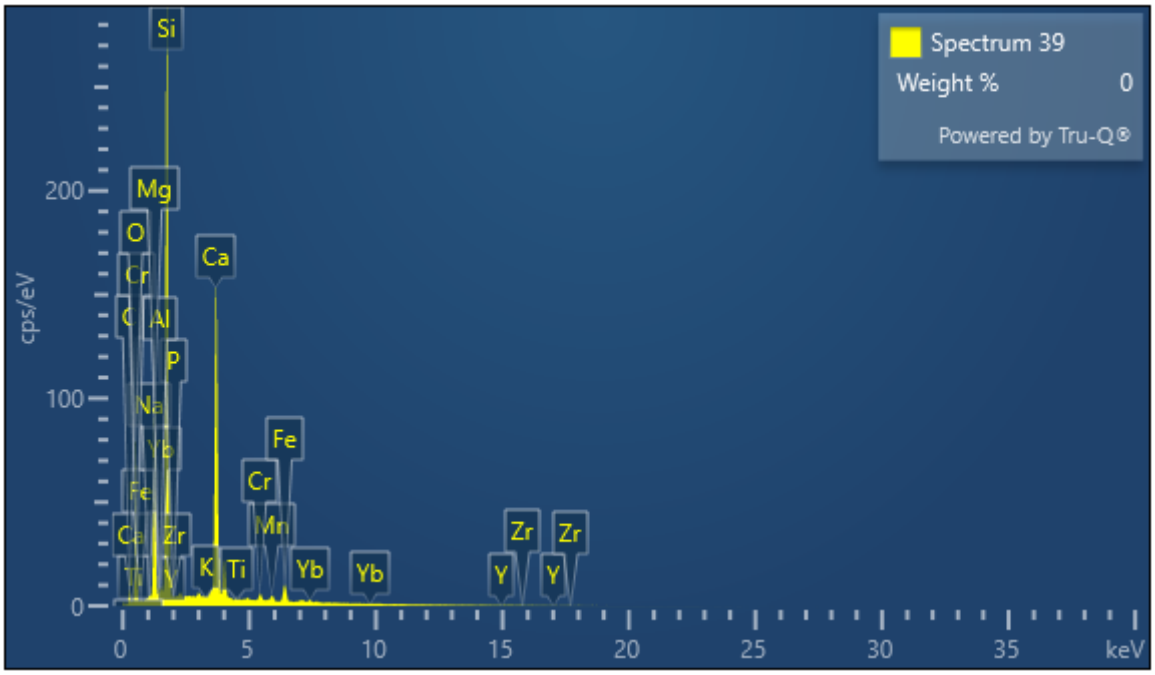
Spectrum 39
Weight % 0
Powered by Tru-Q®
cps/eV
keV
Si
Mg
O
Ca
Cr
Al
P
Na
Yb
Fe
Mn
Zr
K
Ti
Y
Br

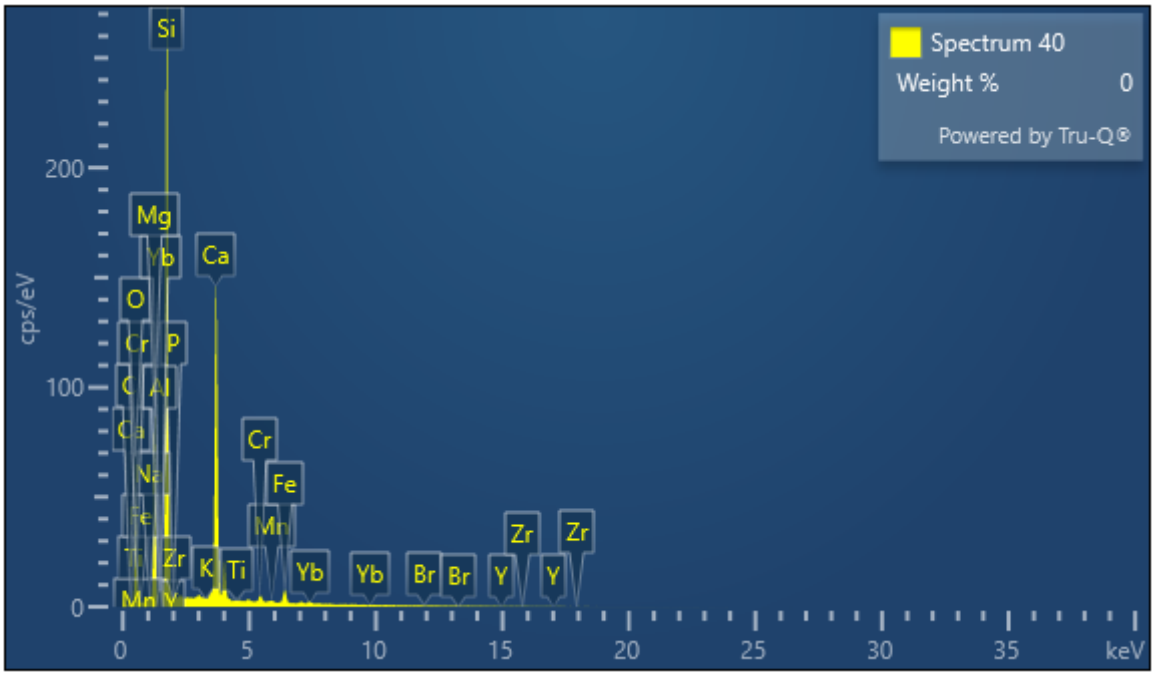
Spectrum 40
Weight % 0
Powered by Tru-Q®
cps/eV
keV
Si
Mg
Yb
Ca
O
Cr
P
Al
Na
Fe
Mn
Zr
K
Ti
Y
Br

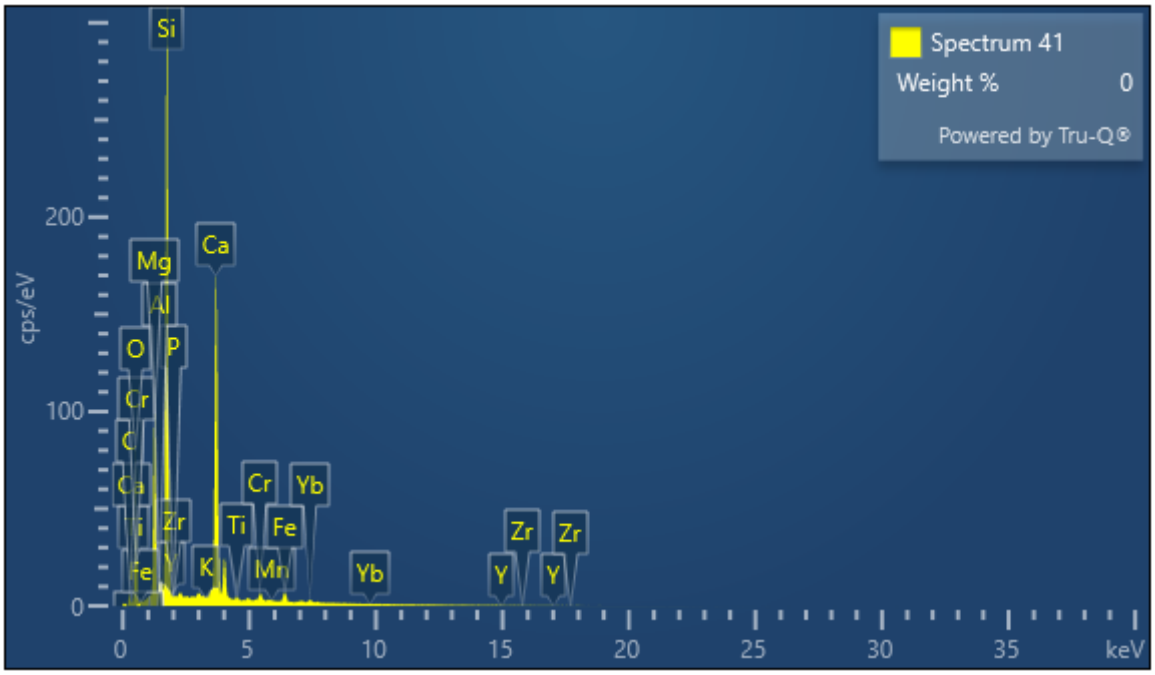
Spectrum 41
Weight % 0
Powered by Tru-Q®
cps/eV
keV
Si
Mg
Ca
Al
O
P
Cr
C
Yb
Zr
Ti
Fe
K
Mn
Y

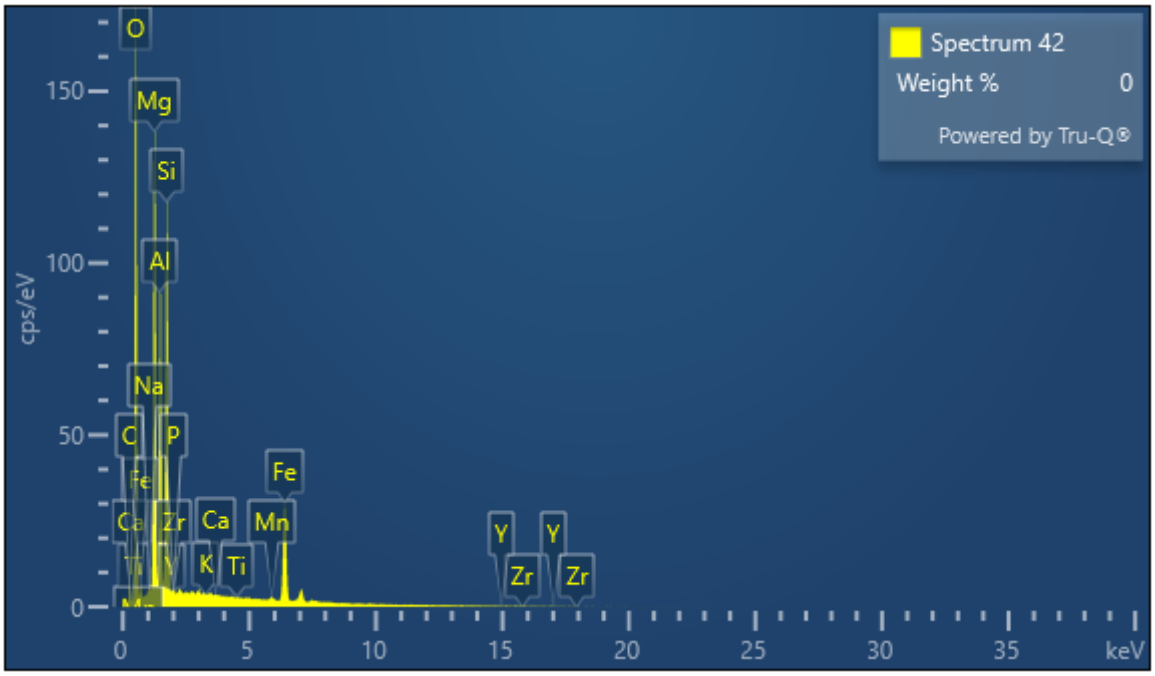
Spectrum 42
Weight % 0
Powered by Tru-Q®
cps/eV
keV
O
Mg
Si
Al
Na
C
P
Fe
Ca
Zr
Mn
K
Ti
Y

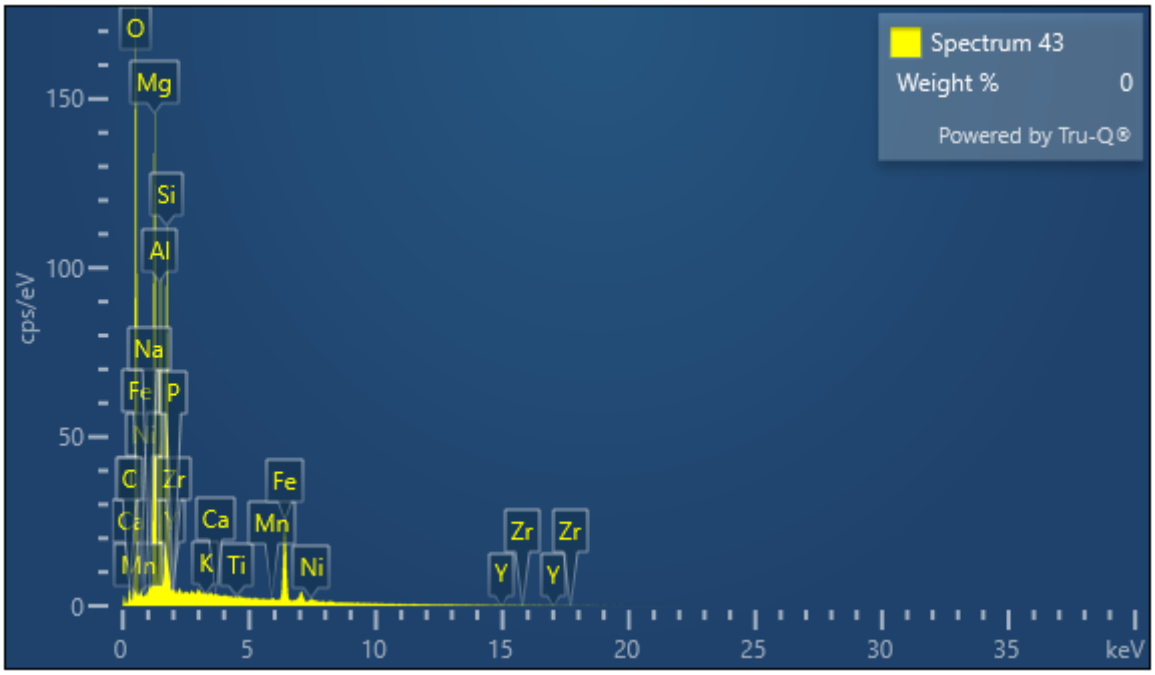
Spectrum 43
Weight % 0
Powered by Tru-Q®
cps/eV
keV
O
Mg
Si
Al
Na
Fe
P
C
Zr
Ca
Mn
K
Ti
Ni
Y

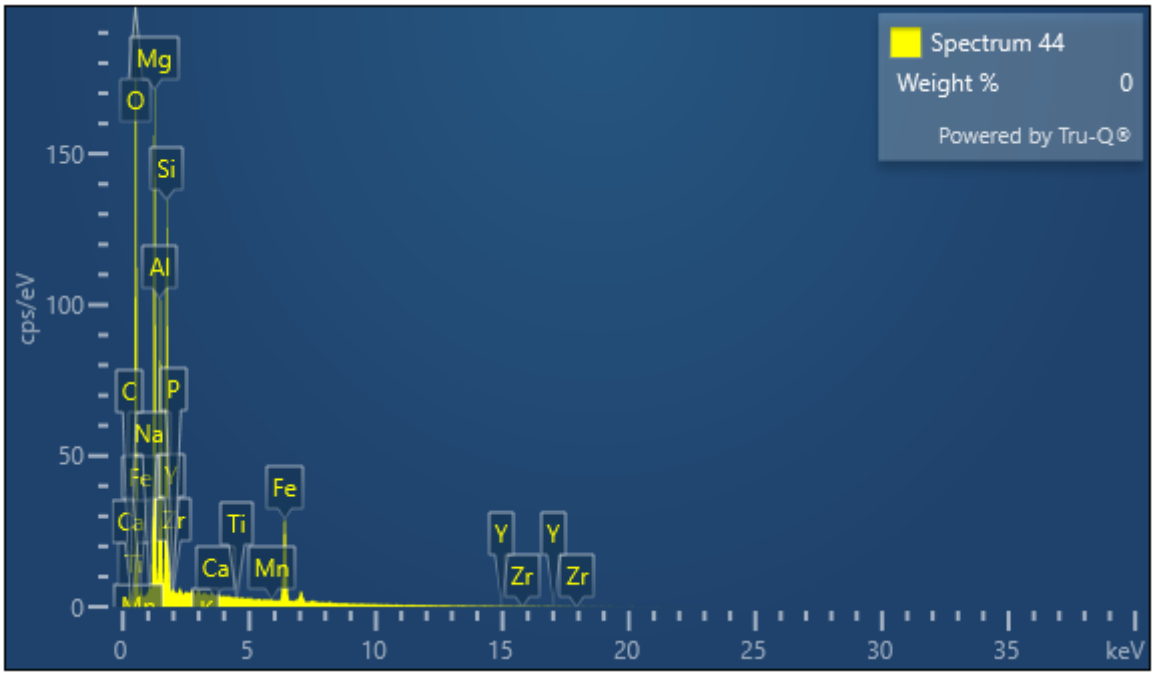
Spectrum 44
Weight % 0
Powered by Tru-Q®
cps/eV
keV
Mg
O
Si
Al
C
P
Na
Fe
Y
Ca
Zr
Ti
Mn

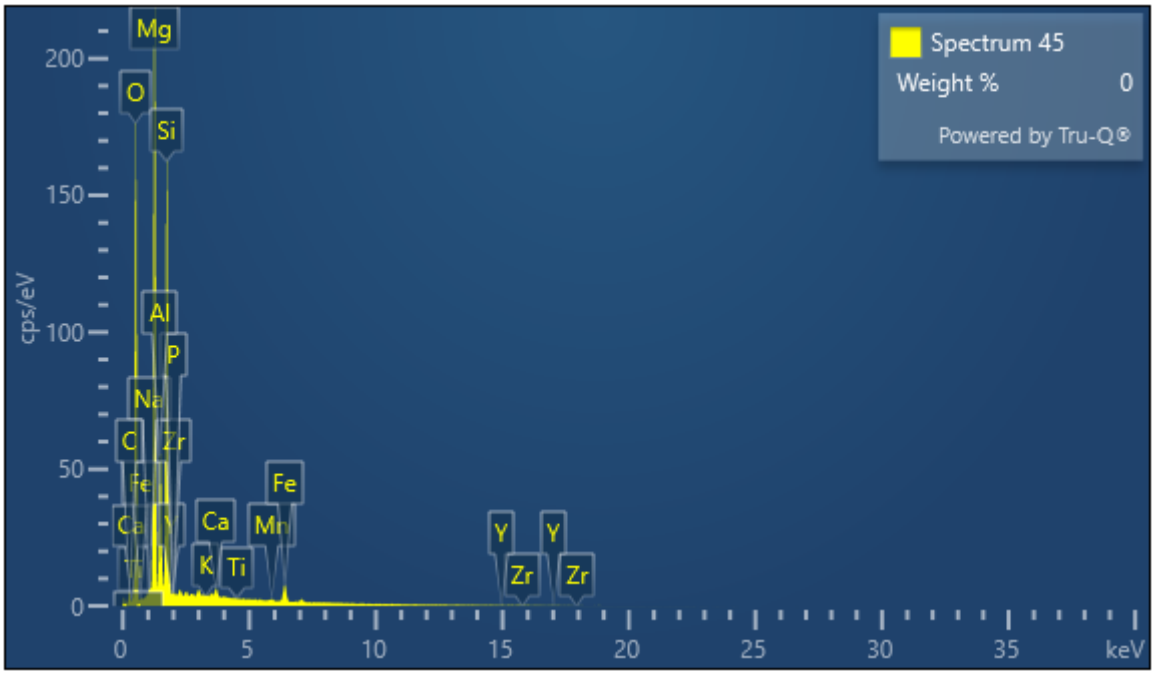
Spectrum 45
Weight % 0
Powered by Tru-Q®
cps/eV
keV
Mg
O
Si
Al
P
Na
C
Zr
Fe
Ca
Mn
K
Ti
Y

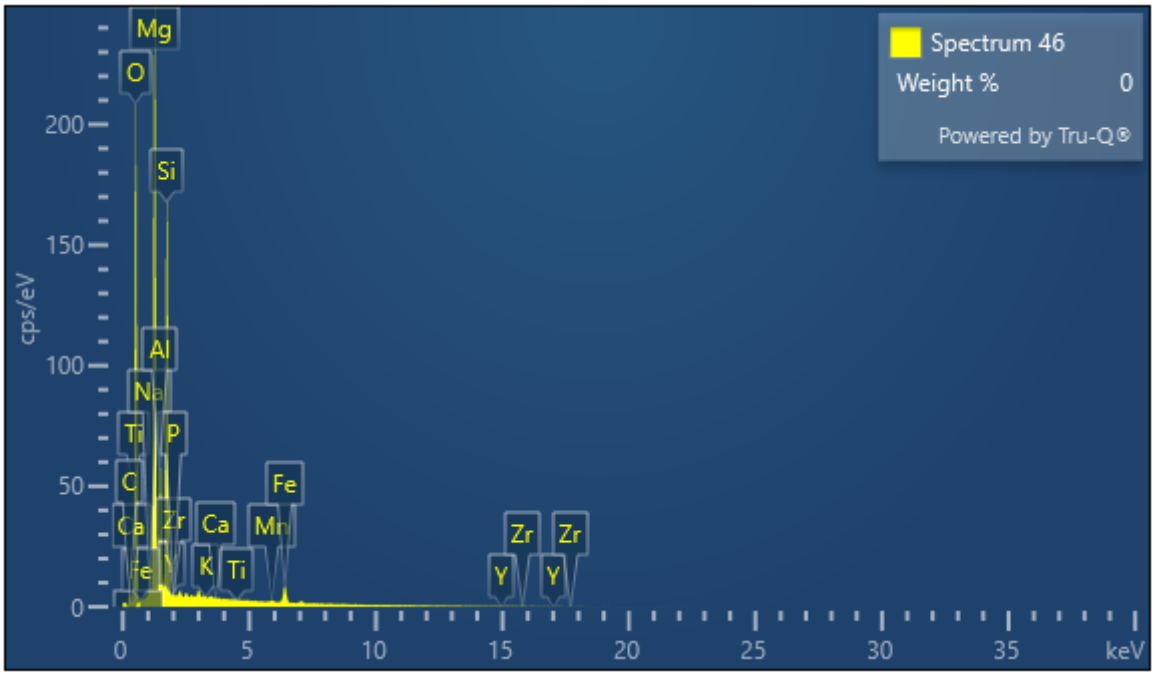
Spectrum 46
Weight % 0
Powered by Tru-Q®
cps/eV
keV
Mg
O
Si
Al
Na
Ti
P
C
Ca
Zr
Fe
Mn
K
Y

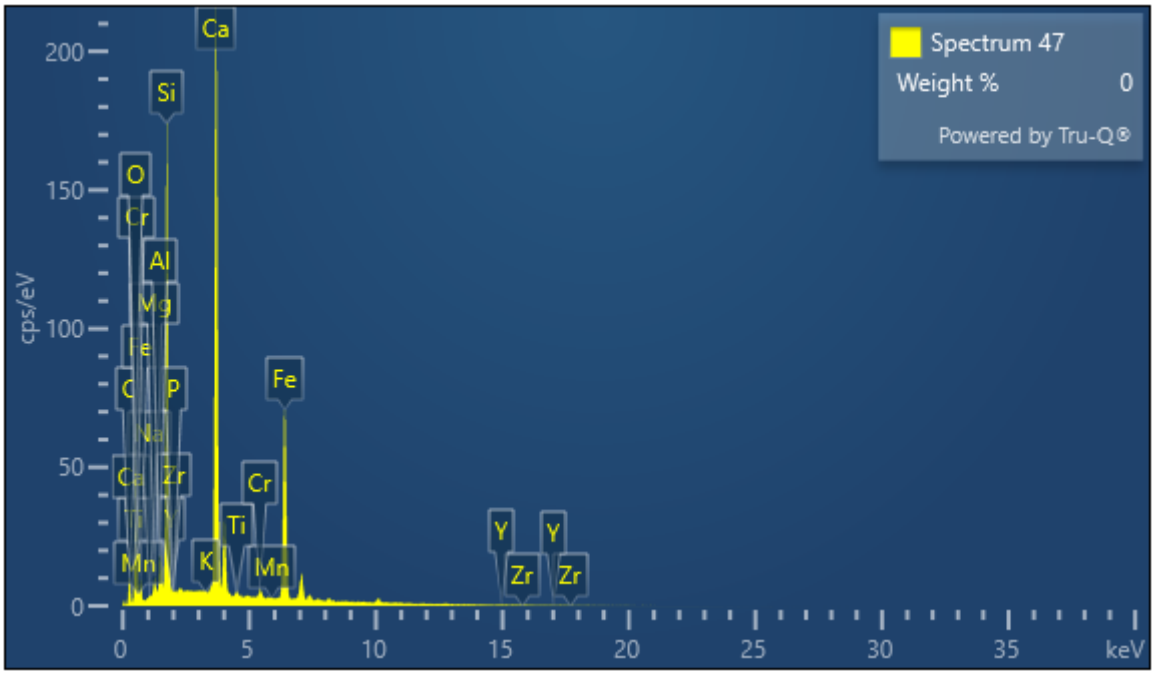
Spectrum 47
Weight % 0
Powered by Tru-Q®
cps/eV
200
150
100
50
0
0
5
10
15
20
25
30
35
keV
Ca
Si
O
Cr
Al
Mg
Fe
P
Zr
Ti
K
Mn
Y
Zr

Electron Image 5

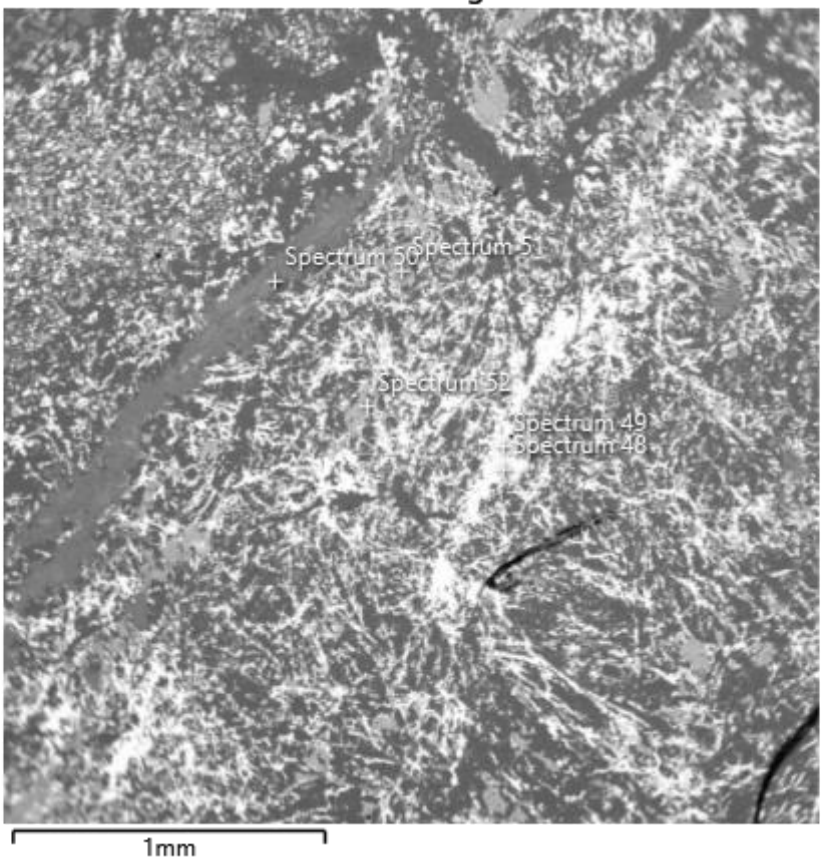

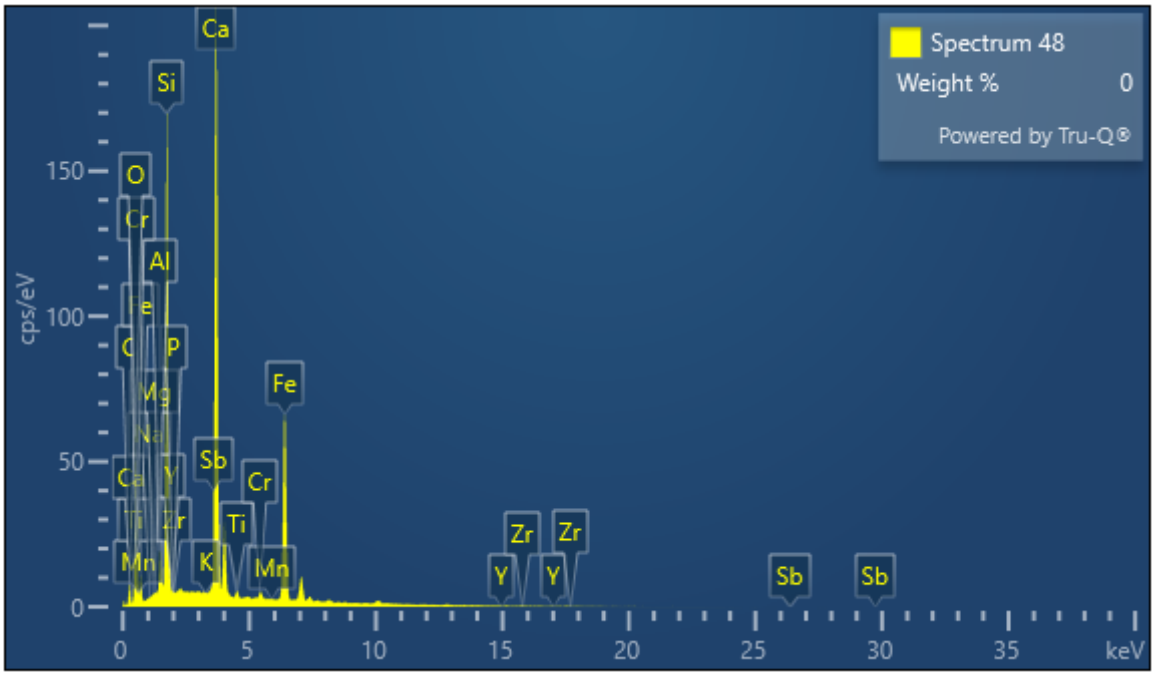

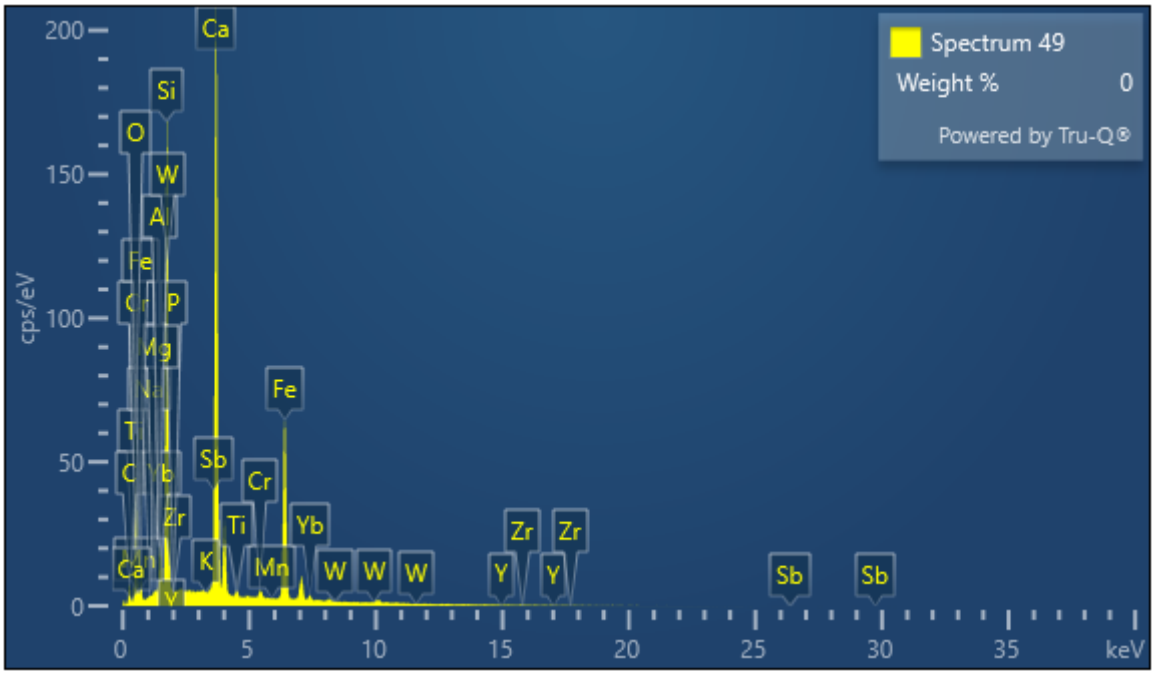
Spectrum 49
Weight % 0
Powered by Tru-Q®
cps/eV
keV
Ca
Si
O
W
Al
Fe
P
Mg
Sb
Cr
Ti
Yb
Zr
K
Mn
Y
Sb

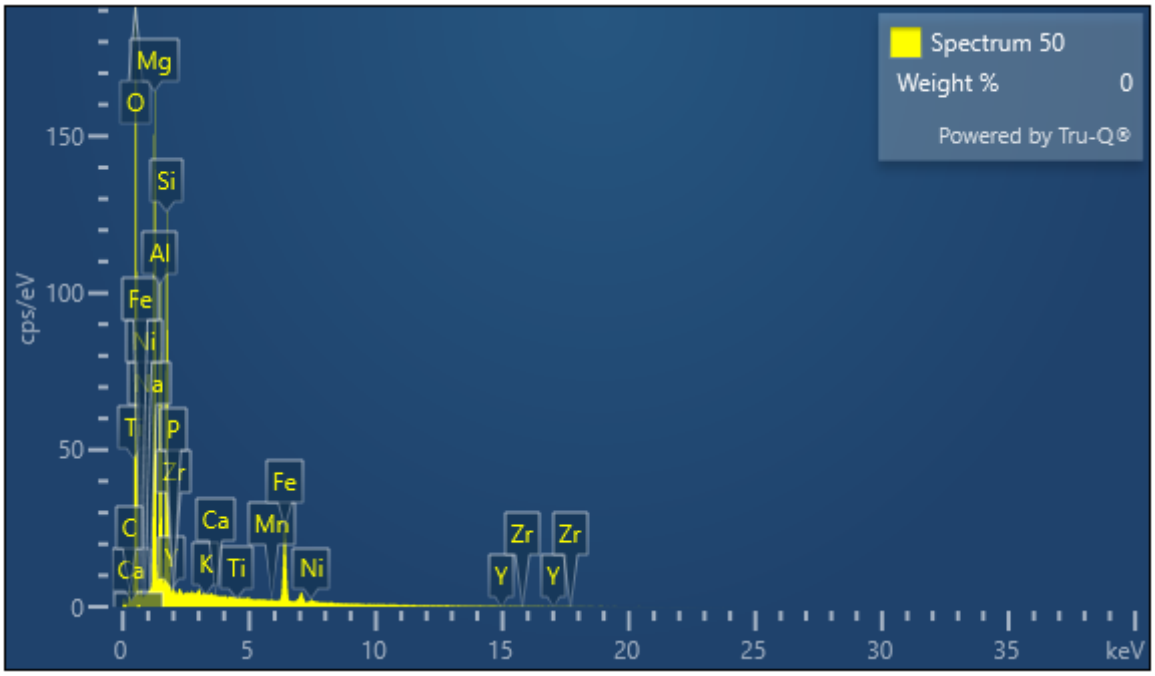
Spectrum 50
Weight % 0
Powered by Tru-Q®
cps/eV
keV
Mg
O
Si
Al
Fe
P
Zr
Ca
Mn
K
Ti
Ni
Y

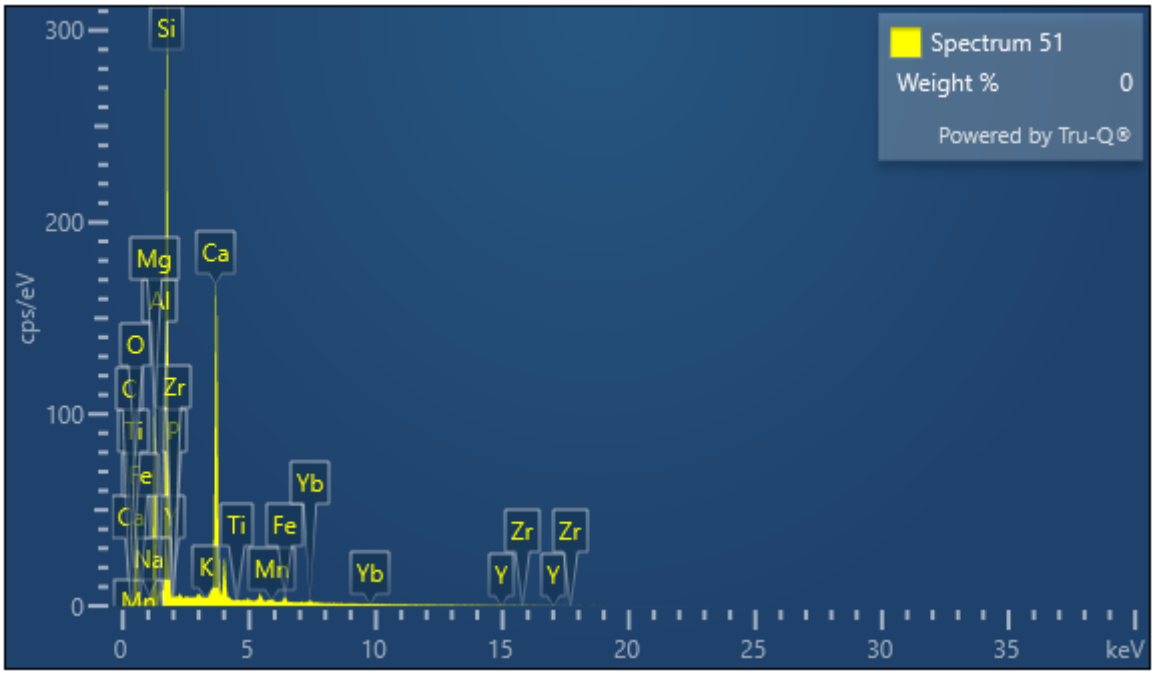
Spectrum 51
Weight % 0
Powered by Tru-Q®
cps/eV
keV
Si
Mg
Ca
Al
O
C
Zr
Ti
P
Fe
Yb
Na
K
Mn
Y

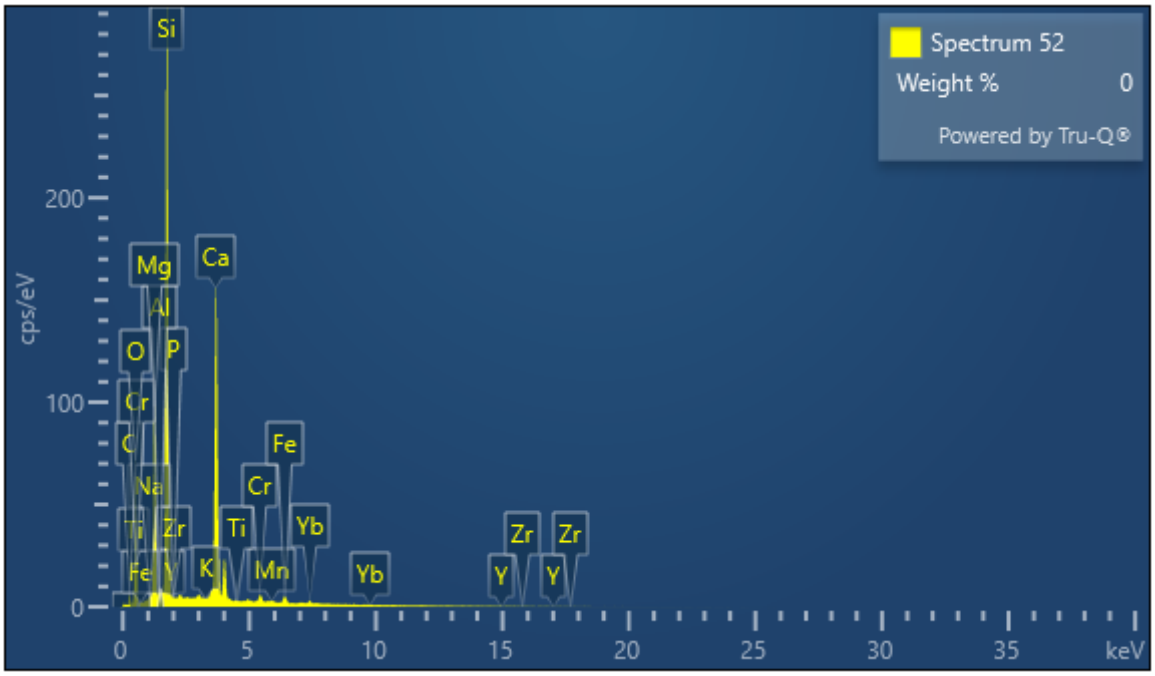
Spectrum 52
Weight % 0
Powered by Tru-Q®
cps/eV
keV
Si
Mg
Ca
Al
O
P
Cr
C
Fe
Na
Ti
Zr
K
Mn
Yb
Y

Electron Image 6

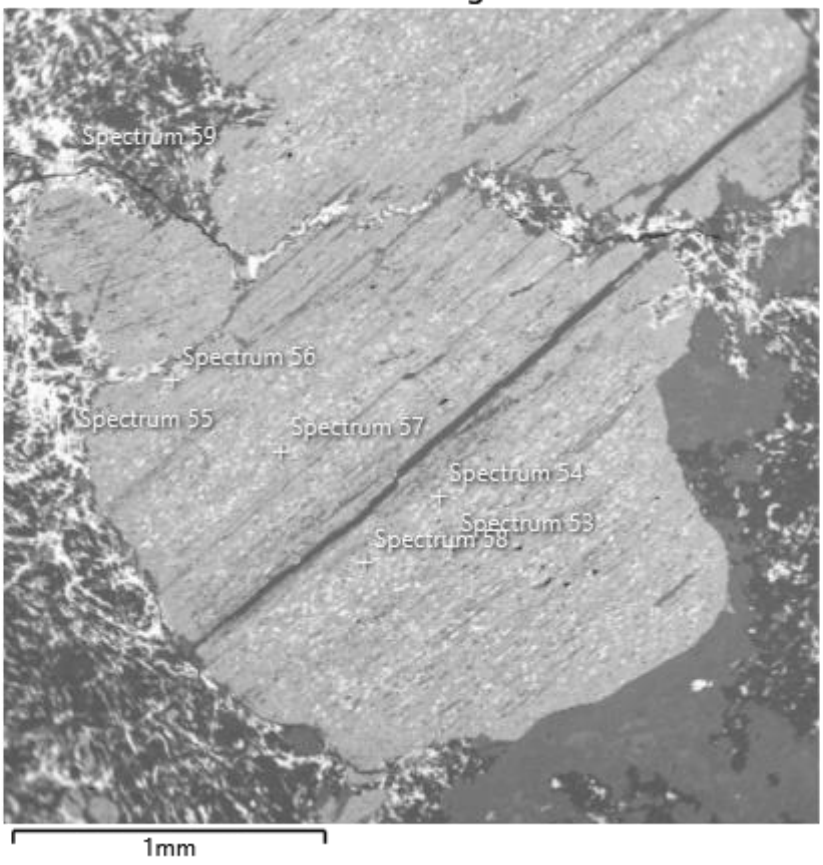

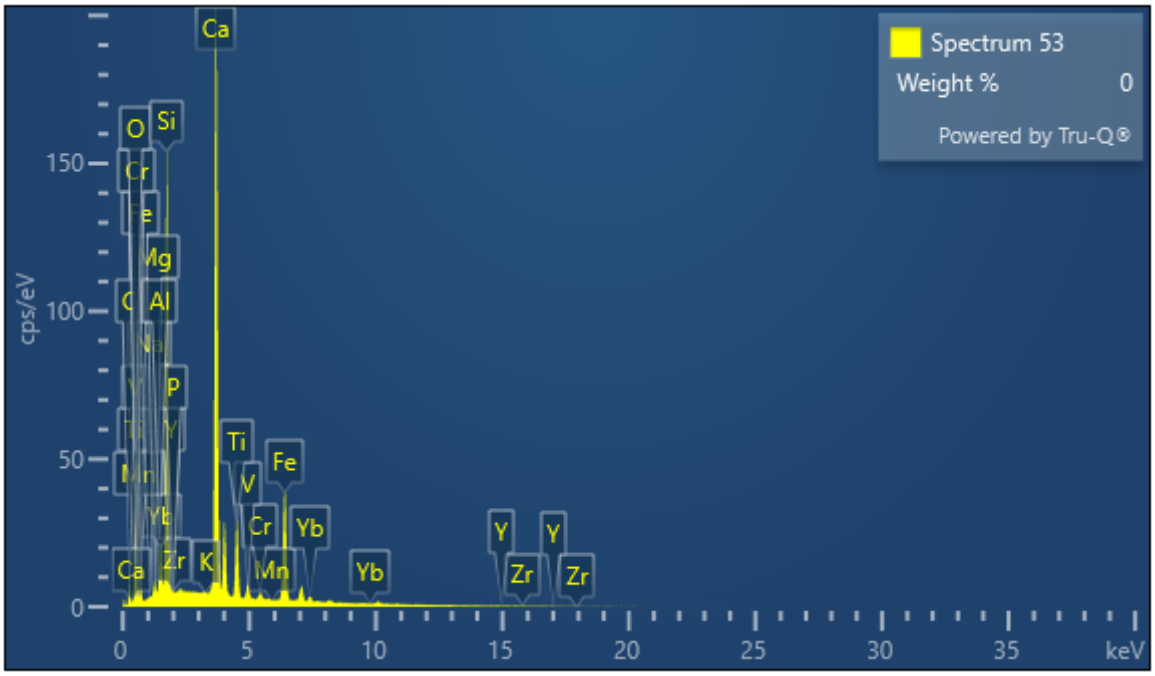

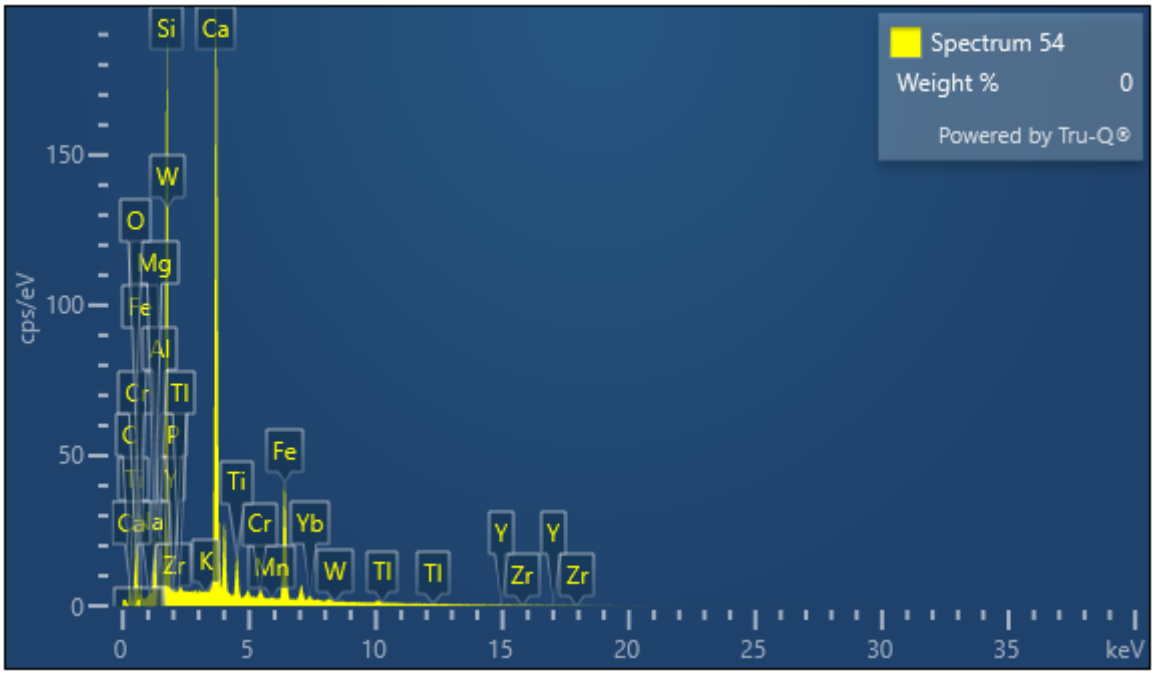
Spectrum 54
Weight % 0
Powered by Tru-Q®
cps/eV
keV
Si
Ca
W
O
Mg
Fe
Al
Cr
Tl
C
P
Ti
Yb
Y
Zr
K
Mn

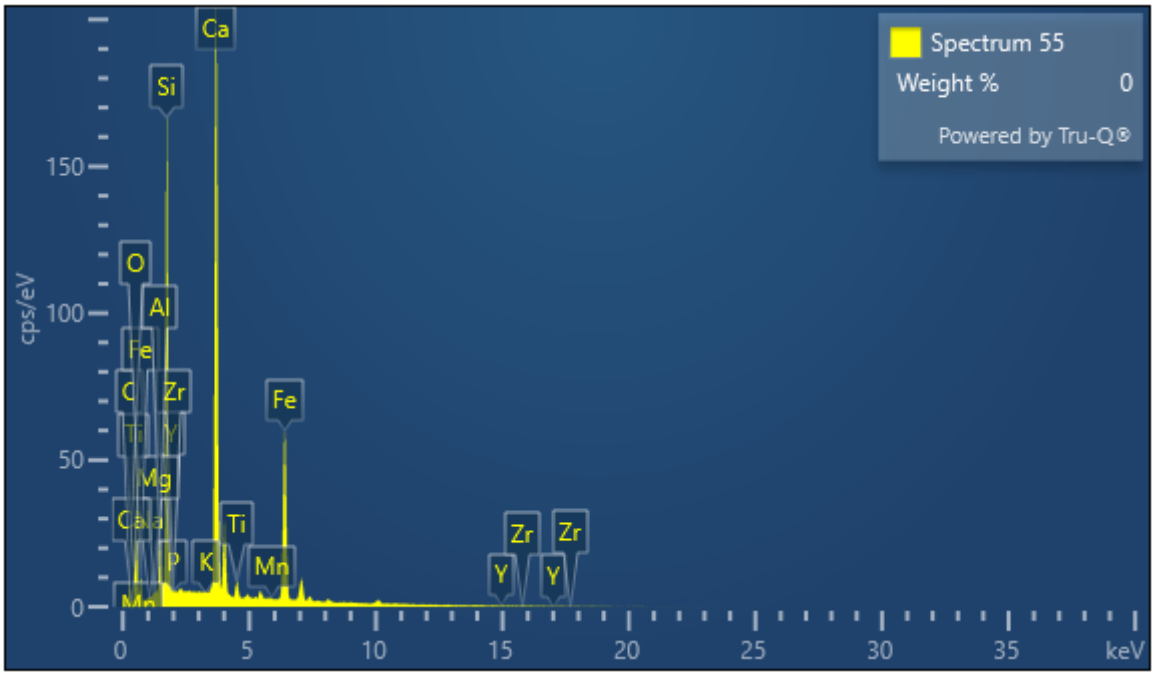
Spectrum 55
Weight % 0
Powered by Tru-Q®
cps/eV
keV
Ca
Si
O
Al
Fe
C
Zr
Ti
Y
Mg
P
K
Mn

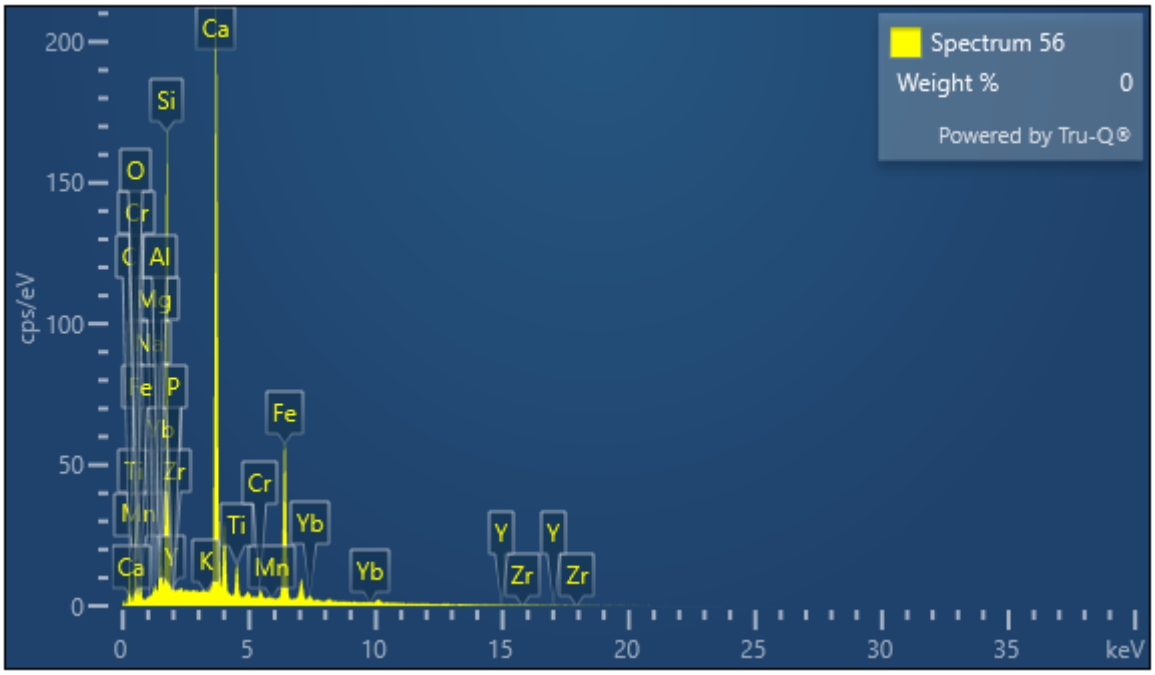
Spectrum 56
Weight % 0
Powered by Tru-Q®
cps/eV
keV
Ca
Si
O
Cr
Al
Mg
P
Fe
Ti
Zr
Mn
K
Yb
Y

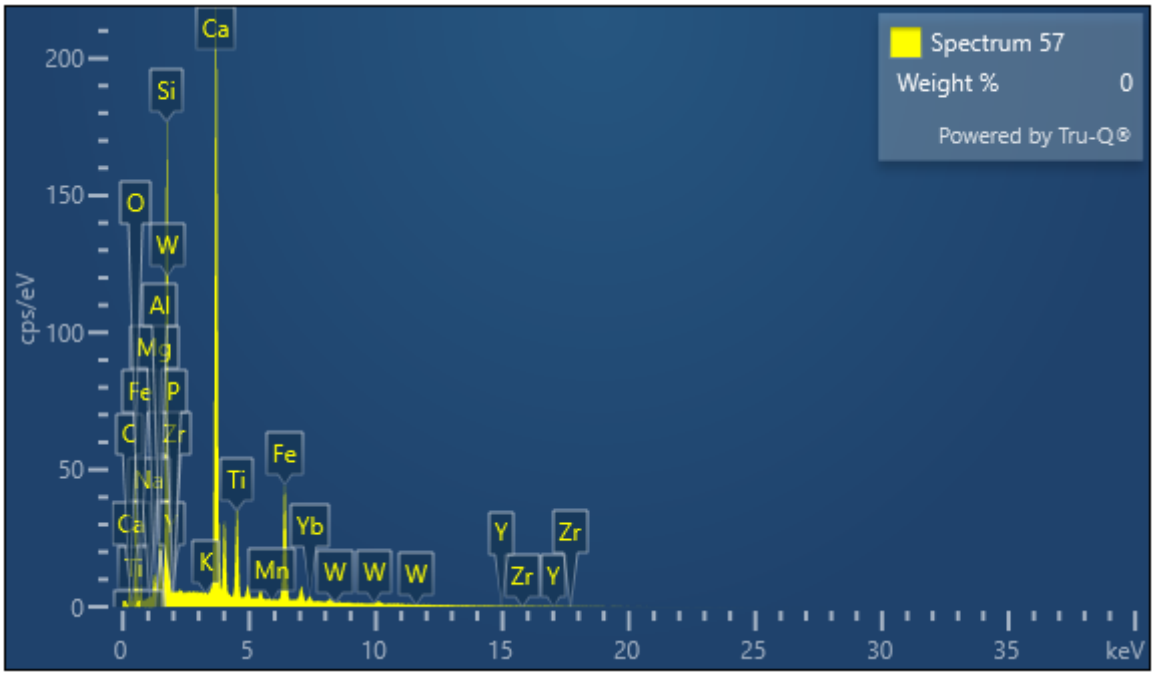
Spectrum 57
Weight % 0
Powered by Tru-Q®
cps/eV
keV
Ca
Si
O
W
Al
Mg
Fe
P
C
Zr
Na
Ti
K
Mn
Yb
Y

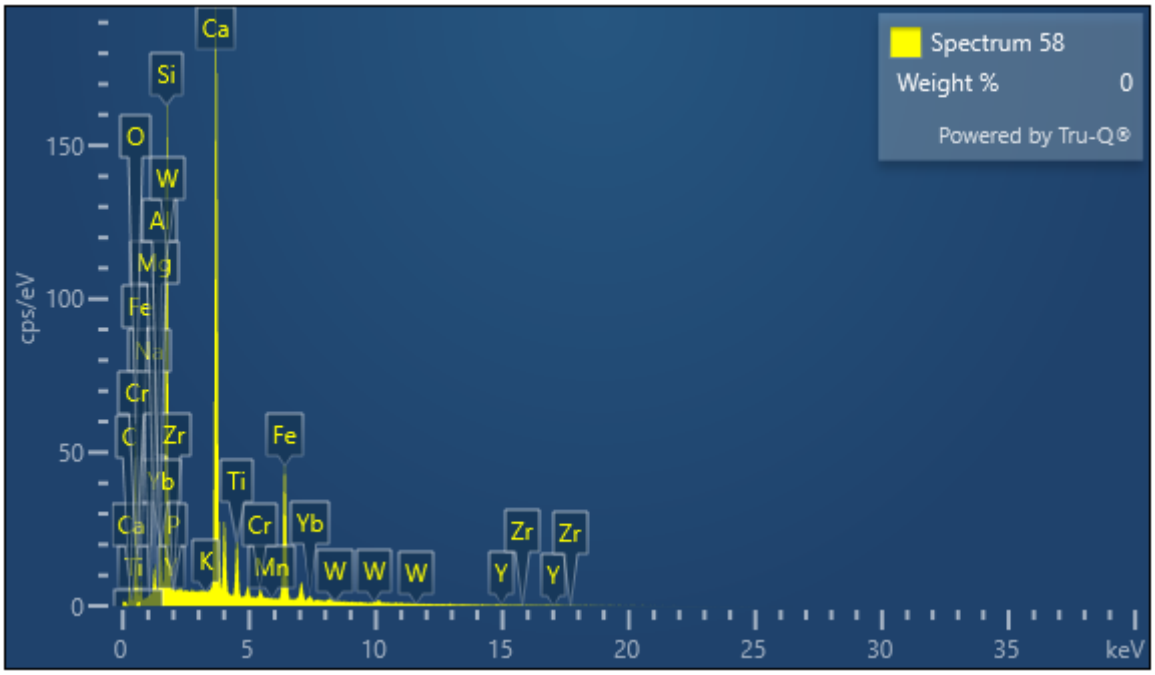
Spectrum 58
Weight % 0
Powered by Tru-Q®
cps/eV
keV
Ca
Si
O
W
Al
Mg
Fe
Cr
C
Zr
Yb
Ti
P
K
Mn
Y

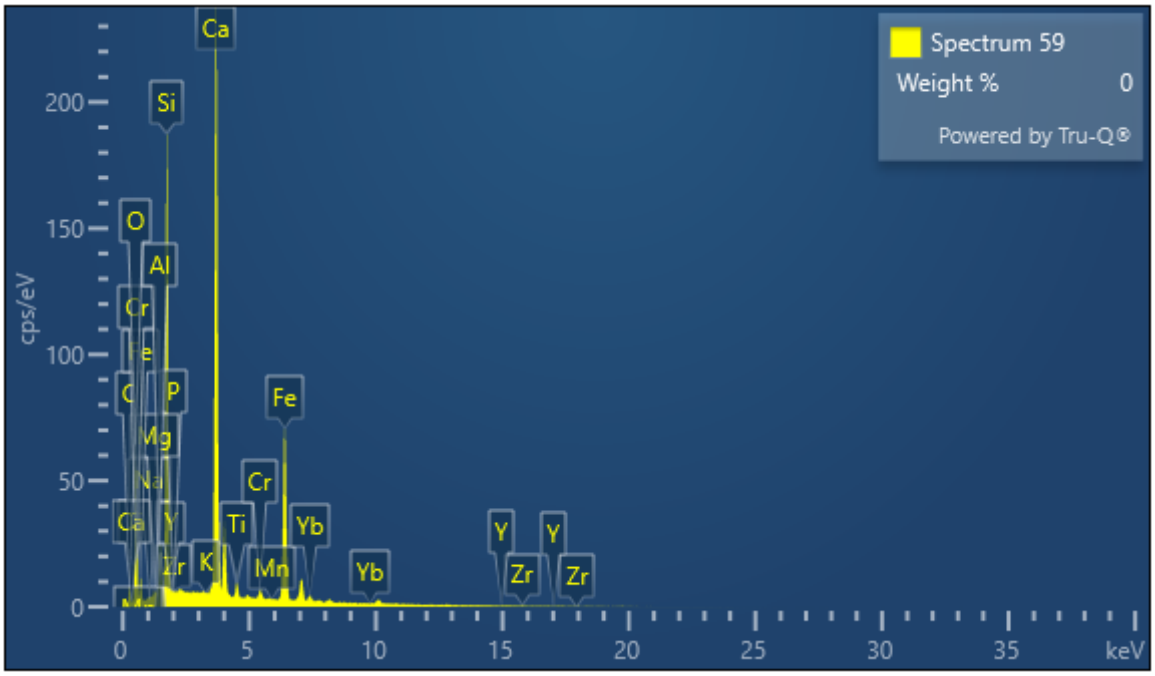
Spectrum 59
Weight % 0
Powered by Tru-Q®
cps/eV
keV
Ca
Si
O
Al
Cr
C
P
Mg
Fe
Ti
Yb
K
Mn
Y
Zr

Electron Image 7

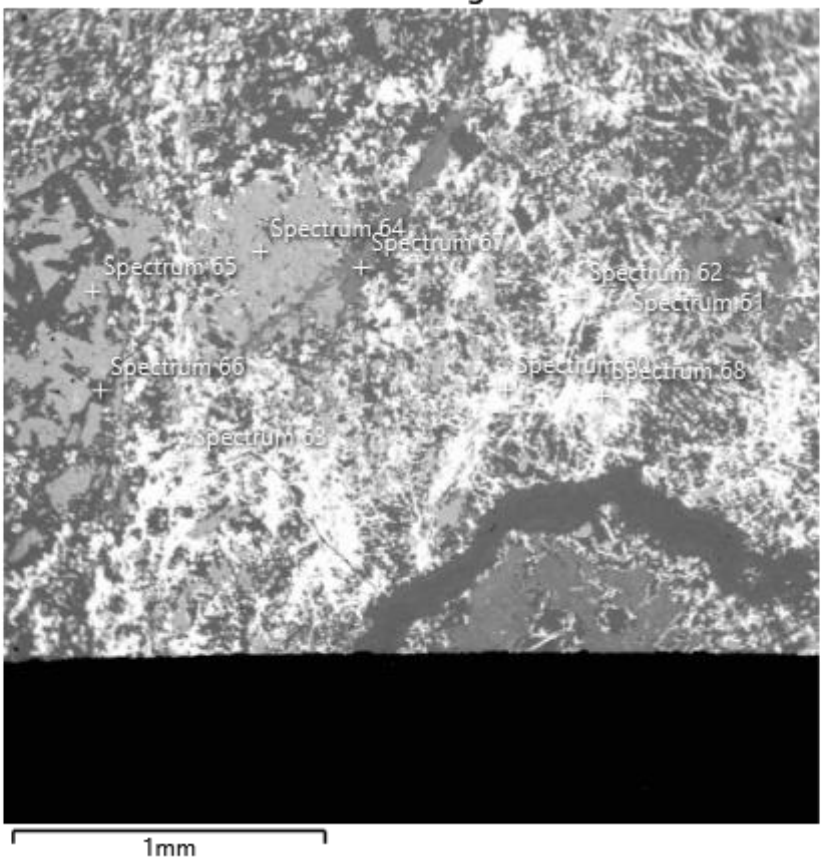

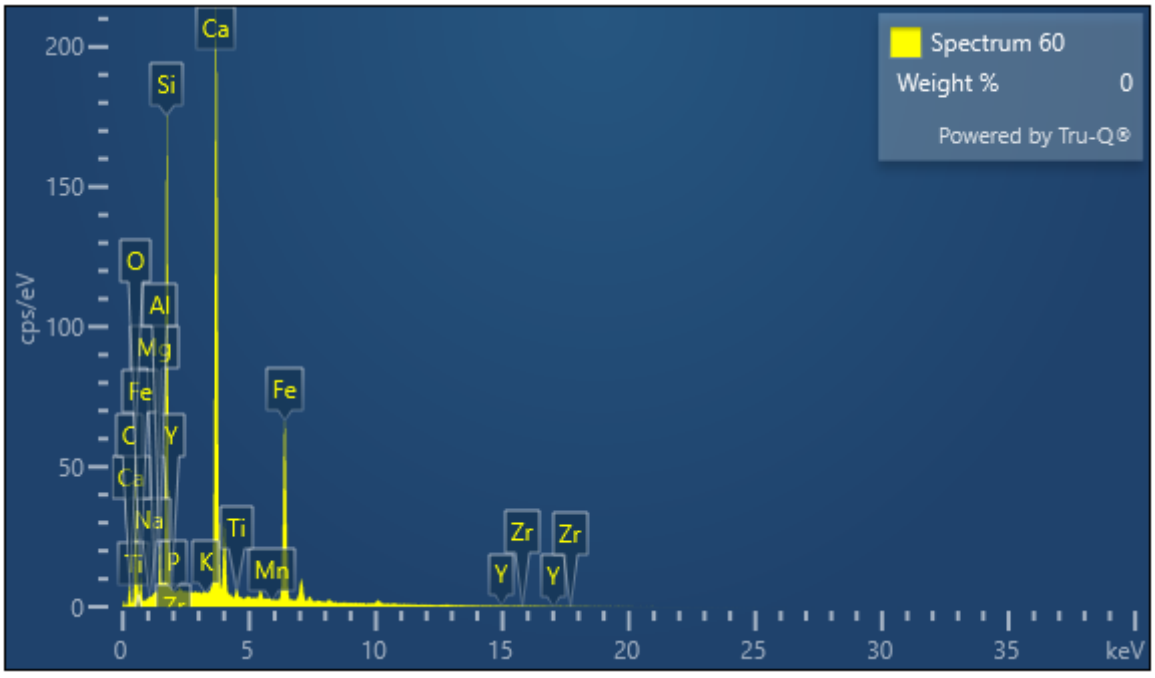

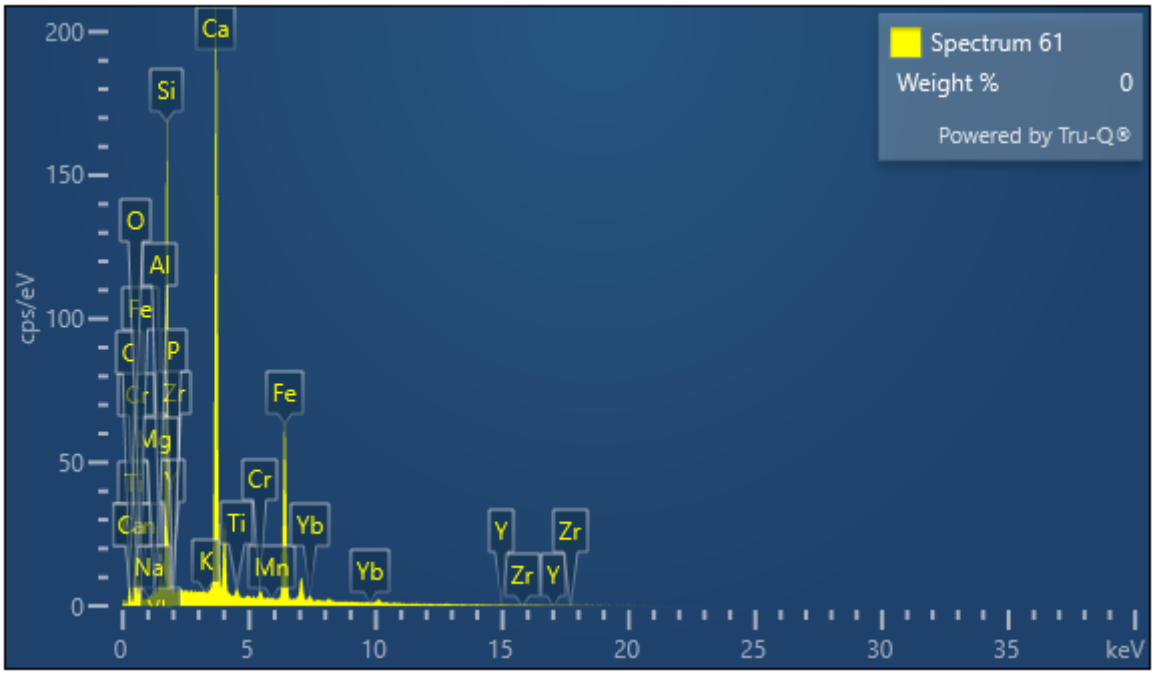
Spectrum 61
Weight % 0
Powered by Tru-Q®
cps/eV
keV
Ca
Si
O
Al
Fe
C
P
Cr
Zr
Mg
Ti
Yb
K
Mn
Na
Y

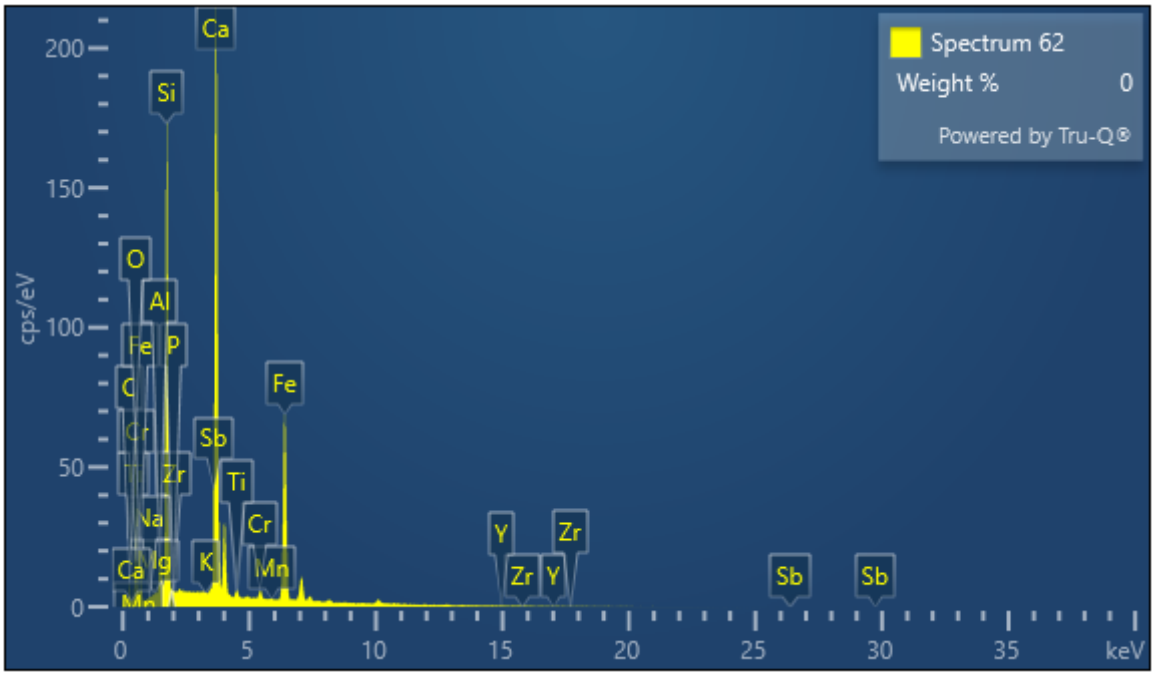
Spectrum 62
Weight % 0
Powered by Tru-Q®
cps/eV
keV
Ca
Si
O
Al
Fe
P
C
Sb
Zr
Ti
Na
Cr
K
Mn
Y
Sb

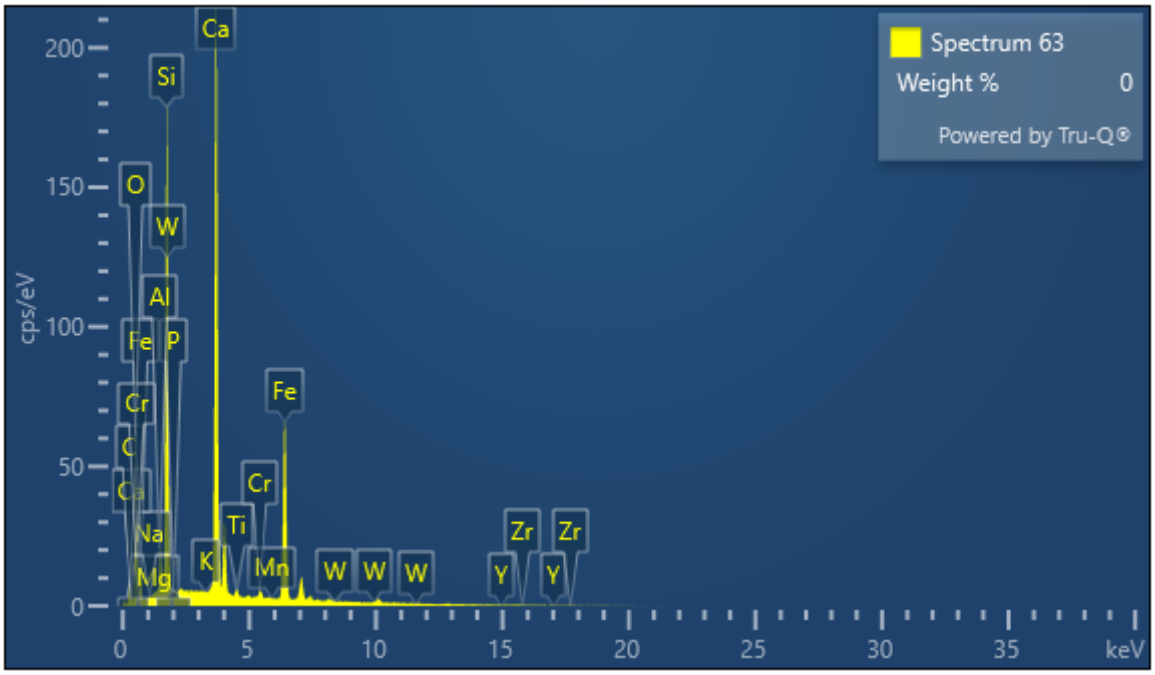
Spectrum 63
Weight % 0
Powered by Tru-Q®
cps/eV
keV
Ca
Si
O
W
Al
Fe
P
Cr
C
Ca
Na
Mg
K
Ti
Mn
W
W
W
Fe
Cr
Zr
Zr
Y
Y

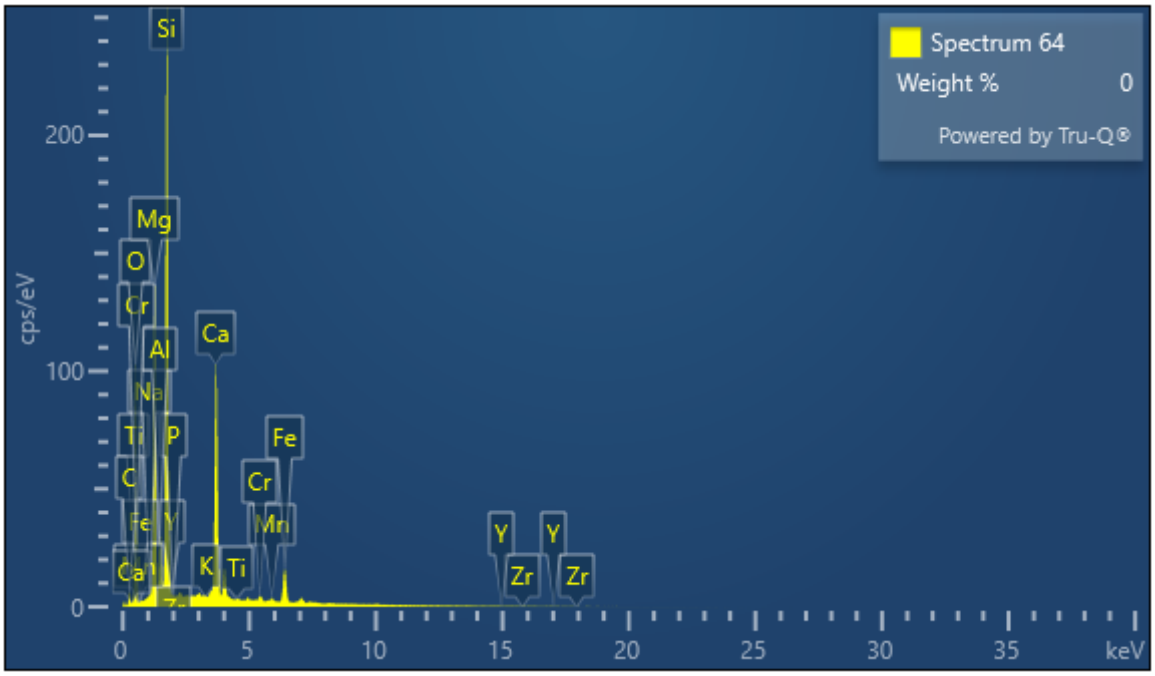
Spectrum 64
Weight % 0
Powered by Tru-Q®
cps/eV
keV
Si
Mg
O
Cr
Al
Ca
Na
Ti
P
C
Fe
Cr
Mn
Y
Y
Zr
Zr
K
Ti

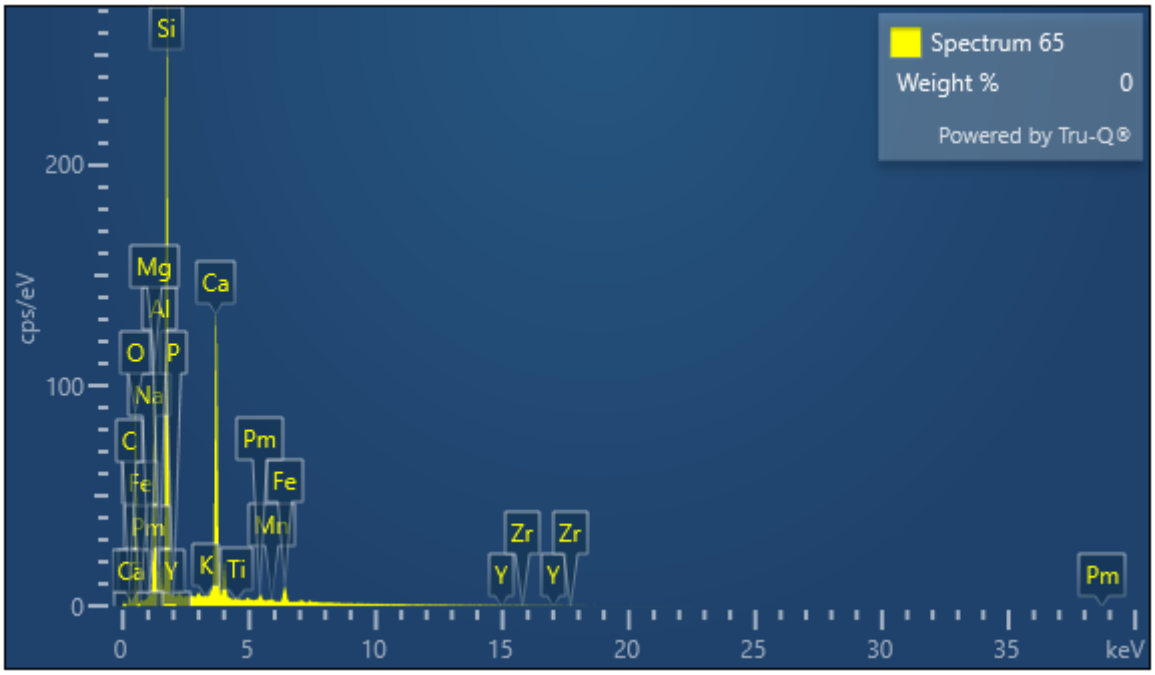
Spectrum 65
Weight % 0
Powered by Tru-Q®
cps/eV
keV
Si
Mg
Ca
Al
O
P
Na
C
Pm
Fe
Mn
Ti
K
Y
Zr

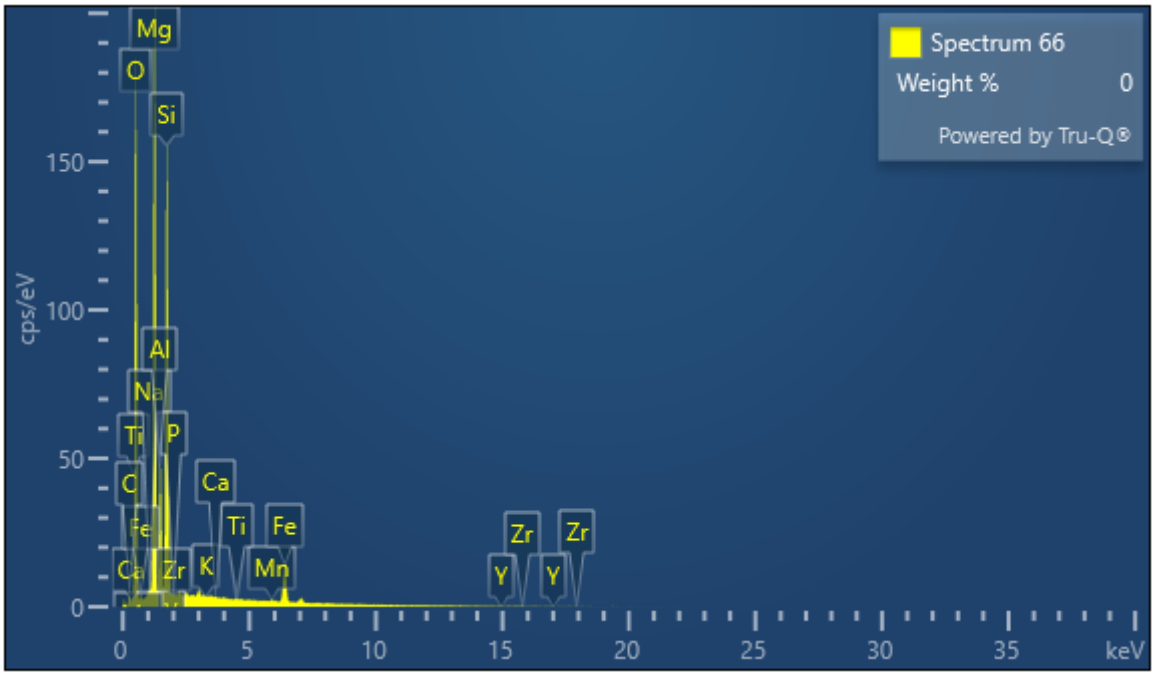
Spectrum 66
Weight % 0
Powered by Tru-Q®
cps/eV
keV
Mg
O
Si
Al
Na
Ti
P
C
Ca
Fe
Mn
K
Zr
Y

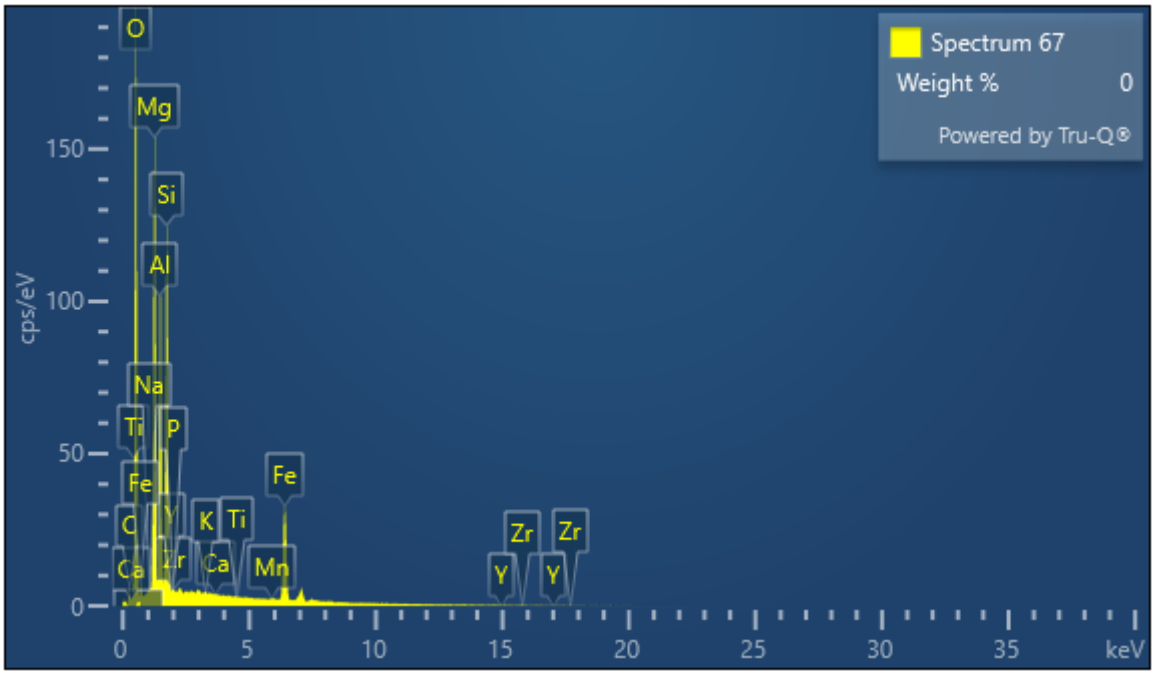
Spectrum 67
Weight % 0
Powered by Tru-Q®
cps/eV
keV
O
Mg
Si
Al
Na
Ti
P
Fe
C
Y
K
Ti
Zr
Ca
Ca
Mn
Fe
Zr
Zr
Y
Y

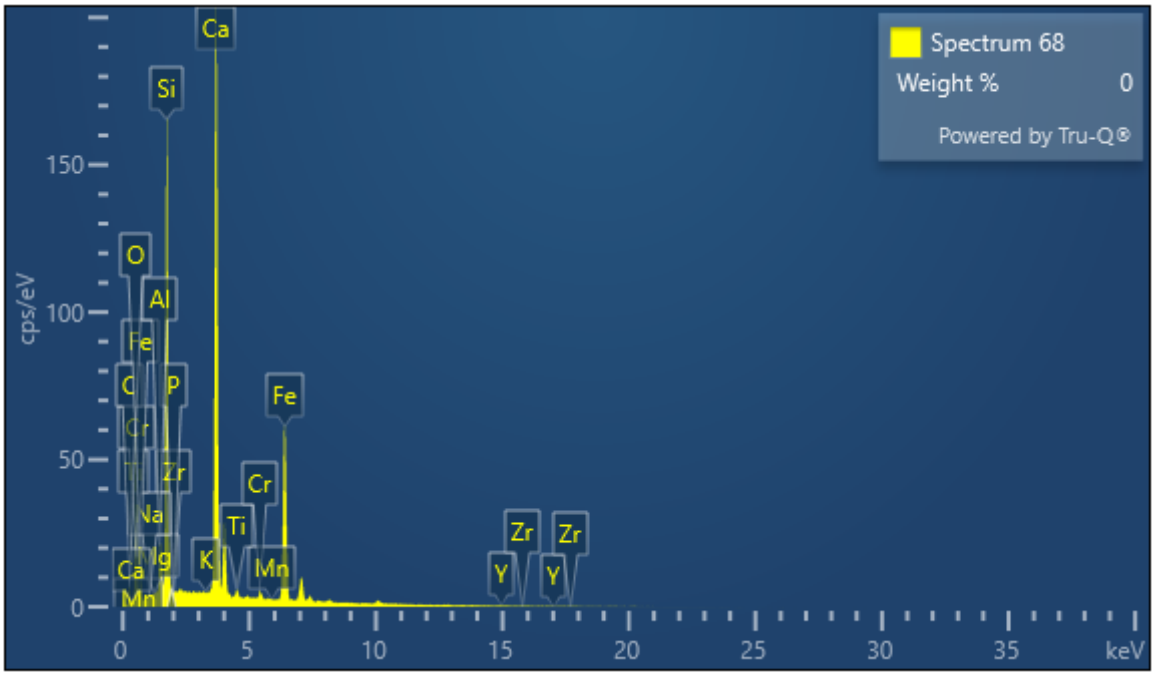
Spectrum 68
Weight % 0
Powered by Tru-Q®
cps/eV
keV
Ca
Si
O
Al
Fe
C
P
Cr
Fe
Zr
Cr
Na
Ti
Ca
Mg
K
Mn
Mn
Zr
Zr
Y
Y

Electron Image 8

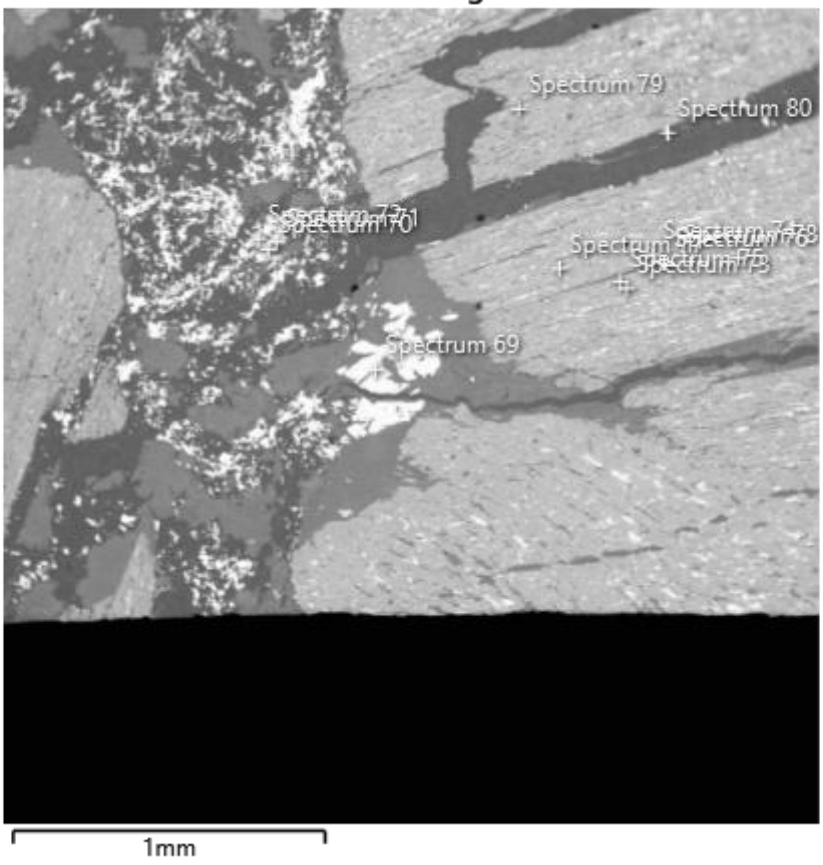

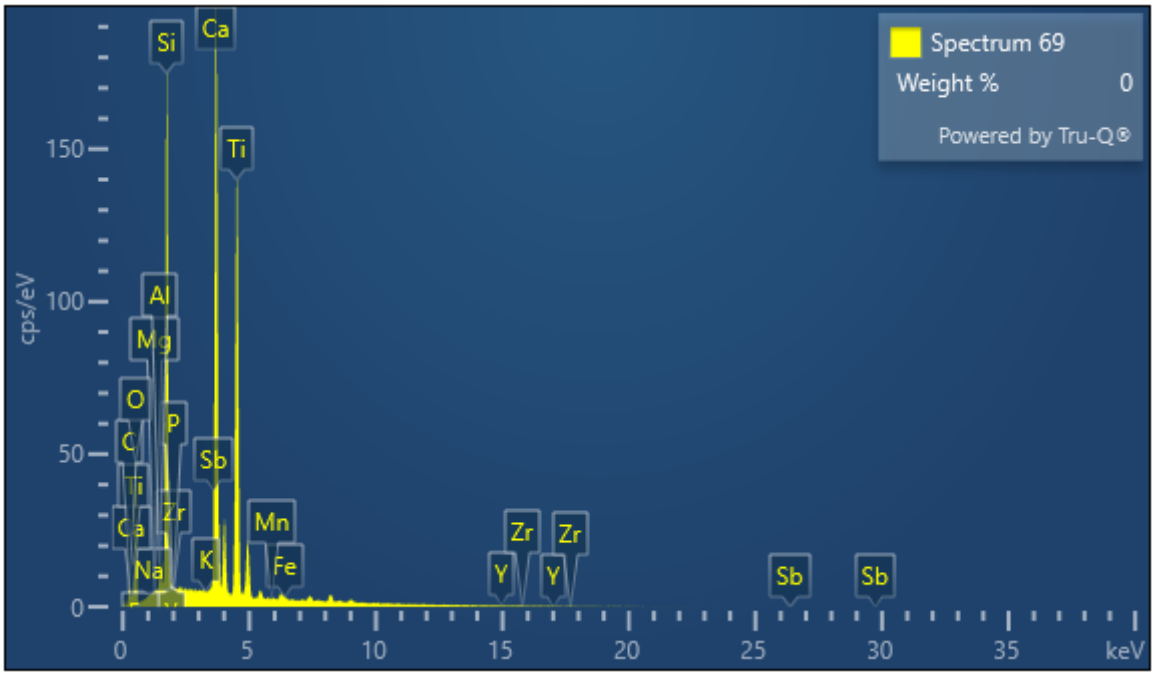

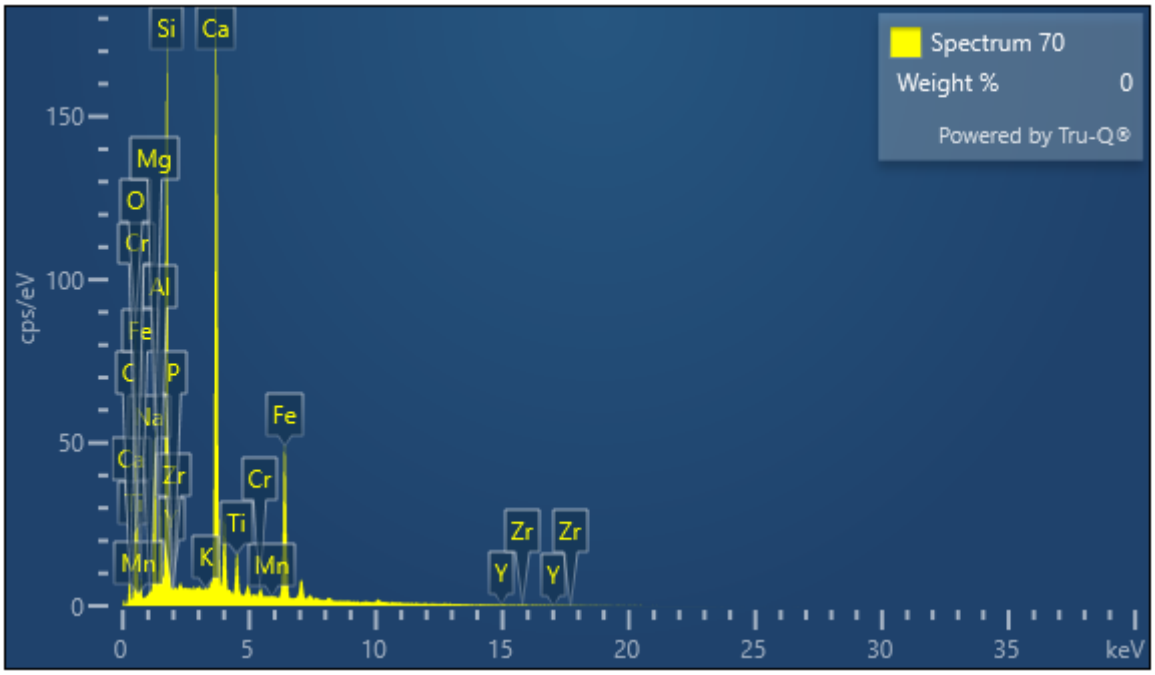
Spectrum 70
Weight % 0
Powered by Tru-Q®
cps/eV
keV
Si
Ca
Mg
O
Cr
Al
Fe
C
P
Na
Ca
Zr
Ti
K
Mn
Fe
Cr
Mn
Zr
Zr
Y
Y

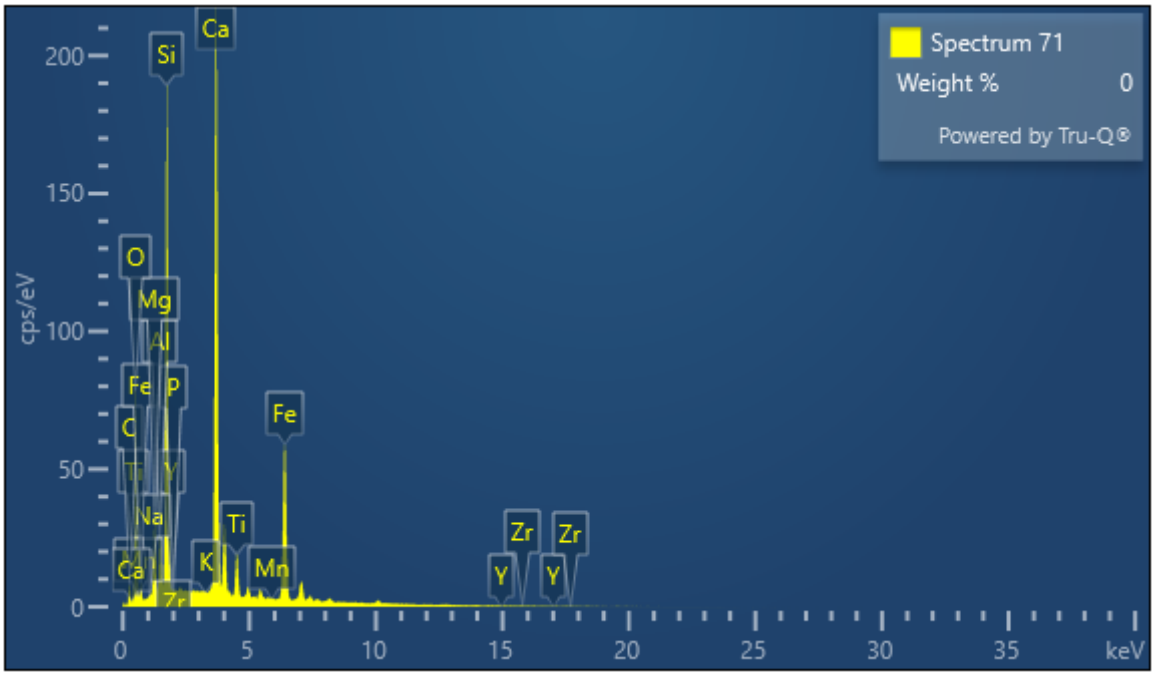
Spectrum 71
Weight % 0
Powered by Tru-Q®
cps/eV
keV
Si
Ca
O
Mg
Al
Fe
P
C
Y
Na
Ti
Ca
K
Mn
Zr
Fe
Zr
Zr
Y
Y

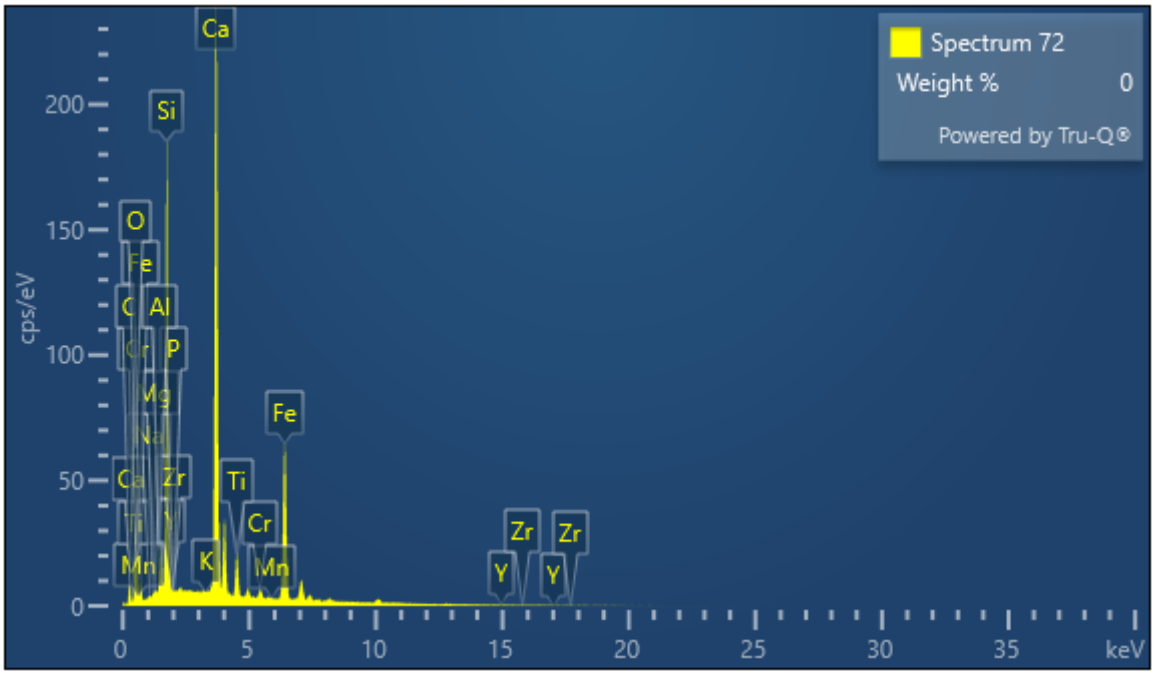
Spectrum 72
Weight % 0
Powered by Tru-Q®
cps/eV
keV
Ca
Si
O
Fe
C
Al
Cr
P
Mg
Ti
K
Mn
Zr
Y

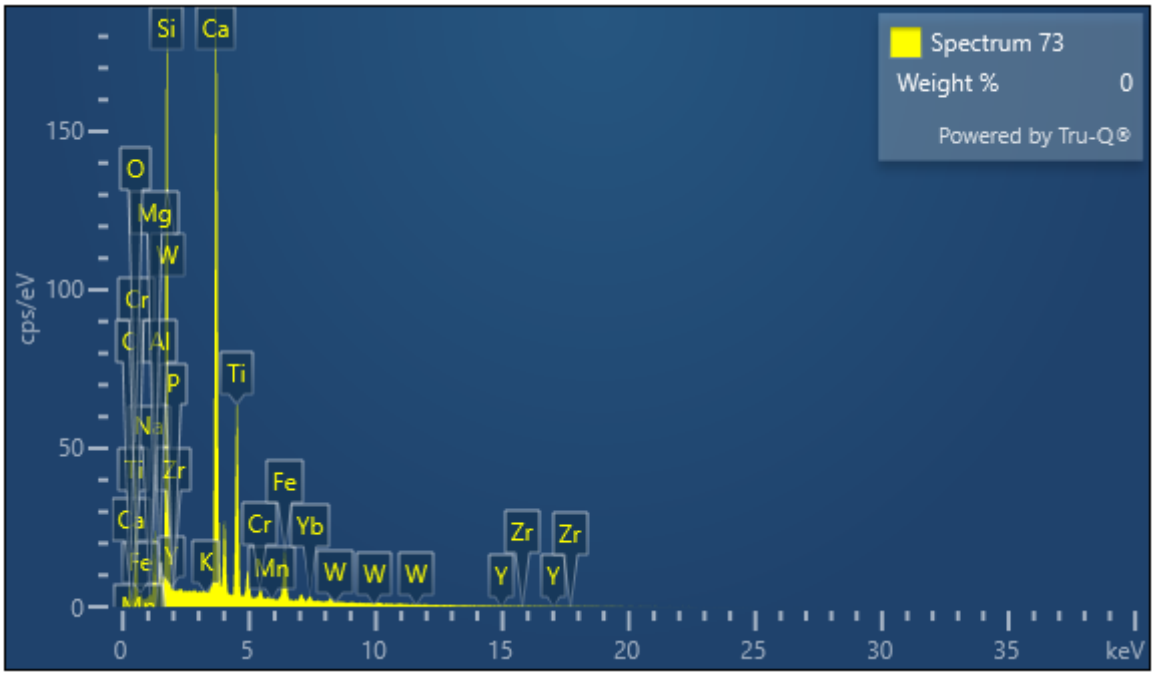
Spectrum 73
Weight % 0
Powered by Tru-Q®
cps/eV
keV
Si
Ca
O
Mg
W
Cr
C
Al
P
Ti
Fe
Yb
K
Mn
Zr
Y

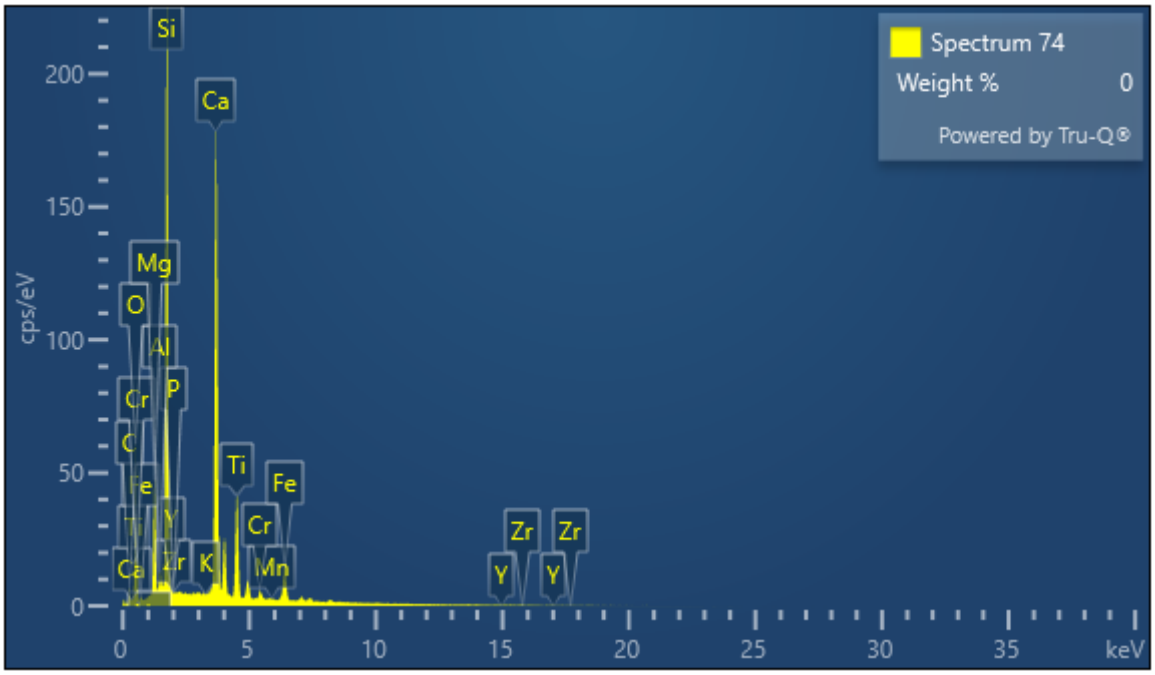
Spectrum 74
Weight % 0
Powered by Tru-Q®
cps/eV
keV
Si
Ca
Mg
O
Al
P
Cr
C
Ti
Fe
Y
Zr
K
Mn

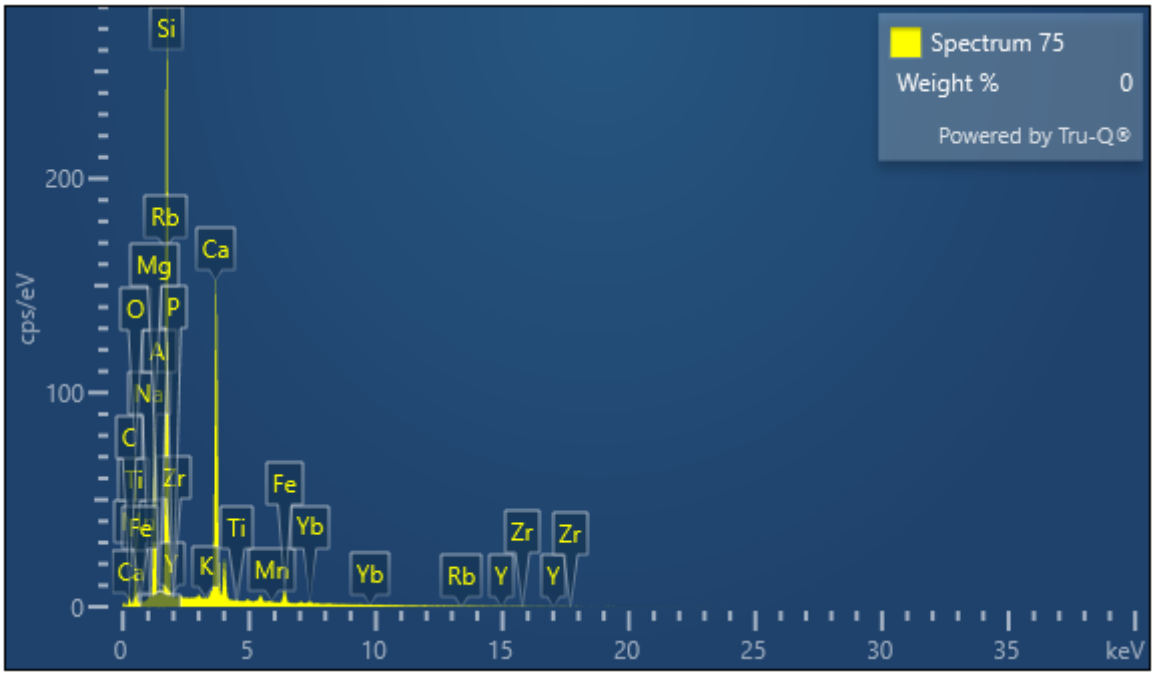
Spectrum 75
Weight % 0
Powered by Tru-Q®
cps/eV
keV
Si
Rb
Ca
Mg
O
P
Al
C
Ti
Zr
Fe
Yb
K
Mn
Y

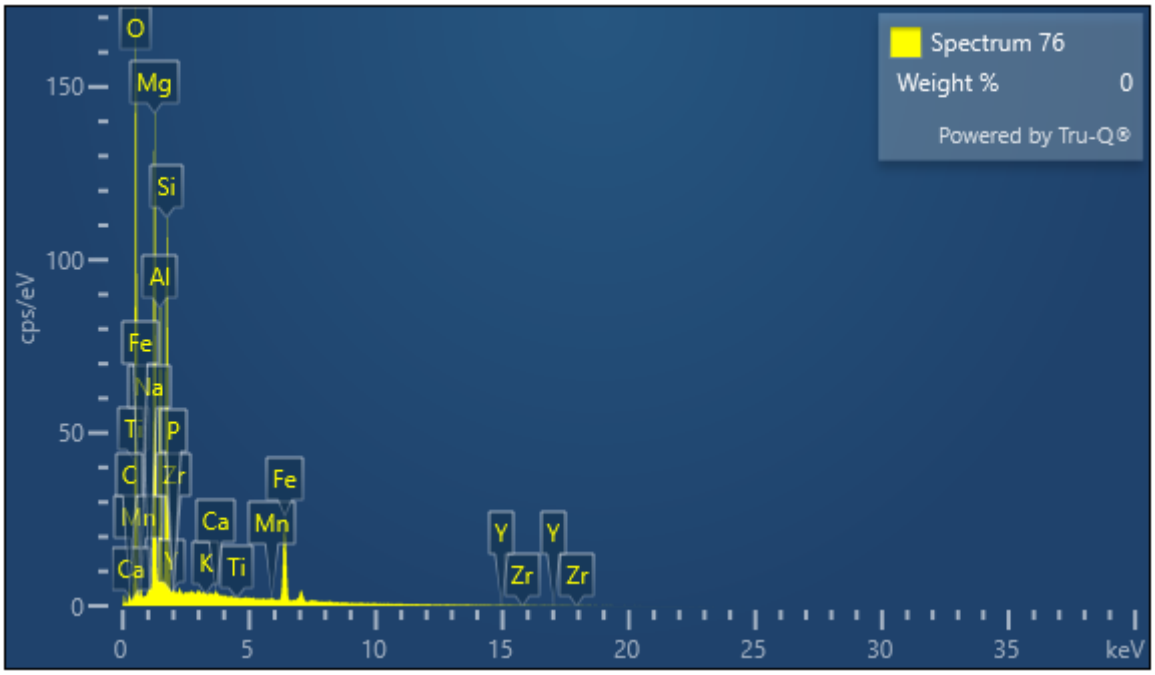
Spectrum 76
Weight % 0
Powered by Tru-Q®
cps/eV
keV
O
Mg
Si
Al
Fe
Na
Ti
P
C
Zr
Mn
Ca
K
Y
Zr

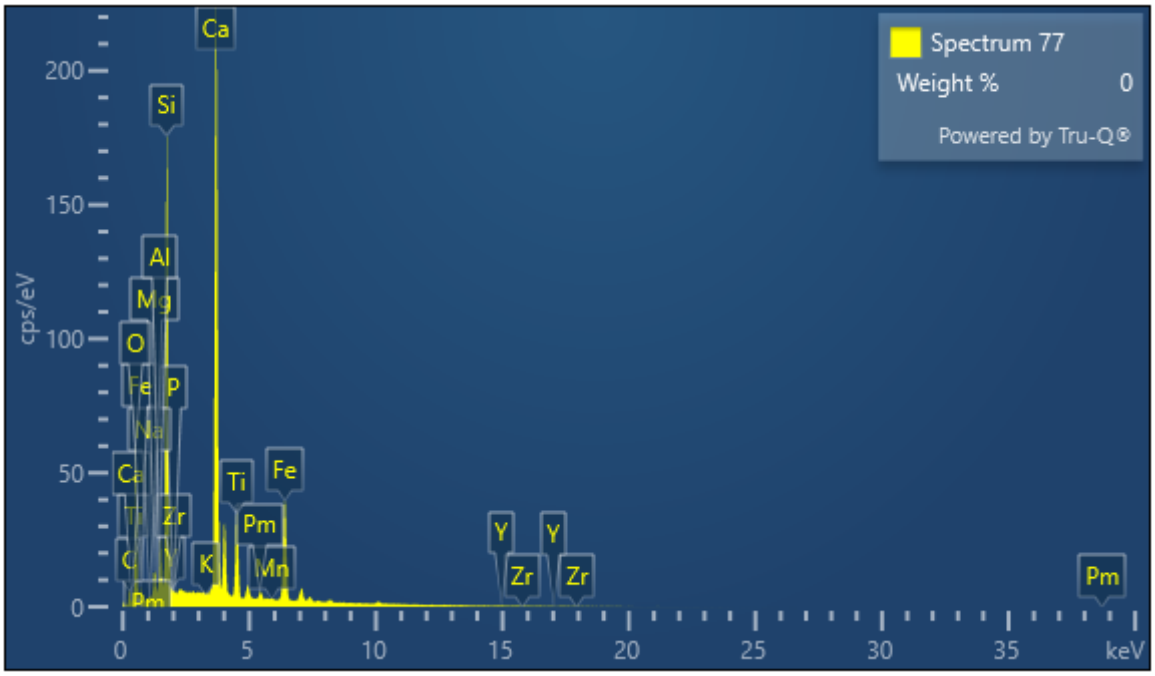
Spectrum 77
Weight % 0
Powered by Tru-Q®
cps/eV
keV
Ca
Si
Al
Mg
O
Fe
P
Ti
Pm
K
Mn
Y
Zr
Pm

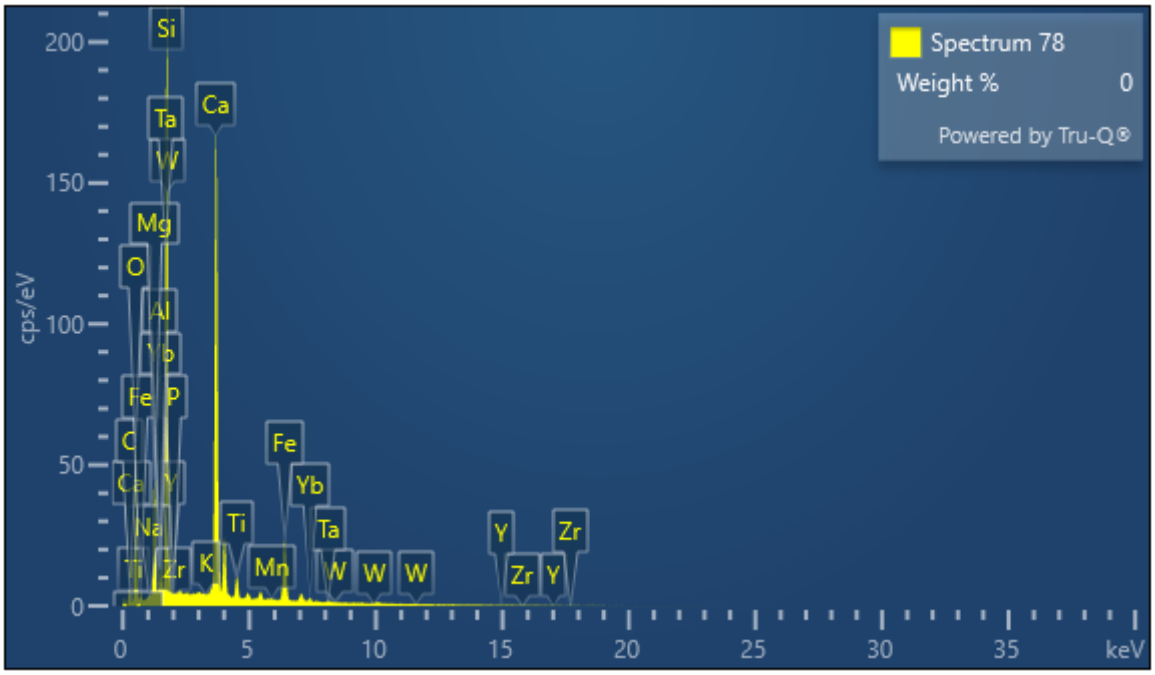
Spectrum 78
Weight % 0
Powered by Tru-Q®
cps/eV
keV
Si
Ca
Ta
W
Mg
O
Al
Yb
Fe
P
C
Ca
Y
Na
Ti
Zr
K
Mn
Fe
Yb
Ta
W
W
W
Y
Zr
Y
Zr

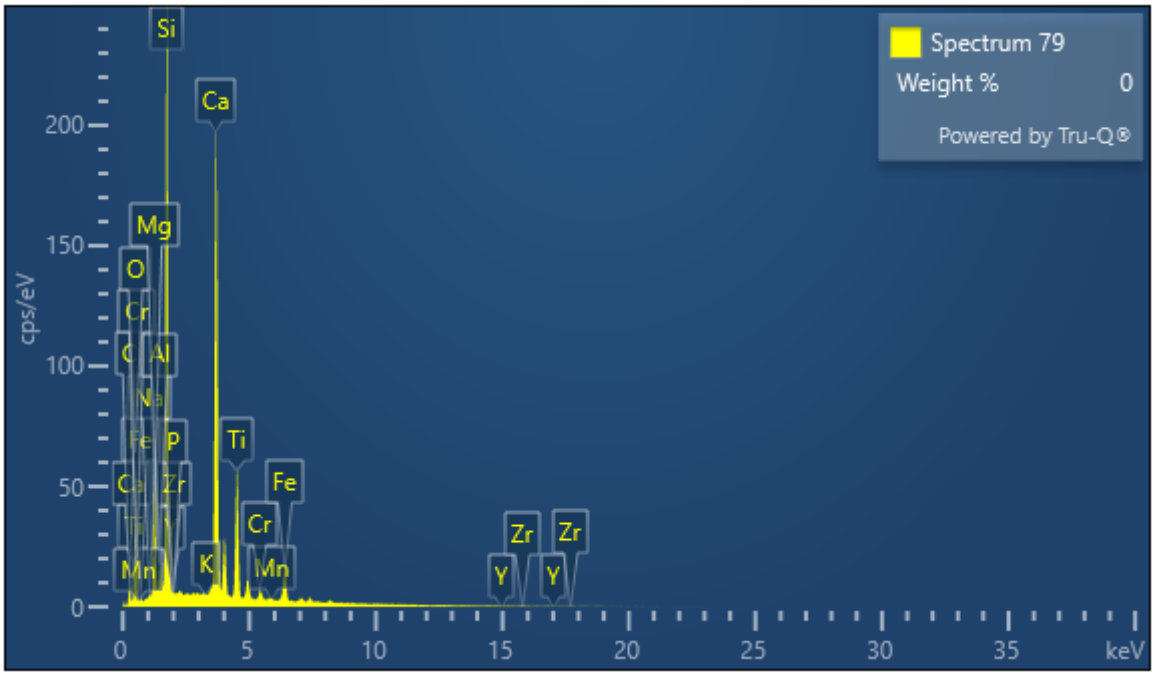
Spectrum 79
Weight % 0
Powered by Tru-Q®
cps/eV
keV
Si
Ca
Mg
O
Cr
C
Al
Na
Fe
P
Ti
Ca
Zr
Fe
Cr
Mn
K
Mn
Zr
Zr
Y
Y

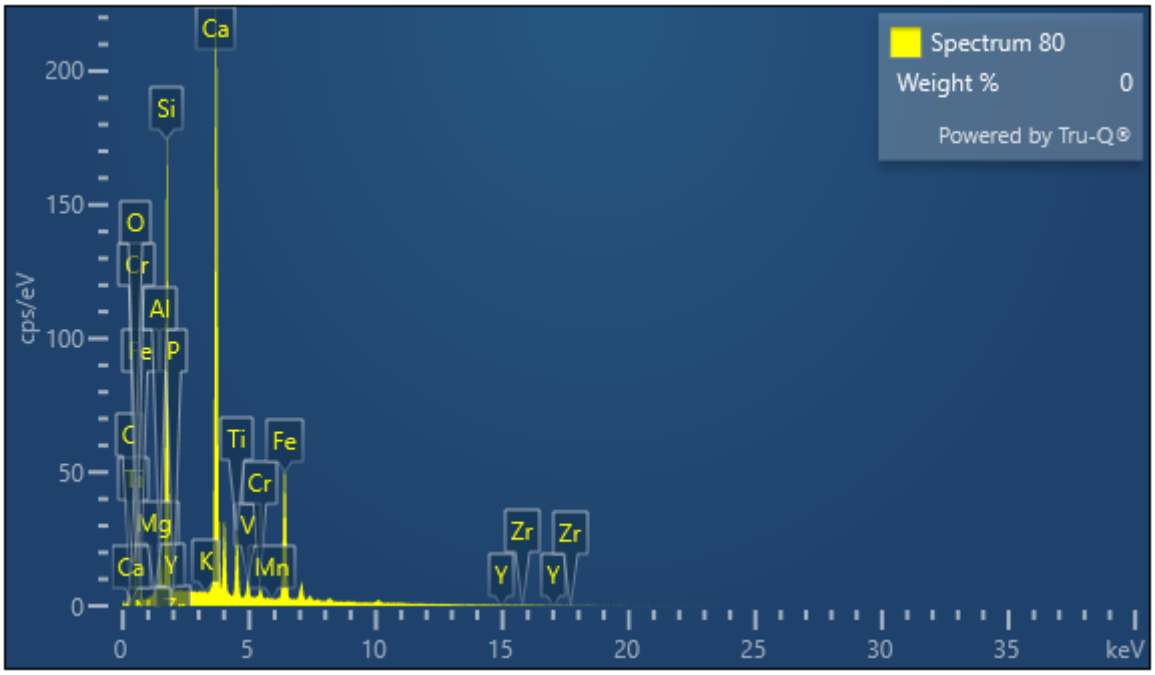
Spectrum 80
Weight % 0
Powered by Tru-Q®
cps/eV
200
150
100
50
0
0
5
10
15
20
25
30
35
keV
Ca
Si
O
Cr
Al
Fe
P
C
Ti
Fe
Cr
V
Mg
Ca
Y
K
Mn
Zr
Zr
Y
Y

Table 6

21LAP SPIKE SHEET SUMMARY

Sample:	87/86 Exp Pre Spk	87/86 Exp	2sig error	2sig error ppm	Sr ppm
21LAP-UCR-1.15-2F	0.7063440	0.7071529	0.0000054	7.62	4.0
21LAP-UCR-4.62-2F	0.701121	0.707410	0.000010	14.43	1.5
21LAP-UCR-15.92-2F	0.7049694	0.7074441	0.0000051	7.17	1.4
21LAP-UCR-25.17-2C	0.7033625	0.7042272	0.0000034	4.79	5.1
21LAP-UCR-38.66-2C	0.7031087	0.7045154	0.0000064	9.07	4.7
21LAP-UCR-45.04-2C	0.7034307	0.7049024	0.0000072	10.23	4.0
21LAP-UCR-50.29-2C	0.703791	0.705194	0.000017	23.55	3.9
21LAP-UCR-61.95-2C	0.7041258	0.7064034	0.0000061	8.61	3.0
21LAP-UCR-68.72-2C	0.7042080	0.7068201	0.0000028	3.89	2.5
21LAP-UCR-79.91-2C	0.7046504	0.7062277	0.0000062	8.83	4.4
21LAP-UCR-90.51-2C	0.703983	0.705775	0.000049	69.09	4.2
21LAP-UCR-101.88-2C	0.704141	0.705778	0.000040	55.97	4.2
21LAP-UCR-118.67-2C	0.7049091	0.7060975	0.0000053	7.51	5.5
21LAP-UCR-124.52-2C	0.7046650	0.7060638	0.0000048	6.83	5.1
21LAP-UCR-140.55-2C	0.7049154	0.7067043	0.0000044	6.21	4.0
21LAP-UCR-149.29-2C	0.7047943	0.7067745	0.0000051	7.23	3.3
21LAP-UCR-166.20-2C	0.7046541	0.7064641	0.0000030	4.25	3.9
21LAP-UCR-175.99-2C	0.7046979	0.7061800	0.0000079	11.17	4.6
21LAP-UCR-186.19-2C	0.705054	0.706817	0.000013	18.69	3.7
21LAP-UCR-188.62-2C	0.7050691	0.7063913	0.0000042	5.93	2.4
21LAP-UCR-205.40-2C	0.7040992	0.7061456	0.0000052	7.37	4.4
21LAP-UCR-215.02-2C	0.7045688	0.7061698	0.0000039	5.48	4.3
21LAP-UCR-234.94-2C	0.7045303	0.7061616	0.0000032	4.60	4.3
21LAP-LCR-1.98-2E	0.7050688	0.7069310	0.0000042	5.91	5.2
21LAP-LCC-0.86-2E	0.7066665	0.7072816	0.0000036	5.12	5.0
21LAP-UCS-110.68-2H	0.7063344	0.7078154	0.0000040	5.67	14.4
21LAP-UCS-90.19-2H	0.7055775	0.7060988	0.0000088	12.42	12.4
21LAP-UCS-85.11-2H	0.7054179	0.7057023	0.0000041	5.76	24.0
21LAP-UCS-80.23-2H	0.7055166	0.7058462	0.0000046	6.48	19.9
21LAP-UCS-76.82-2H	0.7056672	0.7059913	0.0000042	5.96	20.2
21LAP-UCS-68.94-2H	0.7064864	0.7071382	0.0000060	8.50	10.5
21LAP-UCS-39.72-2H	0.7065577	0.7078921	0.0000066	9.27	5.0
21LAP-UCS-24.93-2F	0.7046121	0.7068454	0.0000061	8.57	3.1
21LAP-UCS-10.76-2F	0.7047925	0.7065992	0.0000059	8.39	3.1
21LAP-UCS-2.04-2F	0.7054376	0.7070286	0.0000043	6.02	4.3
21LAP-LCS-3.76-2E	0.7047980	0.7079137	0.0000057	8.11	2.2
21LAP-LCS-6.55-2E	0.704889	0.707904	0.000033	46.03	2.3
21LAP-LCS-25.85-2E	0.7051865	0.7081513	0.0000048	6.84	2.3
21LAP-LCS-49.91-2E	0.7074763	0.7086356	0.0000060	8.48	2.1
21LAP-LCS-76.81-2E	0.7055409	0.7086460	0.0000044	6.26	1.9
21LAP-LCS-100.85-2E	0.7062707	0.7090363	0.0000052	7.34	2.6

Sample:	**21LAP-UCR-1.15-2F**	Turret(Bead):	12
Operator:	**CTL**	Date:	4/7/2022
		Time:	

	Rspike Values: Sr84-3(x10)#2		
Name	Rsp84\88	Rsp86\88	Rsp87\88
Value	**5.96961**	**0.33048**	**0.12894**

[Sr84-3(x10)#2]
Conc.Spike
8.84500

Final Results

Wt.Sample	**0.105790**	g
Wt.Spike	**0.008780**	g

Unspike subtracted grand mean ratios (Measured Ratios)

	RI_84\88	RI_86\88	RI_87\86
Ratios	2.60E-02	0.11940	7.06E-01
%StdErr	1.22E-03	0	3.81E-04
	# Ratios	Enter # of ratios	

discrimination corrected (Sr86/Sr88)m= 0.1201

Spike subtracted grand mean ratios (Reported Ratios)

	84/88	87/88	87/86	88s/84t
Ratios	0.006747	0.084434	**0.707153**	**50.829314**
2Sigma errors	0.000000	0.000000	**0.000005**	**0.000000**
2*Sig. err. (ppm)=(epsilon*100)	0	0	**7.6176038**	**0.001224846**

[Sr86]= **4.455** nm/g
± **0.000**

[Sr]= **3.958** ppm 418.6861869
± **0.000** nanograms of Sr

Epsilon (Sr)= **37.66**
(± **0.08**)

Discrimination= #VALUE! to #VALUE!
w/Average of #VALUE!

Enter ion guage pressure in first set x10-8 mbar
Enter ion guage pressure in last set x10-8 mbar
Average Sr88 Intensity= ditted Sr88 Intensity x10-11A

Sample:	**21LAP-UCR-4.62-2F**	Turret(Bead):	17
Operator:	**CTL**	Date:	5/23/2022
		Time:	

	Rspike Values: Sr84-3(x10)#2		
Name	Rsp84\88	Rsp86\88	Rsp87\88
Value	**5.96961**	**0.33048**	**0.12894**

[Sr84-3(x10)#2]
Conc.Spike
8.84500

Final Results

Wt.Sample	**0.051341**	g
Wt.Spike	**0.013350**	g

Unspike subtracted grand mean ratios (Measured Ratios)

	RI_84\88	RI_86\88	RI_87\86
Ratios	1.51E-01	0.11940	7.01E-01
%StdErr	1.02E-02	0.00000	7.22E-04
	# Ratios	Enter # of ratios	

discrimination corrected (Sr86/Sr88)m= 0.1250

Spike subtracted grand mean ratios (Reported Ratios)

	84/88	87/88	87/86	88s/84t
Ratios	0.006747	0.084465	**0.707410**	**6.109528**
2Sigma errors	0.000000	0.000000	**0.000010**	**0.000000**
2*Sig. err. (ppm)=(epsilon*100)	0	0	**14.4344848**	**0.010245328**

[Sr86]=	**1.678**	nm/g	
±	**0.000**		
[Sr]=	**1.490**	ppm	76.52084124
±	**0.000**		nanograms of Sr
Epsilon (Sr)=	**41.31**		
(±	**0.14**)		

Discrimination= #VALUE! to #VALUE!
w/Average of #VALUE!

Enter ion guage pressure in first set x10-8 mbar
Enter ion guage pressure in last set x10-8 mbar
Average Sr88 Intensity= ditted Sr88 Intensity x10-11A

Sample:	**21LAP-LCS-15.92-2F**	Turret(Bead):	11
Operator:	**CTL**	Date:	4/6/2022
		Time:	

	Rspike Values: Sr84-3(x10)#2		
Name	Rsp84\88	Rsp86\88	Rsp87\88
Value	**5.96961**	**0.33048**	**0.12894**

[Sr84-3(x10)#2]
Conc.Spike
8.84500

Final Results

Wt.Sample	**0.093750**	g
Wt.Spike	**0.008830**	g

Unspike subtracted grand mean ratios (Measured Ratios)

	RI_84\88	RI_86\88	RI_87\86
Ratios	6.50E-02	0.11940	7.05E-01
%StdErr	1.24E-03	0	3.59E-04
	# Ratios	Enter # of ratios	

discrimination corrected (Sr86/Sr88)m= 0.1215

Spike subtracted grand mean ratios (Reported Ratios)

	84/88	87/88	87/86	88s/84t
Ratios	0.006747	0.084469	**0.707444**	**16.311606**
2Sigma errors	0.000000	0.000000	**0.000005**	**0.000000**
2*Sig. err. (ppm)=(epsilon*100)	0	0	**7.1718942**	**0.001237736**

[Sr86]= **1.623** nm/g
± **0.000**

[Sr]= **1.441** ppm
± **0.000**

135.1293421 nanograms of Sr

Epsilon (Sr)= **41.79**
(± **0.07**)

Discrimination= #VALUE! to #VALUE!
w/Average of #VALUE!

Enter ion guage pressure in first set x10-8 mbar
Enter ion guage pressure in last set x10-8 mbar
Average Sr88 Intensity= ditted Sr88 Intensity x10-11A

Sample:	**21LAP-UCR-25.17-2C**	Turret(Bead):	5
Operator:	**CTL**	Date:	6/20/2022
		Time:	

	Rspike Values: Sr84-3(x10)#2		
Name	Rsp84\88	Rsp86\88	Rsp87\88
Value	**5.96961**	**0.33048**	**0.12894**

[Sr84-3(x10)#2]
Conc.Spike
8.84500

Final Results

Wt.Sample	**0.112880**	g
Wt.Spike	**0.013260**	g

Unspike subtracted grand mean ratios (Measured Ratios)

	RI_84\88	RI_86\88	RI_87\86
Ratios	2.78E-02	0.11940	7.03E-01
%StdErr	1.40E-03	0.00000	2.39E-04
	# Ratios	Enter # of ratios	

discrimination corrected (Sr86/Sr88)m= 0.1202

Spike subtracted grand mean ratios (Reported Ratios)

	84/88	87/88	87/86	88s/84t
Ratios	0.006747	0.084085	**0.704227**	**46.442793**
2Sigma errors	0.000000	0.000000	**0.000003**	**0.000000**
2*Sig. err. (ppm)=(epsilon*100)	0	0	**4.7893674**	**0.001400043**

[Sr86]= **5.762** nm/g
± **0.000**

[Sr]= **5.117** ppm
± **0.000**

577.5869814 nanograms of Sr

Epsilon (Sr)= **-3.87**
(± **0.05**)

Discrimination= #VALUE! to #VALUE!
w/Average of #VALUE!

Enter ion guage pressure in first set x10-8 mbar
Enter ion guage pressure in last set x10-8 mbar
Average Sr88 Intensity= ditted Sr88 Intensity x10-11A

Sample:	**21LAP-UCR-38.66-2C**	Turret(Bead):	6
Operator:	**CTL**	Date:	5/20/2022
		Time:	

	Rspike Values: Sr84-3(x10)#2		
Name	Rsp84\88	Rsp86\88	Rsp87\88
Value	**5.96961**	**0.33048**	**0.12894**

[Sr84-3(x10)#2]
Conc.Spike
8.84500

Final Results

Wt.Sample	**0.073968**	g
Wt.Spike	**0.012990**	g

Unspike subtracted grand mean ratios (Measured Ratios)

	RI_84\88	RI_86\88	RI_87\86
Ratios	4.08E-02	0.11940	7.03E-01
%StdErr	1.61E-03	0.00000	4.54E-04
	# Ratios	Enter # of ratios	

discrimination corrected (Sr86/Sr88)m= 0.1206

Spike subtracted grand mean ratios (Reported Ratios)

	84/88	87/88	87/86	88s/84t
Ratios	0.006747	0.084119	**0.704515**	**28.419249**
2Sigma errors	0.000000	0.000000	**0.000006**	**0.000000**
2*Sig. err. (ppm)=(epsilon*100)	0	0	**9.0721922**	**0.001605606**

[Sr86]= **5.271** nm/g
± **0.000**

[Sr]= **4.681** ppm
± **0.000**

346.2498099 nanograms of Sr

Epsilon (Sr)= **0.22**
(± **0.09**)

Discrimination= #VALUE! to #VALUE!
w/Average of #VALUE!

Enter ion guage pressure in first set x10-8 mbar
Enter ion guage pressure in last set x10-8 mbar
Average Sr88 Intensity= ditted Sr88 Intensity x10-11A

Sample:	**21LAP-UCR-45.04-2C**	Turret(Bead):	6
Operator:	**CTL**	Date:	6/20/2022
		Time:	

	Rspike Values: Sr84-3(x10)#2		
Name	Rsp84\88	Rsp86\88	Rsp87\88
Value	**5.96961**	**0.33048**	**0.12894**

[Sr84-3(x10)#2]
Conc.Spike
8.84500

Final Results

Wt.Sample	**0.084564**	g
Wt.Spike	**0.013390**	g

Unspike subtracted grand mean ratios (Measured Ratios)

	RI_84\88	RI_86\88	RI_87\86
Ratios	4.23E-02	0.11940	7.03E-01
%StdErr	2.79E-03	0.00000	5.12E-04
	# Ratios	Enter # of ratios	

discrimination corrected (Sr86/Sr88)m= 0.1207

Spike subtracted grand mean ratios (Reported Ratios)

	84/88	87/88	87/86	88s/84t
Ratios	0.006747	0.084165	**0.704902**	**27.226001**
2Sigma errors	0.000000	0.000000	**0.000007**	**0.000000**
2*Sig. err. (ppm)=(epsilon*100)	0	0	**10.23169**	**0.002786853**

[Sr86]= **4.553** nm/g
± **0.000**

[Sr]= **4.044** ppm
± **0.000**

341.9390285 nanograms of Sr

Epsilon (Sr)= **5.71**
(± **0.10**)

Discrimination= #VALUE! to #VALUE!
w/Average of #VALUE!

Enter ion guage pressure in first set x10-8 mbar
Enter ion guage pressure in last set x10-8 mbar
Average Sr88 Intensity= ditted Sr88 Intensity x10-11A

Sample:	**21LAP-UCR-50.29-2C**	Turret(Bead):	7
Operator:	**CTL**	Date:	6/20/2022
		Time:	

	Rspike Values: Sr84-3(x10)#2		
Name	Rsp84\88	Rsp86\88	Rsp87\88
Value	**5.96961**	**0.33048**	**0.12894**

[Sr84-3(x10)#2]
Conc.Spike
8.84500

Final Results

Wt.Sample	**0.092481**	g
Wt.Spike	**0.013390**	g

Unspike subtracted grand mean ratios (Measured Ratios)

	RI_84\88	RI_86\88	RI_87\86
Ratios	4.05E-02	0.11940	7.04E-01
%StdErr	8.43E-03	0.00000	1.18E-03
	# Ratios	Enter # of ratios	

discrimination corrected (Sr86/Sr88)m= 0.1206

Spike subtracted grand mean ratios (Reported Ratios)

	84/88	87/88	87/86	88s/84t
Ratios	0.006747	0.084200	**0.705194**	**28.660511**
2Sigma errors	0.000000	0.000000	**0.000017**	**0.000000**
2*Sig. err. (ppm)=(epsilon*100)	0	0	**23.5494**	**0.0084269**

[Sr86]= **4.382** nm/g
± **0.000**

[Sr]= **3.892** ppm
± **0.000**

359.965699 nanograms of Sr

Epsilon (Sr)= **9.85**
(± **0.24**)

Discrimination= #VALUE! to #VALUE!
w/Average of #VALUE!

Enter ion guage pressure in first set x10-8 mbar
Enter ion guage pressure in last set x10-8 mbar
Average Sr88 Intensity= ditted Sr88 Intensity x10-11A

Sample:	**21LAP-UCR-61.95-2C**	Turret(Bead):	8
Operator:	**CTL**	Date:	6/20/2022
		Time:	

	Rspike Values: Sr84-3(x10)#2		
Name	Rsp84\88	Rsp86\88	Rsp87\88
Value	**5.96961**	**0.33048**	**0.12894**

[Sr84-3(x10)#2]
Conc.Spike
8.84500

Final Results

Wt.Sample	**0.073953**	g
Wt.Spike	**0.013410**	g

Unspike subtracted grand mean ratios (Measured Ratios)

	RI_84\88	RI_86\88	RI_87\86
Ratios	6.08E-02	0.11940	7.04E-01
%StdErr	1.29E-03	0.00000	4.30E-04
	# Ratios	Enter # of ratios	

discrimination corrected (Sr86/Sr88)m= 0.1214

Spike subtracted grand mean ratios (Reported Ratios)

	84/88	87/88	87/86	88s/84t
Ratios	0.006747	0.084345	**0.706403**	**17.622218**
2Sigma errors	0.000000	0.000000	**0.000006**	**0.000000**
2*Sig. err. (ppm)=(epsilon*100)	0	0	**8.6068926**	**0.001287554**

[Sr86]= **3.375** nm/g
± **0.000**

[Sr]= **2.998** ppm
± **0.000**

221.6855395 nanograms of Sr

Epsilon (Sr)= **27.02**
(± **0.09**)

Discrimination= #VALUE! to #VALUE!
w/Average of #VALUE!

Enter ion guage pressure in first set x10-8 mbar
Enter ion guage pressure in last set x10-8 mbar
Average Sr88 Intensity= ditted Sr88 Intensity x10-11A

Sample:	**21LAP-UCR-68.72-2C**	Turret(Bead):	9
Operator:	**CTL**	Date:	6/21/2022
		Time:	

	Rspike Values: Sr84-3(x10)#2		
Name	Rsp84\88	Rsp86\88	Rsp87\88
Value	**5.96961**	**0.33048**	**0.12894**

[Sr84-3(x10)#2]
Conc.Spike
8.84500

Final Results

Wt.Sample	**0.077070**	g
Wt.Spike	**0.013430**	g

Unspike subtracted grand mean ratios (Measured Ratios)

	RI_84\88	RI_86\88	RI_87\86
Ratios	6.84E-02	0.11940	7.04E-01
%StdErr	7.83E-04	0.00000	1.95E-04
	# Ratios	Enter # of ratios	

discrimination corrected (Sr86/Sr88)m= 0.1217

Spike subtracted grand mean ratios (Reported Ratios)

	84/88	87/88	87/86	88s/84t
Ratios	0.006747	0.084394	**0.706820**	**15.350931**
2Sigma errors	0.000000	0.000000	**0.000003**	**0.000000**
2*Sig. err. (ppm)=(epsilon*100)	0	0	**3.8933588**	**0.000782615**

[Sr86]= **2.825** nm/g
± **0.000**

[Sr]= **2.510** ppm
± **0.000**

193.4088995 nanograms of Sr

Epsilon (Sr)= **32.93**
(± **0.04**)

Discrimination= #VALUE! to #VALUE!
w/Average of #VALUE!

Enter ion guage pressure in first set x10-8 mbar
Enter ion guage pressure in last set x10-8 mbar
Average Sr88 Intensity= ditted Sr88 Intensity x10-11A

Sample:	**21LAP-UCR-79.91-2C**	Turret(Bead):	10
Operator:	**CTL**	Date:	6/21/2022
		Time:	

	Rspike Values: Sr84-3(x10)#2		
Name	Rsp84\88	Rsp86\88	Rsp87\88
Value	**5.96961**	**0.33048**	**0.12894**

[Sr84-3(x10)#2]
Conc.Spike
8.84500

Final Results

Wt.Sample	**0.073590**	g
Wt.Spike	**0.013320**	g

Unspike subtracted grand mean ratios (Measured Ratios)

	RI_84\88	RI_86\88	RI_87\86
Ratios	4.44E-02	0.11940	7.05E-01
%StdErr	1.53E-03	0.00000	4.42E-04
	# Ratios	Enter # of ratios	

discrimination corrected (Sr86/Sr88)m= 0.1208

Spike subtracted grand mean ratios (Reported Ratios)

	84/88	87/88	87/86	88s/84t
Ratios	0.006747	0.084324	**0.706228**	**25.635277**
2Sigma errors	0.000000	0.000000	**0.000006**	**0.000000**
2*Sig. err. (ppm)=(epsilon*100)	0	0	**8.8300888**	**0.001528977**

[Sr86]= **4.900** nm/g
± **0.000**

[Sr]= **4.353** ppm
± **0.000**

320.3190651 nanograms of Sr

Epsilon (Sr)= **24.52**
(± **0.09**)

Discrimination= #VALUE! to #VALUE!
w/Average of #VALUE!

Enter ion guage pressure in first set x10-8 mbar
Enter ion guage pressure in last set x10-8 mbar
Average Sr88 Intensity= ditted Sr88 Intensity x10-11A

Sample:	**21LAP-UCR-90.51-2C**	Turret(Bead):	11
Operator:	**CTL**	Date:	6/21/2022
		Time:	

	Rspike Values: Sr84-3(x10)#2		
Name	Rsp84\88	Rsp86\88	Rsp87\88
Value	**5.96961**	**0.33048**	**0.12894**

[Sr84-3(x10)#2]
Conc.Spike
8.84500

Final Results

Wt.Sample	**0.066546**	g
Wt.Spike	**0.013270**	g

Unspike subtracted grand mean ratios (Measured Ratios)

	RI_84\88	RI_86\88	RI_87\86
Ratios	4.96E-02	0.11940	7.04E-01
%StdErr	2.82E-02	0.00000	3.45E-03
	# Ratios	Enter # of ratios	

discrimination corrected (Sr86/Sr88)m= 0.1210

Spike subtracted grand mean ratios (Reported Ratios)

	84/88	87/88	87/86	88s/84t
Ratios	0.006747	0.084269	**0.705775**	**22.433449**
2Sigma errors	0.000000	0.000000	**0.000049**	**0.000001**
2*Sig. err. (ppm)=(epsilon*100)	0	0	**69.093782**	**0.028235514**

[Sr86]= **4.724** nm/g
± **0.000**

[Sr]= **4.196** ppm
± **0.000**

279.2468409 nanograms of Sr

Epsilon (Sr)= **18.09**
(± **0.69**)

Discrimination= #VALUE! to #VALUE!
w/Average of #VALUE!

Enter ion guage pressure in first set x10-8 mbar
Enter ion guage pressure in last set x10-8 mbar
Average Sr88 Intensity= ditted Sr88 Intensity x10-11A

Sample:	**21LAP-UCR-101.88-2C**	Turret(Bead):	7
Operator:	**CTL**	Date:	5/20/2022
		Time:	

	Rspike Values: Sr84-3(x10)#2		
Name	Rsp84\88	Rsp86\88	Rsp87\88
Value	**5.96961**	**0.33048**	**0.12894**

[Sr84-3(x10)#2]
Conc.Spike
8.84500

Final Results

Wt.Sample	**0.071748**	g
Wt.Spike	**0.012980**	g

Unspike subtracted grand mean ratios (Measured Ratios)

	RI_84\88	RI_86\88	RI_87\86
Ratios	4.60E-02	0.11940	7.04E-01
%StdErr	1.09E-02	0.00000	2.80E-03
	# Ratios	Enter # of ratios	

discrimination corrected (Sr86/Sr88)m= 0.1208

Spike subtracted grand mean ratios (Reported Ratios)

	84/88	87/88	87/86	88s/84t
Ratios	0.006747	0.084270	**0.705778**	**24.596627**
2Sigma errors	0.000000	0.000000	**0.000040**	**0.000000**
2*Sig. err. (ppm)=(epsilon*100)	0	0	**55.973662**	**0.010879673**

[Sr86]= **4.699** nm/g
± **0.000**

[Sr]= **4.174** ppm
± **0.000**

299.482655 nanograms of Sr

Epsilon (Sr)= **18.14**
(± **0.56**)

Discrimination= #VALUE! to #VALUE!
w/Average of #VALUE!

Enter ion guage pressure in first set x10-8 mbar
Enter ion guage pressure in last set x10-8 mbar
Average Sr88 Intensity= ditted Sr88 Intensity x10-11A

Sample:	**21LAP-UCR-118.67-2C**	Turret(Bead):	12
Operator:	**CTL**	Date:	6/21/2022
		Time:	

	Rspike Values: Sr84-3(x10)#2		
Name	Rsp84\88	Rsp86\88	Rsp87\88
Value	**5.96961**	**0.33048**	**0.12894**

[Sr84-3(x10)#2]
Conc.Spike
8.84500

Final Results

Wt.Sample	**0.077835**	g
Wt.Spike	**0.013400**	g

Unspike subtracted grand mean ratios (Measured Ratios)

	RI_84\88	RI_86\88	RI_87\86
Ratios	3.52E-02	0.11940	7.05E-01
%StdErr	1.33E-03	0.00000	3.75E-04
	# Ratios	Enter # of ratios	

discrimination corrected (Sr86/Sr88)m= 0.1204

Spike subtracted grand mean ratios (Reported Ratios)

	84/88	87/88	87/86	88s/84t
Ratios	0.006747	0.084308	**0.706098**	**34.151678**
2Sigma errors	0.000000	0.000000	**0.000005**	**0.000000**
2*Sig. err. (ppm)=(epsilon*100)	0	0	**7.507424**	**0.001326869**

[Sr86]= **6.209** nm/g
± **0.000**

[Sr]= **5.515** ppm
± **0.000**

429.2910898 nanograms of Sr

Epsilon (Sr)= **22.68**
(± **0.08**)

Discrimination= #VALUE! to #VALUE!
w/Average of #VALUE!

Enter ion guage pressure in first set x10-8 mbar
Enter ion guage pressure in last set x10-8 mbar
Average Sr88 Intensity= ditted Sr88 Intensity x10-11A

Sample:	**21LAP-UCR-124.52-2C**	Turret(Bead):	13
Operator:	**CTL**	Date:	6/21/2022
		Time:	

	Rspike Values: Sr84-3(x10)#2		
Name	Rsp84\88	Rsp86\88	Rsp87\88
Value	**5.96961**	**0.33048**	**0.12894**

[Sr84-3(x10)#2]
Conc.Spike
8.84500

Final Results

Wt.Sample	**0.071044**	g
Wt.Spike	**0.013310**	g

Unspike subtracted grand mean ratios (Measured Ratios)

	RI_84\88	RI_86\88	RI_87\86
Ratios	4.02E-02	0.11940	7.05E-01
%StdErr	1.67E-03	0.00000	3.41E-04
	# Ratios	Enter # of ratios	

discrimination corrected (Sr86/Sr88)m= 0.1206

Spike subtracted grand mean ratios (Reported Ratios)

	84/88	87/88	87/86	88s/84t
Ratios	0.006747	0.084304	**0.706064**	**28.933015**
2Sigma errors	0.000000	0.000000	**0.000005**	**0.000000**
2*Sig. err. (ppm)=(epsilon*100)	0	0	**6.8260594**	**0.001672414**

[Sr86]= **5.725** nm/g
± **0.000**

[Sr]= **5.085** ppm
± **0.000**

361.2479056 nanograms of Sr

Epsilon (Sr)= **22.20**
(± **0.07**)

Discrimination= #VALUE! to #VALUE!
w/Average of #VALUE!

Enter ion guage pressure in first set x10-8 mbar
Enter ion guage pressure in last set x10-8 mbar
Average Sr88 Intensity= ditted Sr88 Intensity x10-11A

Sample:	**21LAP-UCR-140.55-2C**	Turret(Bead):	14
Operator:	**CTL**	Date:	6/22/2022
		Time:	

	Rspike Values: Sr84-3(x10)#2		
Name	Rsp84\88	Rsp86\88	Rsp87\88
Value	**5.96961**	**0.33048**	**0.12894**

[Sr84-3(x10)#2]
Conc.Spike
8.84500

Final Results

Wt.Sample	**0.068813**	g
Wt.Spike	**0.012950**	g

Unspike subtracted grand mean ratios (Measured Ratios)

	RI_84\88	RI_86\88	RI_87\86
Ratios	4.93E-02	0.11940	7.05E-01
%StdErr	1.28E-03	0.00000	3.10E-04
	# Ratios	Enter # of ratios	

discrimination corrected (Sr86/Sr88)m= 0.1210

Spike subtracted grand mean ratios (Reported Ratios)

	84/88	87/88	87/86	88s/84t
Ratios	0.006747	0.084380	**0.706704**	**22.627867**
2Sigma errors	0.000000	0.000000	**0.000004**	**0.000000**
2*Sig. err. (ppm)=(epsilon*100)	0	0	**6.2090436**	**0.001278657**

[Sr86]= **4.497** nm/g
± **0.000**

[Sr]= **3.995** ppm
± **0.000**

274.8996529 nanograms of Sr

Epsilon (Sr)= **31.29**
(± **0.06**)

Discrimination= #VALUE! to #VALUE!
w/Average of #VALUE!

Enter ion guage pressure in first set x10-8 mbar
Enter ion guage pressure in last set x10-8 mbar
Average Sr88 Intensity= ditted Sr88 Intensity x10-11A

Sample:	**21LAP-UCR-149.29-2C**	Turret(Bead):	8
Operator:	**CTL**	Date:	5/20/2022
		Time:	

	Rspike Values: Sr84-3(x10)#2		
Name	Rsp84\88	Rsp86\88	Rsp87\88
Value	**5.96961**	**0.33048**	**0.12894**

[Sr84-3(x10)#2]
Conc.Spike
8.84500

Final Results

Wt.Sample	**0.073118**	g
Wt.Spike	**0.012650**	g

Unspike subtracted grand mean ratios (Measured Ratios)

	RI_84\88	RI_86\88	RI_87\86
Ratios	5.37E-02	0.11940	7.05E-01
%StdErr	1.49E-03	0.00000	3.62E-04
	# Ratios	Enter # of ratios	

discrimination corrected (Sr86/Sr88)m= 0.1211

Spike subtracted grand mean ratios (Reported Ratios)

	84/88	87/88	87/86	88s/84t
Ratios	0.006747	0.084389	**0.706774**	**20.404158**
2Sigma errors	0.000000	0.000000	**0.000005**	**0.000000**
2*Sig. err. (ppm)=(epsilon*100)	0	0	**7.2326196**	**0.001488381**

[Sr86]= **3.728** nm/g
± **0.000**

[Sr]= **3.312** ppm
± **0.000**

242.1436005 nanograms of Sr

Epsilon (Sr)= **32.29**
(± **0.07**)

Discrimination= #VALUE! to #VALUE!
w/Average of #VALUE!

Enter ion guage pressure in first set x10-8 mbar
Enter ion guage pressure in last set x10-8 mbar
Average Sr88 Intensity= ditted Sr88 Intensity x10-11A

Sample:	**21LAP-UCR-166.20-2C**	Turret(Bead):	15
Operator:	**CTL**	Date:	6/22/2022
		Time:	

	Rspike Values: Sr84-3(x10)#2		
Name	Rsp84\88	Rsp86\88	Rsp87\88
Value	**5.96961**	**0.33048**	**0.12894**

[Sr84-3(x10)#2]
Conc.Spike
8.84500

Final Results

Wt.Sample	**0.071284**	g
Wt.Spike	**0.013400**	g

Unspike subtracted grand mean ratios (Measured Ratios)

	RI_84\88	RI_86\88	RI_87\86
Ratios	4.98E-02	0.11940	7.05E-01
%StdErr	7.00E-04	0.00000	2.12E-04
	# Ratios	Enter # of ratios	

discrimination corrected (Sr86/Sr88)m= 0.1210

Spike subtracted grand mean ratios (Reported Ratios)

	84/88	87/88	87/86	88s/84t
Ratios	0.006747	0.084352	**0.706464**	**22.316142**
2Sigma errors	0.000000	0.000000	**0.000003**	**0.000000**
2*Sig. err. (ppm)=(epsilon*100)	0	0	**4.2476038**	**0.000699923**

[Sr86]= **4.430** nm/g
± **0.000**

[Sr]= **3.935** ppm
± **0.000**

280.5269065 nanograms of Sr

Epsilon (Sr)= **27.88**
(± **0.04**)

Discrimination= #VALUE! to #VALUE!
w/Average of #VALUE!

Enter ion guage pressure in first set x10-8 mbar
Enter ion guage pressure in last set x10-8 mbar
Average Sr88 Intensity= ditted Sr88 Intensity x10-11A

Sample:	**21LAP-UCR-175.99-2C**	Turret(Bead):	16
Operator:	**CTL**	Date:	6/22/2022
		Time:	

	Rspike Values: Sr84-3(x10)#2		
Name	Rsp84\88	Rsp86\88	Rsp87\88
Value	**5.96961**	**0.33048**	**0.12894**

[Sr84-3(x10)#2]
Conc.Spike
8.84500

Final Results

Wt.Sample	**0.073190**	g
Wt.Spike	**0.013190**	g

Unspike subtracted grand mean ratios (Measured Ratios)

	RI_84\88	RI_86\88	RI_87\86
Ratios	4.22E-02	0.11940	7.05E-01
%StdErr	2.93E-03	0.00000	5.58E-04
	# Ratios	Enter # of ratios	

discrimination corrected (Sr86/Sr88)m= 0.1207

Spike subtracted grand mean ratios (Reported Ratios)

	84/88	87/88	87/86	88s/84t
Ratios	0.006747	0.084318	**0.706180**	**27.304304**
2Sigma errors	0.000000	0.000000	**0.000008**	**0.000000**
2*Sig. err. (ppm)=(epsilon*100)	0	0	**11.1696844**	**0.002933134**

[Sr86]= **5.197** nm/g
± **0.000**

[Sr]= **4.616** ppm
± **0.000**

337.8426163 nanograms of Sr

Epsilon (Sr)= **23.85**
(± **0.11**)

Discrimination= #VALUE! to #VALUE!
w/Average of #VALUE!

Enter ion guage pressure in first set x10-8 mbar
Enter ion guage pressure in last set x10-8 mbar
Average Sr88 Intensity= ditted Sr88 Intensity x10-11A

Sample:	**21LAP-UCR-186.19-2C**	Turret(Bead):	9
Operator:	**CTL**	Date:	5/21/2022
		Time:	

	Rspike Values: Sr84-3(x10)#2		
Name	Rsp84\88	Rsp86\88	Rsp87\88
Value	**5.96961**	**0.33048**	**0.12894**

[Sr84-3(x10)#2]
Conc.Spike
8.84500

Final Results

Wt.Sample	**0.074488**	g
Wt.Spike	**0.012850**	g

Unspike subtracted grand mean ratios (Measured Ratios)

	RI_84\88	RI_86\88	RI_87\86
Ratios	4.86E-02	0.11940	7.05E-01
%StdErr	2.19E-03	0.00000	9.34E-04
	# Ratios	Enter # of ratios	

discrimination corrected (Sr86/Sr88)m= 0.1209

Spike subtracted grand mean ratios (Reported Ratios)

	84/88	87/88	87/86	88s/84t
Ratios	0.006747	0.084394	**0.706817**	**22.979985**
2Sigma errors	0.000000	0.000000	**0.000013**	**0.000000**
2*Sig. err. (ppm)=(epsilon*100)	0	0	**18.6862068**	**0.002190417**

[Sr86]= **4.187** nm/g
± **0.000**

[Sr]= **3.719** ppm
± **0.000**

277.024691 nanograms of Sr

Epsilon (Sr)= **32.89**
(± **0.19**)

Discrimination= #VALUE! to #VALUE!
w/Average of #VALUE!

Enter ion guage pressure in first set x10-8 mbar
Enter ion guage pressure in last set x10-8 mbar
Average Sr88 Intensity= ditted Sr88 Intensity x10-11A

Sample:	**21LAP-UCR-188.62-2C**	Turret(Bead):	10
Operator:	**CTL**	Date:	4/6/2022
		Time:	

	Rspike Values: Sr84-3(x10)#2		
Name	Rsp84\88	Rsp86\88	Rsp87\88
Value	**5.96961**	**0.33048**	**0.12894**

[Sr84-3(x10)#2]
Conc.Spike
8.84500

Final Results

Wt.Sample	**0.099753**	g
Wt.Spike	**0.008290**	g

Unspike subtracted grand mean ratios (Measured Ratios)

	RI_84\88	RI_86\88	RI_87\86
Ratios	3.83E-02	0.11940	7.05E-01
%StdErr	1.30E-03	0	2.97E-04
	# Ratios	Enter # of ratios	

discrimination corrected (Sr86/Sr88)m= 0.1205

Spike subtracted grand mean ratios (Reported Ratios)

	84/88	87/88	87/86	88s/84t
Ratios	0.006747	0.084343	**0.706391**	**30.714744**
2Sigma errors	0.000000	0.000000	**0.000004**	**0.000000**
2*Sig. err. (ppm)=(epsilon*100)	0	0	**5.9329552**	**0.001303003**

[Sr86]= **2.696** nm/g
± **0.000**

[Sr]= **2.395** ppm
± **0.000**

238.8630316 nanograms of Sr

Epsilon (Sr)= **26.85**
(± **0.06**)

Discrimination= #VALUE! to #VALUE!
w/Average of #VALUE!

Enter ion guage pressure in first set x10-8 mbar
Enter ion guage pressure in last set x10-8 mbar
Average Sr88 Intensity= ditted Sr88 Intensity x10-11A

Sample:	**21LAP-UCR-205.40-2C**	Turret(Bead):	10
Operator:	**CTL**	Date:	5/21/2022
		Time:	

	Rspike Values: Sr84-3(x10)#2		
Name	Rsp84\88	Rsp86\88	Rsp87\88
Value	**5.96961**	**0.33048**	**0.12894**

[Sr84-3(x10)#2]
Conc.Spike
8.84500

Final Results

Wt.Sample	**0.053981**	g
Wt.Spike	**0.013030**	g

Unspike subtracted grand mean ratios (Measured Ratios)

	RI_84\88	RI_86\88	RI_87\86
Ratios	5.55E-02	0.11940	7.04E-01
%StdErr	1.18E-03	0.00000	3.69E-04

Ratios Enter # of ratios

discrimination corrected (Sr86/Sr88)m= 0.1212

Spike subtracted grand mean ratios (Reported Ratios)

	84/88	87/88	87/86	88s/84t
Ratios	0.006747	0.084314	**0.706146**	**19.630053**
2Sigma errors	0.000000	0.000000	**0.000005**	**0.000000**
2*Sig. err. (ppm)=(epsilon*100)	0	0	**7.3745094**	**0.001183216**

[Sr86]= **5.004** nm/g
± **0.000**

[Sr]= **4.445** ppm
± **0.000**

239.9401661 nanograms of Sr

Epsilon (Sr)= **23.36**
(± **0.07**)

Discrimination= #VALUE! to #VALUE!
w/Average of #VALUE!

Enter ion guage pressure in first set x10-8 mbar
Enter ion guage pressure in last set x10-8 mbar
Average Sr88 Intensity= ditted Sr88 Intensity x10-11A

Sample:	**21LAP-UCR-215.02_2C**	Turret(Bead):	19
Operator:	**CTL**	Date:	5/23/2022
		Time:	

	Rspike Values: Sr84-3(x10)#2		
Name	Rsp84\88	Rsp86\88	Rsp87\88
Value	**5.96961**	**0.33048**	**0.12894**

[Sr84-3(x10)#2]
Conc.Spike
8.84500

Final Results

Wt.Sample	**0.073299**	g
Wt.Spike	**0.013340**	g

Unspike subtracted grand mean ratios (Measured Ratios)

	RI_84\88	RI_86\88	RI_87\86
Ratios	4.50E-02	0.11940	7.05E-01
%StdErr	1.16E-03	0.00000	2.74E-04
	# Ratios	Enter # of ratios	

discrimination corrected (Sr86/Sr88)m= 0.1208

Spike subtracted grand mean ratios (Reported Ratios)

	84/88	87/88	87/86	88s/84t
Ratios	0.006747	0.084317	**0.706170**	**25.235885**
2Sigma errors	0.000000	0.000000	**0.000004**	**0.000000**
2*Sig. err. (ppm)=(epsilon*100)	0	0	**5.4775206**	**0.001163727**

[Sr86]= **4.850** nm/g
± **0.000**

[Sr]= **4.308** ppm
± **0.000**

315.8002501 nanograms of Sr

Epsilon (Sr)= **23.70**
(± **0.05**)

Discrimination= #VALUE! to #VALUE!
w/Average of #VALUE!

Enter ion guage pressure in first set x10-8 mbar
Enter ion guage pressure in last set x10-8 mbar
Average Sr88 Intensity= ditted Sr88 Intensity x10-11A

Sample:	**21LAP-UCR-234.94-2C**	Turret(Bead):	20
Operator:	**CTL**	Date:	6/23/2022
		Time:	

	Rspike Values: Sr84-3(x10)#2		
Name	Rsp84\88	Rsp86\88	Rsp87\88
Value	**5.96961**	**0.33048**	**0.12894**

[Sr84-3(x10)#2]
Conc.Spike
8.84500

Final Results

Wt.Sample	**0.072749**	g
Wt.Spike	**0.013410**	g

Unspike subtracted grand mean ratios (Measured Ratios)

	RI_84\88	RI_86\88	RI_87\86
Ratios	4.57E-02	0.11940	7.05E-01
%StdErr	1.04E-03	0.00000	2.30E-04
	# Ratios	Enter # of ratios	

discrimination corrected (Sr86/Sr88)m= 0.1208

Spike subtracted grand mean ratios (Reported Ratios)

	84/88	87/88	87/86	88s/84t
Ratios	0.006747	0.084316	**0.706162**	**24.756644**
2Sigma errors	0.000000	0.000000	**0.000003**	**0.000000**
2*Sig. err. (ppm)=(epsilon*100)	0	0	**4.5953542**	**0.001036568**

[Sr86]=	**4.819**	nm/g	
±	**0.000**		
[Sr]=	**4.281**	ppm	311.4284616
±	**0.000**		nanograms of Sr
Epsilon (Sr)=	**23.59**		
(±	**0.05**)		

Discrimination= #VALUE! to #VALUE!
w/Average of #VALUE!

Enter ion guage pressure in first set x10-8 mbar
Enter ion guage pressure in last set x10-8 mbar
Average Sr88 Intensity= ditted Sr88 Intensity x10-11A

Sample:	**21LAP-LCR-1.98-2E**	Turret(Bead):	18
Operator:	**CTL**	Date:	5/23/2022
		Time:	

	Rspike Values: Sr84-3(x10)#2		
Name	Rsp84\88	Rsp86\88	Rsp87\88
Value	**5.96961**	**0.33048**	**0.12894**

[Sr84-3(x10)#2]
Conc.Spike
8.84500

Final Results

Wt.Sample	**0.050438**	g
Wt.Spike	**0.012940**	g

Unspike subtracted grand mean ratios (Measured Ratios)

	RI_84\88	RI_86\88	RI_87\86
Ratios	5.09E-02	0.11940	7.05E-01
%StdErr	1.37E-03	0.00000	2.96E-04
	# Ratios	Enter # of ratios	

discrimination corrected (Sr86/Sr88)m= 0.1210

Spike subtracted grand mean ratios (Reported Ratios)

	84/88	87/88	87/86	88s/84t
Ratios	0.006747	0.084408	**0.706931**	**21.754596**
2Sigma errors	0.000000	0.000000	**0.000004**	**0.000000**
2*Sig. err. (ppm)=(epsilon*100)	0	0	**5.9101548**	**0.00137078**

[Sr86]= **5.894** nm/g
± **0.000**

[Sr]= **5.236** ppm
± **0.000**

264.0922999 nanograms of Sr

Epsilon (Sr)= **34.51**
(± **0.06**)

Discrimination= #VALUE! to #VALUE!
w/Average of #VALUE!

Enter ion guage pressure in first set x10-8 mbar
Enter ion guage pressure in last set x10-8 mbar
Average Sr88 Intensity= ditted Sr88 Intensity x10-11A

Sample:	**21LAP-LCC-0.86-2E**		Turret(Bead):	9	
Operator:	**CTL**		Date:	4/6/2022	
			Time:		

	Rspike Values: Sr84-3(x10)#2			[Sr84-3(x10)#2]
Name	Rsp84\88	Rsp86\88	Rsp87\88	Conc.Spike
Value	**5.96961**	**0.33048**	**0.12894**	**8.84500**

Final Results

Wt.Sample	**0.111310**	g
Wt.Spike	**0.008780**	g

Unspike subtracted grand mean ratios (Measured Ratios)

	RI_84\88	RI_86\88	RI_87\86
Ratios	2.14E-02	0.11940	7.07E-01
%StdErr	1.12E-03	0	2.56E-04
	# Ratios	Enter # of ratios	

discrimination corrected (Sr86/Sr88)m= 0.1199

Spike subtracted grand mean ratios (Reported Ratios)

	84/88	87/88	87/86	88s/84t
Ratios	0.006747	0.084449	**0.707282**	**67.061985**
2Sigma errors	0.000000	0.000000	**0.000004**	**0.000000**
2*Sig. err. (ppm)=(epsilon*100)	0	0	**5.1161308**	**0.001117294**

[Sr86]= **5.586** nm/g
± **0.000**

[Sr]= **4.963** ppm
± **0.000**

552.4032858 nanograms of Sr

Epsilon (Sr)= **39.48**
(± **0.05**)

Discrimination= #VALUE! to #VALUE!
w/Average of #VALUE!

Enter ion guage pressure in first set x10-8 mbar
Enter ion guage pressure in last set x10-8 mbar
Average Sr88 Intensity= ditted Sr88 Intensity x10-11A

Sample:	**21LAP-UCS-110.68-2H**	Turret(Bead):	3
Operator:	**CTL**	Date:	6/19/2022
		Time:	

	Rspike Values: Sr84-3(x10)#2		
Name	Rsp84\88	Rsp86\88	Rsp87\88
Value	**5.96961**	**0.33048**	**0.12894**

[Sr84-3(x10)#2]
Conc.Spike
8.84500

Final Results

Wt.Sample	**0.032347**	g
Wt.Spike	**0.017890**	g

Unspike subtracted grand mean ratios (Measured Ratios)

	RI_84\88	RI_86\88	RI_87\86
Ratios	4.17E-02	0.11940	7.06E-01
%StdErr	1.80E-03	0.00000	2.84E-04
	# Ratios	Enter # of ratios	

discrimination corrected (Sr86/Sr88)m= 0.1207

Spike subtracted grand mean ratios (Reported Ratios)

	84/88	87/88	87/86	88s/84t
Ratios	0.006747	0.084513	**0.707815**	**27.674639**
2Sigma errors	0.000000	0.000000	**0.000004**	**0.000000**
2*Sig. err. (ppm)=(epsilon*100)	0	0	**5.6747326**	**0.001802146**

[Sr86]= **16.164** nm/g
± **0.000**

[Sr]= **14.360** ppm
± **0.000**

464.5156156 nanograms of Sr

Epsilon (Sr)= **47.06**
(± **0.06**)

Discrimination= #VALUE! to #VALUE!
w/Average of #VALUE!

Enter ion guage pressure in first set x10-8 mbar
Enter ion guage pressure in last set x10-8 mbar
Average Sr88 Intensity= ditted Sr88 Intensity x10-11A

Sample:	**21LAP-UCS-90.19-2H**	Turret(Bead):	3
Operator:	**CTL**	Date:	5/19/2022
		Time:	

	Rspike Values: Sr84-3(x10)#2		
Name	Rsp84\88	Rsp86\88	Rsp87\88
Value	**5.96961**	**0.33048**	**0.12894**

[Sr84-3(x10)#2]
Conc.Spike
8.84500

Final Results

Wt.Sample	**0.075930**	g
Wt.Spike	**0.012810**	g

Unspike subtracted grand mean ratios (Measured Ratios)

	RI_84\88	RI_86\88	RI_87\86
Ratios	1.93E-02	0.11940	7.06E-01
%StdErr	1.75E-03	0.00000	6.21E-04
	# Ratios	Enter # of ratios	

discrimination corrected (Sr86/Sr88)m= 0.1198

Spike subtracted grand mean ratios (Reported Ratios)

	84/88	87/88	87/86	88s/84t
Ratios	0.006747	0.084308	**0.706099**	**78.510769**
2Sigma errors	0.000000	0.000000	**0.000009**	**0.000000**
2*Sig. err. (ppm)=(epsilon*100)	0	0	**12.4190106**	**0.001746009**

[Sr86]= **13.988** nm/g
± **0.000**

[Sr]= **12.425** ppm
± **0.000**

943.438158 nanograms of Sr

Epsilon (Sr)= **22.69**
(± **0.12**)

Discrimination= #VALUE! to #VALUE!
w/Average of #VALUE!

Enter ion guage pressure in first set x10-8 mbar
Enter ion guage pressure in last set x10-8 mbar
Average Sr88 Intensity= ditted Sr88 Intensity x10-11A

Sample:	**21LAP-UCS-85.11-2H**	Turret(Bead):	14
Operator:	**CTL**	Date:	5/22/2022
		Time:	

	Rspike Values: Sr84-3(x10)#2		
Name	Rsp84\88	Rsp86\88	Rsp87\88
Value	**5.96961**	**0.33048**	**0.12894**

[Sr84-3(x10)#2]
Conc.Spike
8.84500

Final Results

Wt.Sample	**0.074360**	g
Wt.Spike	**0.013200**	g

Unspike subtracted grand mean ratios (Measured Ratios)

	RI_84\88	RI_86\88	RI_87\86
Ratios	1.36E-02	0.11940	7.05E-01
%StdErr	1.17E-03	0.00000	2.88E-04
	# Ratios	Enter # of ratios	

discrimination corrected (Sr86/Sr88)m= 0.1196

Spike subtracted grand mean ratios (Reported Ratios)

	84/88	87/88	87/86	88s/84t
Ratios	0.006747	0.084261	**0.705702**	**143.899666**
2Sigma errors	0.000000	0.000000	**0.000004**	**0.000000**
2*Sig. err. (ppm)=(epsilon*100)	0	0	**5.7603038**	**0.001165201**

[Sr86]= **26.977** nm/g
± **0.000**

[Sr]= **23.961** ppm
± **0.000**

1781.771246 nanograms of Sr

Epsilon (Sr)= **17.07**
(± **0.06**)

Discrimination= #VALUE! to #VALUE!
w/Average of #VALUE!

Enter ion guage pressure in first set x10-8 mbar
Enter ion guage pressure in last set x10-8 mbar
Average Sr88 Intensity= ditted Sr88 Intensity x10-11A

Sample:	**21LAP-UCS-80.23-2H**	Turret(Bead):	15
Operator:	**CTL**	Date:	5/22/2022
		Time:	

	Rspike Values: Sr84-3(x10)#2		
Name	Rsp84\88	Rsp86\88	Rsp87\88
Value	**5.96961**	**0.33048**	**0.12894**

[Sr84-3(x10)#2]
Conc.Spike
8.84500

Final Results

Wt.Sample	**0.074815**	g
Wt.Spike	**0.012780**	g

Unspike subtracted grand mean ratios (Measured Ratios)

	RI_84\88	RI_86\88	RI_87\86
Ratios	1.47E-02	0.11940	7.06E-01
%StdErr	1.58E-03	0.00000	3.24E-04
	# Ratios	Enter # of ratios	

discrimination corrected (Sr86/Sr88)m= 0.1197

Spike subtracted grand mean ratios (Reported Ratios)

	84/88	87/88	87/86	88s/84t
Ratios	0.006747	0.084278	**0.705846**	**124.232307**
2Sigma errors	0.000000	0.000000	**0.000005**	**0.000000**
2*Sig. err. (ppm)=(epsilon*100)	0	0	**6.4812638**	**0.001578561**

[Sr86]= **22.412** nm/g
± **0.000**

[Sr]= **19.907** ppm
± **0.000**

1489.325911 nanograms of Sr

Epsilon (Sr)= **19.11**
(± **0.06**)

Discrimination= #VALUE! to #VALUE!
w/Average of #VALUE!

Enter ion guage pressure in first set x10-8 mbar
Enter ion guage pressure in last set x10-8 mbar
Average Sr88 Intensity= ditted Sr88 Intensity x10-11A

Sample:	**21LAP-UCS-76.82-2H**	Turret(Bead):	17
Operator:	**CTL**	Date:	6/22/2022
		Time:	

	Rspike Values: Sr84-3(x10)#2		
Name	Rsp84\88	Rsp86\88	Rsp87\88
Value	**5.96961**	**0.33048**	**0.12894**

[Sr84-3(x10)#2]
Conc.Spike
8.84500

Final Results

Wt.Sample	**0.076914**	g
Wt.Spike	**0.013120**	g

Unspike subtracted grand mean ratios (Measured Ratios)

	RI_84\88	RI_86\88	RI_87\86
Ratios	1.46E-02	0.11940	7.06E-01
%StdErr	2.47E-03	0.00000	2.98E-04
	# Ratios	Enter # of ratios	

discrimination corrected (Sr86/Sr88)m= 0.1197

Spike subtracted grand mean ratios (Reported Ratios)

	84/88	87/88	87/86	88s/84t
Ratios	0.006747	0.084295	**0.705991**	**126.481597**
2Sigma errors	0.000000	0.000000	**0.000004**	**0.000000**
2*Sig. err. (ppm)=(epsilon*100)	0	0	**5.9551428**	**0.002469639**

[Sr86]= **22.785** nm/g
± **0.000**

[Sr]= **20.239** ppm
± **0.000**

1556.652536 nanograms of Sr

Epsilon (Sr)= **21.17**
(± **0.06**)

Discrimination= #VALUE! to #VALUE!
w/Average of #VALUE!

Enter ion guage pressure in first set x10-8 mbar
Enter ion guage pressure in last set x10-8 mbar
Average Sr88 Intensity= ditted Sr88 Intensity x10-11A

Sample:	**21LAP-UCS-68.94-2H**	Turret(Bead):	4
Operator:	**CTL**	Date:	5/19/2022
		Time:	

	Rspike Values: Sr84-3(x10)#2		
Name	Rsp84\88	Rsp86\88	Rsp87\88
Value	**5.96961**	**0.33048**	**0.12894**

[Sr84-3(x10)#2]
Conc.Spike
8.84500

Final Results

Wt.Sample	**0.073838**	g
Wt.Spike	**0.013110**	g

Unspike subtracted grand mean ratios (Measured Exponentilaly Normalized Ratios)

	RI_84\88	RI_86\88	RI_87\86
Ratios	2.23E-02	0.11940	7.06E-01
%StdErr	2.45E-03	0.00000	4.25E-04
	# Ratios	Enter # of ratios	

discrimination corrected (Sr86/Sr88)m= 0.1200

Spike subtracted grand mean ratios (Reported Ratios)

	84/88	87/88	87/86	88s/84t
Ratios	0.006747	0.084432	**0.707138**	**63.192546**
2Sigma errors	0.000000	0.000000	**0.000006**	**0.000000**
2*Sig. err. (ppm)=(epsilon*100)	0	0	**8.5000716**	**0.002454448**

[Sr86]= **11.849** nm/g
± **0.000**

[Sr]= **10.526** ppm
± **0.000**

777.2268297 nanograms of Sr

Epsilon (Sr)= **37.45**
(± **0.09**)

Discrimination= #VALUE! to #VALUE!
w/Average of #VALUE!

Enter ion guage pressure in first set x10-8 mbar
Enter ion guage pressure in last set x10-8 mbar
Average Sr88 Intensity= ditted Sr88 Intensity x10-11A

Sample:	**21LAP-UCS-39.72-2H**	Turret(Bead):	5
Operator:	**CTL**	Date:	5/19/2022
		Time:	

	Rspike Values: Sr84-3(x10)#2		
Name	Rsp84\88	Rsp86\88	Rsp87\88
Value	**5.96961**	**0.33048**	**0.12894**

[Sr84-3(x10)#2]
Conc.Spike
8.84500

Final Results

Wt.Sample	**0.075937**	g
Wt.Spike	**0.013050**	g

Unspike subtracted grand mean ratios (Measured Ratios)

	RI_84\88	RI_86\88	RI_87\86
Ratios	3.83E-02	0.11940	7.07E-01
%StdErr	1.26E-03	0.00000	4.63E-04
	# Ratios	Enter # of ratios	

discrimination corrected (Sr86/Sr88)m= 0.1205

Spike subtracted grand mean ratios (Reported Ratios)

	84/88	87/88	87/86	88s/84t
Ratios	0.006747	0.084522	**0.707892**	**30.786426**
2Sigma errors	0.000000	0.000000	**0.000007**	**0.000000**
2*Sig. err. (ppm)=(epsilon*100)	0	0	**9.2677276**	**0.001259663**

[Sr86]= **5.588** nm/g
± **0.000**

[Sr]= **4.964** ppm
± **0.000**

376.9476622 nanograms of Sr

Epsilon (Sr)= **48.15**
(± **0.09**)

Discrimination= #VALUE! to #VALUE!
w/Average of #VALUE!

Enter ion guage pressure in first set x10-8 mbar
Enter ion guage pressure in last set x10-8 mbar
Average Sr88 Intensity= ditted Sr88 Intensity x10-11A

Sample:	**21LAP-UCS-24.93-2F**	Turret(Bead):	18
Operator:	**CTL**	Date:	6/23/2022
		Time:	

	Rspike Values: Sr84-3(x10)#2		
Name	Rsp84\88	Rsp86\88	Rsp87\88
Value	**5.96961**	**0.33048**	**0.12894**

[Sr84-3(x10)#2]
Conc.Spike
8.84500

Final Results

Wt.Sample	**0.073295**	g
Wt.Spike	**0.013450**	g

Unspike subtracted grand mean ratios (Measured Ratios)

	RI_84\88	RI_86\88	RI_87\86
Ratios	5.96E-02	0.11940	7.05E-01
%StdErr	1.38E-03	0.00000	4.28E-04
	# Ratios	Enter # of ratios	

discrimination corrected (Sr86/Sr88)m= 0.1213

Spike subtracted grand mean ratios (Reported Ratios)

	84/88	87/88	87/86	88s/84t
Ratios	0.006747	0.084397	**0.706845**	**18.043853**
2Sigma errors	0.000000	0.000000	**0.000006**	**0.000000**
2*Sig. err. (ppm)=(epsilon*100)	0	0	**8.5655904**	**0.001379602**

[Sr86]= **3.497** nm/g
± **0.000**

[Sr]= **3.106** ppm
± **0.000**

227.6765829 nanograms of Sr

Epsilon (Sr)= **33.29**
(± **0.09**)

Discrimination= #VALUE! to #VALUE!
w/Average of #VALUE!

Enter ion guage pressure in first set x10-8 mbar
Enter ion guage pressure in last set x10-8 mbar
Average Sr88 Intensity= ditted Sr88 Intensity x10-11A

Sample:	**21LAP-UCS-10.76-2F**	Turret(Bead):	4
Operator:	**CTL**	Date:	6/19/2022
		Time:	

	Rspike Values: Sr84-3(x10)#2		
Name	Rsp84\88	Rsp86\88	Rsp87\88
Value	**5.96961**	**0.33048**	**0.12894**

[Sr84-3(x10)#2]
Conc.Spike
8.84500

Final Results

Wt.Sample	**0.089876**	g
Wt.Spike	**0.013380**	g

Unspike subtracted grand mean ratios (Measured Ratios)

	RI_84\88	RI_86\88	RI_87\86
Ratios	4.97E-02	0.11940	7.05E-01
%StdErr	1.98E-03	0.00000	4.20E-04
	# Ratios	Enter # of ratios	

discrimination corrected (Sr86/Sr88)m= 0.1210

Spike subtracted grand mean ratios (Reported Ratios)

	84/88	87/88	87/86	88s/84t
Ratios	0.006747	0.084368	**0.706599**	**22.380262**
2Sigma errors	0.000000	0.000000	**0.000006**	**0.000000**
2*Sig. err. (ppm)=(epsilon*100)	0	0	**8.3922354**	**0.001978379**

[Sr86]= **3.519** nm/g
± **0.000**

[Sr]= **3.126** ppm
± **0.000**

280.9167468 nanograms of Sr

Epsilon (Sr)= **29.80**
(± **0.08**)

Discrimination= #VALUE! to #VALUE!
w/Average of #VALUE!

Enter ion guage pressure in first set x10-8 mbar
Enter ion guage pressure in last set x10-8 mbar
Average Sr88 Intensity= ditted Sr88 Intensity x10-11A

Sample:	**21LAP-UCS-2.04-2F**		Turret(Bead):	16	
Operator:	**CTL**		Date:	5/22/2022	
			Time:		

	Rspike Values: Sr84-3(x10)#2			[Sr84-3(x10)#2]
Name	Rsp84\88	Rsp86\88	Rsp87\88	Conc.Spike
Value	**5.96961**	**0.33048**	**0.12894**	**8.84500**

Final Results

Wt.Sample	**0.074823**	g
Wt.Spike	**0.013310**	g

Unspike subtracted grand mean ratios (Measured Ratios)

	RI_84\88	RI_86\88	RI_87\86
Ratios	4.45E-02	0.11940	7.05E-01
%StdErr	9.13E-04	0.00000	3.01E-04
	# Ratios	Enter # of ratios	

discrimination corrected (Sr86/Sr88)m= 0.1208

Spike subtracted grand mean ratios (Reported Ratios)

	84/88	87/88	87/86	88s/84t
Ratios	0.006747	0.084419	**0.707029**	**25.568014**
2Sigma errors	0.000000	0.000000	**0.000004**	**0.000000**
2*Sig. err. (ppm)=(epsilon*100)	0	0	**6.0170214**	**0.000912791**

[Sr86]=	**4.803**	nm/g	
±	**0.000**		
[Sr]=	**4.267**	ppm	319.2637702
±	**0.000**		nanograms of Sr
Epsilon (Sr)=	**35.89**		
(±	**0.06**)		

Discrimination= #VALUE! to #VALUE!
w/Average of #VALUE!

Enter ion guage pressure in first set x10-8 mbar
Enter ion guage pressure in last set x10-8 mbar
Average Sr88 Intensity= ditted Sr88 Intensity x10-11A

Sample:	**21LAP-LCS-3.76-2E**	Turret(Bead):	19
Operator:	**CTL**	Date:	5/23/2022
		Time:	

	Rspike Values: Sr84-3(x10)#2		
Name	Rsp84\88	Rsp86\88	Rsp87\88
Value	**5.96961**	**0.33048**	**0.12894**

[Sr84-3(x10)#2]
Conc.Spike
8.84500

Final Results

Wt.Sample	**0.073240**	g
Wt.Spike	**0.013510**	g

Unspike subtracted grand mean ratios (Measured Ratios)

	RI_84\88	RI_86\88	RI_87\86
Ratios	7.95E-02	0.11940	7.05E-01
%StdErr	1.38E-03	0.00000	4.06E-04
	# Ratios	Enter # of ratios	

discrimination corrected (Sr86/Sr88)m= 0.1221

Spike subtracted grand mean ratios (Reported Ratios)

	84/88	87/88	87/86	88s/84t
Ratios	0.006747	0.084525	**0.707914**	**12.900384**
2Sigma errors	0.000000	0.000000	**0.000006**	**0.000000**
2*Sig. err. (ppm)=(epsilon*100)	0	0	**8.1128552**	**0.001375563**

[Sr86]= **2.513** nm/g
± **0.000**

[Sr]= **2.233** ppm
± **0.000**

163.5197418 nanograms of Sr

Epsilon (Sr)= **48.46**
(± **0.08**)

Discrimination= #VALUE! to #VALUE!
w/Average of #VALUE!

Enter ion guage pressure in first set x10-8 mbar
Enter ion guage pressure in last set x10-8 mbar
Average Sr88 Intensity= ditted Sr88 Intensity x10-11A

Sample:	**21LAP-LCS-6.55-2E**	Turret(Bead):	20
Operator:	**CTL**	Date:	5/23/2022
		Time:	

	Rspike Values: Sr84-3(x10)#2		
Name	Rsp84\88	Rsp86\88	Rsp87\88
Value	**5.96961**	**0.33048**	**0.12894**

[Sr84-3(x10)#2]
Conc.Spike
8.84500

Final Results

Wt.Sample	**0.072902**	g
Wt.Spike	**0.013320**	g

Unspike subtracted grand mean ratios (Measured Ratios)

	RI_84\88	RI_86\88	RI_87\86
Ratios	7.72E-02	0.11940	7.05E-01
%StdErr	1.01E-02	0.00000	2.30E-03
	# Ratios	Enter # of ratios	

discrimination corrected (Sr86/Sr88)m= 0.1220

Spike subtracted grand mean ratios (Reported Ratios)

	84/88	87/88	87/86	88s/84t
Ratios	0.006747	0.084524	**0.707904**	**13.345773**
2Sigma errors	0.000000	0.000000	**0.000033**	**0.000000**
2*Sig. err. (ppm)=(epsilon*100)	0	0	**46.033464**	**0.010134315**

[Sr86]= **2.575** nm/g
± **0.000**

[Sr]= **2.288** ppm
± **0.000**

166.7860464 nanograms of Sr

Epsilon (Sr)= **48.31**
(± **0.46**)

Discrimination= #VALUE! to #VALUE!
w/Average of #VALUE!

Enter ion guage pressure in first set x10-8 mbar
Enter ion guage pressure in last set x10-8 mbar
Average Sr88 Intensity= ditted Sr88 Intensity x10-11A

Sample:	**21LAP-LCS-25.85-2E**	Turret(Bead):	11
Operator:	**CTL**	Date:	5/21/2022
		Time:	

	Rspike Values: Sr84-3(x10)#2		
Name	Rsp84\88	Rsp86\88	Rsp87\88
Value	**5.96961**	**0.33048**	**0.12894**

[Sr84-3(x10)#2]
Conc.Spike
8.84500

Final Results

Wt.Sample	**0.071633**	g
Wt.Spike	**0.012760**	g

Unspike subtracted grand mean ratios (Measured Ratios)

	RI_84\88	RI_86\88	RI_87\86
Ratios	7.59E-02	0.11940	7.05E-01
%StdErr	1.73E-03	0.00000	3.42E-04
	# Ratios	Enter # of ratios	

discrimination corrected (Sr86/Sr88)m= 0.1220

Spike subtracted grand mean ratios (Reported Ratios)

	84/88	87/88	87/86	88s/84t
Ratios	0.006747	0.084553	**0.708151**	**13.607776**
2Sigma errors	0.000000	0.000000	**0.000005**	**0.000000**
2*Sig. err. (ppm)=(epsilon*100)	0	0	**6.8356946**	**0.001729393**

[Sr86]= **2.560** nm/g
± **0.000**

[Sr]= **2.274** ppm
± **0.000**

162.9146332 nanograms of Sr

Epsilon (Sr)= **51.83**
(± **0.07**)

Discrimination= #VALUE! to #VALUE!
w/Average of #VALUE!

Enter ion guage pressure in first set x10-8 mbar
Enter ion guage pressure in last set x10-8 mbar
Average Sr88 Intensity= ditted Sr88 Intensity x10-11A

Sample:	**21LAP-LCS-49.91-2E**	Turret(Bead):	8
Operator:	**CTL**	Date:	4/6/2022
		Time:	

	Rspike Values: Sr84-3(x10)#2		
Name	Rsp84\88	Rsp86\88	Rsp87\88
Value	**5.96961**	**0.33048**	**0.12894**

[Sr84-3(x10)#2]
Conc.Spike
8.84500

Final Results

Wt.Sample	**0.135660**	g
Wt.Spike	**0.008700**	g

Unspike subtracted grand mean ratios (Measured Ratios)

	RI_84\88	RI_86\88	RI_87\86
Ratios	3.40E-02	0.11940	7.07E-01
%StdErr	1.26E-03	0	4.24E-04
	# Ratios	Enter # of ratios	

discrimination corrected (Sr86/Sr88)m= 0.1204

Spike subtracted grand mean ratios (Reported Ratios)

	84/88	87/88	87/86	88s/84t
Ratios	0.006747	0.084611	**0.708636**	**35.714442**
2Sigma errors	0.000000	0.000000	**0.000006**	**0.000000**
2*Sig. err. (ppm)=(epsilon*100)	0	0	**8.4816962**	**0.001260397**

[Sr86]= **2.419** nm/g
± **0.000**

[Sr]= **2.149** ppm
± **0.000**

291.5452602 nanograms of Sr

Epsilon (Sr)= **58.70**
(± **0.09**)

Discrimination= #VALUE! to #VALUE!
w/Average of #VALUE!

Enter ion guage pressure in first set x10-8 mbar
Enter ion guage pressure in last set x10-8 mbar
Average Sr88 Intensity= ditted Sr88 Intensity x10-11A

Sample:	**21LAP-LCS-76.81-2E**	Turret(Bead):	12
Operator:	**CTL**	Date:	5/21/2022
		Time:	

	Rspike Values: Sr84-3(x10)#2		
Name	Rsp84\88	Rsp86\88	Rsp87\88
Value	**5.96961**	**0.33048**	**0.12894**

[Sr84-3(x10)#2]
Conc.Spike
8.84500

Final Results

Wt.Sample	**0.082942**	g
Wt.Spike	**0.013160**	g

Unspike subtracted grand mean ratios (Measured Ratios)

	RI_84\88	RI_86\88	RI_87\86
Ratios	7.89E-02	0.11940	7.06E-01
%StdErr	1.91E-03	0.00000	3.13E-04
	# Ratios	Enter # of ratios	

discrimination corrected (Sr86/Sr88)m= 0.1221

Spike subtracted grand mean ratios (Reported Ratios)

	84/88	87/88	87/86	88s/84t
Ratios	0.006747	0.084612	**0.708646**	**13.020959**
2Sigma errors	0.000000	0.000000	**0.000004**	**0.000000**
2*Sig. err. (ppm)=(epsilon*100)	0	0	**6.257094**	**0.001914136**

[Sr86]= **2.182** nm/g
± **0.000**

[Sr]= **1.939** ppm
± **0.000**

160.7837525 nanograms of Sr

Epsilon (Sr)= **58.85**
(± **0.06**)

Discrimination= #VALUE! to #VALUE!
w/Average of #VALUE!

Enter ion guage pressure in first set x10-8 mbar
Enter ion guage pressure in last set x10-8 mbar
Average Sr88 Intensity= ditted Sr88 Intensity x10-11A

Sample:	**21LAP-LCS-100.85-2E**	Turret(Bead):	13
Operator:	**CTL**	Date:	5/22/2022
		Time:	

	Rspike Values: Sr84-3(x10)#2		
Name	Rsp84\88	Rsp86\88	Rsp87\88
Value	**5.96961**	**0.33048**	**0.12894**

[Sr84-3(x10)#2]
Conc.Spike
8.84500

Final Results

Wt.Sample	**0.079757**	g
Wt.Spike	**0.014760**	g

Unspike subtracted grand mean ratios (Measured Ratios)

	RI_84\88	RI_86\88	RI_87\86
Ratios	7.09E-02	0.11940	7.06E-01
%StdErr	1.57E-03	0.00000	3.67E-04
	# Ratios	Enter # of ratios	

discrimination corrected (Sr86/Sr88)m= 0.1218

Spike subtracted grand mean ratios (Reported Ratios)

	84/88	87/88	87/86	88s/84t
Ratios	0.006747	0.084659	**0.709036**	**14.725866**
2Sigma errors	0.000000	0.000000	**0.000005**	**0.000000**
2*Sig. err. (ppm)=(epsilon*100)	0	0	**7.3354938**	**0.001567239**

[Sr86]= **2.878** nm/g
± **0.000**

[Sr]= **2.557** ppm
± **0.000**

203.9515841 nanograms of Sr

Epsilon (Sr)= **64.39**
(± **0.07**)

Discrimination= #VALUE! to #VALUE!
w/Average of #VALUE!

Enter ion guage pressure in first set x10-8 mbar
Enter ion guage pressure in last set x10-8 mbar
Average Sr88 Intensity= ditted Sr88 Intensity x10-11A

Table 7

PAV-2D SPIKE SHEET SUMMARY

Sample:	87/86 Exp Pre Spk	87/86 Exp	2sig error	2sig error ppm	Sr ppm
PAV-2D-S-17 Aq1	0.703853	0.707290	0.000014	19.11	0.66
PAV-2D-S-15 Aq1	0.70379	0.70753	0.00013	181.90	0.63
PAV-2D-S-14 Aq1	0.702713	0.707379	0.000012	17.22	0.48
PAV-2D-S-12 Aq1	0.701619	0.707548	0.000037	52.58	0.39
PAV-2D-S-11 Aq1	0.70158	0.70772	0.00020	278.03	3.69
PAV-2D-S-9 Aq1	0.6973	0.7022	0.0041	5797.28	0.47
PAV-2D-S-8 Aq1	0.703298	0.707283	0.000076	107.49	0.53
PAV-2D-S-6 Aq1	0.704144	0.707550	0.000011	15.05	0.75
PAV-2D-S-5 Aq1	0.703901	0.707516	0.000052	73.62	0.76
PAV-2D-S-3 Aq1	0.702888	0.707454	0.000049	68.99	0.54
PAV-2D-S-2B Aq1	0.703846	0.707588	0.000038	53.98	0.62
PAV-2D-S-19 Aq1	0.7052	0.7085	0.0019	2735.74	0.75
PAV-2D-S-20 Aq1	0.704036	0.706861	0.000094	132.56	0.85
PAV-2D-R-24 Aq1	0.6920	0.6999	0.0057	8108.09	3.45
PAV-2D-R-25.1 Aq1	0.683476	0.705021	0.000042	60.12	1.06
PAV-2D-R-26 Aq1	0.68643	0.70551	0.00025	359.17	1.23
PAV-2D-R-31 Aq1	0.68205	0.70637	0.00074	1053.11	0.83
PAV-2D-R-34 Aq1	0.68216	0.70550	0.00055	776.30	1.06
Apen-1	0.7025186	0.7033971	0.0000044	6.25	2.61
Apen-2	0.702500	0.705158	0.000027	37.75	0.81

Sample:	**PAV-2D-S-17-Aq1**	Turret(Bead):	8
Operator:	**CTL**	Date:	9/28/2021
		Time:	

#NAME?

	Rspike Values: Sr84-3(x10)#2		
Name	Rsp84\88	Rsp86\88	Rsp87\88
Value	**5.96961**	**0.33048**	**0.12894**

[Sr84-3(x10)#2]
Conc.Spike
8.84500

Final Results

Wt.Sample	**0.143127**	g
Wt.Spike	**0.008730**	g

Unspike subtracted grand mean ratios (Measured Ratios)

	RI_84\88	RI_86\88	RI_87\86
Ratios	8.72E-02	0.11940	7.04E-01
%StdErr	3.20E-03	0	9.56E-04

Ratios Enter # of ratios

discrimination corrected (Sr86/Sr88)m= 0.1224

Spike subtracted grand mean ratios (Reported Ratios)

	84/88	87/88	87/86	88s/84t
Ratios	0.006747	0.084450	**0.707290**	**11.588046**
2Sigma errors	0.000000	0.000000	**0.000014**	**0.000000**
2*Sig. err. (ppm)=(epsilon*100)	0	0	**19.1107268**	**0.003197069**

[Sr86]= **0.746** nm/g
± **0.000**

[Sr]= **0.663** ppm
± **0.000**

94.90959979 nanograms of Sr

Epsilon (Sr)= **39.60**
(± **0.19**)

Discrimination= #VALUE! to #VALUE!
w/Average of #VALUE!

Enter ion guage pressure in first set x10-8 mbar
Enter ion guage pressure in last set x10-8 mbar
Average Sr88 Intensity= ditted Sr88 Intensity x10-11A

Sample:	**PAV-2D-S-15-Aq1**	Turret(Bead):	6
Operator:	**CTL**	Date:	9/16/2021
		Time:	

	Rspike Values: Sr84-3(x10)#2		
Name	Rsp84\88	Rsp86\88	Rsp87\88
Value	**5.96961**	**0.33048**	**0.12894**

[Sr84-3(x10)#2]
Conc.Spike
8.84500

Final Results

Wt.Sample	**0.138650**	g
Wt.Spike	**0.008790**	g

Unspike subtracted grand mean ratios (Measured Ratios)

	RI_84\88	RI_86\88	RI_87\86
Ratios	0.094010186	0.11940	0.70379308
%StdErr	0.031184608	0	0.00909477
	# Ratios	Enter # of ratios	

discrimination corrected (Sr86/Sr88)m= 0.1227

Spike subtracted grand mean ratios (Reported Ratios)

	84/88	87/88	87/86	88s/84t
Ratios	0.006747	0.084480	**0.707535**	**10.624580**
2Sigma errors	0.000000	0.000000	**0.000129**	**0.000000**
2*Sig. err. (ppm)=(epsilon*100)	0	0	**181.895322**	**0.031184608**

[Sr86]= **0.711** nm/g
± **0.000**

[Sr]= **0.632** ppm
± **0.000**

87.618685 nanograms of Sr

Epsilon (Sr)= **43.08**
(± **1.83**)

Discrimination= #VALUE! to #VALUE!
w/Average of #VALUE!

Enter ion guage pressure in first set x10-8 mbar
Enter ion guage pressure in last set x10-8 mbar
Average Sr88 Intensity= ditted Sr88 Intensity x10-11A

Sample:	**PAV-2D-S-14-Aq1**	Turret(Bead):	9
Operator:	**CTL**	Date:	9/29/2021
		Time:	

	Rspike Values: Sr84-3(x10)#2		
Name	Rsp84\88	Rsp86\88	Rsp87\88
Value	**5.96961**	**0.33048**	**0.12894**

[Sr84-3(x10)#2]
Conc.Spike
8.84500

Final Results

Wt.Sample	**0.144370**	g
Wt.Spike	**0.008860**	g

Unspike subtracted grand mean ratios (Measured Ratios)

	RI_84\88	RI_86\88	RI_87\86
Ratios	0.1150242	0.11940	0.70271328
%StdErr	0.001735506	0	0.00086081
	# Ratios	Enter # of ratios	

discrimination corrected (Sr86/Sr88)m= 0.1235

Spike subtracted grand mean ratios (Reported Ratios)

	84/88	87/88	87/86	88s/84t
Ratios	0.006747	0.084461	**0.707379**	**8.409870**
2Sigma errors	0.000000	0.000000	**0.000012**	**0.000000**
2*Sig. err. (ppm)=(epsilon*100)	0	0	**17.2162342**	**0.001735506**

[Sr86]= **0.545** nm/g
± **0.000**

[Sr]= **0.484** ppm
± **0.000**

69.90568525 nanograms of Sr

Epsilon (Sr)= **40.87**
(± **0.17**)

Discrimination= #VALUE! to #VALUE!
w/Average of #VALUE!

Enter ion guage pressure in first set x10-8 mbar
Enter ion guage pressure in last set x10-8 mbar
Average Sr88 Intensity= ditted Sr88 Intensity x10-11A

Sample:	**PAV-2D-S-12-Aq1**	Turret(Bead):	14
Operator:	**CTL**	Date:	9/18/2021
		Time:	

	Rspike Values: Sr84-3(x10)#2		
Name	Rsp84\88	Rsp86\88	Rsp87\88
Value	**5.96961**	**0.33048**	**0.12894**

[Sr84-3(x10)#2]
Conc.Spike
8.84500

Final Results

Wt.Sample	**0.139534**	g
Wt.Spike	**0.008850**	g

Unspike subtracted grand mean ratios (Measured Ratios)

	RI_84\88	RI_86\88	RI_87\86
Ratios	0.14302123	0.11940	0.70161913
%StdErr	0.008755309	0	0.00262912
	# Ratios	Enter # of ratios	

discrimination corrected (Sr86/Sr88)m= 0.1247

Spike subtracted grand mean ratios (Reported Ratios)

	84/88	87/88	87/86	88s/84t
Ratios	0.006747	0.084481	**0.707548**	**6.519268**
2Sigma errors	0.000000	0.000000	**0.000037**	**0.000000**
2*Sig. err. (ppm)=(epsilon*100)	0	0	**52.582404**	**0.008755309**

[Sr86]= **0.437** nm/g
± **0.000**

[Sr]= **0.388** ppm
± **0.000**

54.13009251 nanograms of Sr

Epsilon (Sr)= **43.27**
(± **0.53**)

Discrimination= #VALUE! to #VALUE!
w/Average of #VALUE!

Enter ion guage pressure in first set x10-8 mbar
Enter ion guage pressure in last set x10-8 mbar
Average Sr88 Intensity= ditted Sr88 Intensity x10-11A

Sample:	**PAV-2D-S-11-Aq1**	Turret(Bead):	7
Operator:	**CTL**	Date:	9/16/2021
		Time:	

	Rspike Values: Sr84-3(x10)#2		
Name	Rsp84\88	Rsp86\88	Rsp87\88
Value	**5.96961**	**0.33048**	**0.12894**

[Sr84-3(x10)#2]
Conc.Spike
8.84500

Final Results

Wt.Sample	**0.014227**	g
Wt.Spike	**0.008910**	g

Unspike subtracted grand mean ratios (Measured Ratios)

	RI_84\88	RI_86\88	RI_87\86
Ratios	0.14752912	0.11940	0.70157506
%StdErr	0.063009901	0	0.01390152

Ratios Enter # of ratios

discrimination corrected (Sr86/Sr88)m= 0.1249

Spike subtracted grand mean ratios (Reported Ratios)

	84/88	87/88	87/86	88s/84t
Ratios	0.006747	0.084501	**0.707716**	**6.285018**
2Sigma errors	0.000000	0.000000	**0.000197**	**0.000000**
2*Sig. err. (ppm)=(epsilon*100)	0	0	**278.03048**	**0.063009901**

[Sr86]= **4.157** nm/g
± **0.000**

[Sr]= **3.693** ppm
± **0.000**

52.53975818 nanograms of Sr

Epsilon (Sr)= **45.66**
(± **2.79**)

Discrimination= #VALUE! to #VALUE!
w/Average of #VALUE!

Enter ion guage pressure in first set x10-8 mbar
Enter ion guage pressure in last set x10-8 mbar
Average Sr88 Intensity= ditted Sr88 Intensity x10-11A

Sample:	**PAV-2D-S-9-Aq1**	Turret(Bead):	14
Operator:	**CTL**	Date:	9/18/2021
		Time:	

	Rspike Values: Sr84-3(x10)#2		
Name	Rsp84\88	Rsp86\88	Rsp87\88
Value	**5.96961**	**0.33048**	**0.12894**

[Sr84-3(x10)#2]
Conc.Spike
8.84500

Final Results

Wt.Sample	**0.134713**	g
Wt.Spike	**0.008830**	g

Unspike subtracted grand mean ratios (Measured Ratios)

	RI_84\88	RI_86\88	RI_87\86
Ratios	0.1239316	0.11940	0.69729988
%StdErr	0.2795662	0	0.28986412

Ratios Enter # of ratios

discrimination corrected (Sr86/Sr88)m= 0.1239

Spike subtracted grand mean ratios (Reported Ratios)

	84/88	87/88	87/86	88s/84t
Ratios	0.006747	0.083838	**0.702159**	**7.710547**
2Sigma errors	0.000000	0.000000	**0.004071**	**0.000002**
2*Sig. err. (ppm)=(epsilon*100)	0	0	**5797.2824**	**0.2795662**

[Sr86]= **0.534** nm/g
± **0.000**

[Sr]= **0.474** ppm
± **0.000**

63.84303906 nanograms of Sr

Epsilon (Sr)= **-33.23**
(± **57.78**)

Discrimination= #VALUE! to #VALUE!
w/Average of #VALUE!

Enter ion guage pressure in first set x10-8 mbar
Enter ion guage pressure in last set x10-8 mbar
Average Sr88 Intensity= ditted Sr88 Intensity x10-11A

Sample:	**PAV-2D-S-8-Aq1**	Turret(Bead):	10
Operator:	**CTL**	Date:	9/29/2021
		Time:	

	Rspike Values: Sr84-3(x10)#2		
Name	Rsp84\88	Rsp86\88	Rsp87\88
Value	**5.96961**	**0.33048**	**0.12894**

[Sr84-3(x10)#2]
Conc.Spike
8.84500

Final Results

Wt.Sample	**0.155311**	g
Wt.Spike	**0.008860**	g

Unspike subtracted grand mean ratios (Measured Ratios)

	RI_84\88	RI_86\88	RI_87\86
Ratios	0.099706924	0.11940	0.70329793
%StdErr	0.011211523	0	0.00537449

Ratios Enter # of ratios

discrimination corrected (Sr86/Sr88)m= 0.1229

Spike subtracted grand mean ratios (Reported Ratios)

	84/88	87/88	87/86	88s/84t
Ratios	0.006747	0.084450	**0.707283**	**9.925364**
2Sigma errors	0.000000	0.000000	**0.000076**	**0.000000**
2*Sig. err. (ppm)=(epsilon*100)	0	0	**107.489766**	**0.011211523**

[Sr86]= **0.598** nm/g
± **0.000**

[Sr]= **0.531** ppm
± **0.000**

82.5022083 nanograms of Sr

Epsilon (Sr)= **39.50**
(± **1.08**)

Discrimination= #VALUE! to #VALUE!
w/Average of #VALUE!

Enter ion guage pressure in first set x10-8 mbar
Enter ion guage pressure in last set x10-8 mbar
Average Sr88 Intensity= ditted Sr88 Intensity x10-11A

Sample:	**PAV-2D-S-6-Aq1**	Turret(Bead):	18
Operator:	**CTL**	Date:	11/12/2021
		Time:	

	Rspike Values: Sr84-3(x10)#2		
Name	Rsp84\88	Rsp86\88	Rsp87\88
Value	**5.96961**	**0.33048**	**0.12894**

[Sr84-3(x10)#2]
Conc.Spike
8.84500

Final Results

Wt.Sample	**0.131470**	g
Wt.Spike	**0.008970**	g

Unspike subtracted grand mean ratios (Measured Ratios)

	RI_84\88	RI_86\88	RI_87\86
Ratios	0.086324023	0.11940	0.7041444
%StdErr	0.003642768	0	0.00075253

Ratios Enter # of ratios

discrimination corrected (Sr86/Sr88)m= 0.1224

Spike subtracted grand mean ratios (Reported Ratios)

	84/88	87/88	87/86	88s/84t
Ratios	0.006747	0.084481	**0.707550**	**11.726492**
2Sigma errors	0.000000	0.000000	**0.000011**	**0.000000**
2*Sig. err. (ppm)=(epsilon*100)	0	0	**15.0505618**	**0.003642768**

[Sr86]= **0.845** nm/g
± **0.000**

[Sr]= **0.751** ppm
± **0.000**

98.68639559 nanograms of Sr

Epsilon (Sr)= **43.29**
(± **0.15**)

Discrimination= #VALUE! to #VALUE!
w/Average of #VALUE!

Enter ion guage pressure in first set x10-8 mbar
Enter ion guage pressure in last set x10-8 mbar
Average Sr88 Intensity= ditted Sr88 Intensity x10-11A

Sample:	**PAV-2D-S-5-Aq1**	Turret(Bead):	16
Operator:	**CTL**	Date:	11/12/2021
		Time:	

	Rspike Values: Sr84-3(x10)#2		
Name	Rsp84\88	Rsp86\88	Rsp87\88
Value	**5.96961**	**0.33048**	**0.12894**

[Sr84-3(x10)#2]
Conc.Spike
8.84500

Final Results

Wt.Sample	**0.120590**	g
Wt.Spike	**0.008910**	g

Unspike subtracted grand mean ratios (Measured Ratios)

	RI_84\88	RI_86\88	RI_87\86
Ratios	0.091147498	0.11940	0.70390077
%StdErr	0.009079132	0	0.00368113
	# Ratios	Enter # of ratios	

discrimination corrected (Sr86/Sr88)m= 0.1226

Spike subtracted grand mean ratios (Reported Ratios)

	84/88	87/88	87/86	88s/84t
Ratios	0.006747	0.084477	**0.707516**	**11.011547**
2Sigma errors	0.000000	0.000000	**0.000052**	**0.000000**
2*Sig. err. (ppm)=(epsilon*100)	0	0	**73.622522**	**0.009079132**

[Sr86]= **0.859** nm/g
± **0.000**

[Sr]= **0.763** ppm
± **0.000**

92.04948054 nanograms of Sr

Epsilon (Sr)= **42.82**
(± **0.74**)

Discrimination= #VALUE! to #VALUE!
w/Average of #VALUE!

Enter ion guage pressure in first set x10-8 mbar
Enter ion guage pressure in last set x10-8 mbar
Average Sr88 Intensity= ditted Sr88 Intensity x10-11A

Sample:	**PAV-2D-S-3-Aq1**	Turret(Bead):	11
Operator:	**CTL**	Date:	9/29/2021
		Time:	

	Rspike Values: Sr84-3(x10)#2		
Name	Rsp84\88	Rsp86\88	Rsp87\88
Value	**5.96961**	**0.33048**	**0.12894**

[Sr84-3(x10)#2]
Conc.Spike
8.84500

Final Results

Wt.Sample	**0.131360**	g
Wt.Spike	**0.008830**	g

Unspike subtracted grand mean ratios (Measured Ratios)

	RI_84\88	RI_86\88	RI_87\86
Ratios	0.11273099	0.11940	0.7028877
%StdErr	0.009075311	0	0.00344972
	# Ratios	Enter # of ratios	

discrimination corrected (Sr86/Sr88)m= 0.1234

Spike subtracted grand mean ratios (Reported Ratios)

	84/88	87/88	87/86	88s/84t
Ratios	0.006747	0.084470	**0.707454**	**8.608910**
2Sigma errors	0.000000	0.000000	**0.000049**	**0.000000**
2*Sig. err. (ppm)=(epsilon*100)	0	0	**68.994474**	**0.009075311**

[Sr86]= **0.611** nm/g
± **0.000**

[Sr]= **0.543** ppm
± **0.000**

71.31839598 nanograms of Sr

Epsilon (Sr)= **41.93**
(± **0.69**)

Discrimination= #VALUE! to #VALUE!
w/Average of #VALUE!

Enter ion guage pressure in first set x10-8 mbar
Enter ion guage pressure in last set x10-8 mbar
Average Sr88 Intensity= ditted Sr88 Intensity x10-11A

Sample:	**PAV-2D-S-2B-Aq1**	Turret(Bead):	12
Operator:	**CTL**	Date:	9/29/2021
		Time:	

	Rspike Values: Sr84-3(x10)#2		
Name	Rsp84\88	Rsp86\88	Rsp87\88
Value	**5.96961**	**0.33048**	**0.12894**

[Sr84-3(x10)#2]
Conc.Spike
8.84500

Final Results

Wt.Sample	**0.141022**	g
Wt.Spike	**0.008830**	g

Unspike subtracted grand mean ratios (Measured Ratios)

	RI_84\88	RI_86\88	RI_87\86
Ratios	0.093968672	0.11940	0.70384601
%StdErr	0.009933912	0	0.0026988
	# Ratios	Enter # of ratios	

discrimination corrected (Sr86/Sr88)m= 0.1227

Spike subtracted grand mean ratios (Reported Ratios)

	84/88	87/88	87/86	88s/84t
Ratios	0.006747	0.084486	**0.707588**	**10.630010**
2Sigma errors	0.000000	0.000000	**0.000038**	**0.000000**
2*Sig. err. (ppm)=(epsilon*100)	0	0	**53.975992**	**0.009933912**

[Sr86]= **0.703** nm/g
± **0.000**

[Sr]= **0.624** ppm
± **0.000**

88.06284475 nanograms of Sr

Epsilon (Sr)= **43.83**
(± **0.54**)

Discrimination= #VALUE! to #VALUE!
w/Average of #VALUE!

Enter ion guage pressure in first set x10-8 mbar
Enter ion guage pressure in last set x10-8 mbar
Average Sr88 Intensity= ditted Sr88 Intensity x10-11A

Sample:	**PAV-2D-S-19-Aq1**	Turret(Bead):	13
Operator:	**CTL**	Date:	9/17/2017
		Time:	

	Rspike Values: Sr84-3(x10)#2		
Name	Rsp84\88	Rsp86\88	Rsp87\88
Value	**5.96961**	**0.33048**	**0.12894**

[Sr84-3(x10)#2]
Conc.Spike
8.84500

Final Results

Wt.Sample	**0.135878**	g
Wt.Spike	**0.008820**	g

Unspike subtracted grand mean ratios (Measured Ratios)

	RI_84\88	RI_86\88	RI_87\86
Ratios	0.082738814	0.11940	0.70522725
%StdErr	0.13063846	0	0.13678718

Ratios Enter # of ratios

discrimination corrected (Sr86/Sr88)m= 0.1222

Spike subtracted grand mean ratios (Reported Ratios)

	84/88	87/88	87/86	88s/84t
Ratios	0.006747	0.084595	**0.708499**	**12.316659**
2Sigma errors	0.000000	0.000000	**0.001938**	**0.000002**
2*Sig. err. (ppm)=(epsilon*100)	0	0	**2735.7436**	**0.13063846**

[Sr86]= **0.844** nm/g
± **0.000**

[Sr]= **0.750** ppm
± **0.000**

101.9291871 nanograms of Sr

Epsilon (Sr)= **56.77**
(± **27.51**)

Discrimination= #VALUE! to #VALUE!
w/Average of #VALUE!

Enter ion guage pressure in first set x10-8 mbar
Enter ion guage pressure in last set x10-8 mbar
Average Sr88 Intensity= ditted Sr88 Intensity x10-11A

Sample:	**PAV-2D-S-20-Aq1**	Turret(Bead):	9
Operator:	**CTL**	Date:	9/17/2021
		Time:	

	Rspike Values: Sr84-3(x10)#2		
Name	Rsp84\88	Rsp86\88	Rsp87\88
Value	**5.96961**	**0.33048**	**0.12894**

[Sr84-3(x10)#2]
Conc.Spike
8.84500

Final Results

Wt.Sample	**0.138229**	g
Wt.Spike	**0.008850**	g

Unspike subtracted grand mean ratios (Measured Ratios)

	RI_84\88	RI_86\88	RI_87\86
Ratios	0.073344678	0.11940	0.70403633
%StdErr	0.017698499	0	0.00662785
	# Ratios	Enter # of ratios	

discrimination corrected (Sr86/Sr88)m= 0.1219

Spike subtracted grand mean ratios (Reported Ratios)

	84/88	87/88	87/86	88s/84t
Ratios	0.006747	0.084399	**0.706861**	**14.164225**
2Sigma errors	0.000000	0.000000	**0.000094**	**0.000000**
2*Sig. err. (ppm)=(epsilon*100)	0	0	**132.55708**	**0.017698499**

[Sr86]= **0.958** nm/g
± **0.000**

[Sr]= **0.851** ppm
± **0.000**

117.5989758 nanograms of Sr

Epsilon (Sr)= **33.51**
(± **1.33**)

Discrimination= #VALUE! to #VALUE!
w/Average of #VALUE!

Enter ion guage pressure in first set x10-8 mbar
Enter ion guage pressure in last set x10-8 mbar
Average Sr88 Intensity= ditted Sr88 Intensity x10-11A

Sample:	**PAV-2D-R-24-Aq1**	Turret(Bead):	10
Operator:	**CTL**	Date:	9/17/2021
		Time:	

	Rspike Values: Sr84-3(x10)#2		
Name	Rsp84\88	Rsp86\88	Rsp87\88
Value	**5.96961**	**0.33048**	**0.12894**

[Sr84-3(x10)#2]
Conc.Spike
8.84500

Final Results

Wt.Sample	**0.026787**	g
Wt.Spike	**0.022270**	g

Unspike subtracted grand mean ratios (Measured Ratios)

	RI_84\88	RI_86\88	RI_87\86
Ratios	0.19744809	0.11940	0.69200066
%StdErr	1.022219	0	0.40540457
	# Ratios	Enter # of ratios	

discrimination corrected (Sr86/Sr88)m= 0.1271

Spike subtracted grand mean ratios (Reported Ratios)

	84/88	87/88	87/86	88s/84t
Ratios	0.006747	0.083572	**0.699937**	**4.429563**
2Sigma errors	0.000000	0.000000	**0.005675**	**0.000005**
2*Sig. err. (ppm)=(epsilon*100)	0	0	**8108.0914**	**1.022219**

[Sr86]= **3.889** nm/g
± **0.000**

[Sr]= **3.453** ppm
± **0.000**

92.48136303 nanograms of Sr

Epsilon (Sr)= **-64.77**
(± **80.56**)

Discrimination= #VALUE! to #VALUE!
w/Average of #VALUE!

Enter ion guage pressure in first set x10-8 mbar
Enter ion guage pressure in last set x10-8 mbar
Average Sr88 Intensity= ditted Sr88 Intensity x10-11A

Sample:	**PAV-2D-R-25.1-Aq1**	Turret(Bead):	16
Operator:	**CTL**	Date:	9/17/2021
		Time:	

	Rspike Values: Sr84-3(x10)#2		
Name	Rsp84\88	Rsp86\88	Rsp87\88
Value	**5.96961**	**0.33048**	**0.12894**

[Sr84-3(x10)#2]
Conc.Spike
8.84500

Final Results

Wt.Sample	**0.026591**	g
Wt.Spike	**0.021830**	g

Unspike subtracted grand mean ratios (Measured Ratios)

	RI_84\88	RI_86\88	RI_87\86
Ratios	0.45855413	0.11940	0.68347592
%StdErr	0.005470628	0	0.00300596

Ratios Enter # of ratios

discrimination corrected (Sr86/Sr88)m= 0.1423

Spike subtracted grand mean ratios (Reported Ratios)

	84/88	87/88	87/86	88s/84t
Ratios	0.006747	0.084179	**0.705021**	**1.375422**
2Sigma errors	0.000000	0.000000	**0.000042**	**0.000000**
2*Sig. err. (ppm)=(epsilon*100)	0	0	**60.119244**	**0.005470628**

[Sr86]=	**1.193**	nm/g	
±	**0.000**		
[Sr]=	**1.059**	ppm	28.16299708
±	**0.000**		nanograms of Sr
Epsilon (Sr)=	**7.39**		
(±	**0.60**)		

Discrimination= #VALUE! to #VALUE!
w/Average of #VALUE!

Enter ion guage pressure in first set x10-8 mbar
Enter ion guage pressure in last set x10-8 mbar
Average Sr88 Intensity= ditted Sr88 Intensity x10-11A

Sample:	**PAV-2D-R-26-Aq1**	Turret(Bead):	17
Operator:	**CTL**	Date:	9/18/2021
		Time:	

	Rspike Values: Sr84-3(x10)#2		
Name	Rsp84\88	Rsp86\88	Rsp87\88
Value	**5.96961**	**0.33048**	**0.12894**

[Sr84-3(x10)#2]
Conc.Spike
8.84500

Final Results

Wt.Sample	**0.026935**	g
Wt.Spike	**0.021700**	g

Unspike subtracted grand mean ratios (Measured Ratios)

	RI_84\88	RI_86\88	RI_87\86
Ratios	0.41274204	0.11940	0.68643471
%StdErr	0.054437501	0	0.01795826
	# Ratios	Enter # of ratios	

discrimination corrected (Sr86/Sr88)m= 0.1390

Spike subtracted grand mean ratios (Reported Ratios)

	84/88	87/88	87/86	88s/84t
Ratios	0.006747	0.084238	**0.705508**	**1.632341**
2Sigma errors	0.000000	0.000000	**0.000253**	**0.000000**
2*Sig. err. (ppm)=(epsilon*100)	0	0	**359.16522**	**0.054437501**

[Sr86]= **1.389** nm/g
± **0.000**

[Sr]= **1.234** ppm
± **0.000**

33.22619222 nanograms of Sr

Epsilon (Sr)= **14.31**
(± **3.60**)

Discrimination= #VALUE! to #VALUE!
w/Average of #VALUE!

Enter ion guage pressure in first set x10-8 mbar
Enter ion guage pressure in last set x10-8 mbar
Average Sr88 Intensity= ditted Sr88 Intensity x10-11A

Sample:	**PAV-2D-R-31 Aq1**	Turret(Bead):	18
Operator:	**CTL**	Date:	9/18/2021
		Time:	

	Rspike Values: Sr84-3(x10)#2		
Name	Rsp84\88	Rsp86\88	Rsp87\88
Value	**5.96961**	**0.33048**	**0.12894**

[Sr84-3(x10)#2]
Conc.Spike
8.84500

Final Results

Wt.Sample	**0.029591**	g
Wt.Spike	**0.022170**	g

Unspike subtracted grand mean ratios (Measured Ratios)

	RI_84\88	RI_86\88	RI_87\86
Ratios	0.50134005	0.11940	0.68205089
%StdErr	0.075776191	0	0.05265565
	# Ratios	Enter # of ratios	

discrimination corrected (Sr86/Sr88)m= 0.1457

Spike subtracted grand mean ratios (Reported Ratios)

	84/88	87/88	87/86	88s/84t
Ratios	0.006747	0.084340	**0.706368**	**1.176148**
2Sigma errors	0.000000	0.000000	**0.000744**	**0.000000**
2*Sig. err. (ppm)=(epsilon*100)	0	0	**1053.11294**	**0.075776191**

[Sr86]= **0.931** nm/g
± **0.000**

[Sr]= **0.827** ppm
± **0.000**

24.46099475 nanograms of Sr

Epsilon (Sr)= **26.51**
(± **10.56**)

Discrimination= #VALUE! to #VALUE!
w/Average of #VALUE!

Enter ion guage pressure in first set x10-8 mbar
Enter ion guage pressure in last set x10-8 mbar
Average Sr88 Intensity= ditted Sr88 Intensity x10-11A

Sample:	**PAV-2D-R-34-Aq1**	Turret(Bead):	11
Operator:	**CTL**	Date:	9/17/2021
		Time:	

	Rspike Values: Sr84-3(x10)#2		
Name	Rsp84\88	Rsp86\88	Rsp87\88
Value	**5.96961**	**0.33048**	**0.12894**

[Sr84-3(x10)#2]
Conc.Spike
8.84500

Final Results

Wt.Sample	**0.025221**	g
Wt.Spike	**0.023030**	g

Unspike subtracted grand mean ratios (Measured Ratios)

	RI_84\88	RI_86\88	RI_87\86
Ratios	0.4878726	0.11940	0.68216352
%StdErr	0.21768006	0	0.03881502
	# Ratios	Enter # of ratios	

discrimination corrected (Sr86/Sr88)m= 0.1446

Spike subtracted grand mean ratios (Reported Ratios)

	84/88	87/88	87/86	88s/84t
Ratios	0.006747	0.084237	**0.705499**	**1.235323**
2Sigma errors	0.000000	0.000000	**0.000548**	**0.000000**
2*Sig. err. (ppm)=(epsilon*100)	0	0	**776.30032**	**0.21768006**

[Sr86]= **1.191** nm/g
± **0.000**

[Sr]= **1.058** ppm
± **0.000**

26.6860388 nanograms of Sr

Epsilon (Sr)= **14.18**
(± **7.77**)

Discrimination= #VALUE! to #VALUE!
w/Average of #VALUE!

Enter ion guage pressure in first set x10-8 mbar
Enter ion guage pressure in last set x10-8 mbar
Average Sr88 Intensity= ditted Sr88 Intensity x10-11A

Sample:	**Apen-1**	Turret(Bead):	19
Operator:	**CTL**	Date:	9/30/2021
		Time:	

	Rspike Values: Sr84-3(x10)#2		
Name	Rsp84\88	Rsp86\88	Rsp87\88
Value	**5.96961**	**0.33048**	**0.12894**

[Sr84-3(x10)#2]
Conc.Spike
8.84500

Final Results

Wt.Sample	**0.144370**	g
Wt.Spike	**0.008860**	g

Unspike subtracted grand mean ratios (Measured Ratios)

	RI_84\88	RI_86\88	RI_87\86
Ratios	0.028290572	0.11940	0.70251859
%StdErr	0.0009744	0	0.00031237
	# Ratios	Enter # of ratios	

discrimination corrected (Sr86/Sr88)m= 0.1202

Spike subtracted grand mean ratios (Reported Ratios)

	84/88	87/88	87/86	88s/84t
Ratios	0.006747	0.083986	**0.703397**	**45.408172**
2Sigma errors	0.000000	0.000000	**0.000004**	**0.000000**
2*Sig. err. (ppm)=(epsilon*100)	0	0	**6.2474346**	**0.0009744**

[Sr86]= **2.943** nm/g
± **0.000**

[Sr]= **2.613** ppm
± **0.000**

377.3010419 nanograms of Sr

Epsilon (Sr)= **-15.65**
(± **0.06**)

Discrimination= #VALUE! to #VALUE!
w/Average of #VALUE!

Enter ion guage pressure in first set x10-8 mbar
Enter ion guage pressure in last set x10-8 mbar
Average Sr88 Intensity= ditted Sr88 Intensity x10-11A

Sample:	**Apen-2**	Turret(Bead):	20
Operator:	**CTL**	Date:	9/30/2021
		Time:	

	Rspike Values: Sr84-3(x10)#2		
Name	Rsp84\88	Rsp86\88	Rsp87\88
Value	**5.96961**	**0.33048**	**0.12894**

[Sr84-3(x10)#2]
Conc.Spike
8.84500

Final Results

Wt.Sample	**0.149570**	g
Wt.Spike	**0.008730**	g

Unspike subtracted grand mean ratios (Measured Ratios)

	RI_84\88	RI_86\88	RI_87\86
Ratios	0.070296902	0.11940	0.70250019
%StdErr	0.005084486	0	0.00188768
	# Ratios	Enter # of ratios	

discrimination corrected (Sr86/Sr88)m= 0.1217

Spike subtracted grand mean ratios (Reported Ratios)

	84/88	87/88	87/86	88s/84t
Ratios	0.006747	0.084196	**0.705158**	**14.880930**
2Sigma errors	0.000000	0.000000	**0.000027**	**0.000000**
2*Sig. err. (ppm)=(epsilon*100)	0	0	**37.753566**	**0.005084486**

[Sr86]= **0.917** nm/g
± **0.000**

[Sr]= **0.815** ppm
± **0.000**

121.8538929 nanograms of Sr

Epsilon (Sr)= **9.34**
(± **0.38**)

Discrimination= #VALUE! to #VALUE!
w/Average of #VALUE!

Enter ion guage pressure in first set x10-8 mbar
Enter ion guage pressure in last set x10-8 mbar
Average Sr88 Intensity= ditted Sr88 Intensity x10-11A